ESR Studies of Organo-halide Radicals

by

Stanislaw Paul Maj

A thesis submitted
for the degree of
Doctor of Philosophy
in the
Faculty of Science
at the
University of Leicester

Department of Chemistry,
The University,
LEICESTER. LE1 7RH

December 1985

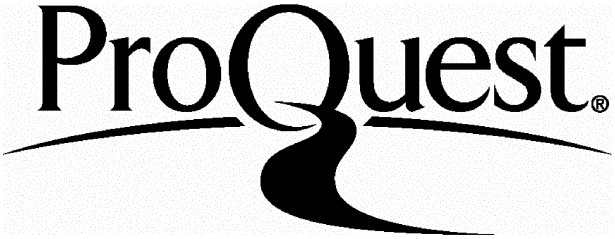

Dedicated to my Mother
and Father

STATEMENT

The work in this Thesis was carried out by the author in the Department of Chemistry at the University of Leicester during the period September 1979 - September 1982. The resolution enhancement technique in Chapter 5 was developed by P. Trousson and the Molecular Orbital calculations, Chapter 3, were performed by Professor A. Hasegawa. Some of the work in Chapter 4 on adducts was carried out in conjunction with Dr. I. G. Smith. The ethyl iodide crystal was grown by Dr. T. Chen (ETH Zürich) who also helped in variable temperature experiments.

This work has not been presented for any other degree.

This thesis may be made available for consultation, photocopying and use through other libraries.

ACKNOWLEDGEMENTS

This thesis would not have been possible without the financial assistance provided by the SERC and ICI Limited (Mond Division).

I would like to thank Professor M. C. R. Symons for all the help and guidance he has given me.

I would like to thank all the members of the Chemistry Department especially members of the Workshop. I would also like to acknowledge Miss Vicky Orson-Wright and Mrs. Ann Crane who have been instrumental in the typing and preparation of diagrams for use in this thesis.

Finally, I would like to acknowledge the help of D. E. Pratt and L. Portwood for work on m-dinitrobenzene.

LIST OF CONTENTS

LIST OF CONTENTS (Continued) ....

[* *This work, though not encompassed by the title of the thesis, was successfully carried out by the author, D. E. Pratt and L. Portwood.*]

CHAPTER 1

Paramagnetic Resonance in Solids

1.1 RESONANCE CONDITION

Electron spin resonance spectroscopy is the study of the interaction between the electronic magnetic moments and the applied magnetic field. The system must have a resultant electronic angular momentum - due to contributions from both intrinsic spin and the orbital angular momentum. Most substances have paired electrons with no resultant electronic angular momentum.[1]

In the absence of a magnetic field the $(2J+1)$ energy levels associated with a chemical entity having a total electronic angular momentum J are degenerate.

An electron interacts with an applied field H according to

$$\mathcal{H} = \beta.H\ (\underline{L} + 2\,\underline{S}) \qquad \ldots\ [1]$$

where $\mathcal{H}$ is the Hamiltonian, β is the Böhr magneton, $\underline{L}$ and $\underline{S}$ are the orbital momentum and spin operators.

For an electron with no orbital momentum the energy of interaction is $g.\beta.H.S$, where g is a dimensionless ratio. The application of H to the Z axis of spin quantisation splits into two levels with the energies $+\beta HS_z$ and $-\beta HS_z$, i.e. the spin vector lies either parallel or antiparallel to the direction of H. Transitions can then be induced between the levels by the application of an oscillating electromagnetic field (Figure 1). The resonance condition is given by

$$h\nu = g\beta H \qquad \ldots\ [2]$$

where ν is the frequency of the photon absorbed and h is Planck's constant. The selection rule is $\Delta M_S = \pm 1$.

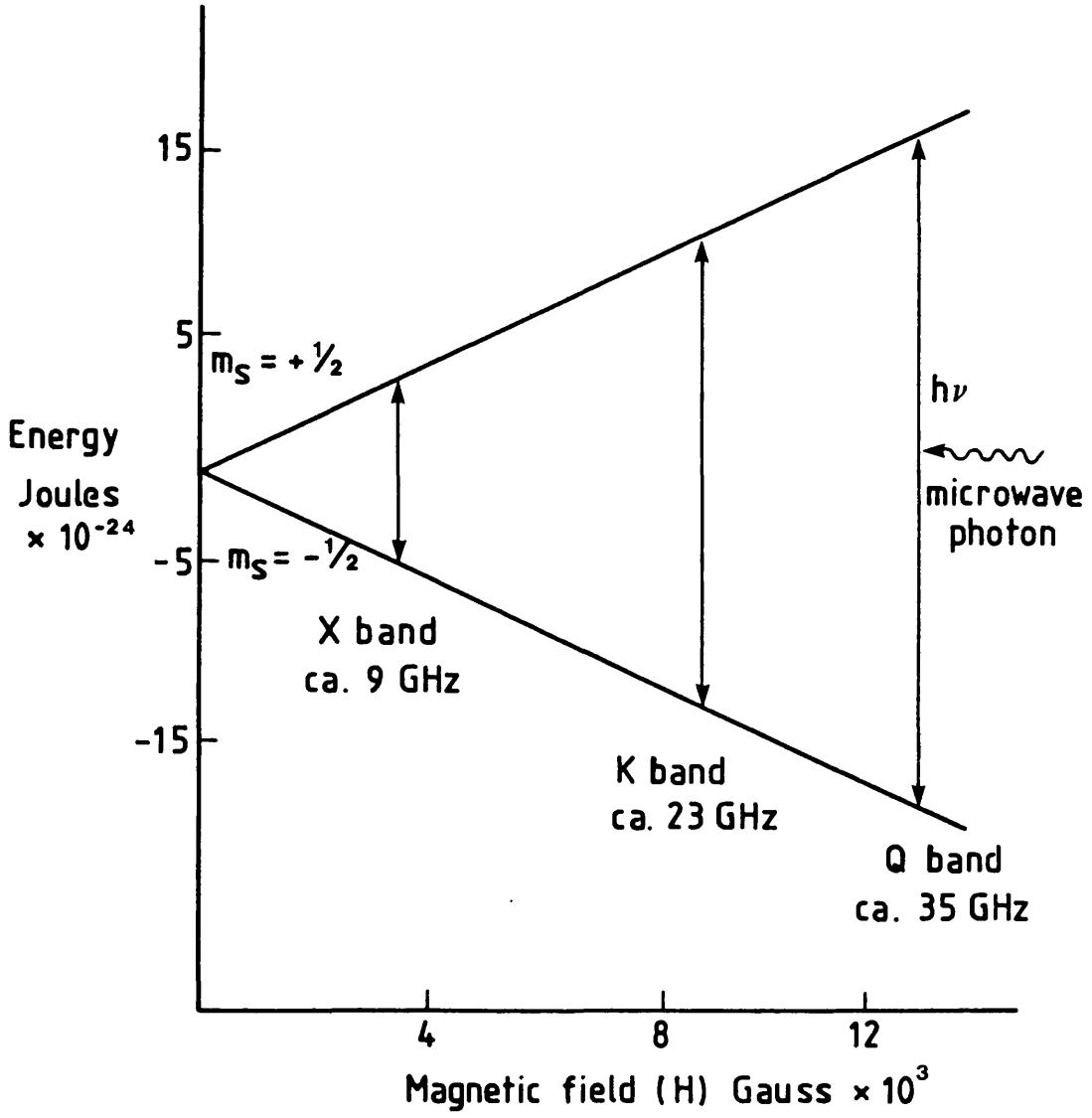

FIGURE 1

Schematic representation of an electron spin resonance transition at different frequencies.

1.2 SPIN HAMILTONIAN

In most systems studied the electron is not free and the energy levels of the simple spin states are modified by perturbations. The spin Hamiltonian takes these into account.[2]

$$\mathcal{H} = \mathcal{H}_{\substack{\text{Electronic}\\\text{Zeeman}}} + \mathcal{H}_{\text{Hyperfine}} + \mathcal{H}_{\text{Quadrupole}} + \mathcal{H}_{\text{Zero-field}} + \mathcal{H}_{\substack{\text{Nuclear}\\\text{Zeeman}}} \quad \ldots\ldots [3]$$

The important features are as follows.

(i) Electronic Zeeman Interaction

The interaction between the external magnetic field and the electron spin lifts the degeneracy of the spin states and is described by the Hamiltonian

$$\mathcal{H} = \beta \, (\underline{g}_{xx} H_x S_x + \underline{g}_{yy} H_y S_y + \underline{g}_{zz} H_z S_z) \quad \ldots\ldots [4]$$

From the above it can be seen there are three principal values, $\underline{g}_{xx}$, $\underline{g}_{yy}$ and $\underline{g}_{zz}$. The orbital part of the electronic magnetic moment depends on the symmetry of the 'crystal field' of the environment.[3] Hence the $\underline{g}$-factors depend on the direction of H with respect to the crystal field and are represented by three principal values lying in orthogonal directions. These include the maximum and minimum values at the symmetric second rank tensor $\underline{g}$.

(ii) Hyperfine Interaction

A spinning nucleus generates a magnetic moment that can interact with the magnetic moment of the associated unpaired electron. This is known as hyperfine interaction. In a magnetic field a nucleus with a spin I has $2I + 1$ orientations giving rise to $2I + 1$ hyperfine lines (Figure 2). The selection rule is $\Delta M_S = \pm 1$ and $\Delta M_I = 0$.

The Hamiltonian is:-

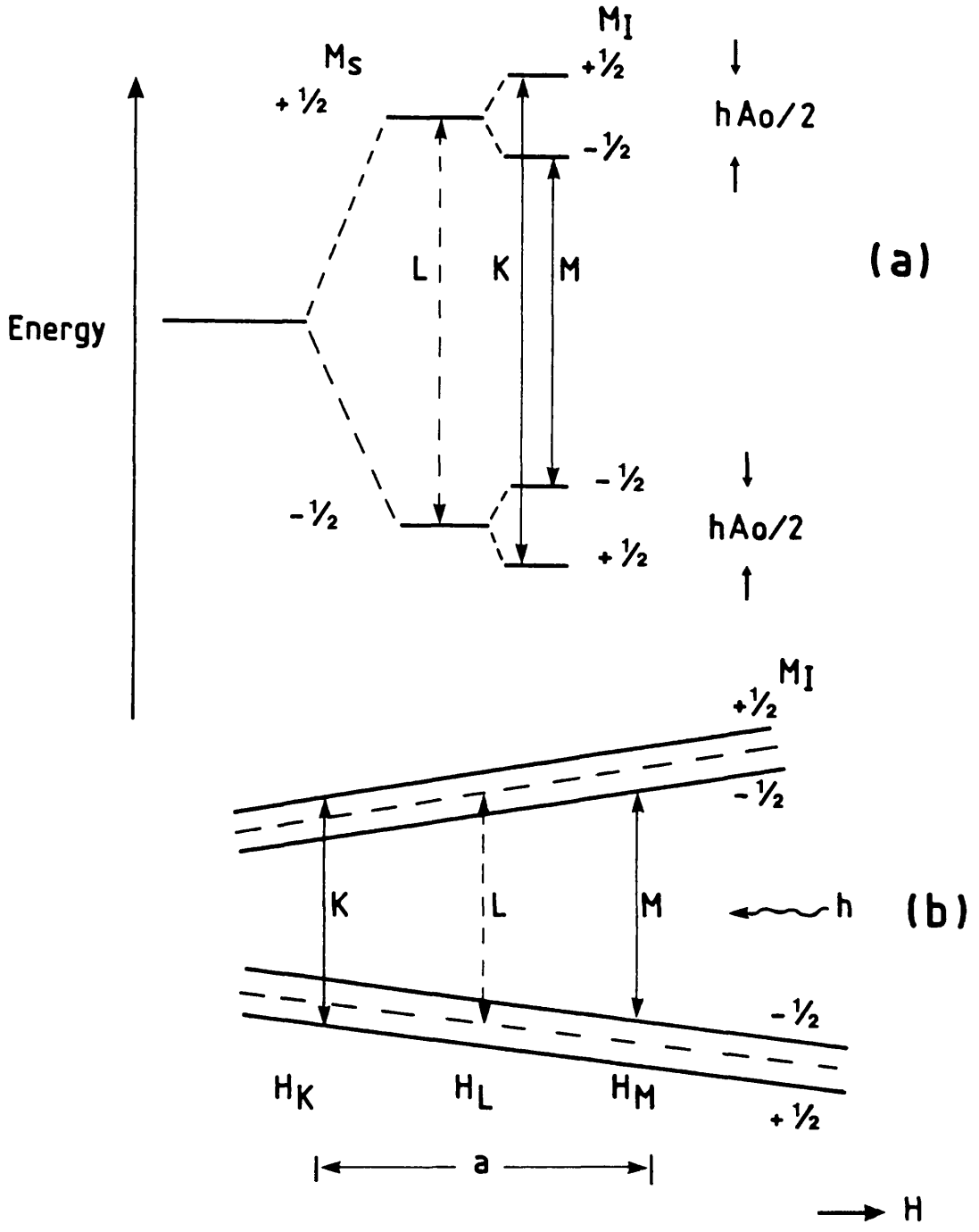

FIGURE 2

(a) Energy levels of the hydrogen atom at a constant magnetic field. Lines K and M are the allowed transitions with hyperfine coupling operative $h\nu = g\beta H \pm \frac{1}{2} h A_o$. A_o (MHz) is the isotropic hyperfine coupling constant.

(b) Energy levels with constant microwave frequency and variable magnetic field. Line K and M are transitions associated with a microwave quantum $h\nu$. The resonant field values are $H_K = \frac{h\nu}{g\beta} + \frac{a}{2}$ and $H_M = \frac{h\nu}{g\beta} - \frac{a}{2}$

where a (gauss) is the hyperfine splitting constant.

$$\mathcal{H} = (A_{xx} I_x S_x + A_{yy} I_y S_y + A_{zz} I_z S_z) \quad \ldots\ [5]$$

A is the hyperfine coupling constant (ergs). When the distribution of the unpaired electron is in an s-orbital, $A_{xx} = A_{yy} = A_{zz}$ and the hyperfine coupling is isotropic. With an aspherical distribution (p, d electrons) the hyperfine coupling is anisotropic.

(iii) Zero Field Interaction

If the system contains more than one unpaired electron, the removal of the spin degeneracy of such triplet spin-states (in the absence of H) by a second order spin-orbit coupling is the 'zero-field splitting' i.e.

$$\mathcal{H} = g\beta H.\hat{S} + D(\hat{S}_z^2 - \tfrac{1}{3}\hat{S}^2) + E(\hat{S}_x^2 - \hat{S}_y^2)$$

where D and E are the zero field splitting constants.

(iv) Quadrupole Interaction

This is the interaction between the electric quadrupole moment of the nucleus and the electric field gradient of the environment. Perturbation of the energy levels of the nuclear spin states are coupled to the electronic spin states. Nuclei with a spin $I \geqslant 1$ have a finite quadrupole moment (eQ) which is a function of the deviation from spherical charge distribution. The action is such as to align the nucleus along its symmetry (spinning) axis whereas the magnetic field produced by the electron (in the direction of H) tries to align the nucleus along the axis of the field. The result of the two competing forces trying to align the nucleus along their respective axes is two-fold. The $2I + 1$ levels are affected in such a way that the normal, $\Delta M_I = 0$, hyperfine lines are not equally spaced and not of equal intensity. The maximum separation is either at the ends or in the middle of the spectrum rather than a progressive change with H.

(v) Nuclear Zeeman Interaction

The nuclear magnetic moment generated by the nuclear spin may be orientated in $2I+1$ ways in an external magnetic field.

It is ignored for experiments at X-band frequencies.

1.3 ESR PARAMETERS

(i) g-values

Generally the g-tensor is not isotropic and there is a shift of the resonance from the free-spin g-value. The deviation is due to a spin/orbital coupling giving the unpaired electron a small amount of orbital angular momentum. This alters its effective magnetic moment.

In terms of M.O. theory this orbital momentum may be visualized as the mixing of excited state configurations with the ground state of the radical. Application of an external field (H) can induce, in the unpaired electron, orbital angular momentum that tends to 'drive' it around a plane perpendicular to H.

If the induced excitation is that of an unpaired electron from a half-filled level into a higher empty orbital, then the orbital momentum produces a magnetic field that is opposed to the external field and the resultant field at the unpaired electron is smaller than the external field. Hence resonance occurs at a larger value of the external field than that required when there is no orbital angular momentum, i.e. a 'negative g-shift', $g < 2.0023$ (Figure 3).

'Positive g-shifts' are observed when the induced excitation is that of an electron from a filled level into a half-filled level. In this situation the orbital motion produces a local field that supplements the external field (Figure 3).

Simply, the size of the g-shift is proportional to the spin orbit coupling constant and inversely proportional to the difference in energy

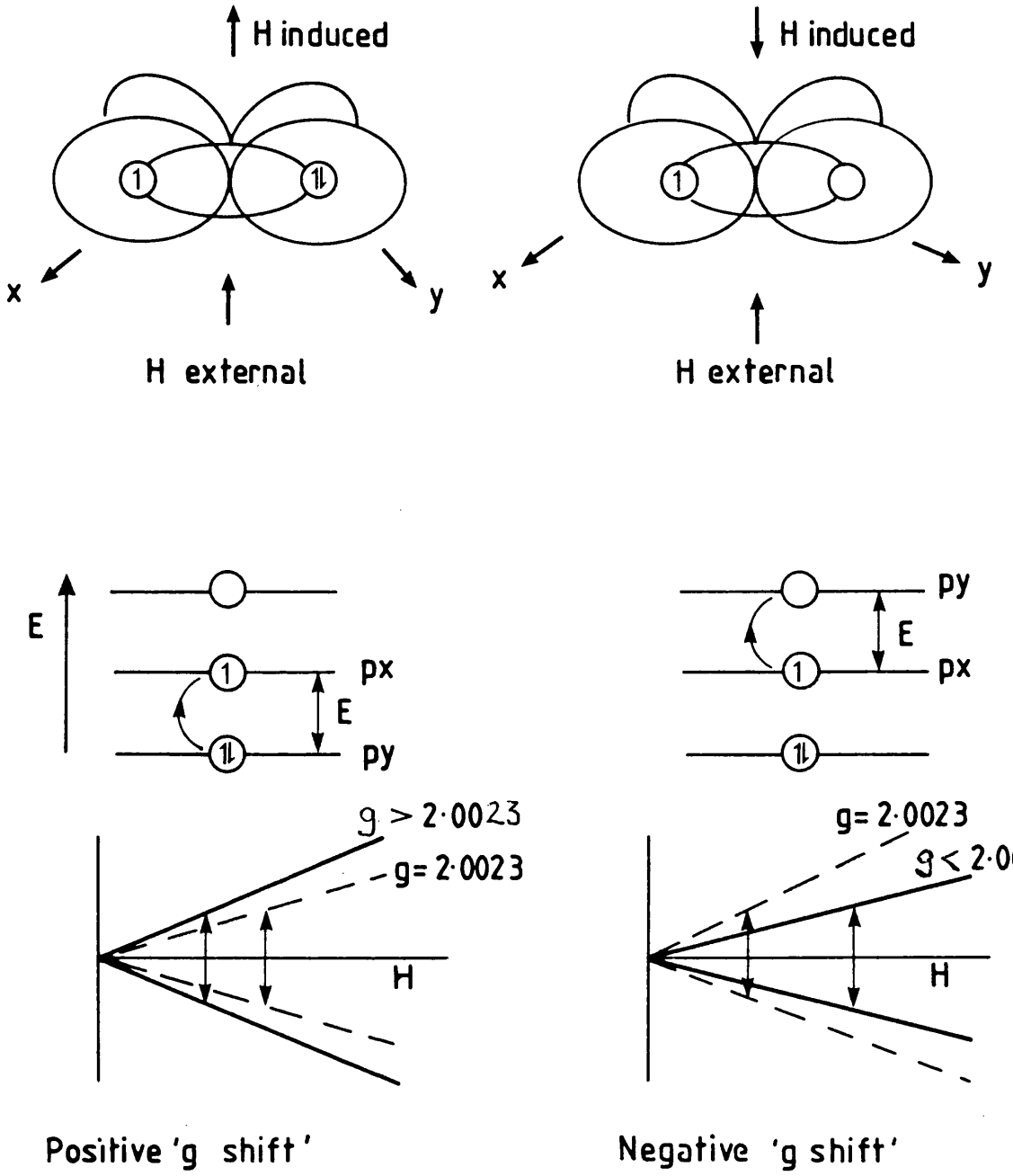

FIGURE 3

Positive and Negative 'g-shifts'.

between the orbitals involved.

$$g = 2.0023 + \sum \frac{\alpha\lambda}{\Delta}$$

α - extent of delocalisation of the unpaired electron in the orbital with which mixing is induced and is a function of the configuration and symmetry of the system

λ - the spin orbit coupling constant

Δ - the difference in energy between the orbital involved.

The spin orbit coupling constant is a measure of the effectiveness of the interaction between the orbital motion and the electron spin. Its magnitude is a function of atomic number and the number of electrons in the valence shell, hence the g-shift for most organic radicals is small.

(ii) Hyperfine Coupling Constants

The experimentally determined A-tensor may be either isotropic or anisotropic depending on the symmetry of the distribution of the unpaired electron about the magnetic nucleus, i.e.

$$\begin{vmatrix} A_{xx} & & \\ & A_{yy} & \\ & & A_{zz} \end{vmatrix} = \begin{vmatrix} A_{iso} & & \\ & A_{iso} & \\ & & A_{iso} \end{vmatrix} + \begin{vmatrix} B_{xx} & & \\ & B_{yy} & \\ & & B_{zz} \end{vmatrix}$$

The first term on the right-hand side represents the isotropic part and the second term the anisotropic part.

(a) Isotropic Hyperfine Coupling

Isotropic hyperfine coupling between the unpaired electron and the magnetic nucleus arises as a result of the Fermi-contact interaction,

$$W_{iso} = -\frac{8\pi}{3} \left|\psi(0)\right|^2 \mu_e \mu_N$$

μ_e electron dipole
μ_N nuclear dipole

where $|\psi(0)|^2$ is the squared amplitude of the electronic wave-function at the nucleus. Only s-electrons have a finite value for $|\psi(0)|^2$ since

s, p, d and f orbitals have nodes at the nucleus. Other mechanisms produce a finite spin-density at the nucleus and isotropic coupling can arise from three main sources:

(i) s-orbital spin density.

(ii) Configurational interaction between the ground state with no s-orbital contribution and an excited state configuration built from s-orbitals.

(iii) Spin-polarisation. Isotropic coupling occurs in isolated paramagnetic atoms where the unpaired electron exists in a p- or d- orbital due to polarisation of the core s-electrons.

The polarisation mechanism is explained by dividing paramagnetic radicals into two classes, i.e. π or σ radicals. In σ-radicals, the electron is in an orbital built from atomic s-orbitals and there is a direct contribution to the isotropic coupling from the Fermi contact interaction. In π-radicals the isotropic coupling is due to spin-polarisation of valence electrons involved in σ-bonding. In planar conjugated systems, the proton hyperfine splittings are proportional to the unpaired π-electron density on the carbon adjacent to the proton,

$$a_i = Q \rho_i$$

a_i - the α-hydrogen isotropic coupling constant
ρ_i - the unpaired spin-density in the carbon $2p_z$-orbital
Q - proportionality constant.

Spin-density is a function of many electrons,

$$\rho_i = P_i(\alpha) - P_i(\beta)$$

where ρ_i is the spin-density in the region i of the molecule and $P_i(\alpha)$ and $P_i(\beta)$ are the total probability densities of electrons with α and β spins respectively, in the region i.

1.4 ANISOTROPIC HYPERFINE INTERACTION

Anisotropic hyperfine interaction comes from the dipolar coupling between the unpaired electron in a p- or d- orbital with the magnetic nucleus associated with it. For a p-orbital the interaction is given by

$$2B = \frac{4}{5} g \beta g_n \beta_n \langle r^{-3} \rangle$$

where 2B is the maximum dipolar coupling, and $\langle r^{-3} \rangle$ is the average value of r^{-3}, r being the distance between the unpaired electron and the nucleus. The interaction magnitude is a function of the relative orientation of the line joining the two dipoles and the external field. It is tensor defined and traceless to a first approximation.

1.5 SPIN DENSITIES AND BOND ANGLES

Experimentally determined hyperfine coupling constants indicate the s- and p- character of the unpaired electron. The signs of the experimental values are often difficult to establish. Isotropic coupling arising from unpaired spin directly on an s-orbital is positive. Polarisation of core s-electrons isotropic coupling can be either positive or negative. When bonding electrons are polarized, a negative coupling is produced. If the isotropic coupling cannot be measured directly, all possible combinations of sign for the principal values have to be tried so that the algebraic average should give the 'expected' isotropic hyperfine coupling constant. This can be approximated by comparison with iso-electronic species. Experimentally determined isotropic coupling constant (A_{iso}) and anisotropic coupling constant (2B) can be compared with corresponding values calculated for a hypothetical atom with unit occupancy of the unpaired electron in an s- or p- orbital. These values are referred to as A° and $2B^\circ$. Hence the ratios A_{iso}/A°

and $2B/2B^{\circ}$ will give the s- and p- character of the unpaired electron. The degree of hybridisation may also be determined.

1.6 RELAXATION

Two processes are involved in the restoration of thermal equilibrium, spin-lattice and spin-spin relaxations.[3]

Spin-lattice relaxation is caused by the interaction between the excited electronic state and the lattice via spin-orbit coupling. This causes fluctuations in the energy levels of the excited states and hence a broadening of the e.s.r. lines due to the uncertainty principle. This is called the T_1 process and is temperature dependent. Lower temperatures reduce the effect. Power saturation, excessive microwave power, causes line broadening because thermal equilibrium cannot be restored. The relaxation time T_1 can be determined by a study of e.s.r. linewidths with respect to microwave power.

Spin-spin relaxation is due to fluctuations in local magnetic fields at the unpaired electron due to the close proximity of unpaired spins. This is called the T_2 process and is considered temperature independent. Dilute solutions of the radical precursors ensure large separations to prevent this type of broadening.

1.7 RADIATION DAMAGE

All the systems reported here involve γ-radiation damage in the solid state and, in a few cases, u.v. rays are used for subsequent bleaching experiments. The source of radiation was a ^{60}Co source having a γ-ray spectrum spread between 10^5 and 10^7 eV.

The radiation incident on the samples is absorbed by both the solvent and the solute and almost entirely by interaction with the electrons of

the constituent molecules. The excited molecules produced undergo their own characteristic chemical change which not only involves the formation of excited species but also leads to subsequent ionisation with the production of secondary electrons and positive ions. Ejected electrons may themselves be sufficiently energetic to produce further ionisation and excitation.

Organic halides are characterised by their high electron affinities and are widely used as electron scavengers. An electron which is captured by an organic halide molecule will initiate one of several reactions (Figure 4). The main effect of radiation is to break the carbon-halogen bond to give alkyl radicals by dissociative electron attachment.[4]

FIGURE 4

SCHEMATIC REPRESENTATION OF RADIATION DAMAGE IN SOLIDS

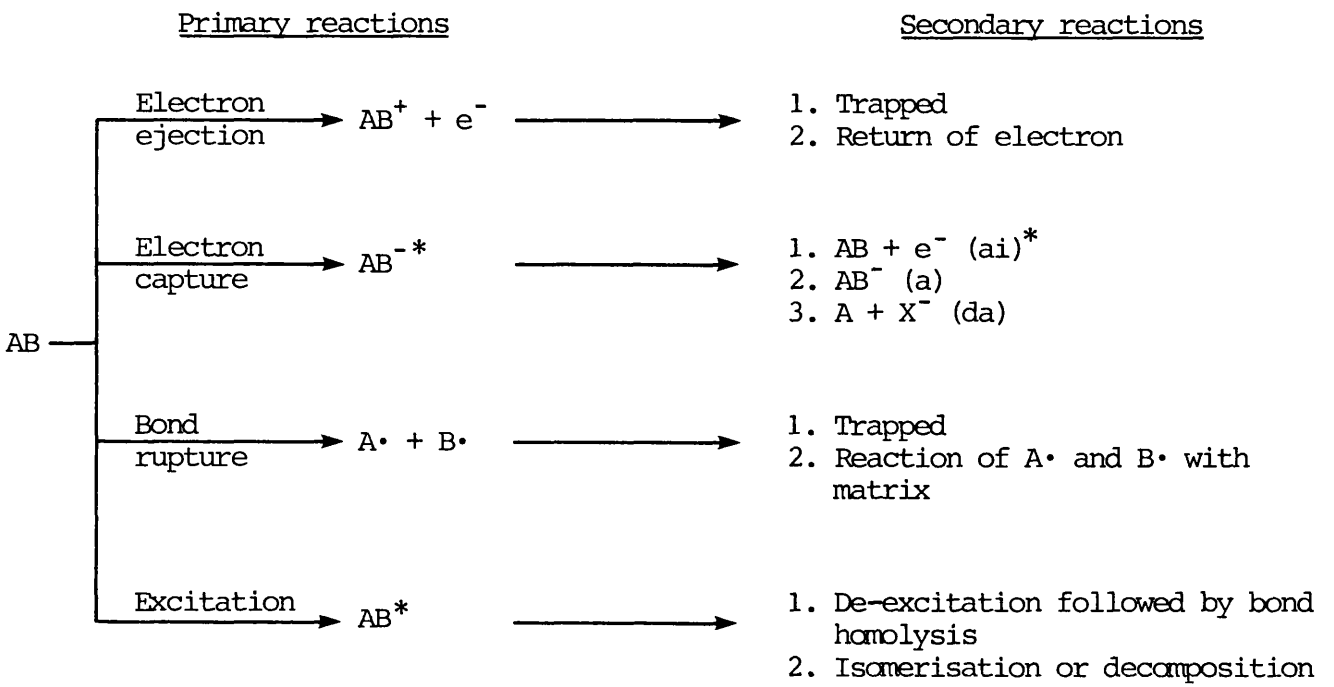

*ai - auto-ionisation
a - attachment
da - dissociative attachment

REFERENCES FOR CHAPTER 1

1. J. E. Wertz, J. R. Bolton, Electron Spin Resonance: Elementary Theory and Practical Applications, McGraw-Hill (1972).

2. D. J. Ingram, Biological and Biochemical Applications of Electron Spin Resonance, Adam Hilger (1969).

3. P. F. Knowles, D. Marsh, H. W. E. Rattle, Magnetic Resonance of Biomolecules, J. Wiley (1976).

4. S. P. Mishra, Electron Spin Resonance Studies of Irradiated Alkyl Halides, Ph.D. Thesis, Leicester University (1976).

CHAPTER 2

Instrumentation

2.1 INTRODUCTION

The resonance condition is $h\nu = g\beta H$ and the main wavelengths of operation are X-band ($\lambda \approx 3$ cm, $H \approx 3000$ gauss) and Q-band ($\lambda \approx 0.8$ cm, $H \approx 12000$ gauss) (Figure 1). All the basic principles of e.s.r. spectro-

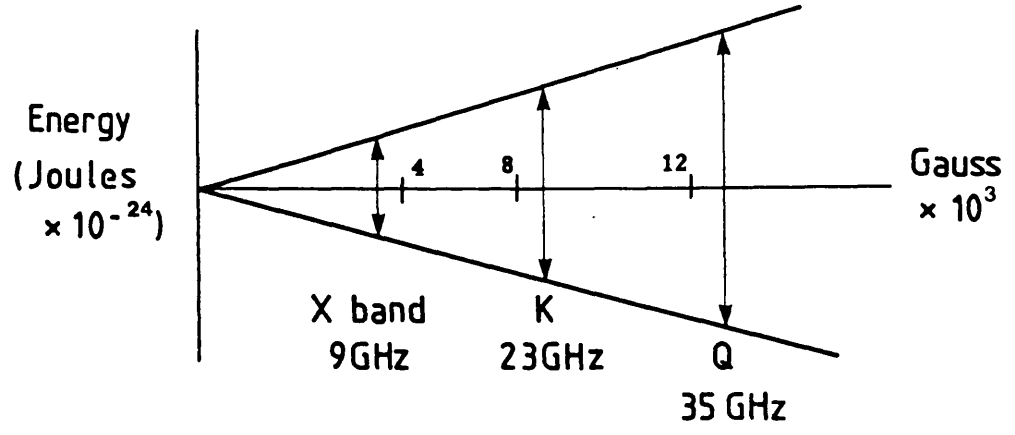

FIGURE 1
Energy levels as a function of magnetic field.

meters are fully described in other texts. All experiments were performed using either a Varian E109 or E3 with a TE_{102} rectangular cavity. The E109 was used in conjunction with the Varian E-900-3 EPR microprocessor based Data Acquisition System. The software package allowed a variety of data acquisition and data manipulation modes. In some experiments variable temperature measurements were made using a variable temperature accessary, and in other instances an Oxford Instruments liquid helium system was used.

Irradiation was carried out using a Vickrad ^{60}Co γ-ray source. The γ-irradiations at 77 K were performed by immersing the samples in a sealed tube in liquid nitrogen.

Photolysis with u.v. light was carried out with both medium and high pressure mercury lamps. Photographs were taken of the emission spectra

and then the relative intensities of the lines plotted by a micro-densitometer. Note the film has not been characterised for its response to intensity and wavelength (Spectra 1 and 2).

2.2 PROPORTIONAL TEMPERATURE CONTROLLER

The Varian low temperature equipment, though suitable for variable temperatures, could not maintain a specific temperature either accurately or for any period of time. To meet the necessary requirements the following equipment was designed and built.[1,2]

The basic principles of operation was as follows:-

(a) The liquid nitrogen was kept at a constant level.
(b) The temperature in the block was determined by the depth of immersion in the liquid nitrogen and the current in the cartridge heater.
(c) Samples were placed in the block and the temperature monitored by a thermocouple.
(d) Accurate temperature control was maintained by a zero voltage switching proportional controller.

No thermistors could be found to give a suitable response at 77 K. A thermocouple was used; the cold junction was immersed in the liquid nitrogen and the hot junction held next to a small heater. The e.m.f. generated was amplified by 60 dB and used to control a relay. The relay, in turn, caused liquid nitrogen to be decanted into the vessel. Different temperatures could be achieved by altering the depth of immersion of the block and the power applied to the cartridge heater. Accurate temperature control was achieved using a proportional temperature control circuit.[3] At the desired temperature just sufficient power was applied to the heater to make up the system losses (Figure 2).

The associated circuits are as shown (Figures 3 and 4).

SPECTRUM 1

Emission spectrum of High Pressure
Mercury Vapour Lamp.

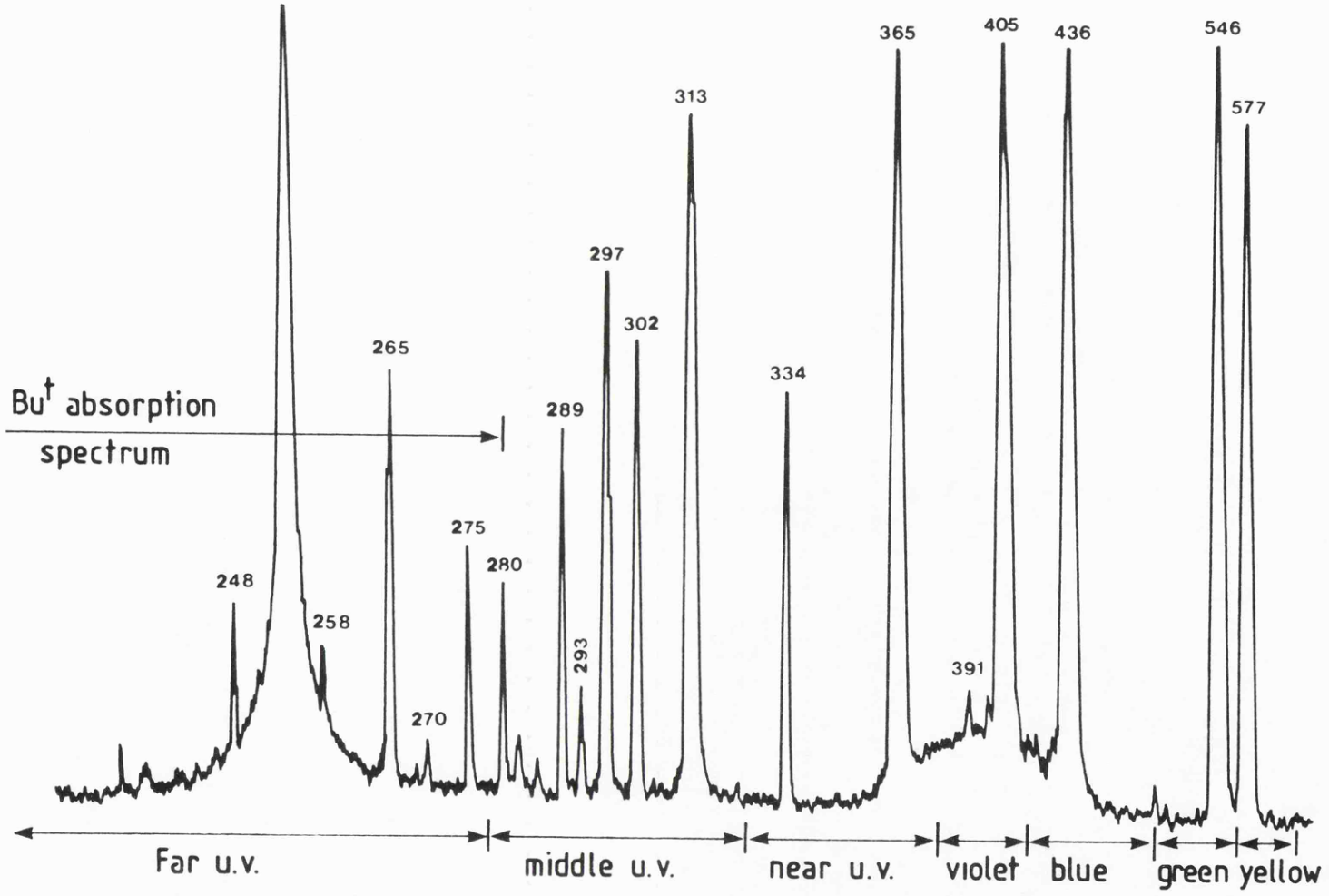

SPECTRUM 2

Emission spectrum of Low Pressure
Mercury Vapour Lamp.

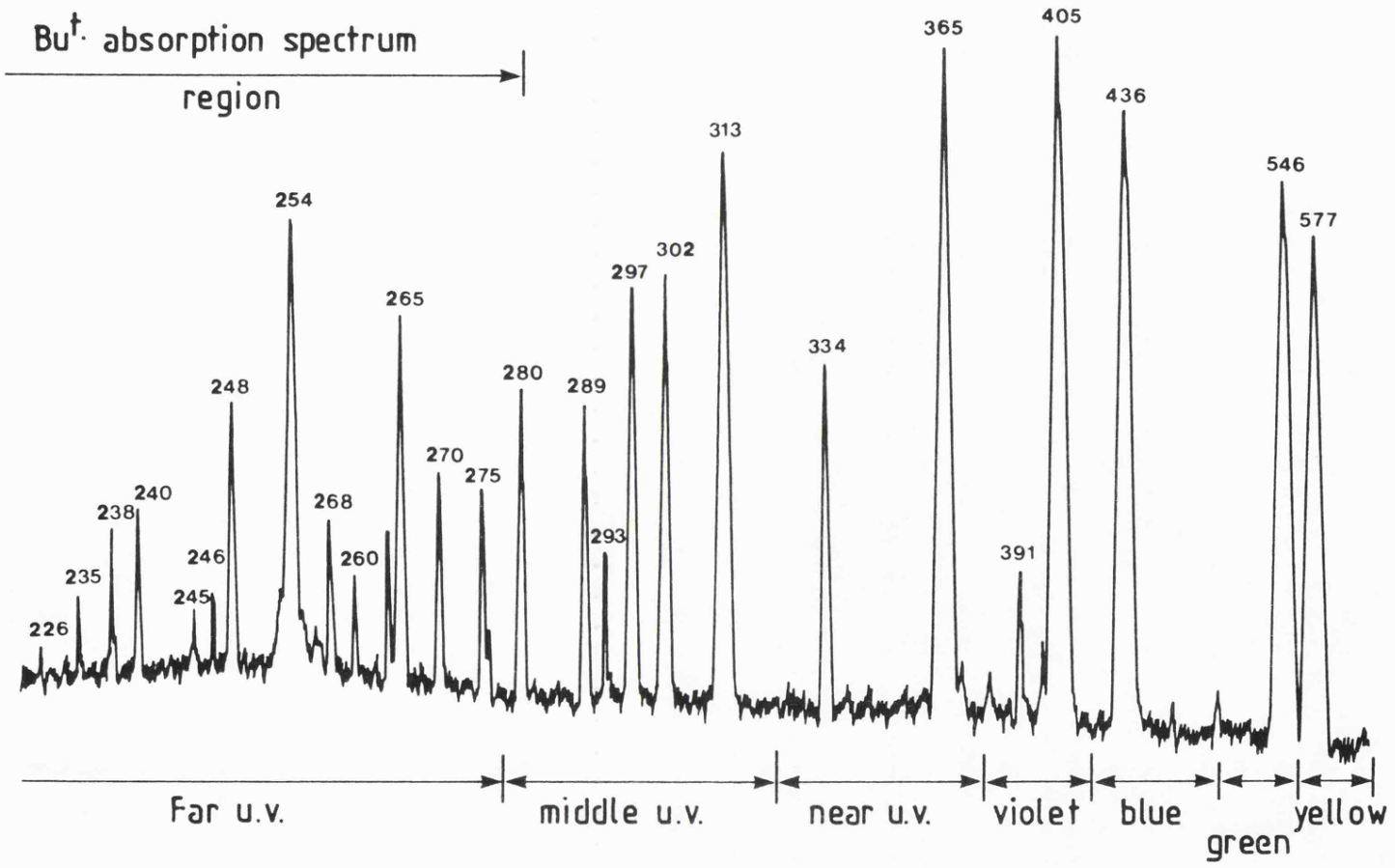

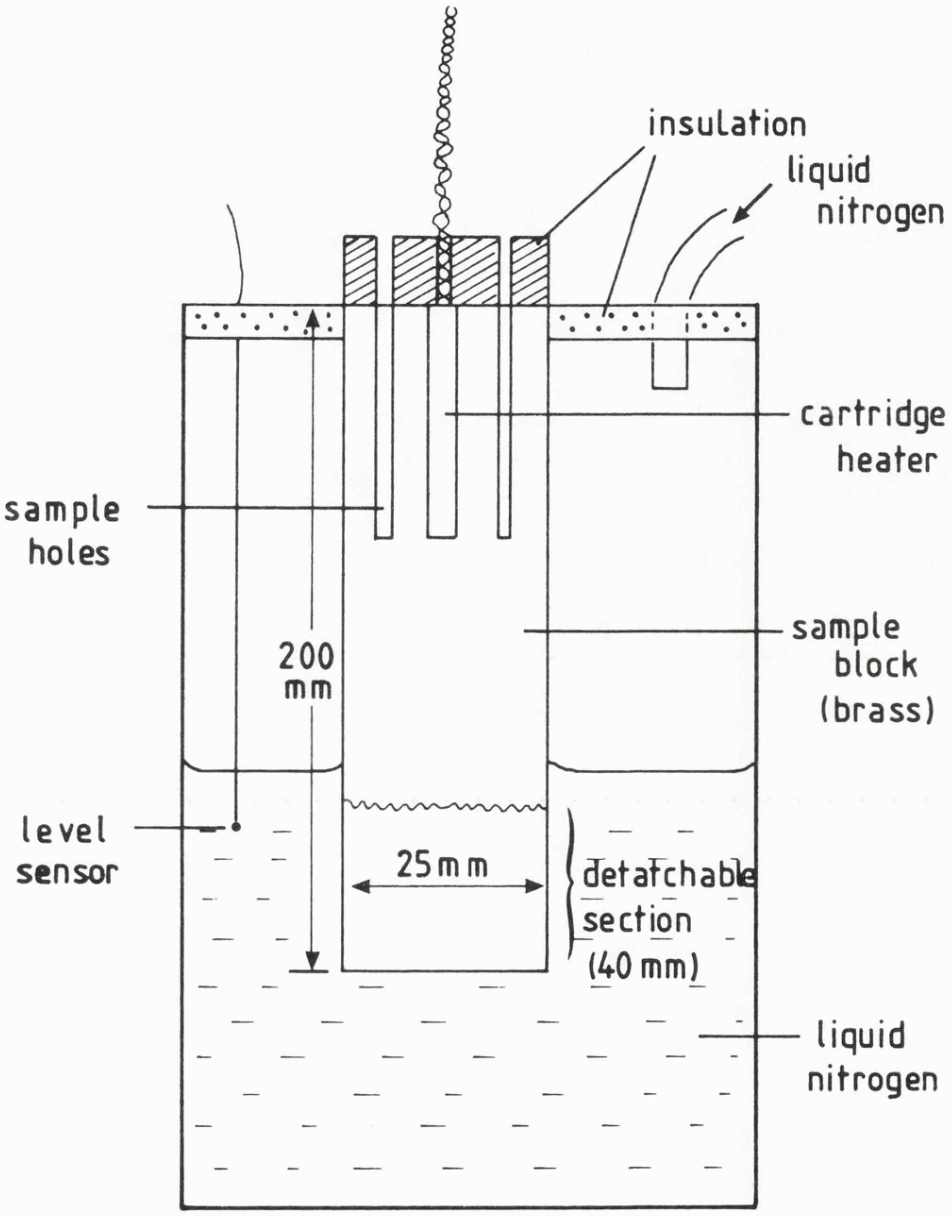

FIGURE 2

Proportional Temperature Block

FIGURE 3
Liquid Nitrogen level control circuit

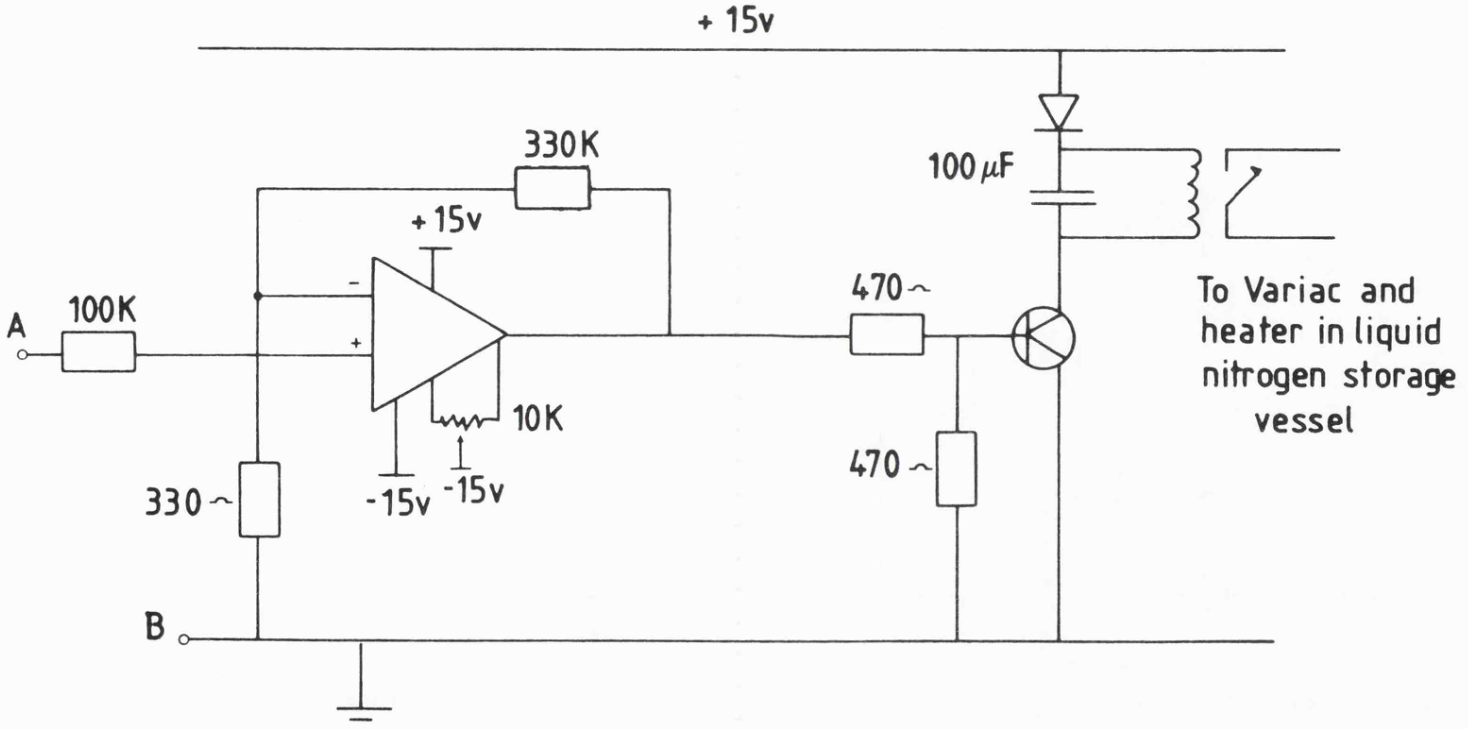

Transistor : NPN Si BFY 51
Amplifier : 741 op amp.

A : Copper connection } Thermocouple
B : Constantan "

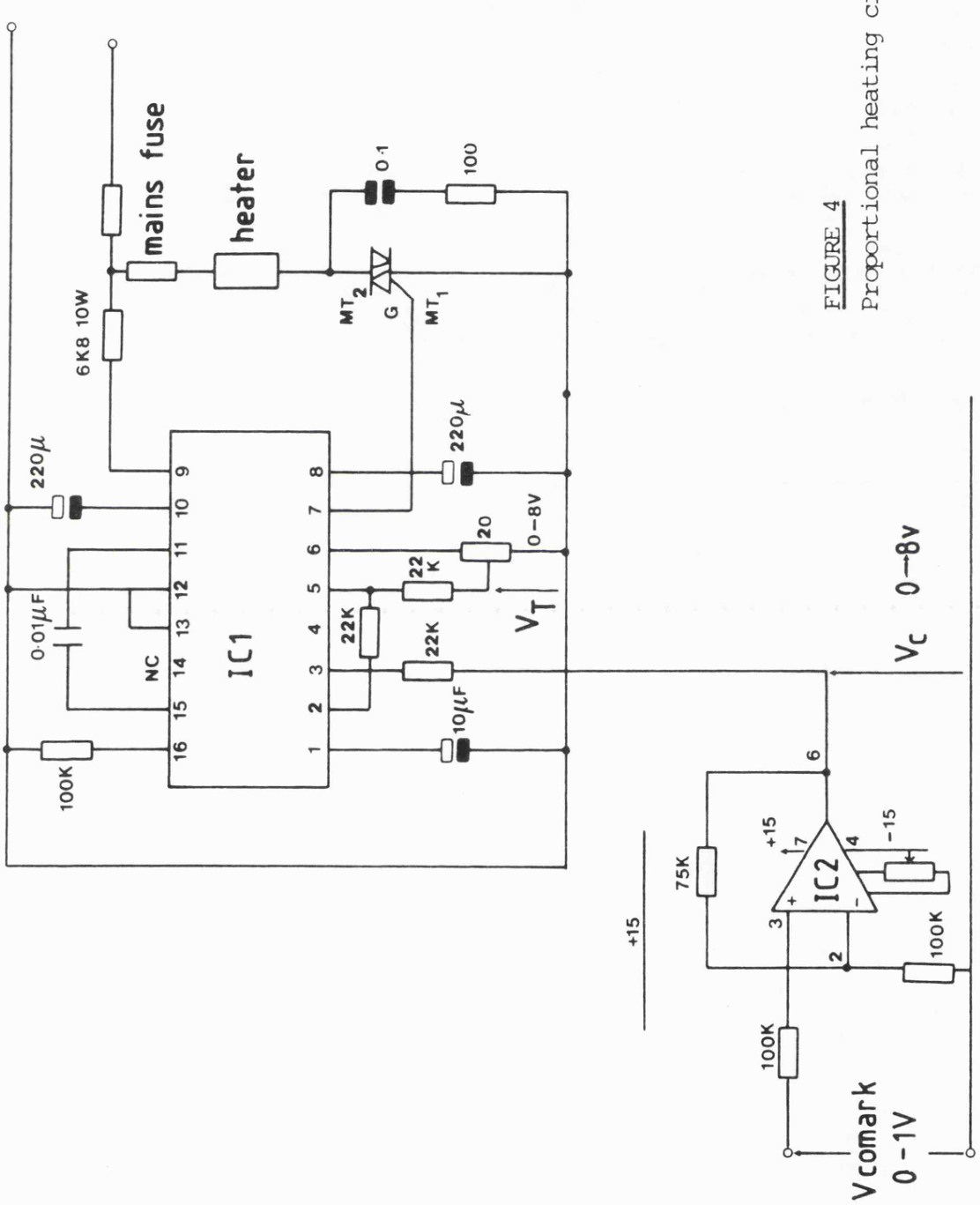

FIGURE 4

Proportional heating circuit

2.3 ENDOR

A technique employed was ENDOR (Electron Nuclear Double Resonance) in some attempts to resolve spectra.[4] This method uses high power microwave radiation to saturate the electron resonance transitions. Variables such as magnetic field and microwave frequency are kept constant and a nuclear resonance frequency is then applied. Signals are detected due to radio frequency induced NMR transitions in the ESR signal. The sensitivity of ESR is thus combined with the resolution of NMR. A principal application is to measure hyperfine splittings that are often not resolved by the ESR method.

Consider a radical ($S = \frac{1}{2}$) that interacts with a single proton ($I = \frac{1}{2}$). The energy levels would split as shown (Figure 5).

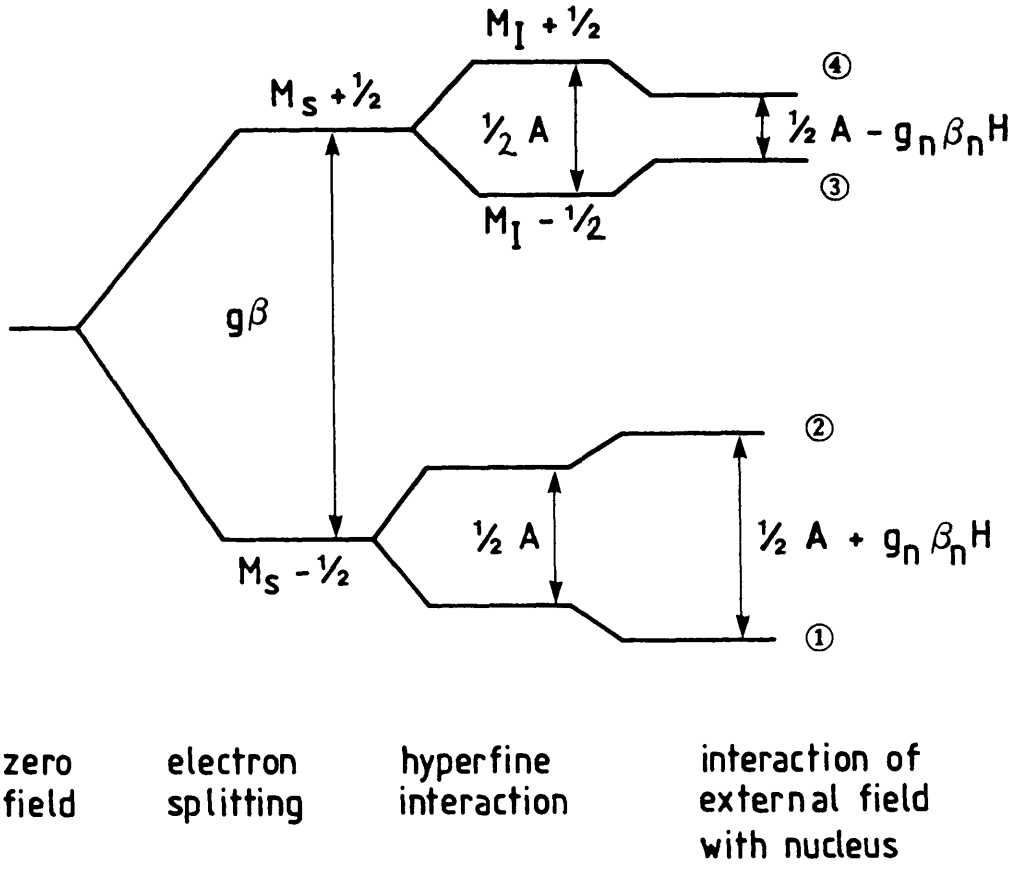

FIGURE 5

Energy level splitting of a radical ($S = \frac{1}{2}$) with a proton.

The largest splitting comes from the electron spin interaction with the magnetic field ($g\,\beta H$). Each level is then further split by the electron-nuclear hyperfine interaction ($\frac{1}{2} A$) and by the interaction between the nuclear spin with the magnetic field. This has the effect of decreasing the splitting of one level by $g_n\,\beta_n H$ and increasing the splitting of the lower level by the same amount.

The (2) to (3) ESR transitions are saturated by microwave frequency radiation, i.e. no further absorption is possible. A radio frequency sweep affects the nuclear transitions (3) to (4) which relieves the saturation in level (3) thus allowing further absorption of microwave power, i.e. an ESR signal. Higher radio frequencies allow the nuclear spin changes (1) and (2).

Level	Energy
1	$\frac{1}{2} g\,\beta H + \frac{1}{4} A - \frac{1}{2} g_N\,\beta_N H$
2	$\frac{1}{2} g\,\beta H - \frac{1}{4} A + \frac{1}{2} g_N\,\beta_N H$
3	$-\frac{1}{2} g\,\beta H + \frac{1}{4} A + \frac{1}{2} g_N\,\beta_N H$
4	$-\frac{1}{2} g\,\beta H - \frac{1}{4} A - \frac{1}{2} g_N\,\beta_N H$

Saturation is relieved when the condition

$$h\nu_{rf} = \tfrac{1}{2} A \pm g_N\,\beta_N H$$

is met. From these two values of rf resonance signals, the values of both A and g_N can be deduced. Of particular interest is that if the ENDOR technique is applied to a system with four equally coupled protons, only two ENDOR lines are obtained. Figure 6 illustrates how there will be only two ENDOR transitions at different frequencies. Differences between ENDOR and ESR become even more apparent as the number of protons increases and if the hyperfine couplings are not the same.

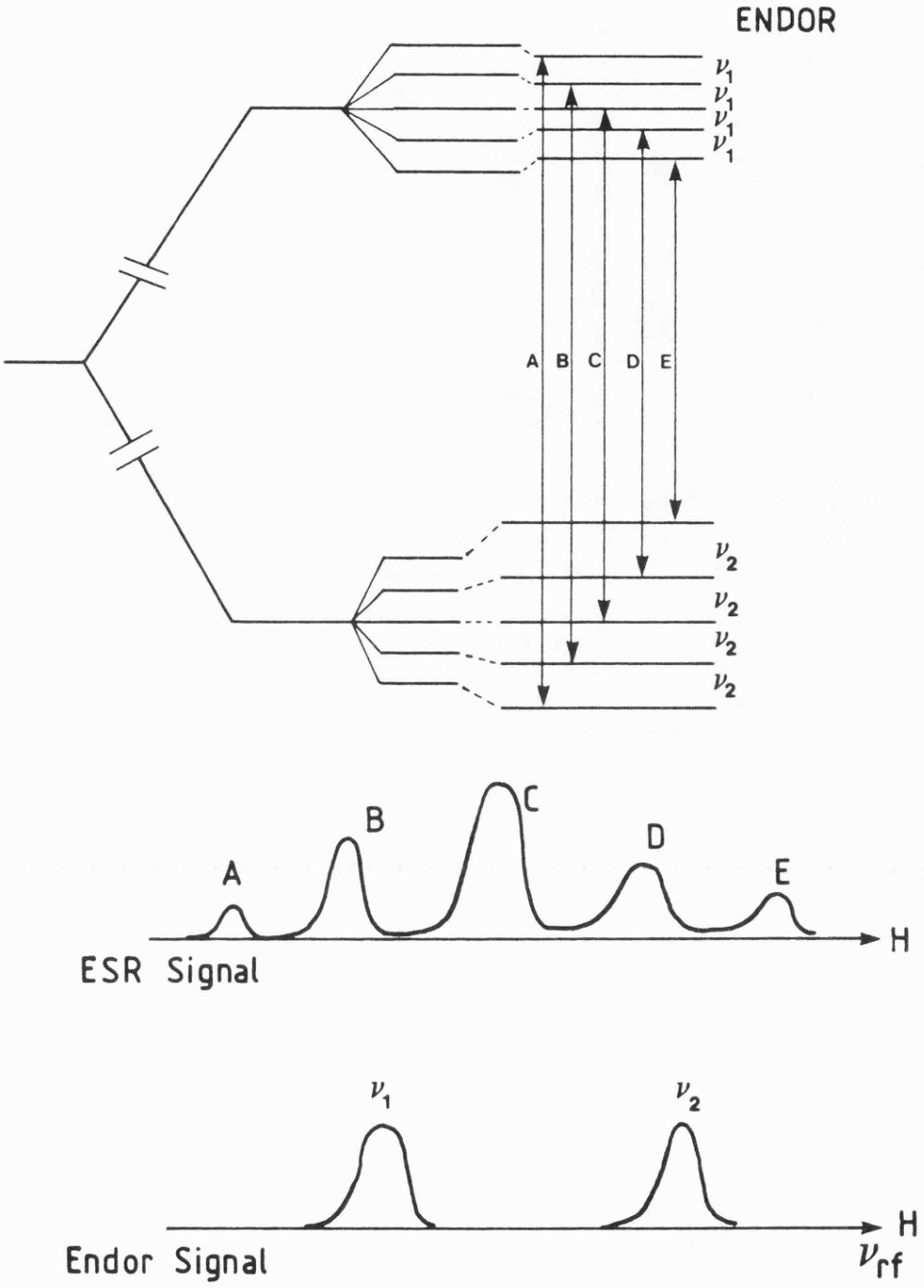

FIGURE 6

Energy level interactions with four equivalent protons.

REFERENCES FOR CHAPTER 2

1. R. F. Coughlin, F. F. Driscoll, Operational Amplifiers and Linear Integrated Circuits, Prentice-Hall (1977).

2. A. C. Rose-Innes, Low Temperature Laboratory Techniques, English Universities Press Ltd. (1973).

3. R. S. Data Sheet R/2129.
Zero Voltage Switch 305-800.

4. D. J. Ingram, Biological and Biochemical Applications of Electron Spin Resonance, A. Hilger Ltd. (1969).

CHAPTER 3

The Bromobenzene Cation

3.1 INTRODUCTION

Powder ESR spectra characteristic of carbon centred α-halo radicals (Cl, Br or I) have been obtained in solid-state radiolysis.[1-3]

The quadrupole moments of the halogen nuclei are relatively large and there are strong asymmetric electric fields at these nuclei. A quadrupole moment will orient in a linear field gradient, just as a dipole orients in a linear field, hence the quadrupolar nuclei will be influenced by the direction in which the molecule containing them is orientated. The effect of this force on the nucleus is to link its motion with molecular motions and hence to provide a spin-lattice relaxation mechanism. This leads to broad nuclear resonances.

These electric fields exert an aligning force on quadrupolar nuclei that may oppose the magnetic aligning forces, hence spectra significantly different than expected.

Considering the following radical (I).

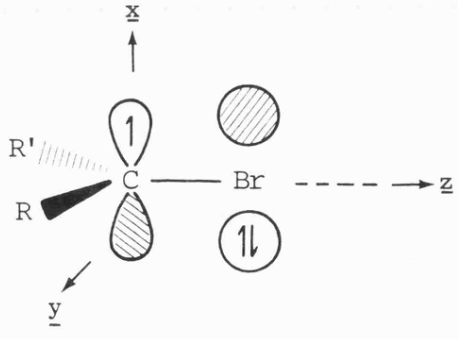

For the fields along x and z, the quadrupole effect for large hyperfine energies (ca. 110 G for the x axis) is to move the spectrum disproportionately such that the hyperfine splitting, A_x, is given approximately by the distance between the two strongest low field lines ($M_I = +3/2$, $M_I = +1/2$) or the two high field lines ($M_I = -1/2$, $M_I = -3/2$). However, when the hyperfine energy is considerably less than the effective quadrupole energy (ca. 35 G for ^{79}Br Ay) then the quadrupole moment

controls alignment and the spectrum comprises of a strong triplet, with weak outer features (Figures 1 and 2).

These spectra gave well-defined features for the maximum hyperfine interaction (xx), but the yy and zz features have to be established by single crystal studies. Hüttermann and co-workers have established these parameters together with accurate g-values and quadrupole coupling tensors.[4-6]

Powder spectra can be used as 'finger-prints' in irradiation studies allowing calculation of the approximate spin densities on the halogen.[7-9]

The absence of any resolution between the ^{81}Br and ^{79}Br features in the $\pm^3/_2$ components is unusual, but has been observed previously for α-bromo radicals and interpreted in terms of differing quadrupole shifts for the two isotopes.

3.2 MOLECULAR ORBITAL ENERGY CALCULATIONS

In halogenobenzene there is overlap of p_π orbitals on adjacent atoms. This overlap allows electrons in these orbitals to be delocalized over the molecular skeleton. Hence the energy states of these electrons may be described in terms of molecular orbitals generated from linear combinations of atomic p-orbitals.

The Hückel molecular orbital approach (HMO) allows the calculation of orbital energies and the unpaired-electron distributions in π-electron systems.

In the molecule the 2s, $2p_x$ and $2p_y$ orbitals of carbon atoms hybridize to form three equivalent (sp^2) σ-bonds at an angle of 120° to each other.

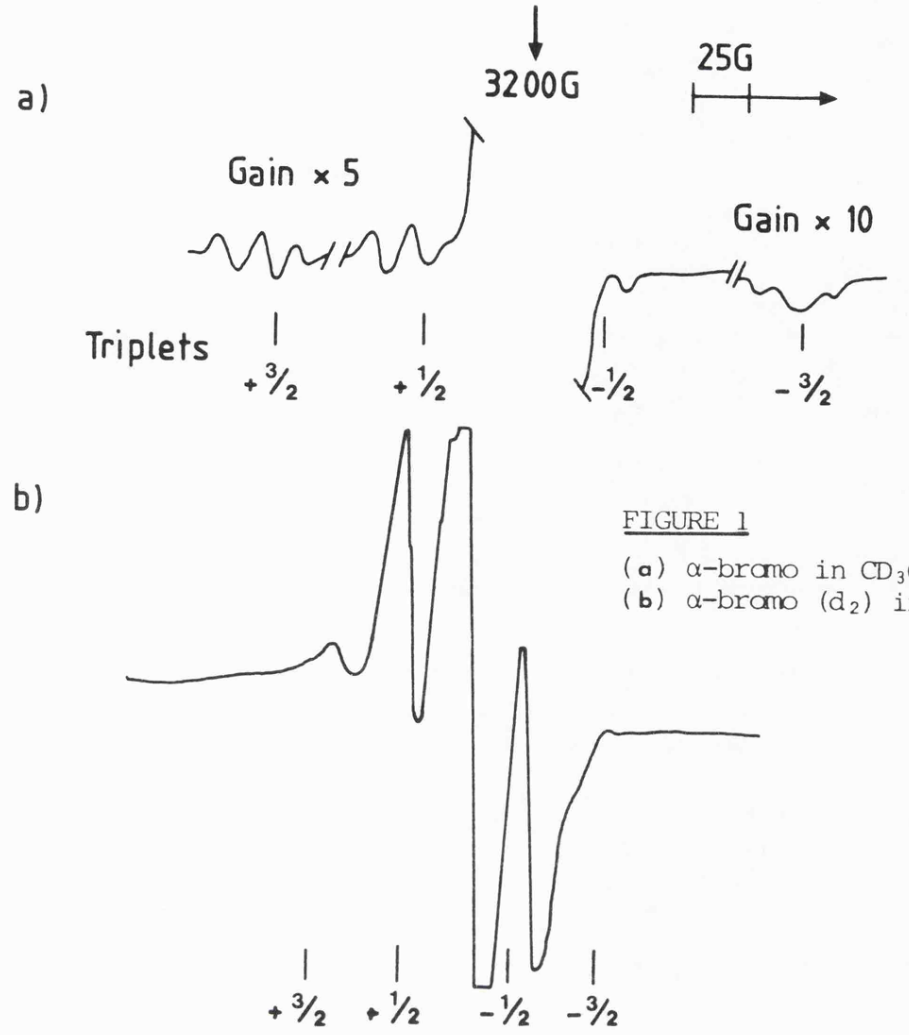

FIGURE 1

(a) α-bromo in CD_3OD $H_2\dot{C}Br$
(b) α-bromo (d_2) in CD_3OD $D_2\dot{C}Br$.

FIGURE 2

X-band powder spectrum for

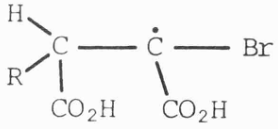

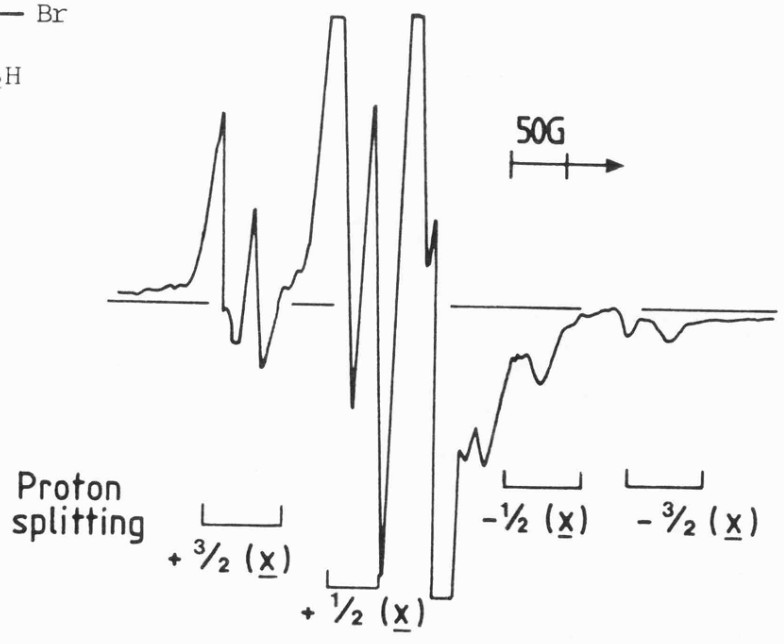

The $2p_z$ orbital is perpendicular to the plane of the other three. The $2p_z$ orbitals on adjacent atoms overlap allowing delocalization of π-electrons over the whole molecule. It is assumed the π-electrons can be treated independently.

Given a molecular framework of n atoms, the molecular orbital wave function, ψ_i, can be defined as a linear combination of atomic $2p_z$ orbitals.

$$\psi_i = C_{i1}\,\phi_1 + C_{i2}\,\phi_2 + \text{-------} C_{ij}\,\phi_j + \text{-------} C_{in}\,\phi_n$$

$$\text{i.e.} \qquad \psi_i = \sum_{j=1}^{n} C_{ij}\,\phi_j$$

The energy W_i corresponding to this wave function is:

$$W_i = \frac{\int_\tau \psi_i^*\, \hat{H}\, \psi_i \, d\tau}{\int_\tau \psi_i^*\, \psi_i \, d\tau}$$

The Hamiltonian operator $\hat{H}$ applies to the interaction of a single π-electron with the potential field due to nuclei and σ-electrons.

The approximate wave function is found using the variational principal, i.e. the best wave function is that for which the values of C_1, C_2, etc. are such that $\partial W/\partial C_1$, etc. are equal to zero.

The following simplifications are made:

$$H_{11} = \int_\tau \phi_1\, \hat{H}\, \phi_1 \, d\tau \qquad S_{11} = \int_\tau \phi_1^2 \, d\tau$$

$$H_{22} = \int_\tau \phi_2\, \hat{H}\, \phi_2 \, d\tau \qquad S_{22} = \int_\tau \phi_2^2 \, d\tau$$

$$H_{33} = \int_\tau \phi_3\, \hat{H}\, \phi_3 \, d\tau \qquad S_{33} = \int_\tau \phi_3^2 \, d\tau$$

etc. etc.

$$H_{12} = \int_\tau \phi_1\, \hat{H}\, \phi_2 \, d\tau \qquad S_{12} = \int_\tau \phi_1\, \phi_2 \, d\tau$$

$$H_{21} = \int_\tau \phi_2\, \hat{H}\, \phi_1 \, d\tau \qquad \text{etc.}$$

where H_{11} is the coulomb integral and H_{12} is the resonance integral. A molecule of n atoms produces n simultaneous linear equations, hence an $n \times n$ secular determinant.

$$\begin{vmatrix} H_{11} - WS_{11} & H_{12} - WS_{12} & H_{in} - WS_{in} \\ H_{12} - WS_{12} & H_{22} - WS_{22} & " \quad " \\ H_{13} - WS_{13} & H_{32} - WS_{32} & " \quad " \\ " \quad " & " \quad " & \\ " \quad " & " \quad " & \\ H_{in} - WS_{in} & & H_{nn} - WS_{nn} \end{vmatrix} = 0$$

The following assumptions are made:-

(i) $S_{ii} = 1$, $S_{ij} = 0 \quad (i \neq j)$.

(ii) If the atoms are bonded

$H_{ij} (i \neq j) = \beta$, the resonance integral;

If atoms are not bonded

$H_{ij} = 0$.

(iii) $H_{ii} = \alpha$, the coulomb integral.

Solution of this determinant yields the orbital energies for the molecule. The coefficients for the wave functions are found by using the normalization condition:

$$\int_{\tau} \psi^2 \, d\tau = 1$$

$$\text{i.e.} \qquad = C_1^2 + C_2^2 + ... = 1$$

Solution of the equations leads to a series of molecular orbitals of increasing energy and increasing number of nodes.

Electron addition to halogeno-benzene can be into π^* or σ^* orbitals. The former give species with small halogen hyperfine coupling constants due to a node through the substituent. In the case of cations, the node avoids the halogen substituents as in (II). The halogen hyperfine coupling for such cations should be large, especially due to the positive charge effect, which should increase electron donation for the

halogen substituents relative to the neutral radicals (I).

3.3 EXPERIMENTAL

The aromatic derivatives were of the highest grades available; their purities were checked by n.m.r. spectroscopy prior to use. Freon ($CFCl_3$) was purified on an activated alumina column and dried over molecular sieves.[10-13] Freon used as received was found to contain too many impurities to be of use. A variety of different concentration solutions were tried. The 0.01 mole-fraction range was used except when dimer cations were required.

All solutions were irradiated at 77 K in a Vickrad ^{60}Co source with doses of ca. 1 Mrad. Radiation doses of less than this produced spectra with poor signal-to-noise ratios. E.s.r. spectra were measured at 77 K with a Varian E109 spectrometer, as previously discussed.

Samples were annealed by decanting the liquid nitrogen and continuously monitoring the e.s.r. spectrum. They were recooled to 77 K whenever significant changes occurred. Specific temperature spectra were obtained using the variable temperature accessory.

The solutions were prepared using micro-litre pipettes and then degassed on a vacuum line using the freeze-thaw method. Degassing was continued until no gas bubbles were evolved. The vacuum was of the order of 0.01 Torr.

3.4 RESULTS AND DISCUSSION

Results for dilute solutions ($\approx$1:1000) are given in Table 1 and typical spectra are shown in Figures 3 and 4. When more concentrated solutions of bromobenzene were used, 7-line spectra indicating hyperfine coupling to two bromine nuclei were detected.

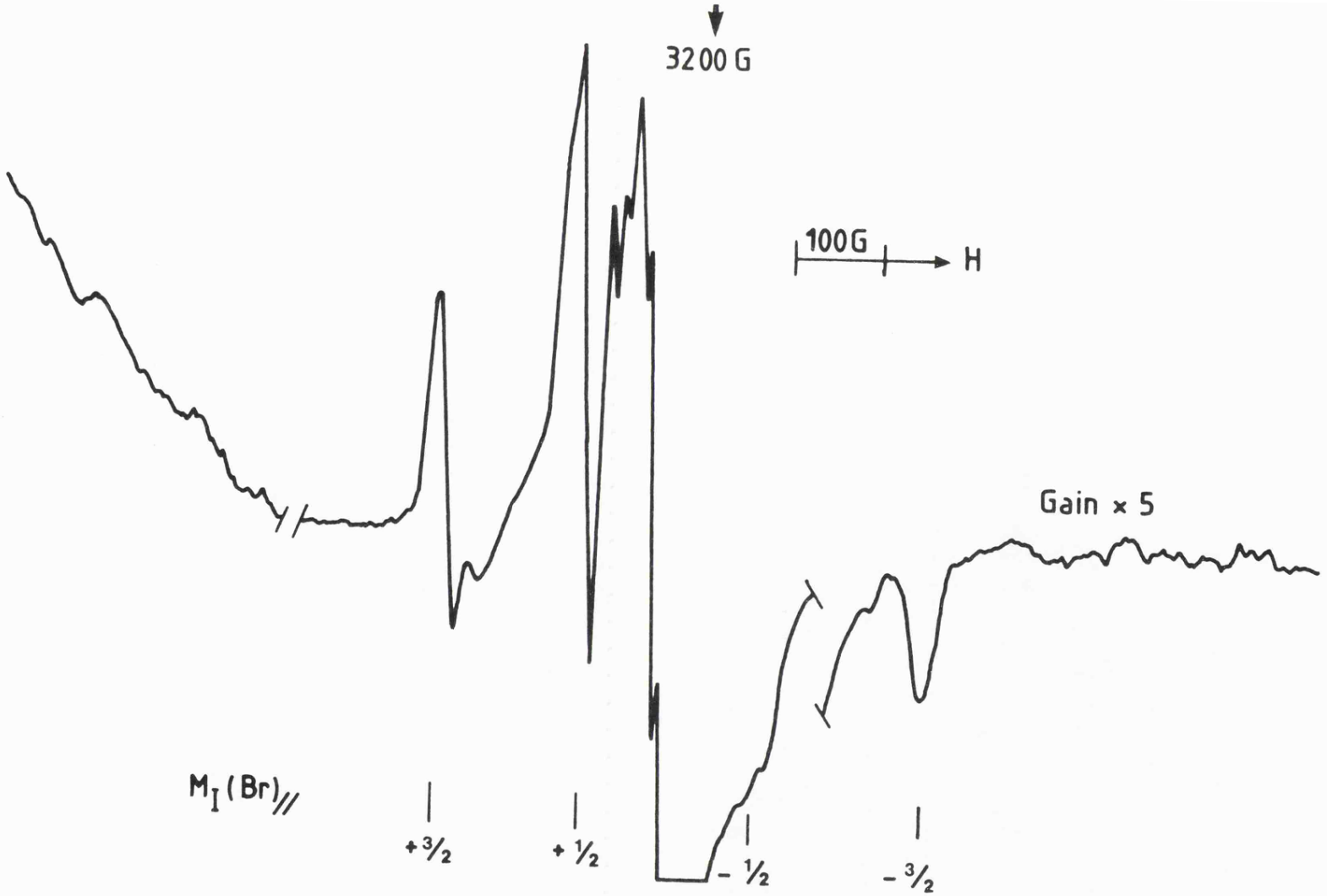

FIGURE 3

First derivative X-band ESR spectrum for C_6H_5Br in freon (1:1000) after exposure to ^{60}Co γ-rays at 77 K, showing features assigned to $(C_6H_5Br)^+$ cations.

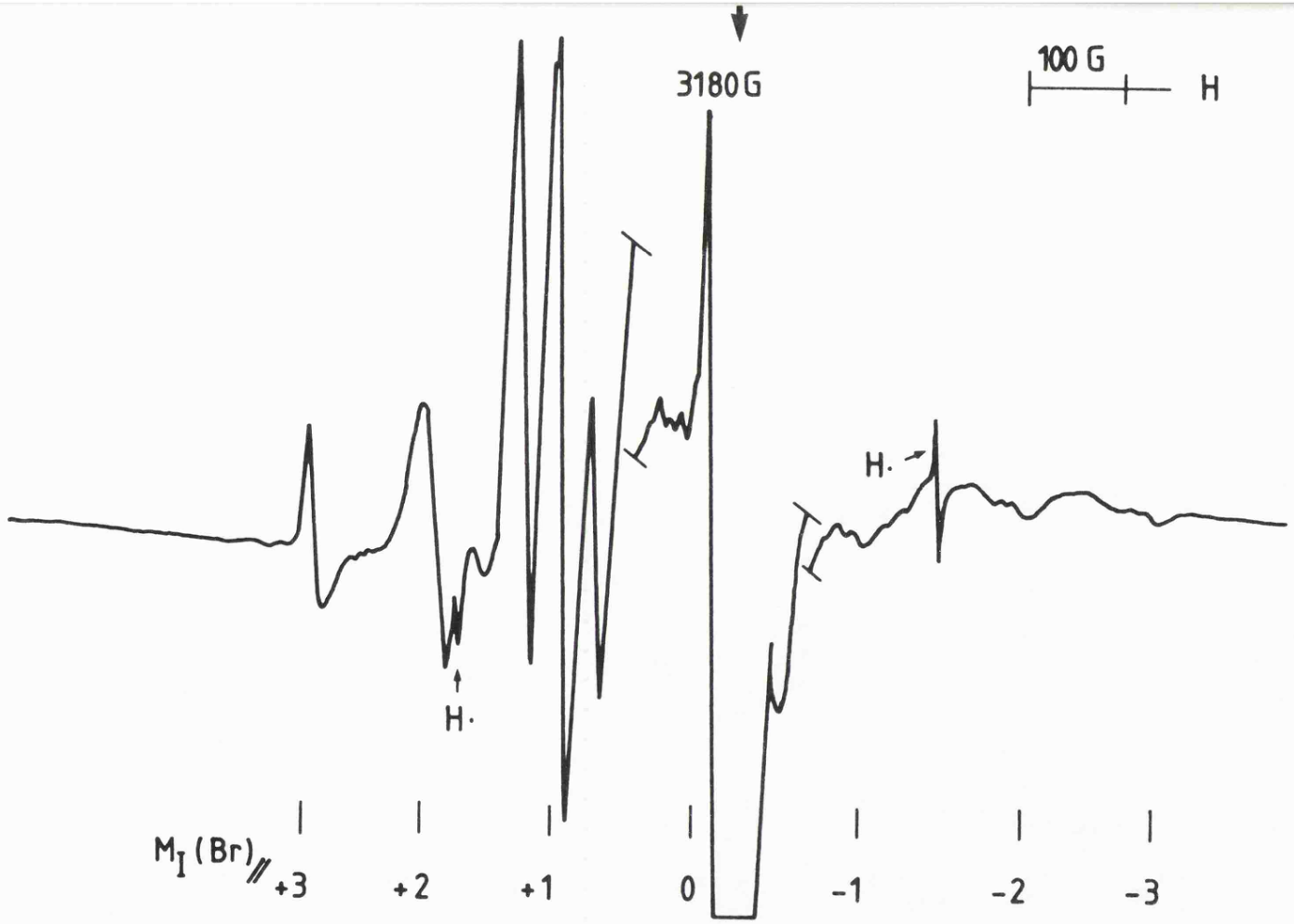

FIGURE 4

First derivative X-band ESR spectrum for p-$C_6H_4Br_2$ in freon (1:1000) after exposure to ^{60}Co γ-rays at 77 K, showing features assigned to $(C_6H_4Br_2)^+$ cations.

TABLE 1

ESR Data and Estimated Spin-Densities on Bromine for a range of α-bromo radicals

Radical	Medium	$A_{//}(^{81}Br)/G$[a]	$g_{//}$	Spin-Density[b]
$C_6H_5Br^+$	$CFCl_3$	185	1.993	0.30
	CCl_4	215	1.992	0.35
$(C_6H_5Br)_2^+$	$CFCl_3$	143	1.992	0.23
$C_6H_4Br_2^+$	$CFCl_3$	141	1.993	0.23
$Br\dot{C}HCO_2H$[c]	CD_3OD	107	2.002	0.17

[a] $G = 10^{-4}$ T;

[b] The magnitudes of spin-density were obtained by use of the atomic hyperfine coupling constants listed in Ref. 14;

[c] Ref. 2.

If simple theory were applicable, there should be a spin-density of $\frac{1}{3}$ on the carbon α to halogen (C_1 in Insert II). Unpaired electron distribution can be determined by HMO theory though, in some cases, its predictions are not fully validated. Consider the expression for the molecular orbital ψ_K occupied by the unpaired electron;

$$\psi_K = C_{K1}\,\phi_1 + C_{K2}\,\phi_2 + \text{------} + C_{Kn}\,\phi_n$$

Normalizing ψ_K gives

$$C_{K_1}^2 + C_{K_2}^2 + \text{----} C_{Kn}^2 = 1.$$

The square of the coefficient of the atomic orbital ϕ_j is the probability that the electron in the molecular orbital ψ_K is an atom j, i.e. C_{Kj}^2 is a measure of the unpaired -π- electron density ρ_j on the atom j,

$$\rho_j = C_{Kj}^2$$

As previously discussed, the halogenobenzene cation has a single node that avoids the halogen substituents. First approximation coefficients are:-

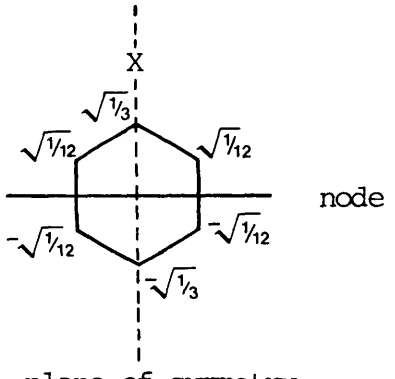

For radicals of class I (Insert I) having formal spin-density on carbon, the A_{xx} values are ≈110 G for bromo substituents. Values of ca. 37 G could be predicted for $(PhBr)^+$. The observed value of ≈185 G is very large compared to this, showing that there is far greater delocalization onto bromine than this theory predicts. The maximum coupling constants are actually greater than those for radicals of structure I, despite the fact that the unpaired electron is delocalized in the benzene ring.

Although the spectra are completely diagnostic of α-bromo radicals of this type, no attempt has been made to derive other hyperfine and g-tensor components from the spectra. Use is made of the equation of Oloff and Hüttermann[7] to deduce approximate values for the spin densities on the halogen;

$$\rho\pi\,(\text{hal}) = (f/2B^\circ)\,A_{xx}\,(\text{hal}), \qquad \ldots\ [1]$$

where $\rho\pi$(hal) is the spin-density on halogen, $f_{Cl} = f_{Br} = 0.81$ and $2B^\circ$ is the major anisotropic hyperfine coupling. The results, given in Table 1, show that there is ≈30% spin-density on halogen.[14]

An interesting feature of the spectra is the absence of the expected

splittings in the $M_I = \pm 3/2$ features due to the difference in magnetic moments for ^{81}Br and ^{79}Br. These have approximately 50% abundance each and the predicted doublet splitting is ca. 18 G for the $M_I = \pm 3/2$ features. However, in the α-bromo radicals, $R_2\dot{C}$-Br, this splitting is fortuitously reduced to zero due to differing quadrupole shifts for the two isotopes. This absence of splitting supports the identification.

Simple theory, as applied to alkyl benzenes,[15] may be unsuitable for halobenzenes because of the non-bonding p-orbital of halogen is expected to participate directly in the π conjugation with the p_π orbitals on the benzene ring. Thus HMO calculations for a Ph-$\ddot{B}r$ molecule were performed, introducing the constants S_x and S_c' into the Coulomb integrals of the halogen and the carbon bonded to the halogen respectively, the purpose of which is to allow for the different electronegativities of the different atoms. $S_x = 1.53$ and $S_c' = 0.19$ were obtained as a result of adjusting the energy of the highest occupied MO, $-\varepsilon_4$, to the average value of the ionization potential[16] (9.30 eV), using the relation of $S_c'/S_x = 1/8$[17] and the values of the Coulomb ($\alpha = -7.2$ eV) and resonance ($\beta = -3.0$ eV) integrals for benzene. The semi-occupied MO of bromobenzene radical cation corresponds to the HOMO of the parent molecule and has, therefore, the energy and coefficients shown in Table 2. The calculated spin-density on bromine is 0.263 (Insert III), which is in good agreement with the estimated experimental value of 0.30.

The spin-density on each of the bromine substituents in p-dibromobenzene is ≈23%. This is close to expectation if the following simple-proportional argument is used. Assuming that the spin distribution within the benzene ring remains that predicted by the Hückel theory, then we get $x + y = 1/3$ and $x/y = 0.3/(0.7/3)$ using the values given in II and IV. This gives a predicted spin-density on each bromine in the

TABLE 2

The energy and the coefficients of AO in the SOMO of the bromobenzene radical cation

Energy	Coefficients of AO[a]						
	CX	C1	C2	C3	C4	C5	C6
$H_4 = \alpha + 0.70\beta$	-0.512	0.425	0.365	-0.169	-0.483	-0.169	0.365
Spin densities	0.263	0.180	0.133	0.029	0.234	0.029	0.133

[a] CX for Br and C1 for the carbon bonded to Br.

TABLE 3

The energy and the coefficients of AO in the SOMO of the dibromobenzene radical cation

Energy	Coefficients of AO[a]							
	CX	C1	C2	C3	C4	CX	C5	C6
$H_5 = \alpha + 0.52\beta$	0.415	-0.419	-0.276	0.276	0.419	-0.415	0.276	-0.276
Spin densities	0.172	0.176	0.076	0.076	0.176	0.172	0.076	0.076

[a] CX for Br; C1 and C4 for the carbon atoms bonded to Br.

INSERT III

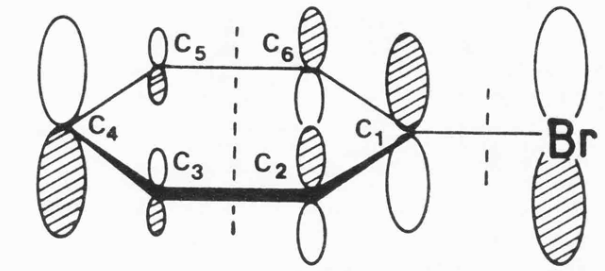

INSERT V

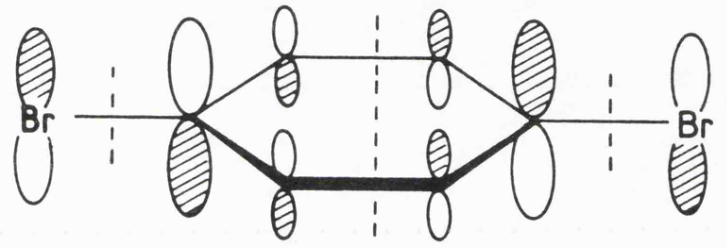

Spin Densities for the bromobenzene and dibromobenzene cations, as per Table 2 and Table 3.

dibromo derivative of between 19 and 21%. This first order approximation is satisfactory if the inaccuracies inherent in equation [1] are considered.

In order to check this argument, Hückel MO calculations were also performed for p-dibromobenzene using the same values of S_x and S_c as used for bromobenzene. The resulting values for the energy and coefficient of the SOMO for the p-dibromobenzene radical cation are given in Table 3. The calculated spin-density on bromine is 0.17 (Insert II). This value is smaller than the estimated (0.23), but it is still a good approximation. The Hückel calculations for these two cases gave smaller spin-densities on halogen than expected from ESR observations. This trend may be interpreted in terms of positive charge effects, in accord with the fact that the constant θ in the McConnell formula is large for cation radicals compared with neutral and anion radicals. Note that the assumption of $x + y = 1/3$, used in the above argument, is reasonable, while the assumption for x/y should be improved.

It is considered coincidental that the estimated spin-density on the dimeric cation, $(PhBr)_2^+$ is also $\approx 23\%$. In this case, one might have expected a factor of two to apply giving 15% on each bromine. Indeed, since there is only 50% positive charge on each ring in the dimer cation, this value might be expected to be reduced rather than increased. This increase may be due to equation [1] failing for the dimer cation or because weak bonding occurs between the two bromine atoms, as in VI or VII. It is most probable that the two molecular planes are close to being parallel, since, if this were not the case, the true $A_{//}(^{81}Br)$ values would be even greater than those observed. Such weak bonding would tend to localize the unpaired electron in the

σ^* ($Br\overset{\bullet}{-}Br$) orbital with loss of spin density in the two rings. Only a minor localization is required and in no sense do these species resemble σ^* radicals such as $(Rhal\overset{\bullet}{-}halR)^+$ ions previously reported.[18]

These results establish the positive charge effect on substituent π delocalization. A similar effect has recently been observed for $(F_2C=CF_2)^+$ cations.[19] The effect can be directly compared with the enhancement of σ-π delocalization (hyperconjugation) for C-H electrons in compounds such as 9,10-dimethyl anthracene[20] and hexamethyl benzene,[21] previously reported by this laboratory.

3.5 CALCULATIONS

For X

$\alpha_x = \alpha + S_x \beta$

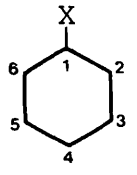

For C_1

$\alpha_{C_1} = \alpha + S\acute{c}\ \beta$

α = coulomb integral

β = resonance integral

$S\acute{c}$, S_x = constant allowing for different electronegativities

For C_2, C_3, C_4, C_5, C_6

α

Hence secular determinant is :

Equation (1)

$$\begin{vmatrix} w+S_x & 1 & 0 & 0 & 0 & 0 & 0 \\ 1 & w+S\acute{c} & 1 & 0 & 0 & 0 & 1 \\ 0 & 1 & w & 1 & 0 & 0 & 0 \\ 0 & 0 & 1 & w & 1 & 0 & 0 \\ 0 & 0 & 0 & 1 & w & 1 & 0 \\ 0 & 0 & 0 & 0 & 1 & w & 1 \\ 0 & 1 & 0 & 0 & 0 & 1 & w \end{vmatrix} = 0$$

where $w = \dfrac{\alpha - E}{\beta}$

Equation (2) Now $\dfrac{S\acute{c}}{S_x} = \dfrac{1}{8}$ [17]

Solving secular determinant (1) for several given values of $S_{c'}$ and S_x that satisfy Equation (2).

By Koopmans theorem, the ionization potential is related to the energy of HOMO.

Equation (3)

$$I = -E_{HOMO} = -E_4$$

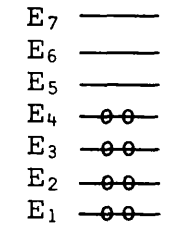

I = ionization potential (eV)

Now for chlorobenzene I(eV) = 9.31 ave.

bromobenzene I(eV) = 9.30 ave.

p-dichlorobenzene I(eV) = 9.07. [16]

The energy of E_4 is

Equation (4) $E_4 = \alpha + U\beta$

Equation (5) $\therefore I = -(\alpha + U\beta) = 9.30\ eV$

Using $\alpha = -7.2$ eV for benzene

$\beta = -3.0$ eV

Equation (6) Then $7.2 + U3.0 = 9.30$

$\therefore \quad U = 0.70$

From calculation results, $S_x = 1.53$ and $S_{c'} = 0.19$ correspond to that of $U = 0.70$.

The SOMO is given by:-

$$\psi_4 = -0.5124X_x + 0.4249X_{c_1} + 0.3647X_{c_2}$$

Equation (7) $$-0.1693X_{c_3} - 0.4833X_{c_4} - 0.16993X_{c_5} + 0.3647X_{c_6}$$

Unpaired electron densities:-

	Theoretical		Actual	
X	0.263	0.443	0.30	0.533
C_1	0.180		0.233 = 0.7/3	
C_2	0.133			
C_3	0.029			
C_4	0.234			
C_5	0.029			
C_6	0.133			

For di-halobenzene species;

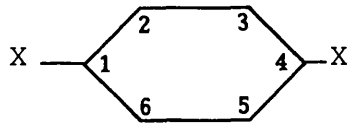

Using $S_X = 1.53$ and $S'_C = 0.190$, as in the case of halobenzene cations, then:-

Equation (8) $E_s = \alpha + 0.5185\beta$

and

$$\psi_s = 0.4145X_X - 0.4192X_{C_1} - 0.2761X_{C_2} + 0.2761X_{C_3} + 0.4192X_{C_4} - 0.4145X_X + 0.2761X_{C_5} - 0.2761X_{C_6}$$

Unpaired electron densities:-

	Theoretical	Actual
X	0.172 } = 0.348	0.23
C_1	0.176 }	
C_2	0.076	
C_3	0.076	
C_4	0.176 } = 0.348	0.23
X	0.172 }	
C_5	0.076	
C_6	0.076	

Adjusting the energy of SOMO to accommodate the ionization potential of 9.07 eV.

Then $S_X = 1.80$, $S_C = 0.255$.

Hence:- $E_s = \alpha + 0.6289\beta$

and

$$\psi_s = -0.3832X_X + 0.4488X_{C_1} + 0.2755X_{C_2} - 0.2755X_{C_3} - 0.4487X_{C_4} + 0.3832X_X - 0.2755X_{C_5} + 0.2755X_{C_6}$$

Unpaired electron densities:-

	Theoretical	Actual
X	0.147 } = 0.348	0.23
C_1	0.201 }	
C_2	0.076	
C_3	0.076	
C_4	0.201 } = 0.348	0.23
X	0.147 }	
C_5	0.076	
C_6	0.076	

Theoretical halogen spin-density ratio

$$\frac{\text{halo species}}{\text{dihalo species}} = \frac{0.263}{0.172} = 1.53$$

or

$$\frac{0.263}{0.147} = 1.79$$

Actual halogen spin-density ratio

$$= \frac{0.30}{0.23} = 1.30$$

INSERTS

I

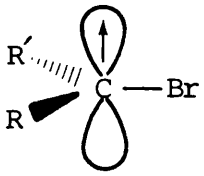

II

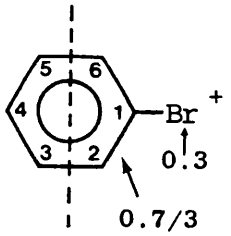

IV

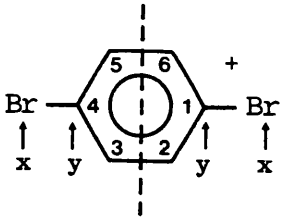

VI

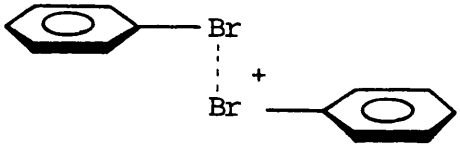

VII

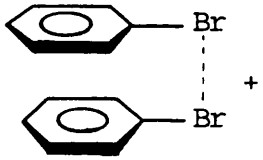

REFERENCES FOR CHAPTER 3

1. S. P. Mishra, G. W. Neilson and M. C. R. Symons, J. Am. Chem. Soc., 1973, 95, 605.
2. S. P. Mishra, G. W. Neilson and M. C. R. Symons, J. Chem. Soc., Faraday Trans. 2, 1973, 69, 1425.
3. S. P. Mishra, G. W. Neilson and M. C. R. Symons, J. Chem. Soc., Faraday Trans. 2, 1974, 70, 1165.
4. J. Hüttermann, W. A. Bernhard, E. Haindl and G. Schmidt, Mol. Phys., 1976, 32, 1111; J. Phys. Chem., 1977, 81, 228.
5. E. Haindl and J. Hüttermann, J. Magn. Reson., 1978, 30, 13.
6. W. Neumüller and J. Hüttermann, Int. J. Radiat. Biol., 1980, 37, 49.
7. H. Oloff and J. Hüttermann, J. Magn. Reson., 1977, 27, 197.
8. H. Oloff, J. Hüttermann and M. C. R. Symons, J. Phys. Chem., 1978, 82, 621.
9. S. P. Mishra and M. C. R. Symons, J. Chem. Soc., Perkin Trans. 2, 1981, 185.
10. T. Shida and T. Kato, Chem. Phys. Lett., 1979, 68, 106; J. Am. Chem. Soc., 1979, 101, 6869.
11. M. C. R. Symons and I. G. Smith, J. Chem. Research (S), 1979, 382.
12. K. Toriyama, K. Nunome and M. Iwasaki, J. Phys. Chem., 1981, 85, 2149.
13. J. T. Wang and F. Williams, J. Phys. Chem., 1980, 89, 3156.
14. M. C. R. Symons, Chemical and Biochemical Aspects of Electron Spin Resonance Spectroscopy, Van Nostrand Reinhold Co. Ltd., Wokingham/Berkshire, 1978.
15. J. R. Bolton and A. Carrington, Mol. Phys., 1961, 4, 497; J. R. Bolton, A. Carrington and L. E. Orgel, Mol. Phys., 1962, 5, 43.
16. J. D. Morrison and J. C. Nicholson, J. Chem. Phys., 1952, 20, 1021; K. Watanabe, J. Chem. Phys., 1957, 26, 542; G. F. Crable and G. L. Kearns, J. Phys. Chem., 1962, 66, 436.
17. H. C. Longuet-Higgins and C. A. Coulson, J. Chem. Soc., 1949, 971.
18. S. P. Mishra and M. C. R. Symons, J. Chem. Soc., Perkin Trans. 2, 1975, 1492.
19. A. Hasegawa and M. C. R. Symons, J. Chem. Soc., Faraday Trans. 1,
20. J. A. Brivati, R. Hulme and M. C. R. Symons, Proc. Chem. Soc., 1961, 384.
21. R. Hulme and M. C. R. Symons, J. Chem. Soc., 1965, 1120.

CHAPTER 4

Halogeno Benzene Cations

4.1 INTRODUCTION

Exposure of dilute solutions of a range of halogeno benzene derivatives in fluorotrichloromethane to ^{60}Co γ-rays at 77 K gave the corresponding radical cations, characterized by their e.s.r. spectra.

Recently there have been developments in the techniques for the generation and spectroscopic measurement of cations in the gas-phase[1-10] and in low temperature inert matrices.[11-14]

Fu and co-workers have studied halobenzene cations in the gas-phase using photo-dissociation spectroscopy[15,16] and Andrews et al. have used low temperature matrices.[17-24]

The results are summarised in Table 1.

4.2 RESULTS AND DISCUSSION

For the fluoro-derivatives (Figure 1), the spectra could be fully interpreted. However, there is ambiguity over the sign of the perpendicular ^{19}F hyperfine coupling constants. The powder spectrum gives the magnitude but not the sign of the perpendicular parameter. If the species are allowed to rotate then if $A_\perp$ is positive, the parallel features would move in twice as fast as the perpendicular features would move out, resulting in a large isotropic nuclear coupling. If $A_\perp$ is negative, all features would move in resulting in a very small isotropic nuclear coupling.[25] Unfortunately, this procedure for estimating relative signs of parallel and perpendicular coupling constants failed in this case as there were no significant librations prior to radical loss. However, for α-fluoroalkyl radicals for which A_{iso} and $A_{//}$ are known, $A_\perp$ must be positive to give reasonable agreement, if $A_{//}$ and A_{iso} are taken as positive.

For chloro- and iodo- derivatives only the $\underline{x}$ features (A_{max}) were

TABLE 1

ESR Parameters for Halobenzene and Related Cations together with estimated Spin-densities on Halogen

Radical	Medium	$A_{//}$(halogen)/G[a]	$A_{\perp}$(^{1}H)/G	$g_{//}$	Spin-density[b]
$C_6H_5F^+$	$CFCl_3$	155(18)	(para)10.5	2.001	0.08
$FUdR^+$ [c]	6.3M H_2SO_4	170(18)		2.000	0.09
$C_6H_4(Me)F^+$	$CFCl_3$	136	(ring)2.9	2.001	0.07
			(Me)19.0		
$C_6H_5Cl^+$	$CFCl_3$	28	(para)ca.9	2.000	0.23
$ClUdR^+$ [c]	6.3M H_2SO_4	22(5,6)		2.000	0.18
$C_6H_5Br^+$	$CFCl_3$	185		1.993	0.30
$C_6H_4Br_2^+$	$CFCl_3$	143		1.992	0.23
$C_6H_4(Me)Br^+$	$CFCl_3$	170		1.994	0.27
$C_6H_4(OH)Br^+$ [d]	90% H_2SO_4	113		1.998	0.18
$C_6H_4(OMe)Br^+$	$CFCl_3$	113		1.998	0.18
$C_6H_4(SH)Br^+$	$CFCl_3$	100		1.998	0.16
$BrUdR^+$	6.3M H_2SO_4	155		1.996	0.25
$C_6H_5I^+$	$CFCl_3$	ca. 210		ca. 1.98	ca. 0.46
$C_6H_4(Me)I^+$	$CFCl_3$	ca. 185		ca. 1.98	ca. 0.41
IUR^+ [c]	6.3M H_2SO_4	ca. 100		ca. 1.94	ca. 0.22
$(C_6H_5Cl)_2^+$	$CFCl_3$	24		2.000	0.20
$(C_6H_5Br)_2^+$	$CFCl_3$	143		1.992	0.23
$(C_6H_5I)_2^+$	$CFCl_3$	ca. 140		ca. 1.98	ca. 0.31

[a] $G = 10^{-4}$ T; [$A_{\perp}$ values in parenthesis when measured].
[b] Estimated using eqn. (1) and atomic parameters listed in Ref. 38; [c] Ref. 32; [d] Ref. 35.

FIGURE 1a

First derivative X-band ESR spectra for fluorobenzene in $CFCl_3$ after exposure to ^{60}Co γ-rays at 77 K, showing features attributable to the cation.

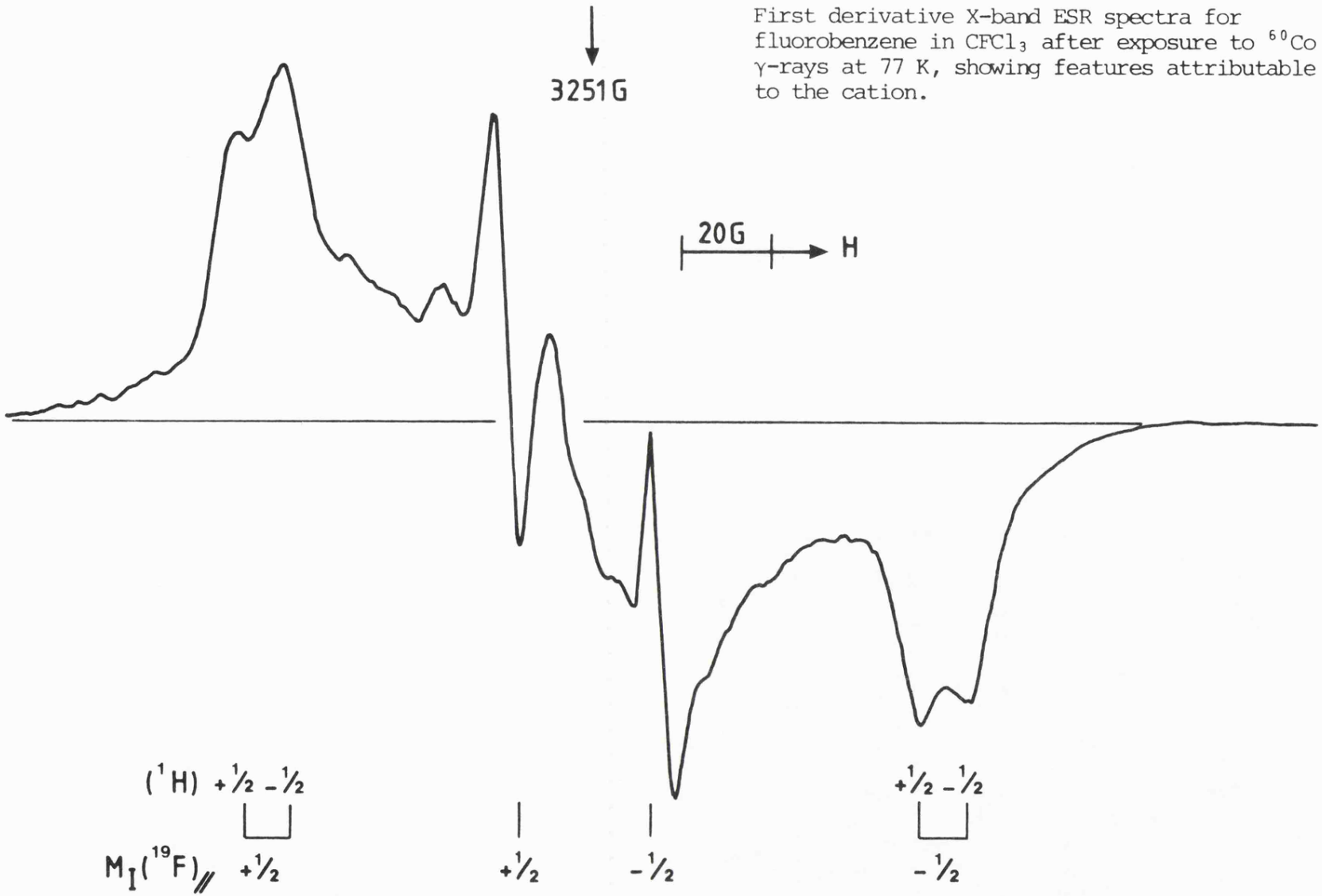

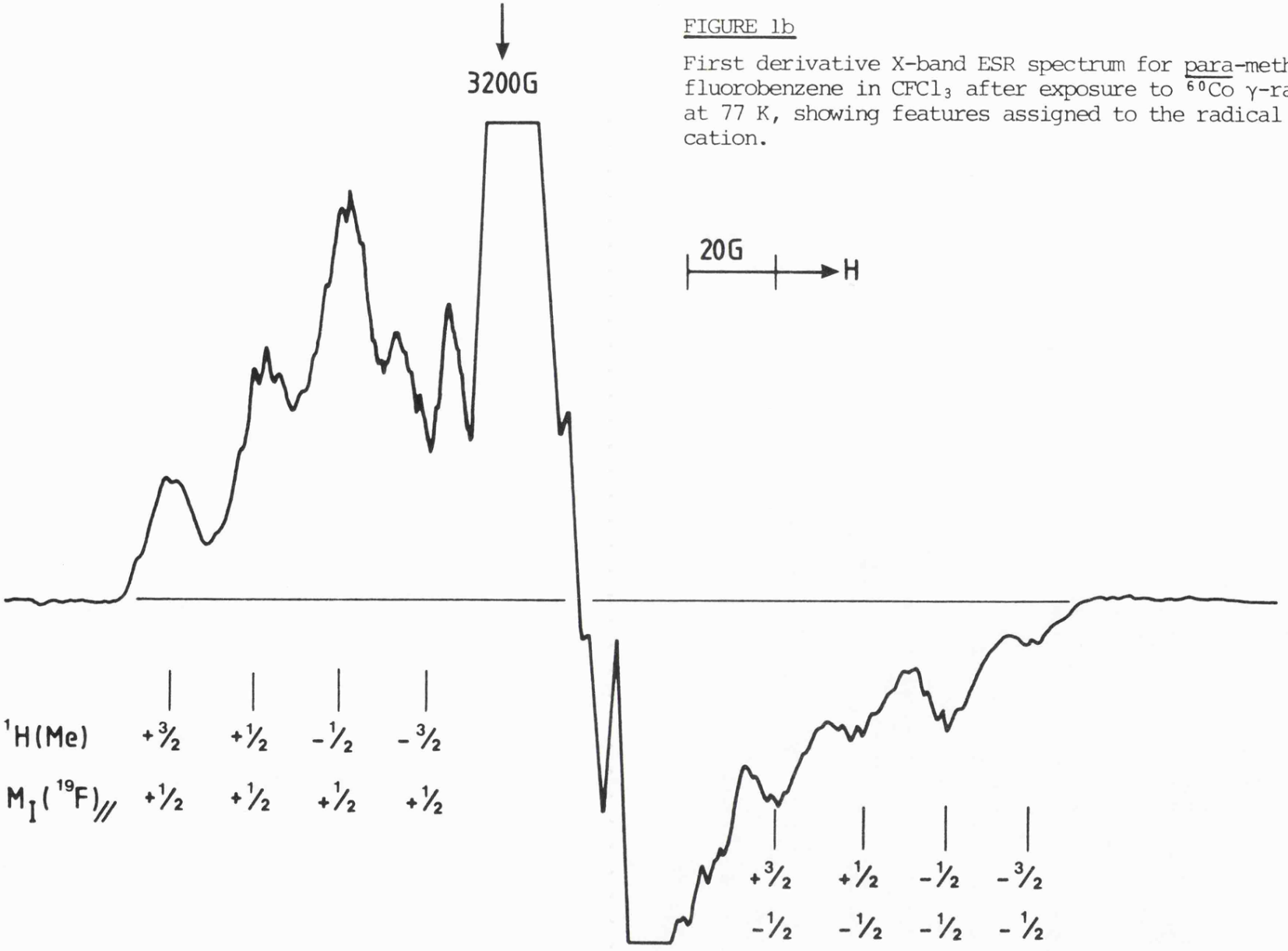

FIGURE 1b

First derivative X-band ESR spectrum for para-methyl fluorobenzene in $CFCl_3$ after exposure to ^{60}Co γ-rays at 77 K, showing features assigned to the radical cation.

well-defined as in the case of bromo derivatives. Using the same method as applied to the bromo derivatives, allowed calculation of the spin-density on the halogen. In the Hüttermann equation $f_x = 0.81$ for ^{35}Cl and ^{81}Br and 1.0 for ^{127}I[26-31] (Figures 2-4).

The most interesting feature of the results is the large positive charge effect, which increases on going from F to I. The estimated spin-densities on halogen are compared with those for neutral radicals, $R_2\dot{C}$-hal in Figure 5. If the substituents were treated only as a minor perturbation, the orbital involved (SOMO) would be that shown in Insert I, with a spin density on C_1 of 0.33, in contrast with the formal spin-density of unity for $R_2\dot{C}$-hal radicals. If this simple model were correct, the extent of delocalisation onto fluorine for PhF^+ should be one-third that for $R_2\dot{C}$-F, whereas in fact they are almost equal. Furthermore, those for the bromo- and iodo- derivatives are greater for the cations. One contributing factor to this charge effect is that electron-donation from halogen into the benzene ring simply shifts positive charge from the ring onto halogen, the trend following the ionization potentials. However, for $R_2\dot{C}$-hal, extensive electron-donation generates charge separation and is consequently opposed by coulombic forces.

The results are presented as a function of halogen atom ionization potentials (Figure 5). The smaller slope compared with results for the neutral radicals illustrates the positive charge effect discussed. The electron affinity of (Ph^+) is much greater than that of the ($R_2\dot{C}$) unit, hence the degree of electron-transfer is also greater. The trends are also compared with those reported by Reiderer and Hüttermann, for certain halo-uracil cations (II) formed in irradiated aqueous sulphuric acid.[32] Their spin-densities are similar to ours, but the trend is in

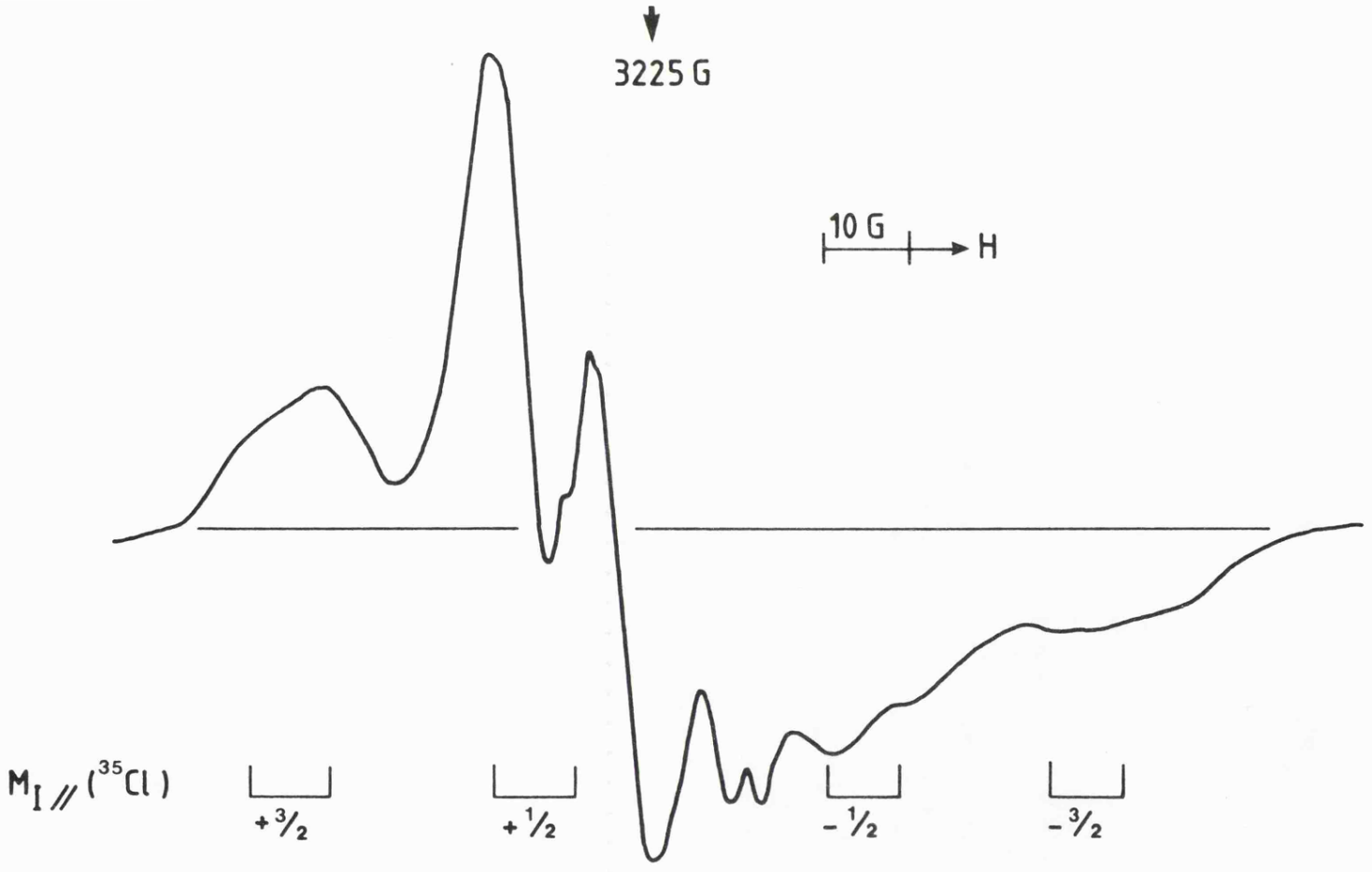

FIGURE 2

First derivative X-band ESR spectrum for chlorobenzene in $CFCl_3$ after exposure to ^{60}Co γ-rays at 77 K, showing features assigned to the chlorobenzene radical cation.

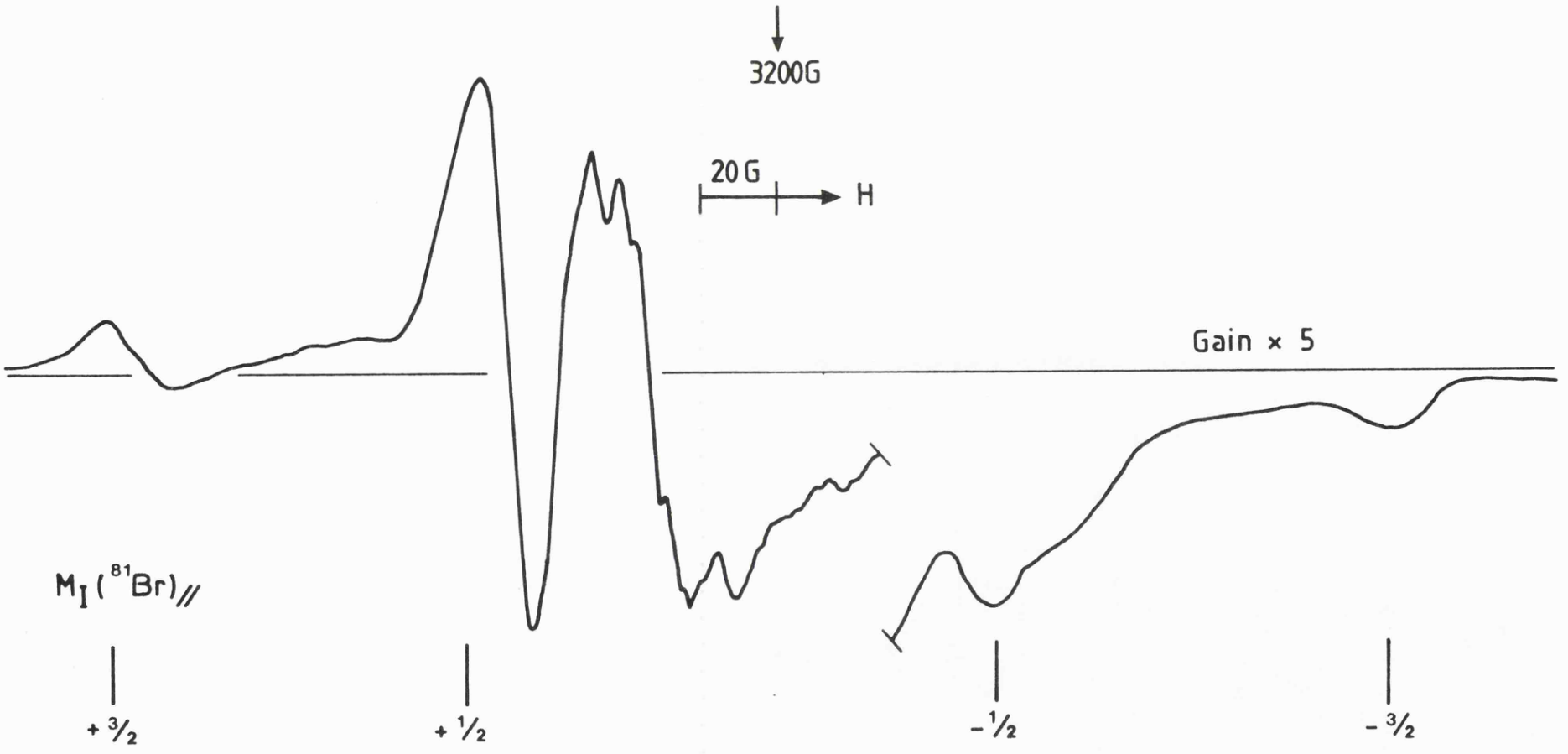

FIGURE 3

First derivative X-band ESR spectrum for para-bromo thiophenol in $CFCl_3$ after exposure to ^{60}Co γ-rays at 77 K, showing features assigned to the cation (see Figure 1 of Chapter 3 for the spectrum of $C_6H_5Br^+$).

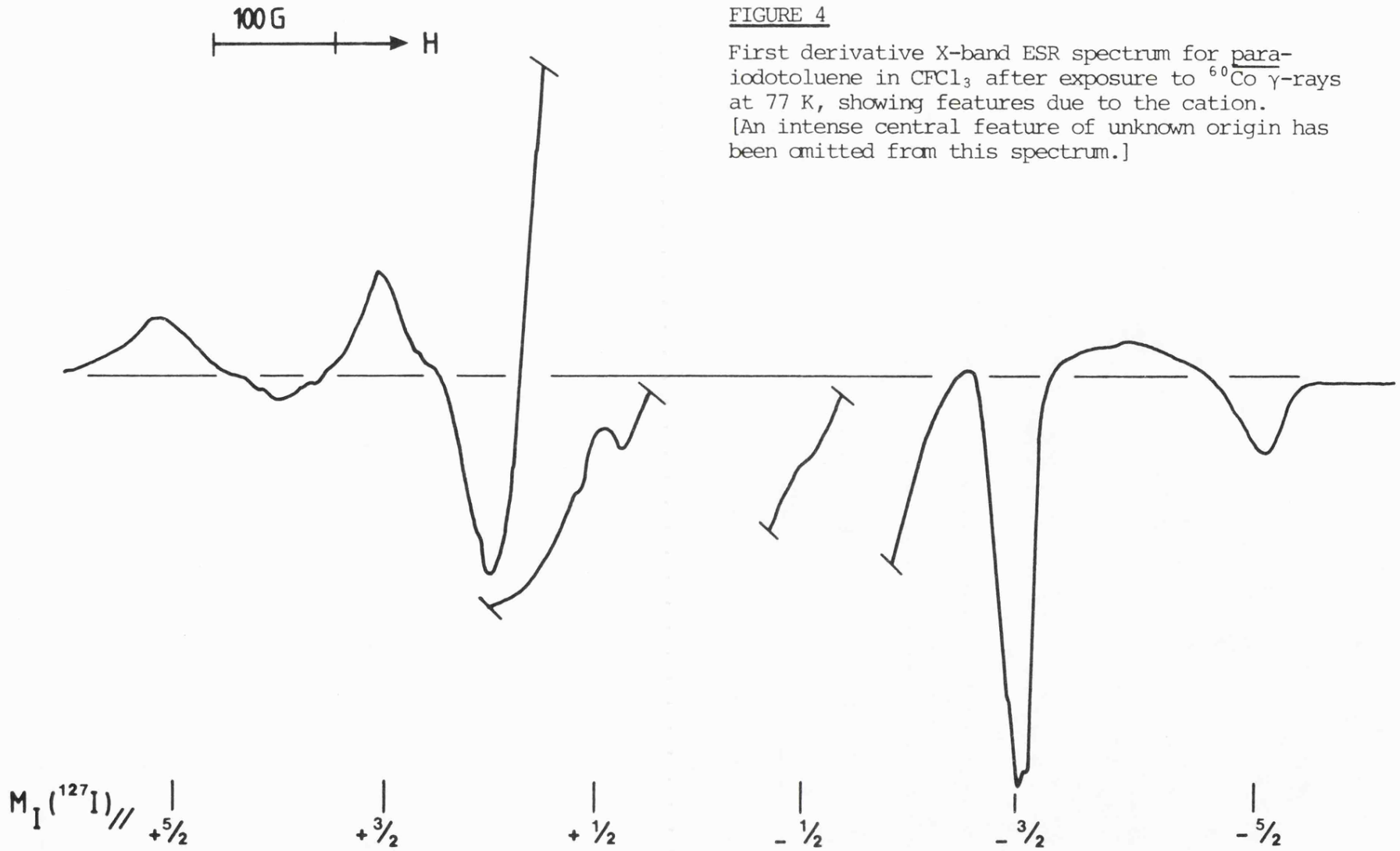

FIGURE 4

First derivative X-band ESR spectrum for para-iodotoluene in $CFCl_3$ after exposure to ^{60}Co γ-rays at 77 K, showing features due to the cation. [An intense central feature of unknown origin has been omitted from this spectrum.]

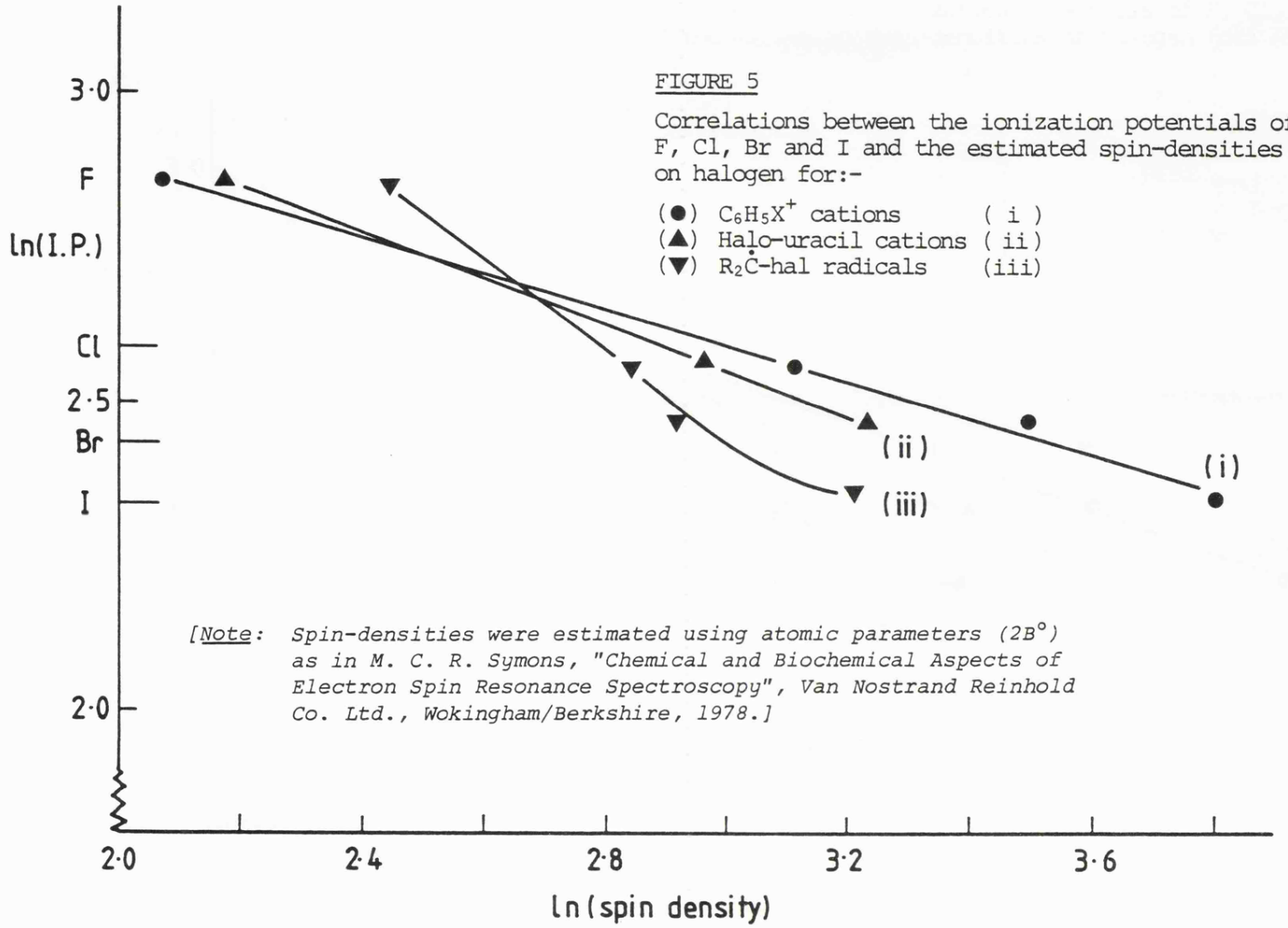

FIGURE 5

Correlations between the ionization potentials of F, Cl, Br and I and the estimated spin-densities on halogen for:-

(●) $C_6H_5X^+$ cations (i)
(▲) Halo-uracil cations (ii)
(▼) $R_2\dot{C}$-hal radicals (iii)

[Note: Spin-densities were estimated using atomic parameters ($2B^\circ$) as in M. C. R. Symons, "Chemical and Biochemical Aspects of Electron Spin Resonance Spectroscopy", Van Nostrand Reinhold Co. Ltd., Wokingham/Berkshire, 1978.]

between those for the phenyl cations and the neutral radicals. [The results for the iodo-derivatives were very uncertain.] This suggests that the electron affinity of the uracil cation group is less than that for the phenyl cation group.

I 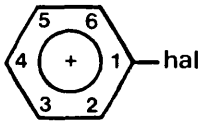

II 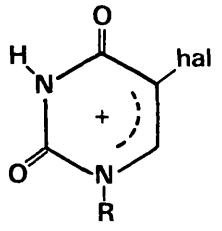

In these studies on Ph hal$^+$ cations, only one well-defined species has been detected for each halo-derivative. This is in contrast with optical studies of the $PhBr^+$ in rare gas matrices, in which two distinct species were detected. These species, formed by photoionization of dilute matrices of PhBr, were thought to have the conventional structure, postulated herein, and the novel structure III. It seems

III 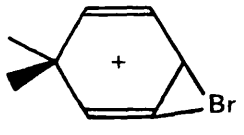

unlikely that these isomers would have similar e.s.r. spectra. If species III has a free-spin signal with only weak hyperfine coupling to bromine, it could contribute to the centre regions of our spectra. One aspect of these studies is that no mention is made of the fate of the ejected electrons. We expect that they would be captured by PhBr molecules to give either $PhBr^-$ radical anions or phenyl radicals. The former might possibly contribute to the observed spectra and should not be formed in freon matrices.

4.3 EFFECTS OF OTHER SUBSTITUENTS

In the particular case of the bromo-derivative cations, we have studied changes in spin-density on bromine on replacing the para-hydrogen atom by other substituents. Para-bromo, -hydroxyl and -sulphydryl groups increasingly reduce the spin-density on bromine.

This effect has already been discussed for the di-bromide, and it has been shown that the fall in spin-density is close to that expected in terms of a simple-proportional π-distribution of spin-density. That -SH groups should be more effective than bromine in gaining spin-density (and positive charge) is to be expected in terms of relative ionization potentials, but the greater delocalisation onto -OH and -OMe than onto bromine is surprising, since the ionization potential for $\cdot OH$ is close to that for $\cdot Cl$. Perhaps the more compatible $2p\pi$ (C) and $2p\pi$ (O) orbitals can explain this discrepancy.

The clear fall in spin-density on methyl substitution was not expected. Presumably, this reflects the direct delocalisation of spin onto the methyl group at the expense of the halogen, as for the other para-substituents. For the fluoro-derivative there is no evidence that the ring protons become inequivalent, and the hyperfine coupling (2.9 G) is actually slightly greater than that estimated for the coupling for the benzene cation (2.6 G).[33]

4.4 FORMATION OF DIMERS

All the halobenzenes formed dimers in more concentrated solutions. The spectra gave 7 "parallel" features for the chloro (and the bromo) and 11 for the iodo-derivative, showing that the two nuclei are equivalent. A typical spectrum is shown (Figure 2). These species are analogous to the $(RhalˑhalR)^+$ σ^* dimer cations previously reported

in certain irradiated alkyl halides.[34]

4.5 CONCLUSIONS

The results confirm that the node selected by all the aromatic mono-halogen cations favours the SOMO that places maximum spin-density on halogen rather than the alternative π-orbital having a nodal plane through the halogen atoms. In contrast, the SOMO for the radical anions do have a node through the halogen. This arrangement contributes to the duality of structures for the anions, which can exist either in the π*-state or with the excess electron in the carbon-halogen σ* orbital.[35]

REFERENCES FOR CHAPTER 4

1. M. Allan and J. P. Maier, Chem. Phys. Lett., 1975, 34, 442.
2. M. Allan, J. P. Maier and O. Marthaler, Chem. Phys., 1977, 26, 131.
3. J. A. Coxon, P. J. Marcoux and D. W. Setser, Chem. Phys., 1976, 17, 403.
4. K. T. Wu and A. T. Yencha, Can. J. Phys., 1977, 55, 767.
5. C. Cossart-Magos, D. Cossart and S. Leach, Mol. Phys., 1979, 37, 793.
6. J. H. Callomon, Proc. Roy. Soc. London, Ser. A, 1958, A244, 220.
7. M. S. King and R. C. Dunbar, Chem. Phys. Lett., 1979, 60, 247.
8. A. Carrington, Proc. Roy. Soc., 1979, 367, 433.
9. J. T. Shy, J. W. Farley, W. E. Lamb and W. H. Wing, Phys. Rev. Lett., 1980, 45, 535.
10. F. J. Grieman, B. H. Mahan and A. O'Keefe, J. Chem. Phys., 1980, 72, 4246.
11. V. E. Bondybey, T. A. Miller and J. H. English, J. Chem. Phys., 1980, 72, 2193.
12. V. E. Bondybey, T. A. Miller and J. H. English, J. Chem. Phys., 1979, 71, 1088.
13. V. E. Bondybey and J. H. English, J. Chem. Phys., 1979, 71, 777.
14. V. E. Bondybey, C. Vaughn, T. A. Miller, J. H. English and R. H. Shiley, J. Am. Chem. Soc., 1981, 103, 6303.
15. E. W. Fu, P. P. Dymerski and R. C. Dunbar, J. Am. Chem. Soc., 1976, 98, 337.
16. R. C. Dunbar, H. H.-I. Teng and E. W. Fu, J. Am. Chem. Soc., 1979, 101, 6506.
17. B. W. Keelan and L. Andrews, J. Am. Chem. Soc., 1981, 103, 99.
18. B. W. Keelan and L. Andrews, J. Am. Chem. Soc., 1981, 103, 829.
19. M. C. R. Symons, A. Hasegawa and S. P. Maj, Chem. Phys. Lett., 1982, 89, 254.
20. T. Shida and T. Kato, Chem. Phys. Lett., 1979, 68, 106.
21. T. Shida, Y. Egawa, J. Kubota and T. Kato, J. Chem. Phys., 1980, 73, 5963.
22. M. C. R. Symons and I. G. Smith, J. Chem. Research (S), 1979, 382.
23. K. Toriyama, K. Nunome and M. Iwasaki, J. Phys. Chem., 1981, 85, 2149.
24. J. T. Wang and F. Williams, J. Phys. Chem., 1980, 84, 3156.
25. M. C. R. Symons and I. G. Smith, J. Chem. Soc., Faraday Trans. 1, 1981, 77, 2701.
26. H. Riederer, J. Hüttermann and M. C. R. Symons, J. Phys. Chem., 1981, 85, 2789.

REFERENCES (Continued)

27. W. Neumuller and J. Hüttermann, Int. J. Radiat. Biol., 1980, 37, 49.

28. H. Oloff, J. Hüttermann and M. C. R. Symons, J. Phys. Chem., 1978, 82, 621.

29. S. P. Mishra, G. W. Neilson and M. C. R. Symons, J. Am. Chem. Soc., 1973, 95, 605; J. Chem. Soc., Faraday Trans. 2, 1973, 69, 1425.

30. S. P. Mishra, G. W. Neilson and M. C. R. Symons, J. Chem. Soc., Faraday Trans. 2, 1974, 70, 1165.

31. H. Oloff and J. Hüttermann, J. Magn. Reson., 1977, 27, 197.

32. H. Riederer and J. Hüttermann, J. Phys. Chem., 1982, 86, 3454.

33. M. C. R. Symons and L. Harris, J. Chem. Research (S), 1982, 268.

34. S. P. Mishra and M. C. R. Symons, J. Chem. Soc., Perkin Trans. 2, 1975, 1492.

35. S. P. Mishra and M. C. R. Symons, J. Chem. Soc., Perkin Trans. 2, 1981, 185.

CHAPTER 5

The [1,2] Hydrogen Atom Shift

5.1 INTRODUCTION

Previous work by this laboratory demonstrated the rearrangement of the $Me_2CH\dot{C}H_2/Br^-$ adduct to the $(CH_3)_3C\cdot/Br^-$ and $(CH_3)_2\dot{C}(CH_2D)/Br^-$ adducts followed by their dissociation into the $(CH_3)_3C\cdot$ and $(CH_3)_2\dot{C}(CH_2D)$ radicals.[1] The competing mechanisms were suggested to be an intramolecular rearrangement [1] and an intermolecular hydrogen atom exchange process with the adamantane-d_{16} matrix [2,3].

[1] $(CH_3)_2CH\dot{C}H_2 \longrightarrow (CH_3)_2\dot{C}CH_3$

[2] $(CH_3)_2CH\dot{C}H_2 + Ada\text{-}D \longrightarrow (CH_3)_2CHCH_2D + Ada\cdot$

[3] $(CH_3)_2CHCH_2D + Ada\cdot \longrightarrow (CH_3)_2\dot{C}CH_2D + Ada\text{-}H$

However, it was thought that ca. 1% impurities present in the adamantane (d_{16}) matrix could give rise to the apparently intramolecular reaction. An analogous reaction, $nPr\cdot/Br^- \longrightarrow IsoPr\cdot/Br^-$, using the same adamantane did not involve any deuterium pick up, providing evidence in favour of the [1,2] hydrogen atom sigmatopic rearrangement.

Iwasaki[2] carried out the following experiments and concluded there to be an intramolecular shift.

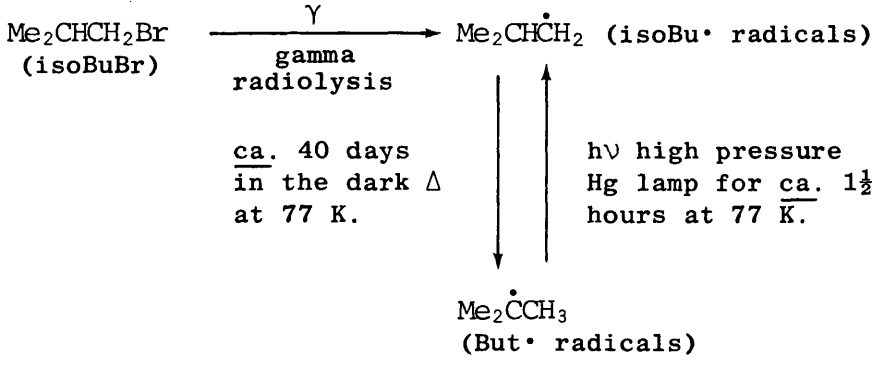

The isoBu· radical, generated from the γ-radiolysis of isoBuBr, rearranged into the But· radical at 77 K, if stored in the dark over a long period of time. It was also found that the But· radical thus generated could be rearranged back into the isoBu· radical by exposure

to ultra-violet light at 77 K. Of particular interest, in the published spectra, are the A(^{1}H) hyperfine couplings of 42 G and 21 G for the β- and α- hydrogen atoms respectively of the isoBu• radical. It is our opinion that these spectra are not of free alkyl radicals but of adducts. Additionally, though the authors assumed the rearrangements were intramolecular, no additional evidence was given.[1,3-5]

The general theory of the principles of orbital symmetry by Woodward and Hoffman predict that 1,2-hydrogen atom shifts are thermally allowed. However, there is no real, unequivocal evidence that 1,2-hydrogen atom or alkyl group migrations do actually occur in radical reactions. In the few systems where such migrations have been postulated, other more probable paths could also explain the products.[6-8]

Two mechanisms were investigated - the intra/inter molecular rearrangements and the effect of the halide ion on the reaction,[9,10] the charge transfer from the halide 'p' orbital to the 'pz' orbital on carbon being ca. 10%.

The reactions may be summarised as follows:-

$$Me_2\dot{C}HCH_2 \underset{h\nu(2)}{\overset{\Delta(1)}{\rightleftharpoons}} Me_2\dot{C}CH_3$$

$$Me_2\dot{C}HCH_2/X^- \underset{h\nu(4)}{\overset{\Delta(3)}{\rightleftharpoons}} Me_2\dot{C}CH_3/X^-$$

(1,2) Iwasaki et al. However, due to reasons just mentioned, his spectra are of adducts.
(3) Previous work in this laboratory.
(4) No previous work.

The following experiments were performed:-

1. (a) The comparison of the photolysis of the $Bu^t\cdot$ radical and the $Bu^t\cdot/Br^-$ adduct in a Bu^tBr matrix.
   (b) The comparison of the photolysis of the $Bu^t\cdot$ radical and the $Bu^t\cdot/Cl^-$ adduct in a Bu^tCl matrix.

2. The comparison of the photolysis of the $But\cdot$ radical and the $But\cdot/Cl^-$, $But\cdot/Br^-$ and $But\cdot/I^-$ adducts in the TMS matrix.
3. Generation of IsoBu· radicals in an adamantane d_{16} matrix and a study of their thermal rearrangement to $But\cdot$ for comparison with the analogous $IsoBu\cdot/Br^-$ and $IsoBu\cdot/I^-$ rearrangements.
4. The photolysis of the $But\cdot$ radical in a CD_3OD matrix.
5. The study of the thermal rearrangement of IsoBu· radical in deuterated matrices.

5.2 THE ADDUCT

Studies of the acetonitrile dimer radical anion produced by γ-irradiation of acetonitrile crystals at 77 K by Williams et al.[11] tried to establish the anionic nature of the paramagnetic colour centre. Addition of a competitive electron scavenger (e.g. MeHal) into the acetonitrile crystal led Sprague and Williams[16] to study γ-irradiated solutions of MeBr in MeCN at 77 K.

The results show four sets of 1:3:3:1 quartets. The quartet splitting of 20.6 G being assigned to protons of Me radicals undergoing weak exchange with Br. Methyl halides normally act as electron scavengers and undergo dissociative electron attachment to give Me· radicals and halide ions. This was the first system showing interaction from ejected halide ions.

The quartet of quartets is assigned to $\cdot CH_3$ radicals interacting with bromide ions. The proton splitting is about 90% of the value (23.04 G) for the free $\cdot CH_3$ radicals. This suggests about 10% of the spin-density is located on the bromine:

$$\frac{20.6}{23.04} \times 100 = 89.4\%$$

Assuming that this 10% of the unpaired electron resides in a 4p orbital and ignoring core polarization effects, we expect an axially

symmetric bromine hyperfine tensor with a parallel value in the region of 50 G, as observed. Annealing produces $\cdot CH_3$ radicals. Hence the $CH_3\cdot/Br^-$ is an intermediate stage in the process of dissociative electron capture.

If there is an anisotropic splitting of B gauss (B is the maximum value of anisotropy) and we know that in the hypothetical atom, having unit occupancy of the particular p-orbital involved, the maximum value of the coupling is B° gauss, then the amount of electron in the p-orbital is:

$$Cp^2 = \frac{B}{B^\circ}$$

Cp^2 = percentage population

B° = maximum coupling

$Cp^2 = 10\%$

$B^\circ = 584$ G

$$\therefore \quad \underline{B = 58.4 \text{ G}}$$

Work by Mishra et al.[12] identified and characterised the parallel and perpendicular features. Note the main features:

(a) Absence of any significant g-value shift.

(b) Absence of any quadrupole effect, even for I despite its very large quadrupole moment. This implies a small electric field gradient.

(c) Absence of anisotropy in proton hyperfine coupling.

5.3 EXPERIMENTAL

Standard methods of sample preparation were employed except in the case of adamantane. Substrates were incorporated into the adamantane matrix by recrystallising the adamantane from the substrate.

Samples were photolysed using a quartz finger Dewar containing liquid nitrogen and then either a high or low pressure mercury lamp focused on the samples.

Three methods of controlled annealing were employed (i) Standard Variable Temperature equipment, (ii) Proportional Temperature Control, (iii) Proportional, Integral and Differential Control (PID), courtesy of Dr. Chen. The major disadvantage of the proportional control system was that samples had to be taken out of the cavity for annealing. In the PID system, the samples remained in the cavity and could be continuously monitored.

Methanol-d_4 (BDH), adamantane-d_{16} (Merck, Sharpe & Dohme), tetramethylsilane-d_{12} (BDH), were all used as supplied. Tertiary butyl chloride (BDH), tertiary butyl bromide (BDH) and tertiary butyl iodide (BDH) were distilled prior to use.

5.4 RESULTS AND DISCUSSION

5.4.1 Photolysis in the Bu^tHal matrix

The gamma radiolysis of Bu^tHal (hal is I, Cl or Br) generates a broad ten-line spectrum attributable to the $Bu^t\cdot/Br^-$ adduct. Mild annealing produces a much narrower spectrum of ten lines due to the $Bu^t\cdot$ radical. Comparisons were made between the photolysis of the adduct and free radical using both high pressure and low pressure mercury lamps.

(a)(i) $Bu^t\cdot/Br^-$ adduct. - IsoBu· radicals were produced on photolysis. However, conversion rates were low due to the matrix absorbing in this region. The IsoBu· radicals could not be sharpened indicating the presence of the free radical (Figures 1a, 1b).

(ii) $Bu^t\cdot$ radical. - Again IsoBu· radicals were produced but, for the same period of illumination, the yield was considerably more than in (i). The spectrum was identical to that produced in (i), i.e. the radical is unadducted (Figures 1c, 1d).

(b)(i) $Bu^t\cdot/Cl^-$ adduct. - Photolysis generated IsoBu· radicals. The

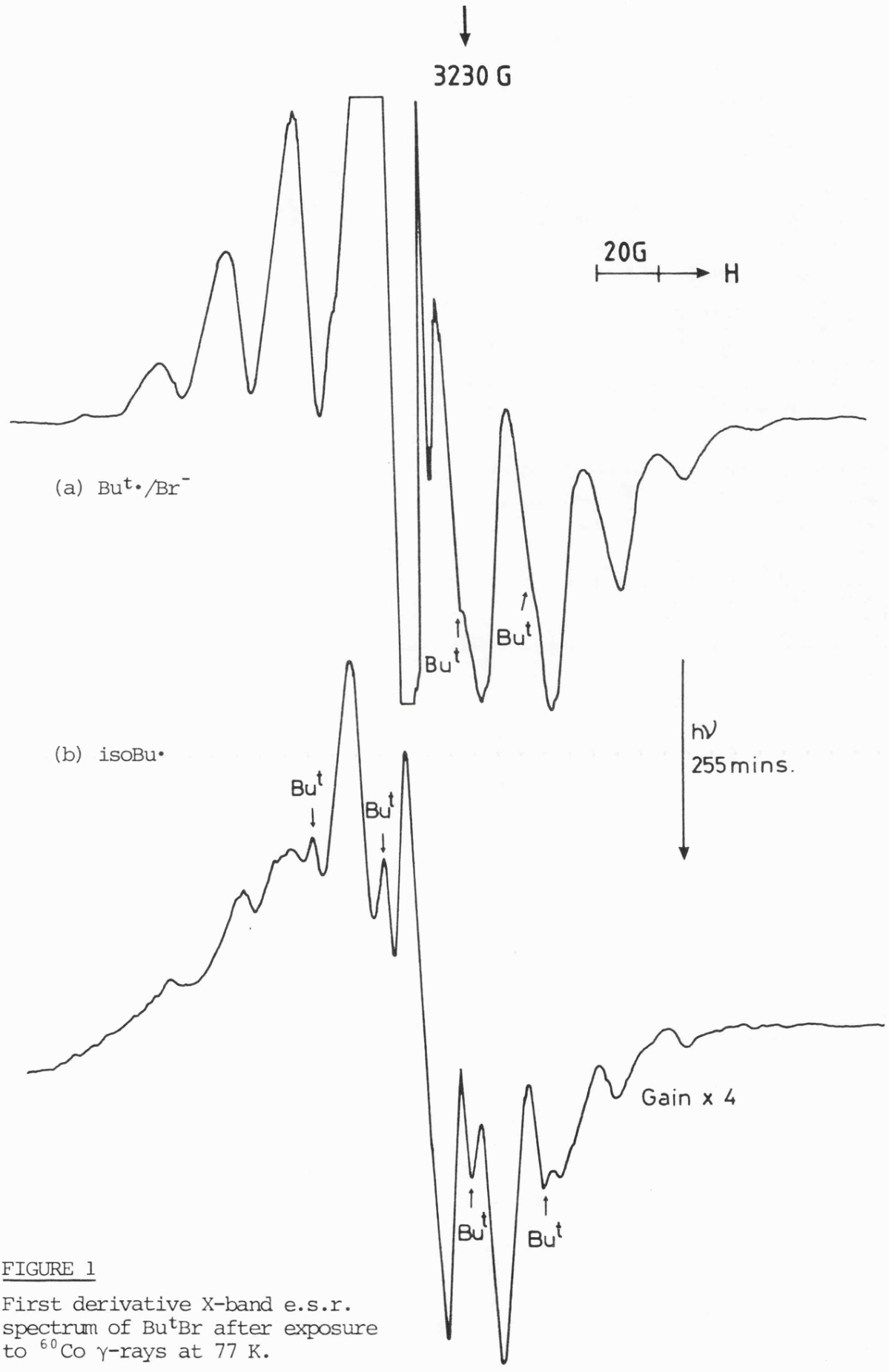

FIGURE 1

First derivative X-band e.s.r. spectrum of Bu^{t}Br after exposure to ^{60}Co γ-rays at 77 K.

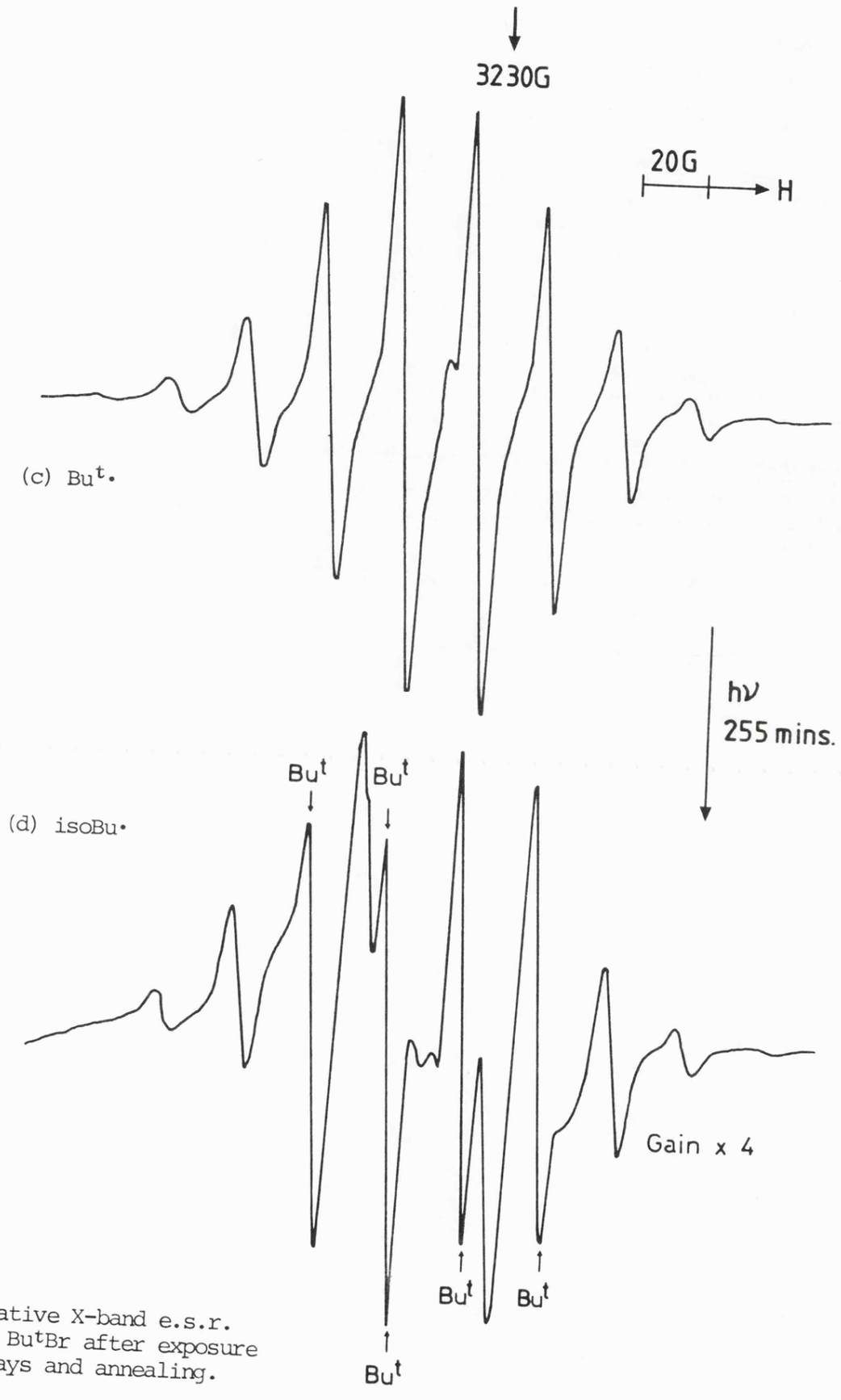

FIGURE 1

First derivative X-band e.s.r. spectrum of Bu^{t}Br after exposure to ^{60}Co γ-rays and annealing.

spectrum could not be sharpened by annealing (Figs. 2a, 2b).

(ii) $Bu^t\cdot$ radicals. - Under identical experimental conditions approximately twice as much IsoBu· was generated with relation to (ii). Annealing did not narrow the radical features (Figs. 2c, 2d).

The results indicate there is a significant conversion of $Bu^t\cdot$ radicals to IsoBu· radicals which is photolytically induced. To a first approximation, the halide ion inhibits this conversion and that the adduct must first split into the free radical prior to rearrangement.

5.4.2 Photolysis in Tetramethylsilane (TMS)

Gamma radiolysis of dilute (1 mol %) solutions of Bu^tHal (Cl, Br, I) in TMS generates the corresponding adduct from which the free radical can be produced. Photolysis of the $Bu^t\cdot$ radical generated IsoBu· radicals but photolysis of the adduct failed to do so. The adduct spectrum was no longer evident and subsequent annealing did not generate IsoBu· radicals. In this system the halide ion totally inhibits any conversion process. Possible mechanisms could be (i) electron transfer from the halide 'p' orbital to the carbon 'p' orbital, (ii) steric hindrance, (iii) both (i) and (ii) (Figs. 3a and b).

5.4.3 Adamantane d_{16} Matrix

All attempts to generate IsoBu· radicals from parent material failed. IsoBuBr and IsoBuI generated adduct only and IsoBuCl generated β-chloro radicals. 3-Methylbutyric acid ($Me_2CHCH_2CO_2H$) was used as a possible precursor to IsoBu· radicals. A high yield of $(CH_3)_3C\cdot$ radicals and $(CH_3)_2\dot{C}(CH_2D)$ radical grew in on annealing but no IsoBu· radicals could be detected either before or after annealing. Thus suggesting a different precursor than the expected IsoBu· radical. Attempts were

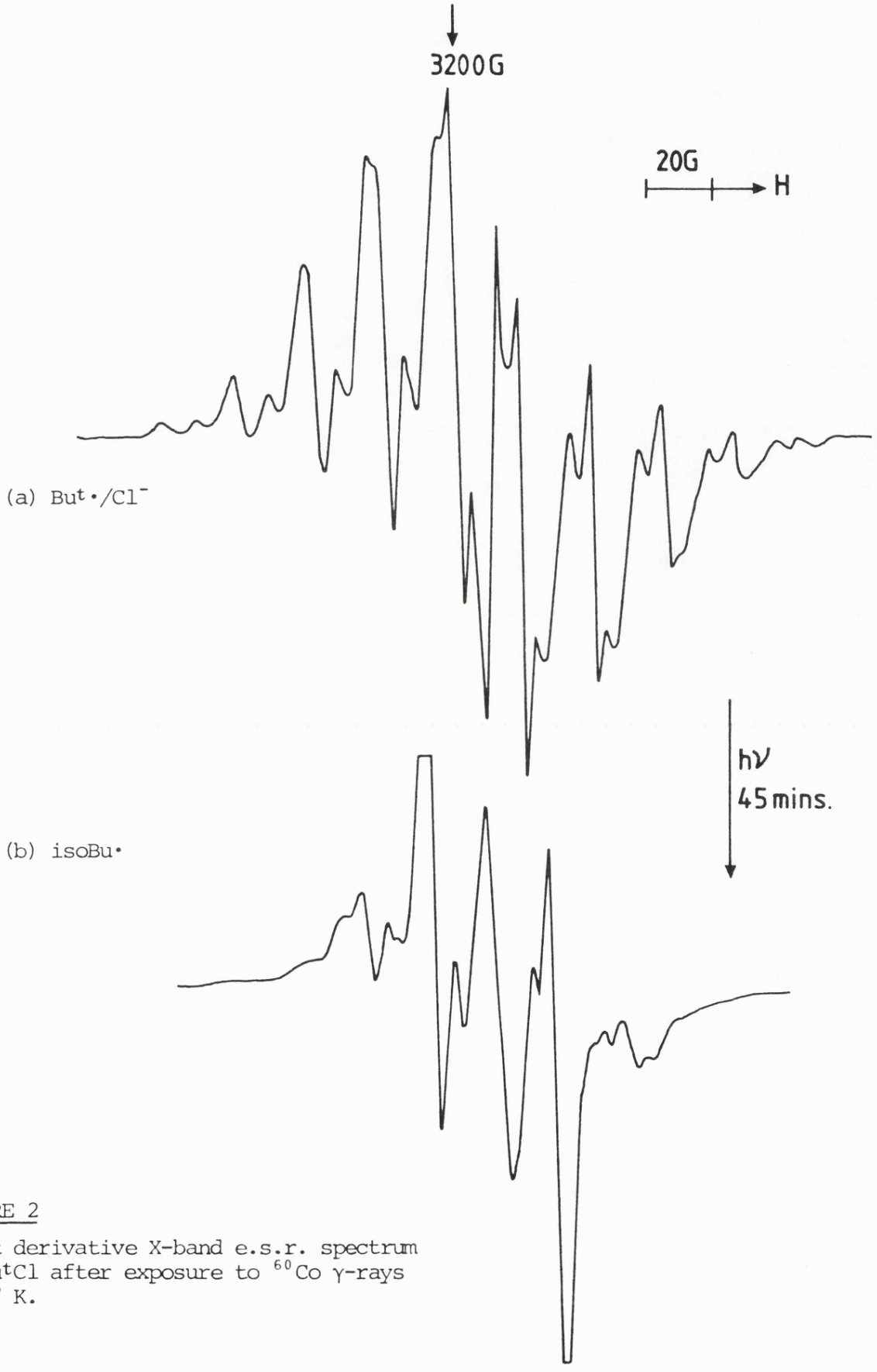

FIGURE 2

First derivative X-band e.s.r. spectrum of Bu^tCl after exposure to ^{60}Co γ-rays at 77 K.

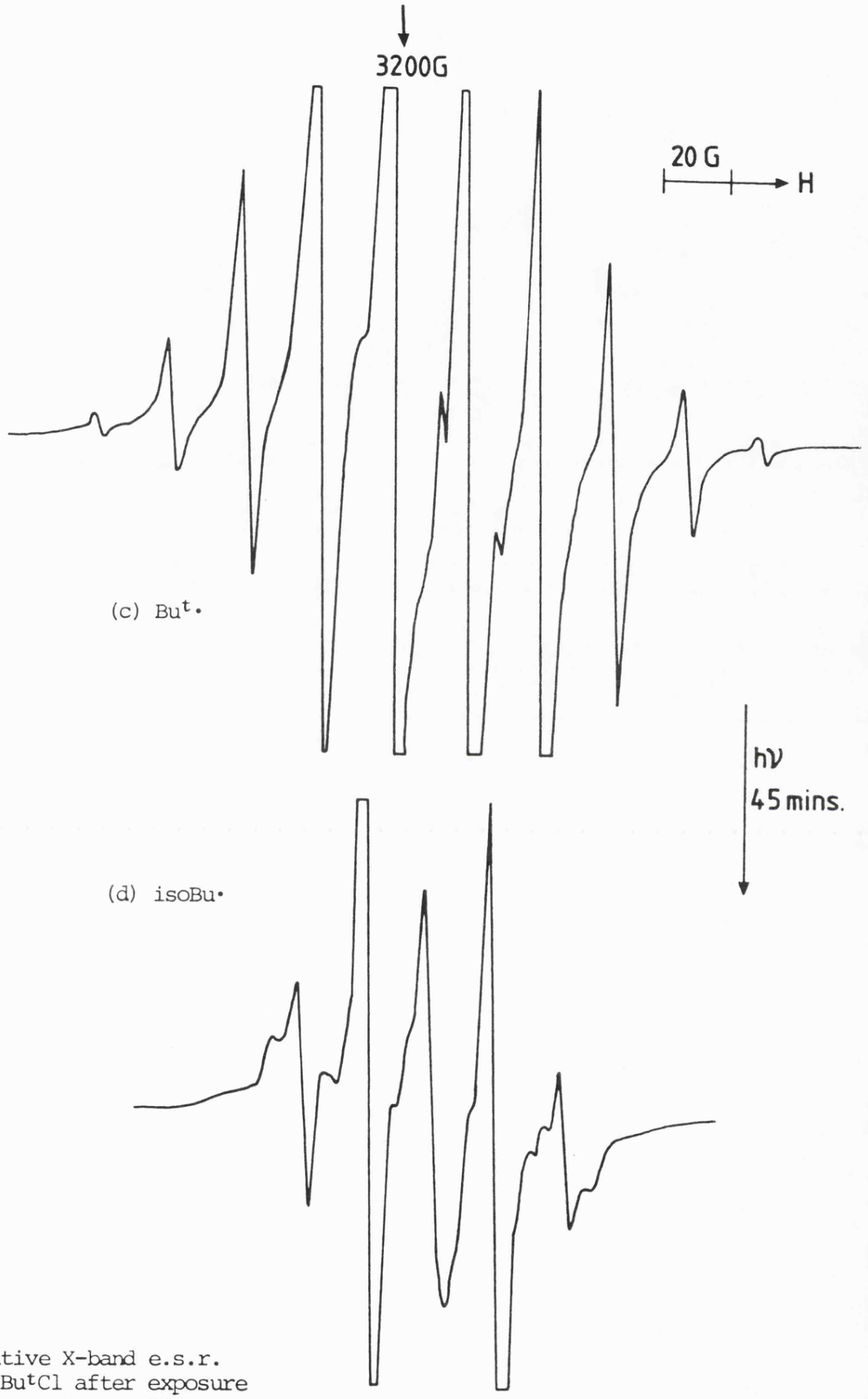

FIGURE 2

First derivative X-band e.s.r. spectrum of Bu^{t}Cl after exposure to ^{60}Co γ-rays and annealing.

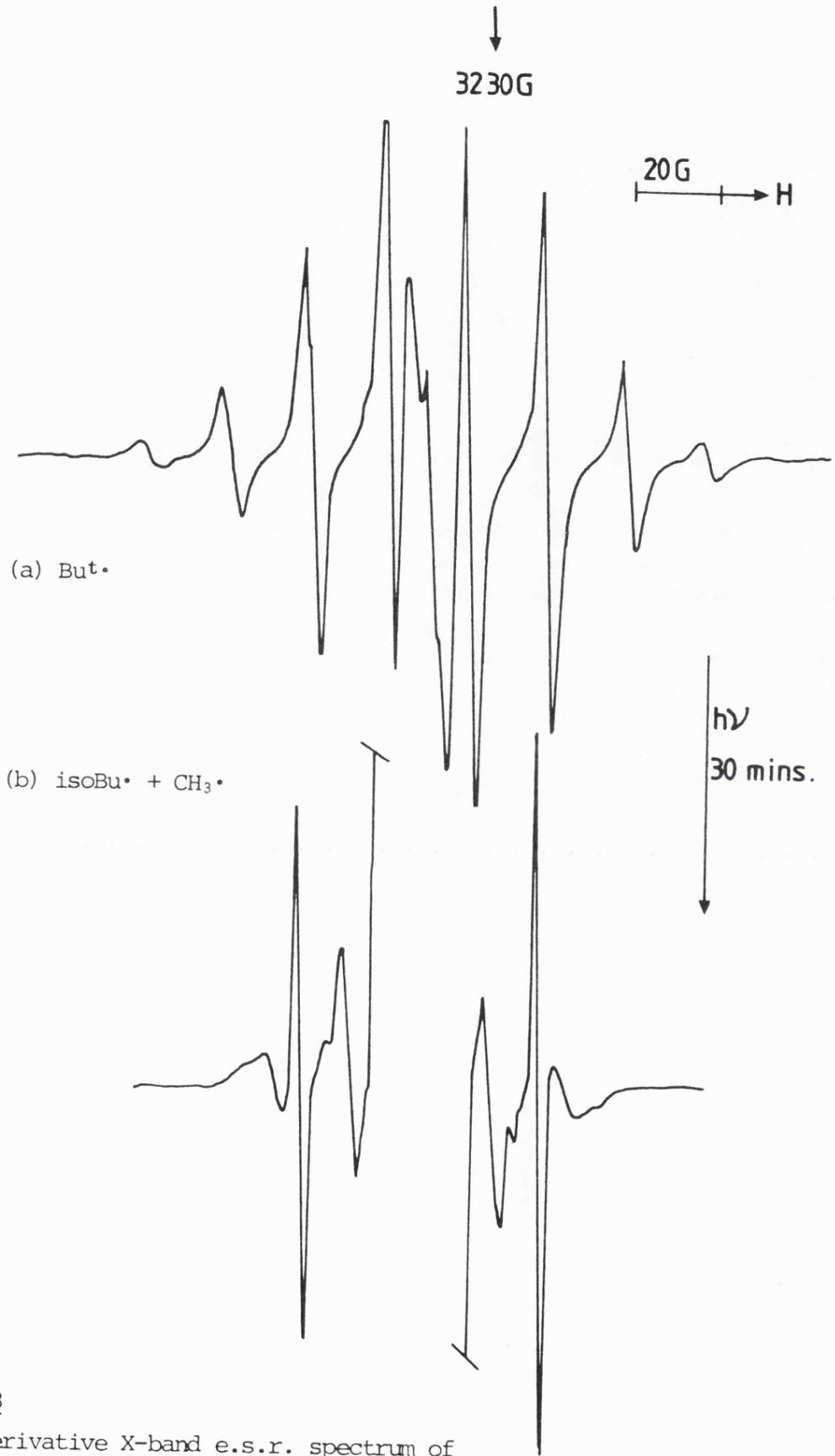

FIGURE 3

First derivative X-band e.s.r. spectrum of Bu^tBr in TMS after exposure to ^{60}Co γ-rays and annealing.

then made to generate IsoBu· radicals from Bu^{t}· radicals by photolysis in adamantane. However, the conversion rate was very low, ca. 10-20%.

5.4.4 Photolysis in CD_3OD

Dilute solutions (1 mol %) of $Bu^{t}Hal$ (Cl, Br, I) in CD_3OD were γ-irradiated. Due to solvation only Bu^{t}· radicals were formed and not adducts. Photolysis generated IsoBu·, $\cdot CH_3$ and $\cdot CD_3$ radicals. No mechanism has yet been assigned for the generation of the $\cdot CD_3$ and $\cdot CH_3$ radicals but it would seem that the Bu^{t}· ⟶ IsoBu· isomerisation process is intramolecular (Figs. 4a, 4b).

Parkes and Quinn[11,12] have detailed the UV absorption spectrum of the Bu^{t}· radical. The profile shows a broad continuum from 220-280 nm with a broad peak at 220-240 nm and a less intense peak at 240-270 nm. The low wavelength band was suggested to be analogous to, but broader than, the spectrum derived from Me· radicals and to be due to Rydberg transitions on the carbon atom. The less intense band was not assigned. It is possible that this band is responsible for the photo-isomerisation process.

Symons has postulated the isomerisation process taking place via electron movement and then a proton shift.[13,14]

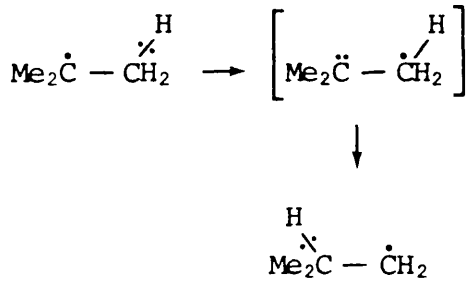

By the use of filters it would appear that the active region is in the 254 nm range.

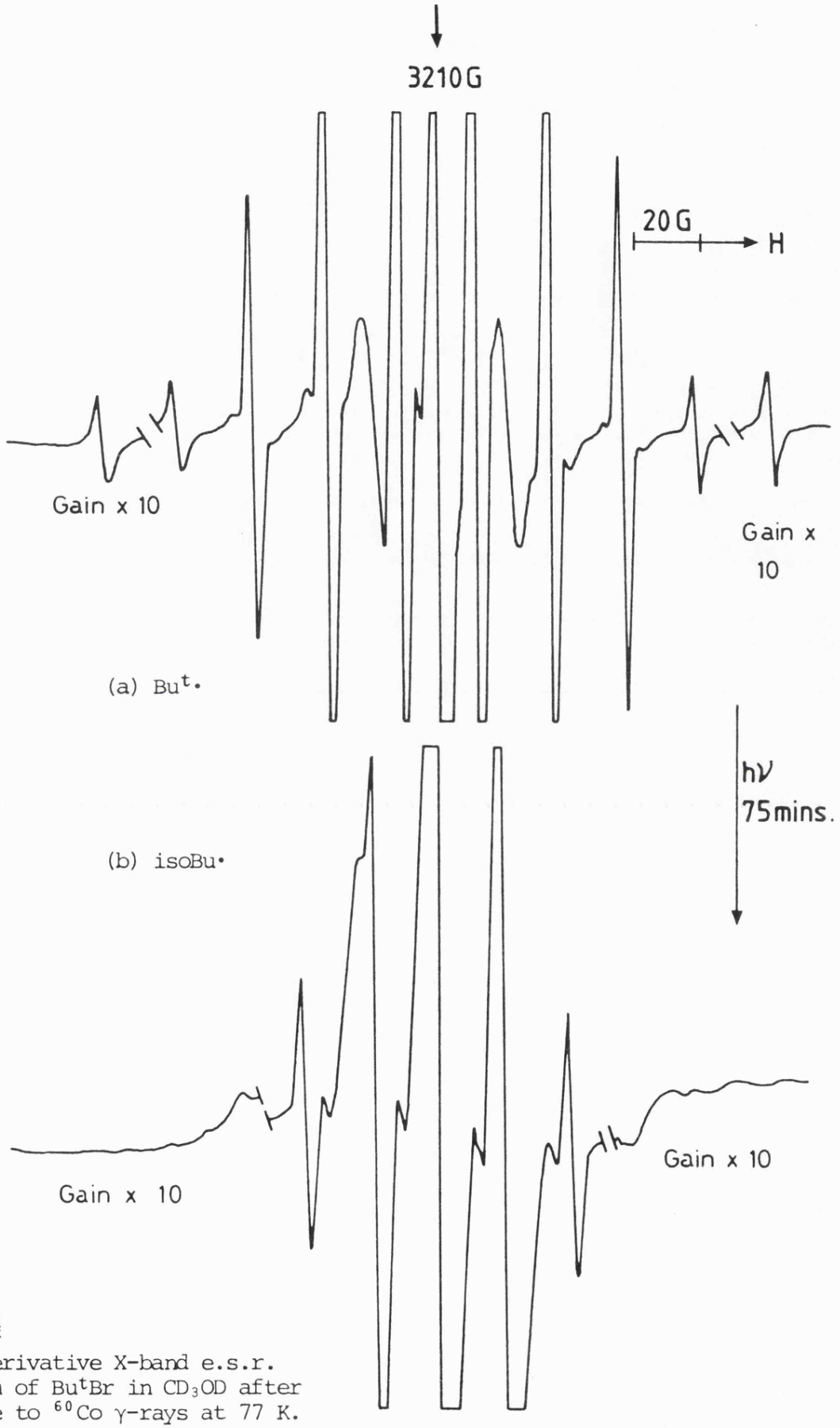

FIGURE 4

First derivative X-band e.s.r. spectrum of Bu^{t}Br in CD_3OD after exposure to ^{60}Co γ-rays at 77 K.

5.4.5 IsoBu• radicals in deuterated matrices

IsoBu• radicals were generated from IsoBuCl in CD_3OD (ca. 1 mol %) and left in the dark at 77 K for seven months. The results show a four-fold increase in Bu^t• radicals with an approximately three-fold decrease in IsoBu• radicals. However the amount of Bu^t• present is of the order of 10^{-2} less than IsoBu•. No $Me_2\dot{C}CH_2D$ was generated. The implications are that an intramolecular shift has occurred.

Possible criticisms are (i) phase separation of IsoBuCl and CD_3OD, (ii) not a 1:1 change in concentrations, (iii) impurities in IsoBuCl, and (iv) reaction too slow to generate kinetic data.

IsoBuCl was distilled and the following experiments tried:-

(i) IsoBu• + MeOH $\longrightarrow$ very slow cf. CD_3OD

(ii) IsoBu• + CD_3OD $\xrightarrow[\text{light}]{\text{visible}}$

(iii) IsoBu• + MeOH $\xrightarrow[\text{light}]{\text{visible}}$

(iv) IsoBu• + CD_3OD $\xrightarrow{\text{VT}}$

(VT = variable temperature)

None of the above gave satisfactory results.

The reaction is an exothermic one and at a suitable temperature the reaction should proceed. With too high a temperature:

(i) Matrix collapse
(ii) Other reactions occur
(iii) Reaction inhibited.

With the temperature too low:

(iv) Reaction not fast enough, cf. CD_3OD at 77 K.

Hence the following requirements were needed: (i) suitable matrix (no protons), (ii) no phase separation, (iii) low temperature VT, and (iv) long term temperature stability with VT.

The VT equipment available failed to come up to specification. Although low temperatures were available, they could not be held for any length of time and were subject to inaccuracies. Various attempts to use 'slush baths' also failed.

The following experiments were carried out using the proportional control system.

1. IsoBu• in CD_3OD. - A variety of temperatures and times failed to generate Bu^t• radicals.

2. IsoBu• in TMS. - Tetramethylsilane was selected, the deuterated material being available. A variety of conditions were tried. Bu^t• radicals started to grow in at -149°C. The apparatus had the facility to hold six sample tubes. In all experiments the following combinations were used:-

(i) IsoBu• + TMS
(ii) Bu^t• + TMS
(iii) IsoBu• + Bu^t• + TMS.

A range of temperatures was selected so that the Bu^t• signal was stable in sample (ii). The growth of Bu^t• in sample (i) could then be monitored. At -142°C Bu^t• radicals could be generated from IsoBu• radicals. At this temperature the signal intensity of sample (ii) remained constant, temperatures other than this caused loss of signal or no change in signal intensity (Fig. 5).

Kinetic data could not be generated due to the inaccuracies involved in placing the sample in the cavity. For the remaining experiments the PID control system was used, i.e. samples kept in the cavity.

(a) IsoBu• in TMS (H)

In this experiment 1 µl of IsoBuBr was dissolved in 0.5 ml of TMS. At -160°C over a period of 4 hours Bu^t• radicals grew in with a loss of

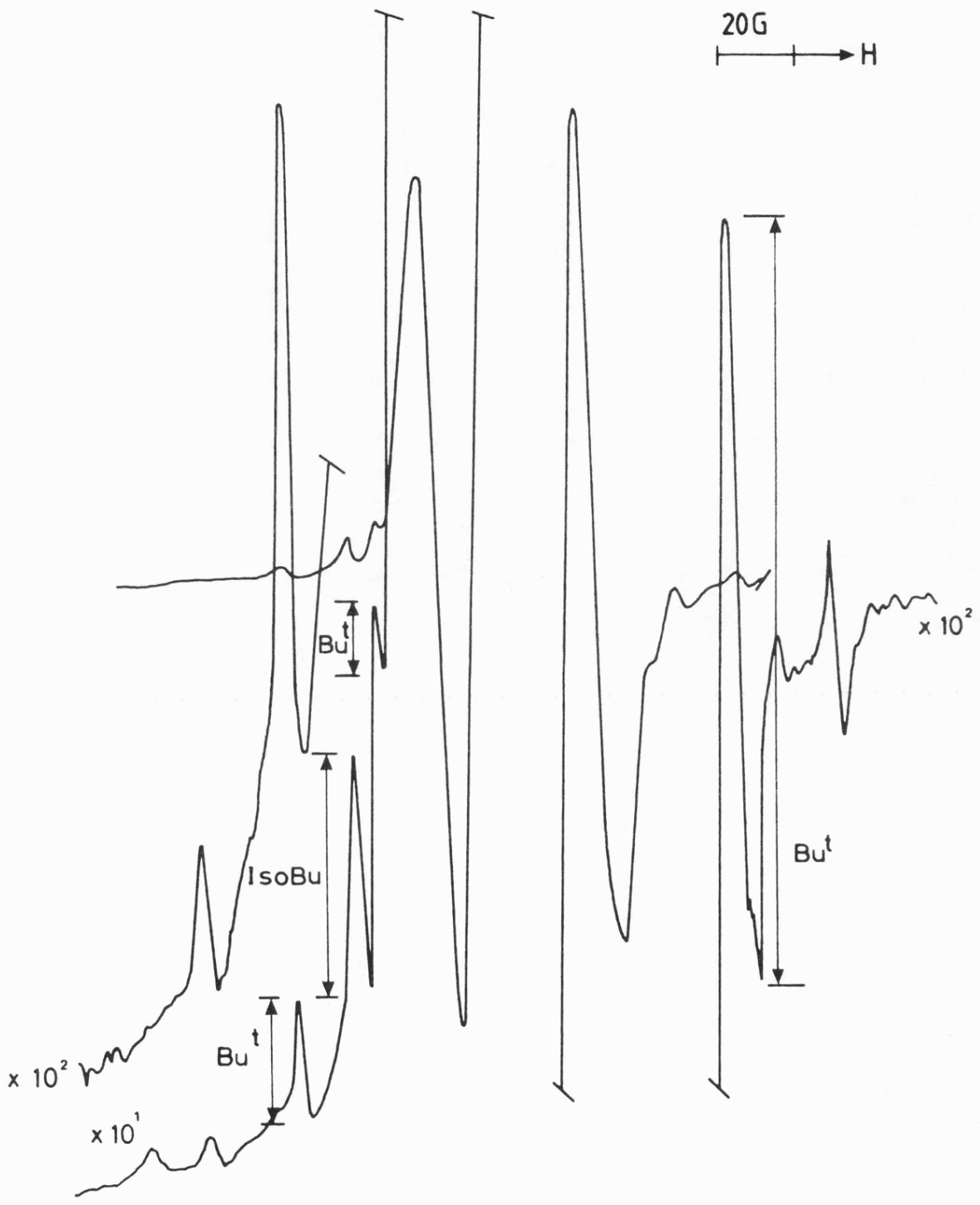

FIGURE 5

First derivative X-band e.s.r. spectrum of Bu^tBr in TMS after exposure to ^{60}Co γ-rays at 77 K and annealing using the proportional control system.

IsoBu•. The degree of temperature control was ±0.5°C using a platinum resistance thermometer (Fig. 6).

(b) Bu^t• in TMS (H)

The Bu^t• was stable over a two-hour period at -160°C.

(c) Bu^t• in TMS (D)

The Bu^t• was stable over a one-hour period at -160°C.

(d) IsoBu• in TMS (D)

IsoBuBr (5 μℓ) was dissolved in TMS (D) (0.5 mℓ). Maintaining the sample within the cavity at various temperatures, spectra were drawn at defined intervals. The results are presented in Graph 1. Over a one-hour period at -170°C (Table 1) there was a small increase in signal due to Bu^t•. At -165°C more Bu^t• grew in. At -160°C for 1½ hours there was a decrease in the IsoBu• signal and an increase in the Bu^t• signal. After this moisture in the cavity prevented further sensible data to be gathered (Fig. 7).

(e) IsoBu• in TMS (D)

IsoBuBr (1 μℓ) was dissolved in TMS (D) (0.5 mℓ). Bu^t• grew in but, due to problems with moisture in the cavity, no accurate determinations could be made.

5.5 CONCLUSIONS

The following points are offered as evidence of a 1,2-intramolecular shift:-

1. In the CD_3OD experiment IsoBu• decayed and Bu^t• radicals grew in. The experiment was over several months and could not be considered as a 'hot' reaction.
2. All solutions used were very dilute, ca. 1:1000, thus reducing chances of self-reaction.

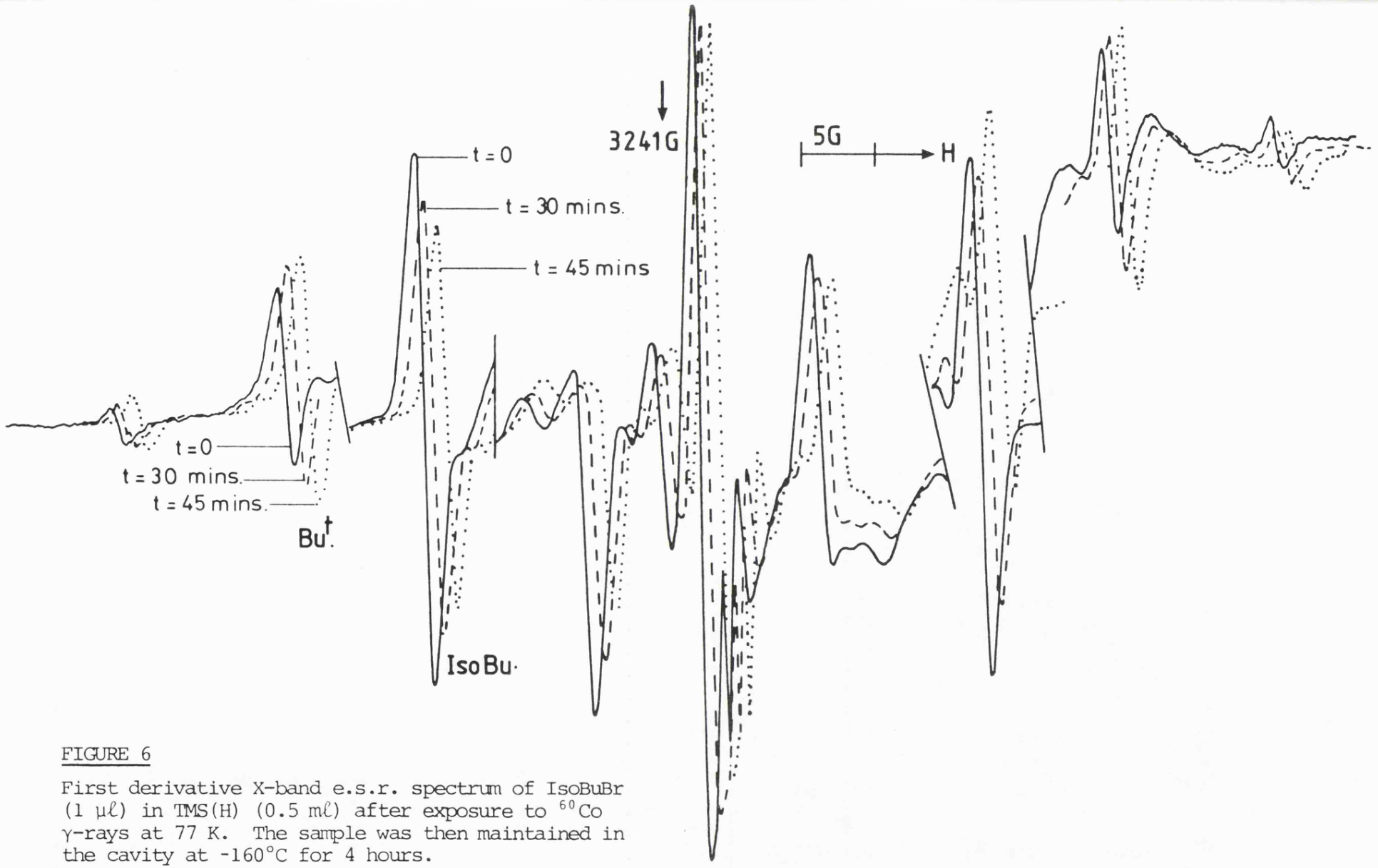

FIGURE 6

First derivative X-band e.s.r. spectrum of IsoBuBr (1 μℓ) in TMS(H) (0.5 mℓ) after exposure to ^{60}Co γ-rays at 77 K. The sample was then maintained in the cavity at -160°C for 4 hours.

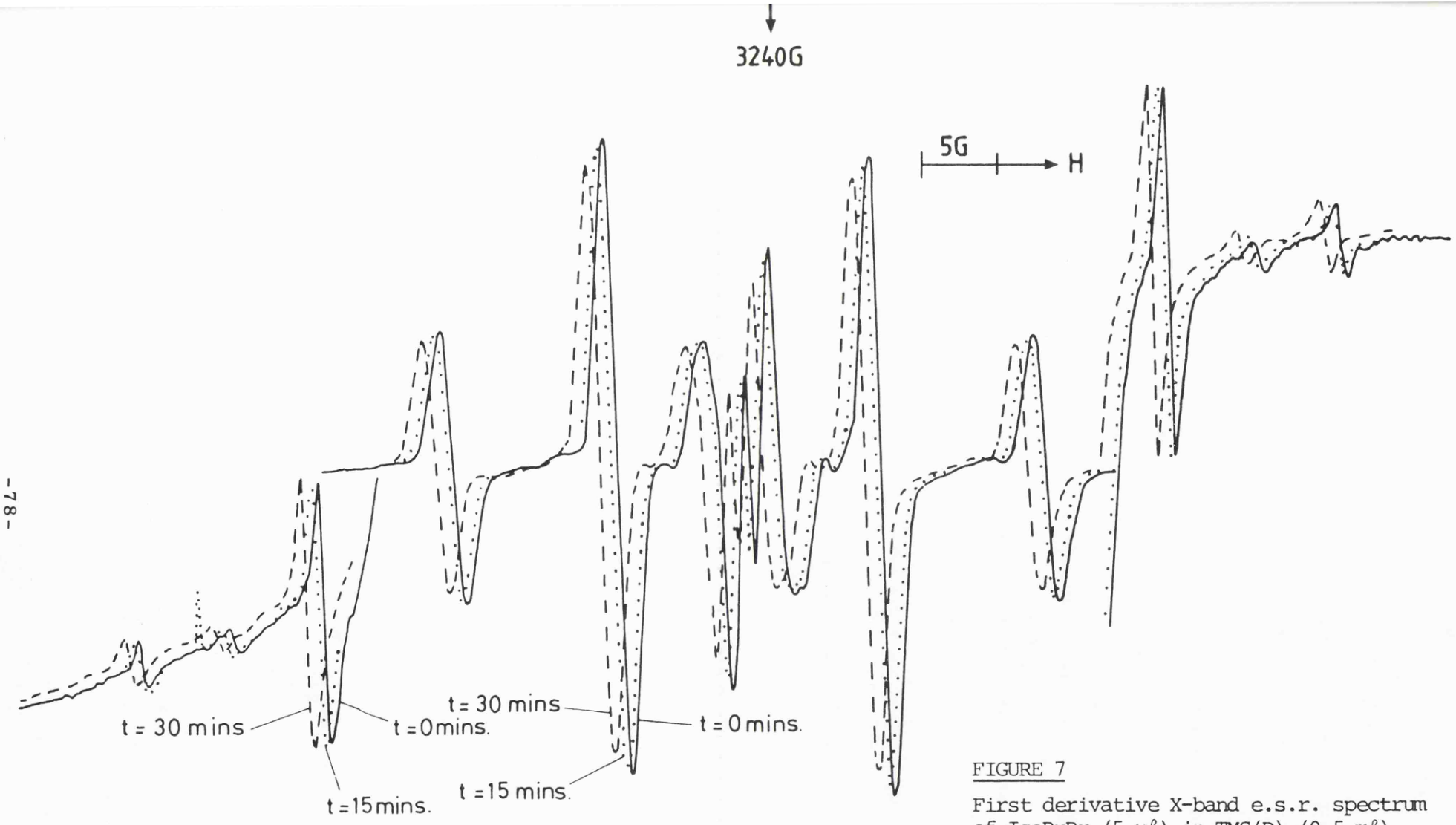

FIGURE 7

First derivative X-band e.s.r. spectrum of IsoBuBr (5 μℓ) in TMS(D) (0.5 mℓ) after exposure to ^{60}Co γ-rays at 77 K. The sample was then maintained in the cavity at a controlled temperature.

TABLE 1

IsoBuBr (5 μℓ) in TMS-d_{16} (0.5 mℓ)

Time (mins)	Temp. (°C)	IsoBu• peak-peak (mm)	IsoBu• gain	Bu^t• peak-peak (mm)	Bu^t• gain
0	-170	80	8×10^1	50	8×10^3
10	"	80	"	52	"
25	"	80	"	54	"
40	"	81	"	55	"
55	"	81	"	55	"
65	"	81	"	55	"
70	-165	80	"	60	"
85	"	80	"	60	"
100	"	80	"	60	"
110	"	80	"	60	"
115	-160	79	"	63	"
120	"	76	"	62	"
135	"	72	"	66	"
137	"	71	"	67	"
150	"	69	"	67	"
165	"	66	"	69	"
180	"	63	"	68	"
195	"	60	"	69	"

GRAPH 1

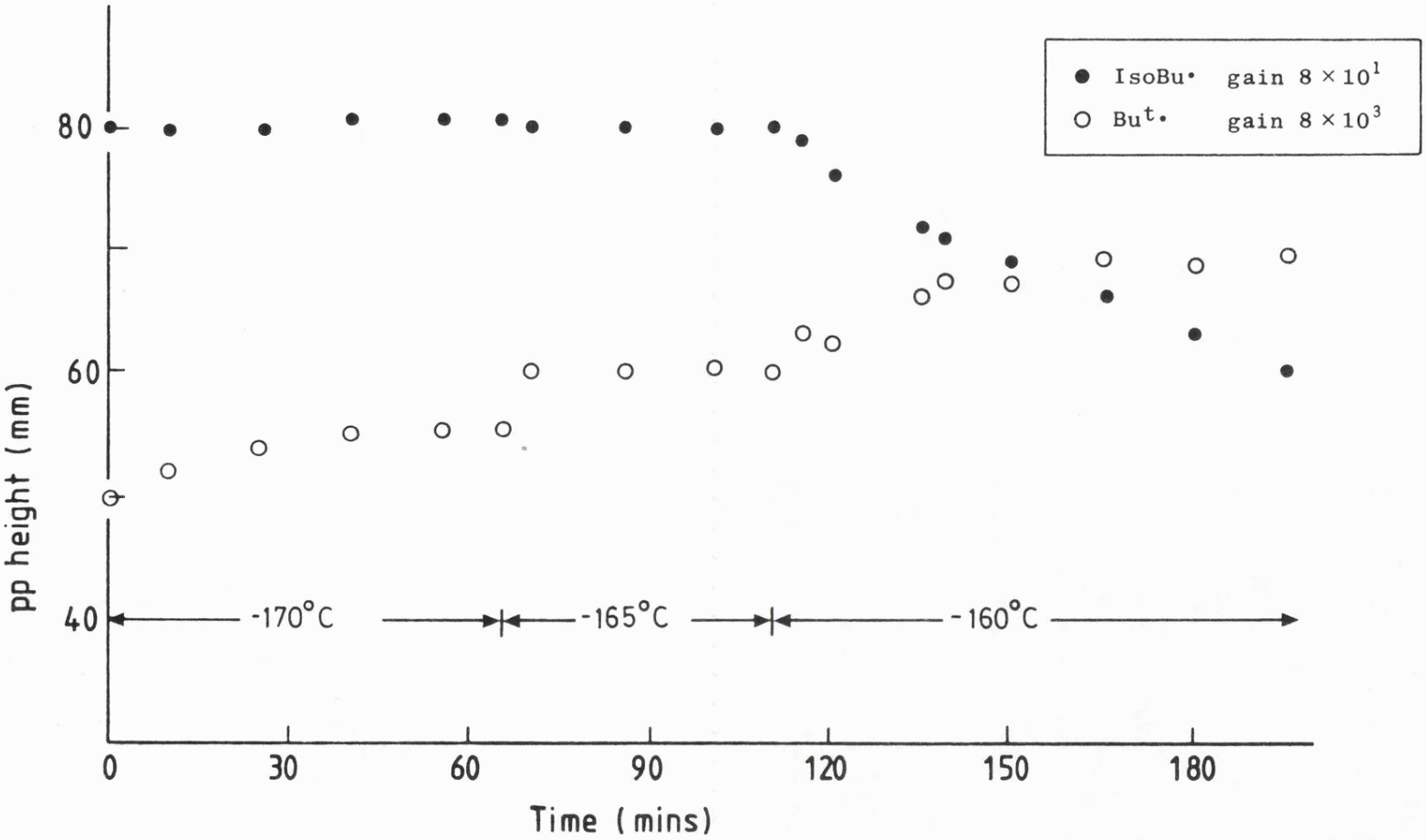
● IsoBu• gain 8 × 10¹
○ But• gain 8 × 10³
80
60
40
pp height (mm)
-170°C
-165°C
-160°C
0
30
60
90
120
150
180
Time (mins)

3. If a self-reaction occurred, i.e. IsoBuBr as a source of protons, α-bromo radicals would be generated. None were seen.
4. The purest available $Si(CD_3)_4$ was used. No ^2H pick-up was observed.
5. Unfortunately, the concentration/rate experiment did not work. This would have enabled the determination of $t_{\frac{1}{2}}$ which is independent of initial concentration in first-order rates.
6. In a CD_3OD matrix diluted $Bu^t\cdot$ could be converted by hν to IsoBu· with no ^2H pick-up.

Considering the above points, it is the opinion of this laboratory that a 1,2-intramolecular shift occurred.

REFERENCES FOR CHAPTER 5

1. I. G. Smith and M. C. R. Symons, J. Chem. Soc., Perkin Trans. 2, 1979, 1362.
2. M. Iwasaki and K. Toriyama, J. Chem. Phys., 1967, 46, 2852.
3. R. V. Lloyd and D. E. Wood, J. Am. Chem. Soc., 1975, 97, 5986.
4. D. E. Wood and R. V. Lloyd, Tetrahedron Letters, 1976, 5, 345.
5. M. C. R. Symons and I. G. Smith, J. Chem. Soc., Perkin Trans. 2, 1980, 1362.
6. P. B. Ayscough and C. Thompson, Trans. Faraday Soc., 1962, 58, 1477.
7. R. W. Fessenden and R. H. Schuler, J. Chem. Phys., 1963, 39, 2147.
8. K. P. Madden and W. A. Bernard, J. Phys. Chem., 1980, 84, 1712.
9. M. C. R. Symons, G. W. Eastland and L. R. Denny, J. Chem. Soc., Faraday Trans. 1, 1980, 76, 1868.
10. G. W. Eastland and M. C. R. Symons, J. Phys. Chem., 1977, 81, 1502.
11. E. D. Sprague and F. Williams, J. Chem. Phys., 1971, 54, 5425.
12. S. P. Mishra, Electron Spin Resonance Studies of Irradiated Alkyl Halides, Ph.D. Thesis, 1976.

CHAPTER 6

The β-Bromo Species

6.1 INTRODUCTION

The mechanism of halogen addition to olefins has long been of interest to organic chemists.[1] Of particular interest has been the geometry of the intermediate $R_2\dot{C}$-CR_2Hal which has been formulated as both symmetric and asymmetric (I and II).

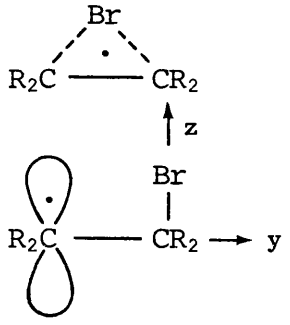

I Symmetric structure

II Asymmetric structure

Most studies have favoured the presence of bridged intermediates but symmetry is not established. Skell *et al.*,[2] using ^{82}Br as a label, concluded that the radical $CH_3CH(Br)$-$\dot{C}HCH_3$ must be either symmetrical or that the bromine atom moves with a frequency greater than 10^{11} sec^{-1}. The chloro-radical analogue is found to be unsymmetrical with migration frequency of less than 10^8 sec^{-1}.

Bowles *et al.*[3] have detected the radical $\dot{C}H_2$-CH_2Cl in fluid conditions at *ca.* -60°C. They deduced from the β-proton hyperfine coupling of 11.5 G that the radical is unsymmetrical and the $H_2\dot{C}$- group normal for an alkyl radical.

In previous work in this laboratory, Symons, Lyons *et al.*,[4] exposure of a variety of alkyl halides to γ-irradiation gave species which exhibited a large hyperfine interaction with the β-halogen atoms. An interesting aspect of this work is the 1,2 halogen migration for radicals derived from *t*-butyl chloride and bromide giving $Me_2\dot{C}$-CH_2Hal even at 77 K.[5]

The ESR spectra of γ-irradiated alkyl bromides are dominated by alkyl

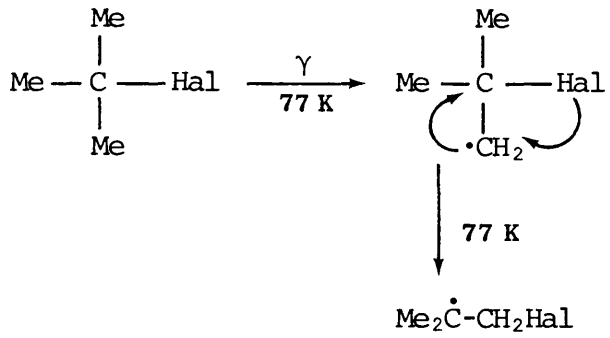

radicals. Additionally, α-halogen radicals can be observed and lines attributable to Br_2^-.

The most characteristic features of the β-bromo radical generated from t-butyl bromide are:-

(i) In tetramethyl silane it was possible to resolve the 6 methyl protons, ca. 13 G on each of the 4 ^{79}Br A_x and 4 ^{81}Br A_x components. This allowed A_x (^{79}Br) and A_x (^{81}Br) to be extracted.
A_x (^{79}Br) = 338.0 G; A_x (^{81}Br) = 362.0 G.

(ii) The $M_I = +\frac{1}{2}$ line was the most intense at X-band.

(iii) The proton couplings of 13 G are in reasonable agreement with the 17 G from the analogous β-chloro radical.

Of interest is the decrease in proton couplings but an increase in halide coupling when comparing chloro- and bromo- radicals. The classical conformation of the β-chloro radical, $Me_2\dot{C}CH_2Cl$, would predict proton couplings of ca. 22 G for the two methyl groups and ca. 13 G for the methylene protons, i.e. a symmetric model with C_1 planar and C_2 tetrahedral. The actual values are ca. 17 G and ca. 5 G respectively. The halide atom lies asymmetric in the radical forcing the methylene protons into the radical plane. This conformation serving to stabilize the radical. It would be expected that the $Me_2\dot{C}CH_2Br$ would also follow this trend with the resulting decrease in proton couplings and an increase in the halide coupling, as is the case.

This Chapter is devoted to experiments on β-bromo radicals generated from t-butyl bromide and from 2,3 dibromo-2,3 dimethyl butane. The rationale being that the two methyl groups on C_2 and C_3 would serve to both stabilize the radical and favour the formation of a symmetric species.

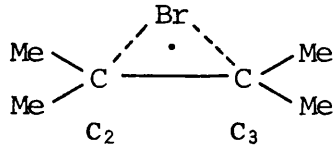

6.2 EXPERIMENTAL

Initially, 2,3 dibromo-2,3 dimethyl butane was prepared: 2,3 dimethyl-but-2-ene (120 cm^3) was dissolved in dry carbon tetrachloride (250 cm^3). The mixture was continuously agitated under an atmosphere of dry nitrogen and kept below 0°C away from direct light. Bromine (47 cm^3) was added in a dropwise fashion, the rate being altered to keep the temperature below 0°C. The white crystalline solid that precipitated out was filtered and washed with cold methanol. The solid was identified by mass spectrometry and found to be NMR pure. It had a melting point of 124°C.

Also prepared was 2 bromo-2,3 dimethyl butane. A similar method of preparation was employed except, in this case, hydrogen bromide was added. Two methods were used to produce bromine as the compound was produced more than once. Initially, hydrogen bromide was produced by adding bromine to tetralin and the gas produced passed through wash bottles of tetralin prior to entering the reaction vessel. Bottled HBr was also used. The white crystalline solid produced was identified by mass spectrometry and found to be NMR pure with a melting point of 24.5°C.

6.3 RESULTS AND DISCUSSION

Previous experimental work using t-butyl bromide as a precursor was repeated.[4,5,7] It was possible to reproduce all the spectra previously reported (Figures 1.1 and 1.2). Additionally, attempts were made to improve resolution by optical bleaching, with no success. Traces of bromine were added to the samples prior to irradiation with the result that no β-bromo radicals were formed. It was hoped that more Br_2^- would be formed, thereby allowing a more detailed examination of this species and the effects of annealing, etc. However, the addition of bromine completely suppressed any formation of β-species. This fact was used to good effect (other dibromo-species).

Prior to using 2,3 dibromo-2,3 dimethyl butane other precursors were tried:

[1] 2,3-Dimethyl-but-2-ene was dissolved in carbon tetrabromide and the solution irradiated. No β-species were generated.

[2] Traces of bromine were added to 2,3 dimethyl-but-2-ene and the mixture rapidly cooled to 77 K. The temperature of the sample was varied in the ESR cavity. No β-species were generated.

The following experiments were tried using $Me_2BrC\text{-}CBrMe_2$.

[1] $Me_2BrC\text{-}CBrMe_2$ in TMS.
[2] $Me_2BrC\text{-}CBrMe_2$ in adamantane (co-sublimation).
[3] $Me_2BrC\text{-}CBrMe_2$ pure.
[4] $Me_2BrC\text{-}CBrMe_2$ + bromine.
[5] $Me_2BrC\text{-}CBrMe_2$ + TMS + bromine.

Irradiation of all the above failed to produce any β-species.

A solution of $Me_2BrC\text{-}CBrMe_2$ in CD_3OD (5% mol), γ-irradiated for 3 hours, produced a β-bromo radical (Figure 2). It had characteristics of previous β-radicals, e.g. $M_I = \frac{1}{2}$ being the most intense line. Additionally, the following factors could be seen; (i) A_x ca. 350 G, (ii) no hyperfine

FIGURE 1.1

First derivative X-band e.s.r. spectrum for Bu^tBr in TMS after exposure to ^{60}Co γ-rays at 77 K.

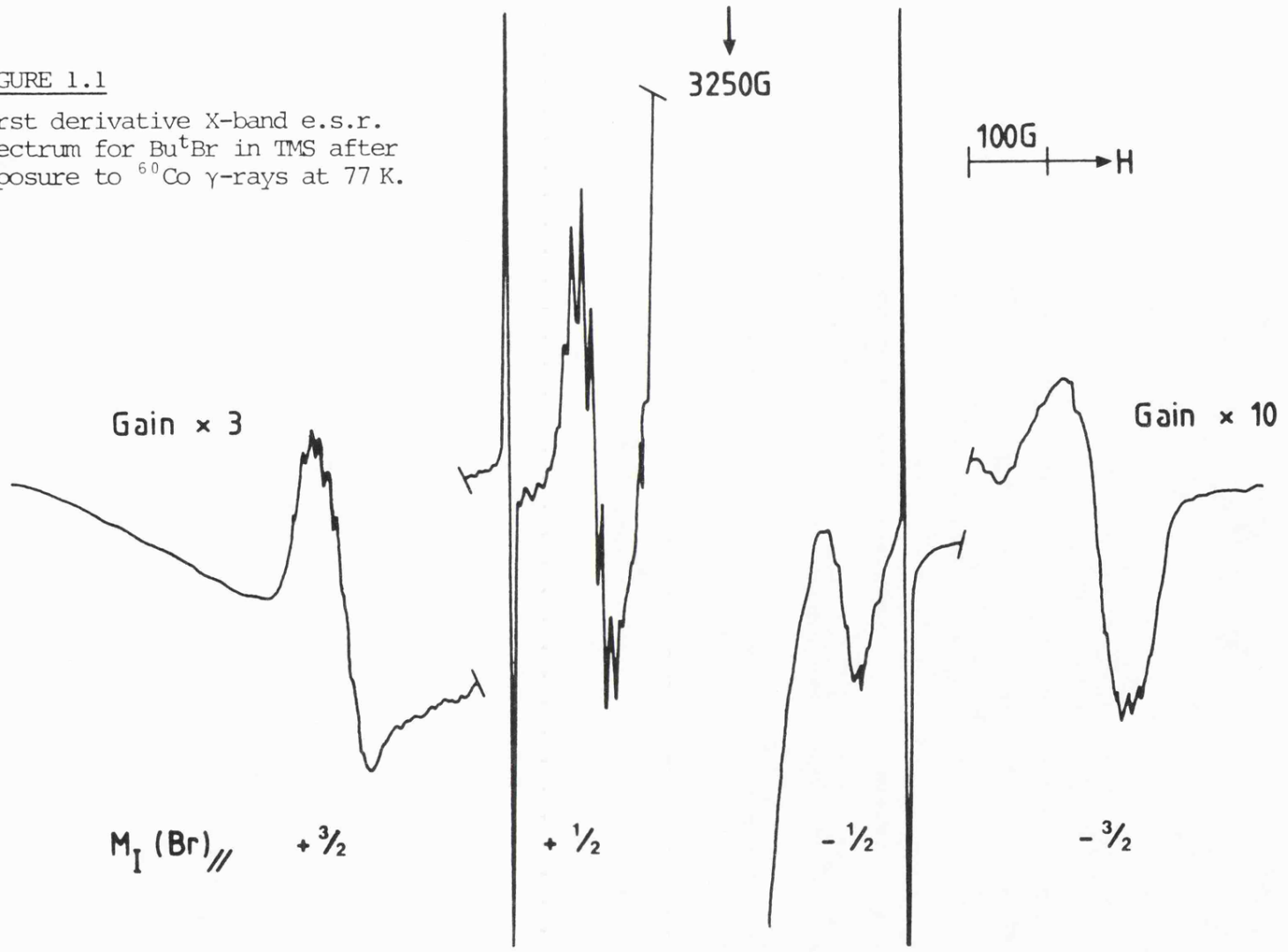

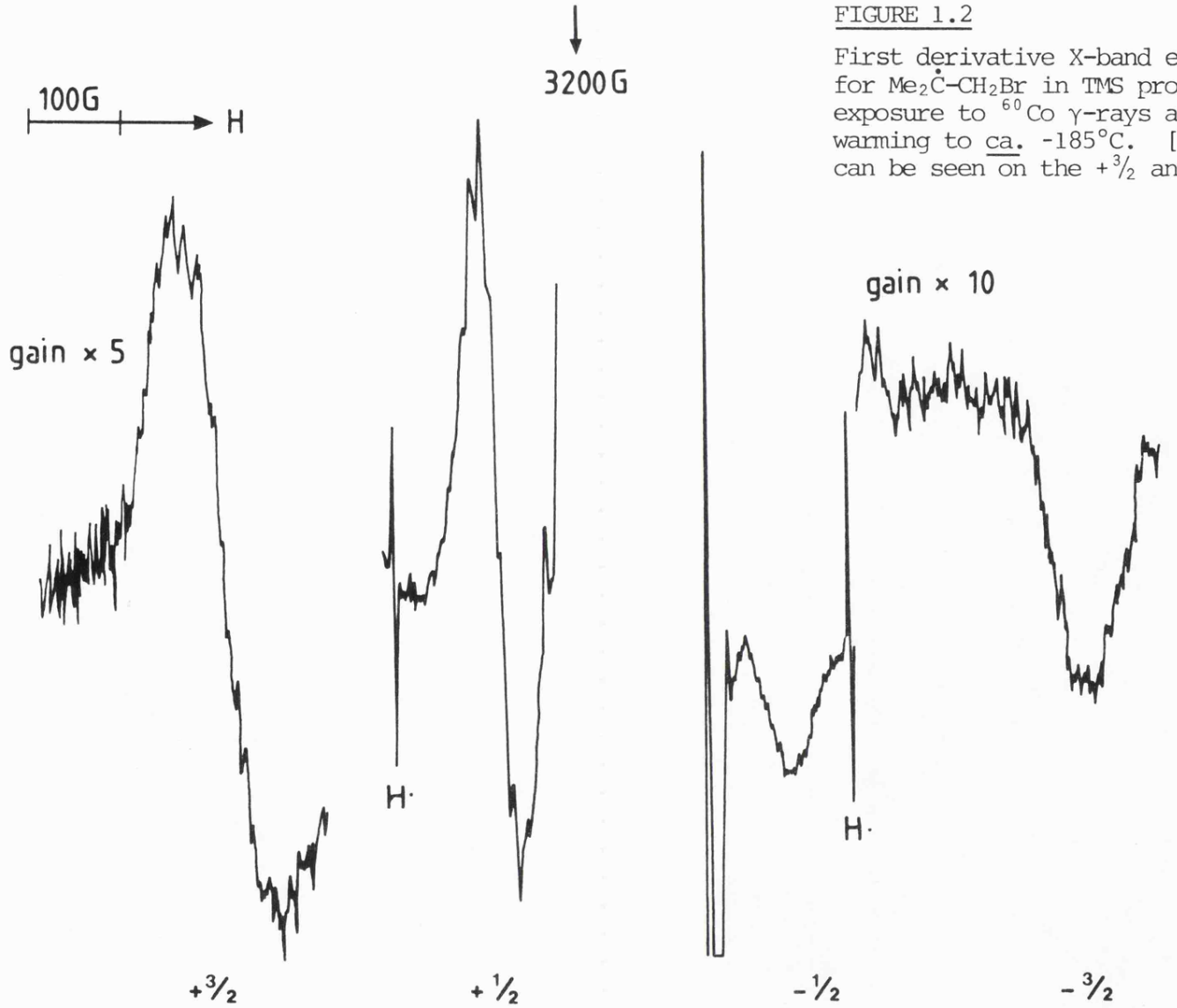

FIGURE 1.2

First derivative X-band e.s.r. spectrum for $Me_2\dot{C}-CH_2Br$ in TMS produced by exposure to ^{60}Co γ-rays at 77 K and warming to ca. -185°C. [Proton resolution can be seen on the $+^3/_2$ and $+^1/_2$ lines.]

FIGURE 2

First derivative X-band e.s.r. spectrum for $Me_2C(Br)-CMe_2(Br)$ in CD_3OD after exposure to ^{60}Co γ-rays at 77 K and warming to ca. 100 K, showing features assigned to $Me_2CCMe_2(Br)$ radicals. The parallel features for ^{81}Br and ^{79}Br are indicated. The splitting resolved for the $M_I = \pm 3/2$ lines is irreversibly lost on cooling to 77 K.

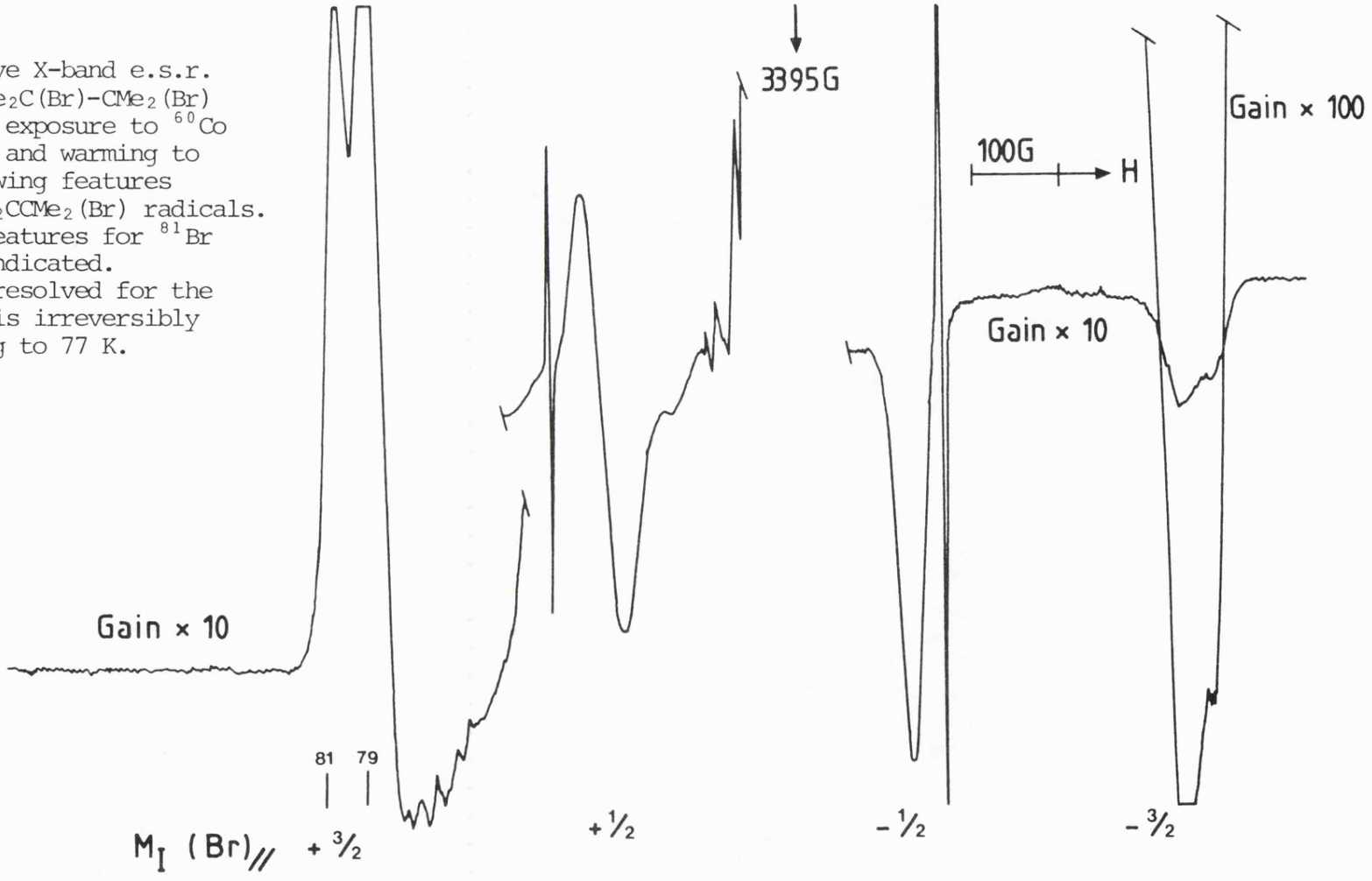

features could be distinguished, (iii) a doublet on the $+^3/_2$ and $-^3/_2$ line of ca. 36 G attributable to isotopic $^{79/81}Br$. In attempts to improve resolution the sample was annealed. This resulted in loss of the β-radical with an increase in the relative intensity of Br_2^-.

An almost identical spectrum was produced by a solution of $Me_2BrC-CBrMe_2$ in MeTHF (Figure 3). Again no hyperfine structure was detected. All attempts to resolve any of the lines by differentiation failed. Solution of $Me_2BrC-CBrMe_2$ in other solvents, e.g. TMS, CD_3CN, etc., failed to generate any β-bromo radicals.

Detailed experimentation on the β-radical in a CD_3OD matrix failed to improve resolution. Variable temperature experiments indicated the species was stable up to -175°C, any higher resulted in a rapid loss of signal. Radiation, e.g. high/low pressure UV, visible, reduced signal intensity. The addition of bromine to the sample prior to irradiation completely suppressed the formation of the β-radical. In an attempt to improve resolution, several samples were run at 4-20 K (Figure 4). There were no significant differences in the spectra except that the parallel features for ^{81}Br and ^{79}Br were lost.

Finally, a single crystal of $Me_2BrC-CBrMe_2$ was grown which would have enabled complete elucidation of all parameters. However, no β-species could be generated in the pure material.

As a check that the spectral lines came from the same species, Q-band experiments were conducted (Figure 5).

Dilute solutions of $Me_2CH-CBrMe_2$ in CD_3OD and MeTHF also on irradiation produced the β-bromo species. It was hoped that, due to some undefined matrix effect, resolution would be better. The spectra were not significantly different.

FIGURE 3

First derivative X-band e.s.r. spectrum for $Me_2\dot{C}-CBrMe_2$ in MeTHF produced by exposure to ^{60}Co γ-rays at 77 K and warming to ca. -185°C. [The parallel features for ^{81}Br and ^{79}Br are indicated.]

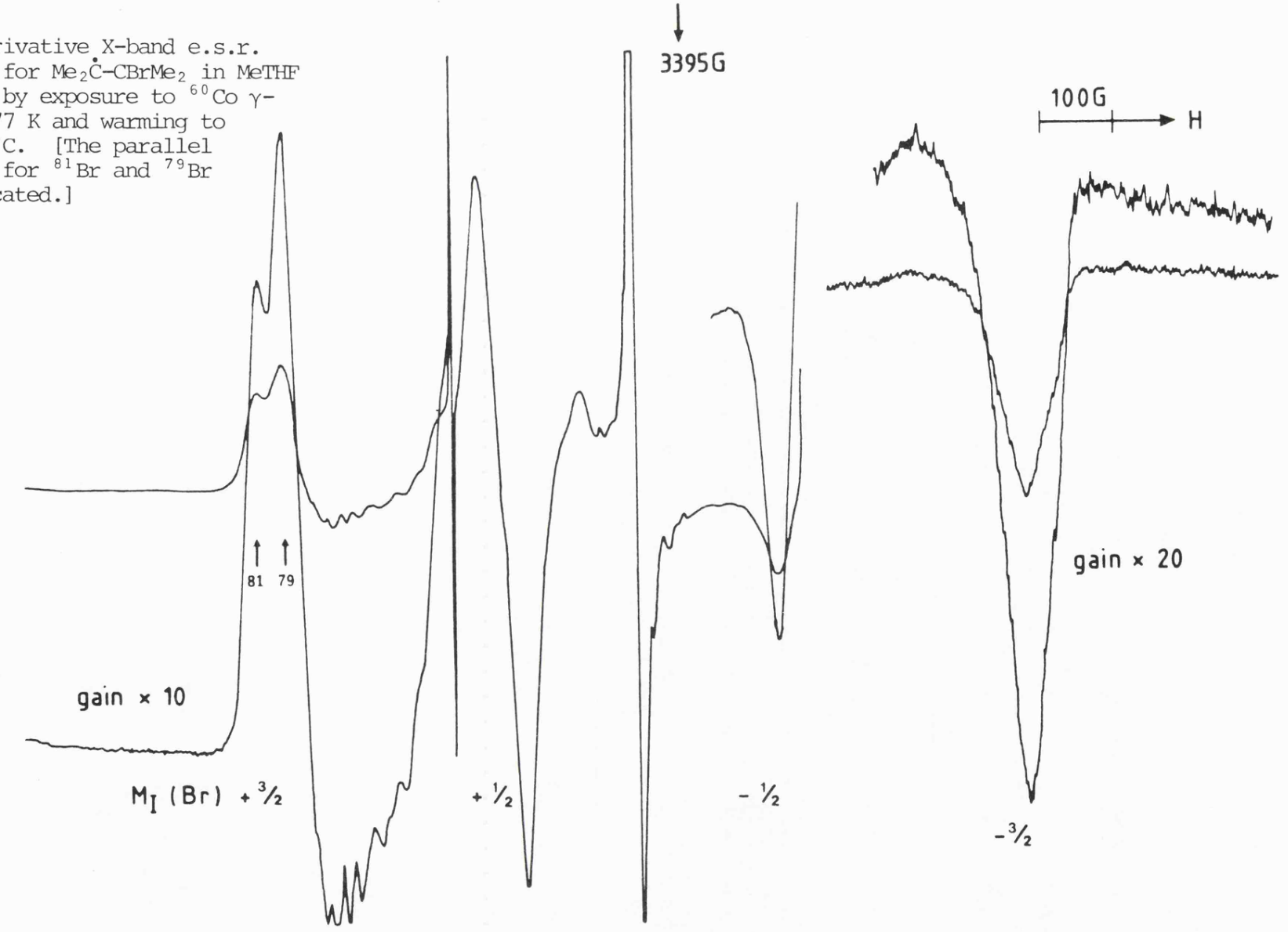

FIGURE 4

First derivative X-band e.s.r. spectrum for $Me_2C(Br)-CMe_2(Br)$ in CD_3OD after exposure to ^{60}Co γ-rays at 77 K and cooling to 20 K.
[Note the parallel features for ^{81}Br and ^{79}Br are lost.]

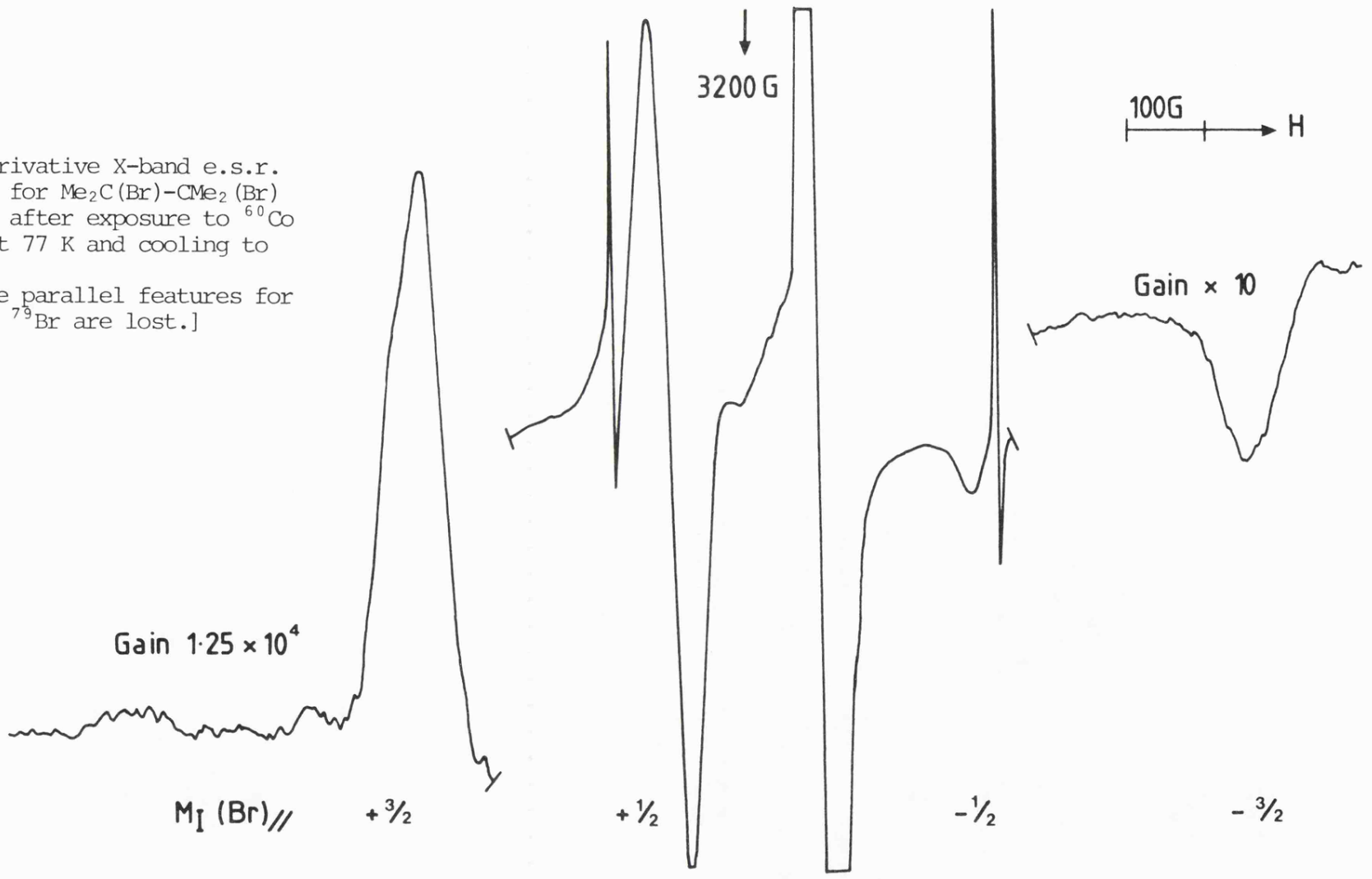

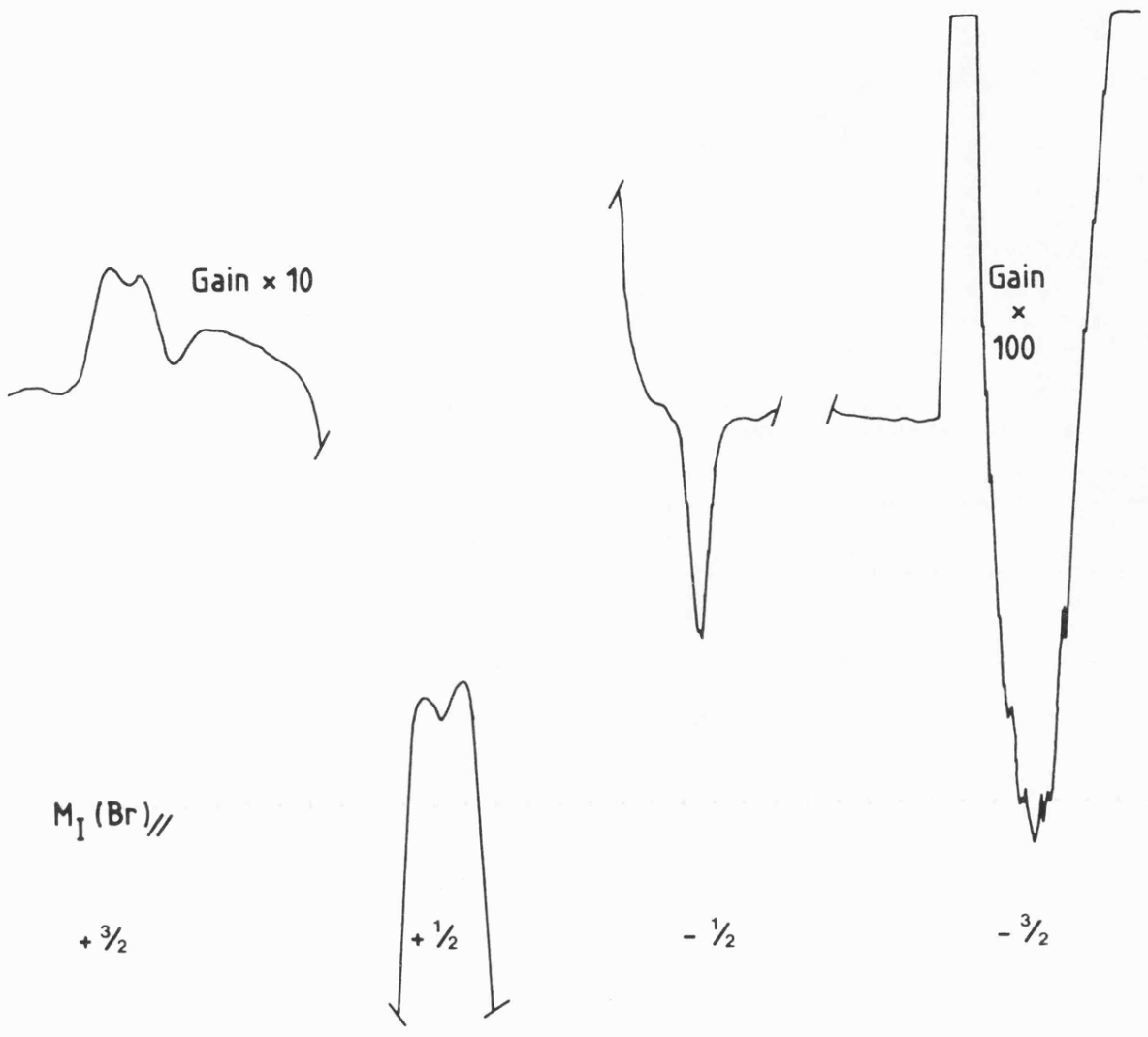

FIGURE 5

First derivative Q-band e.s.r. spectrum for $Me_2C(Br)-CMe_2(Br)$ in CD_3OD after exposure to ^{60}Co γ-rays at 77 K showing features assigned to $Me_2C-CMe_2(Br)$ radicals.

6.4 RESOLUTION ENHANCEMENT

All attempts to improve resolution by conventional methods failed. In the first instance, it was assumed that the species generated was symmetric or asymmetric. In the first case, one would expect 12 equivalent protons with a hyperfine splitting of ca. 6 G. In the second case, there would be inequivalence with 6 equivalent protons being successively split by 6 other equivalent protons with a smaller coupling constant. The actual values of the coupling constants depending on the degree of asymmetry but <13 G.

Simple simulation techniques were employed to determine the characteristics of spectra produced with different numbers of equivalent protons. Not all the parameters of the β-bromo species were known, hence first derivative and absorption curves modulated with hyperfine lines were used. No attempts were made to reproduce the complete spectrum complete with A_x, A_y and A_z, etc. The variables used were (i) line width, (ii) percentage Lorentzian and (iii) truncation width. The number of data points used was 2048.

In order to test the simulation program, the spectra for ^{79}Br (A_x = 338 G) and ^{81}Br (A_x = 362 G) were modulated with 7 lines of ca. 13 G splitting and the two spectra added. The variables were altered until it was possible to produce spectra with the correct number of lines. The addition of absorption curves was also tried.

The outer ($M_I = 3/2$) line with the 36 G doublet splitting from ^{81}Br and ^{79}Br components could be reproduced with 13 binomial components of ca. 6 G. Any other permutation failed to reproduce this doublet (Figures 6 and 7).

Various attempts were tried at resolution enhancement. Due to instrumental limitations, all enhancement techniques employed were done

FIGURE 6.1

Simulated absorption spectrum of $Me_2\dot{C}(Br)CMe_2$, i.e. twelve equivalent protons with a 6 G splitting.

$A_{max}(^{81}Br)$ = 362 G
$A_{max}(^{79}Br)$ = 338 G
Number of data points = 2048
Line width = 5.0
Percentage Lorentzian = 80
Truncation width = 8.0

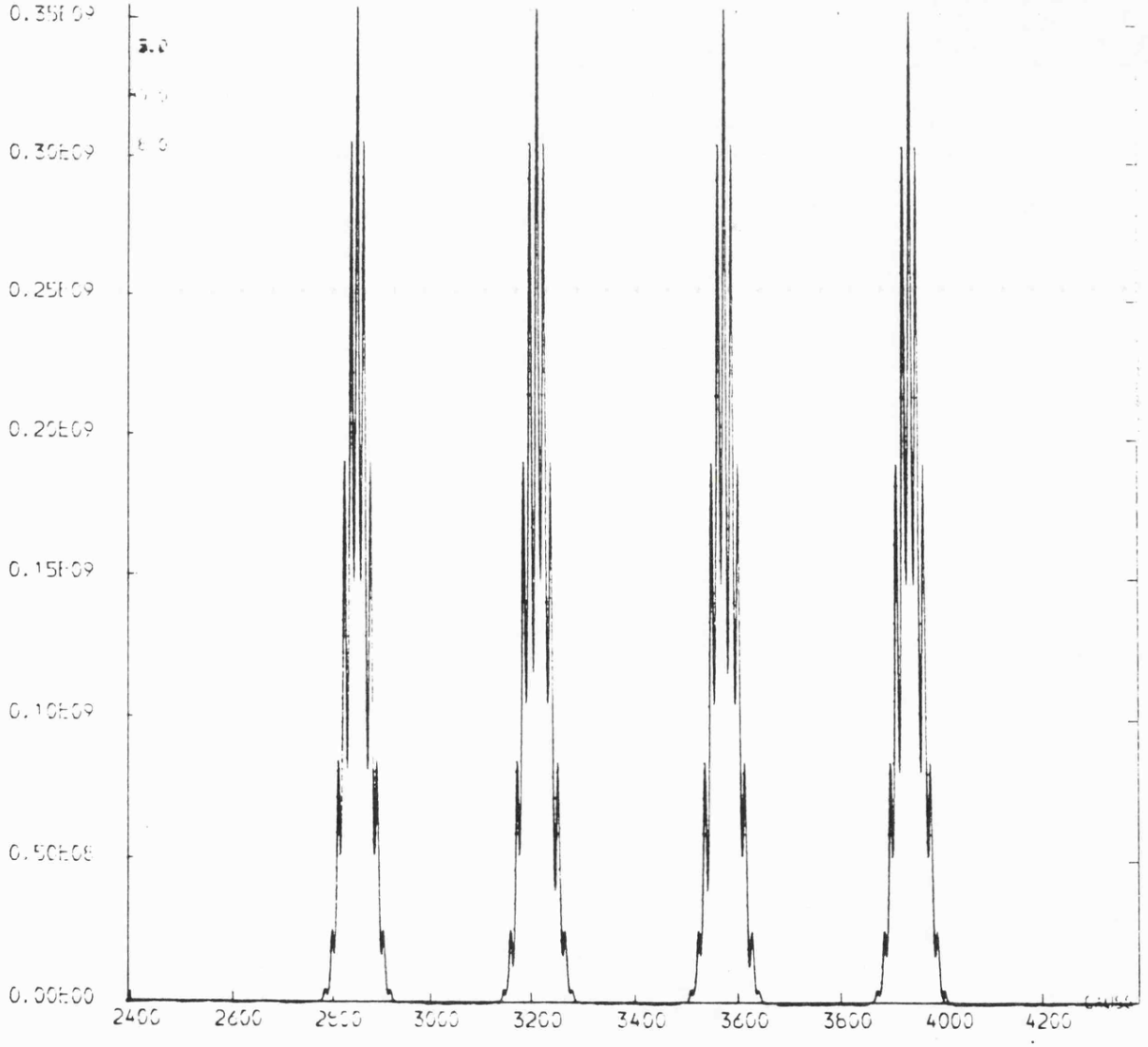

FIGURE 6.2

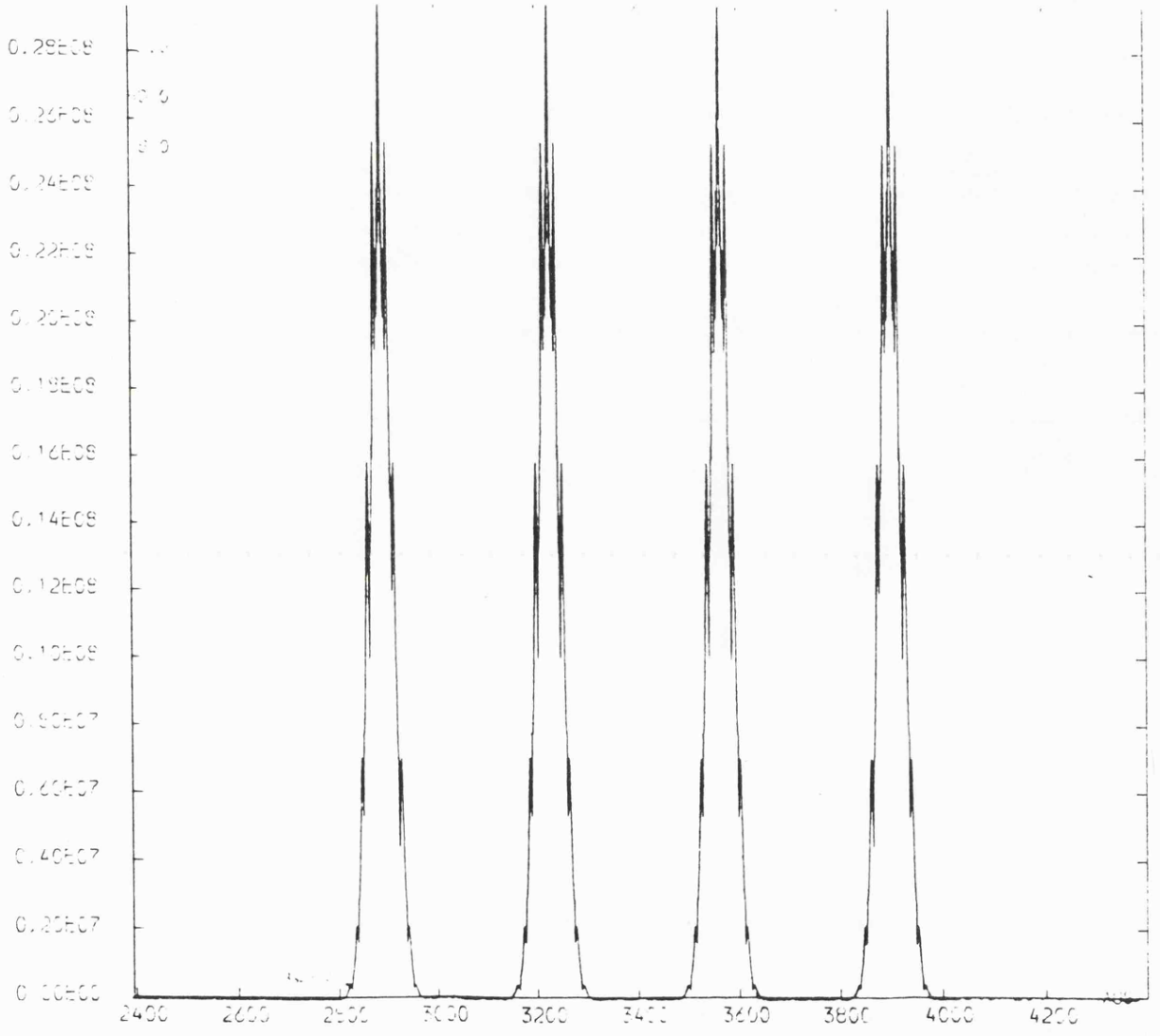

FIGURE 6.3

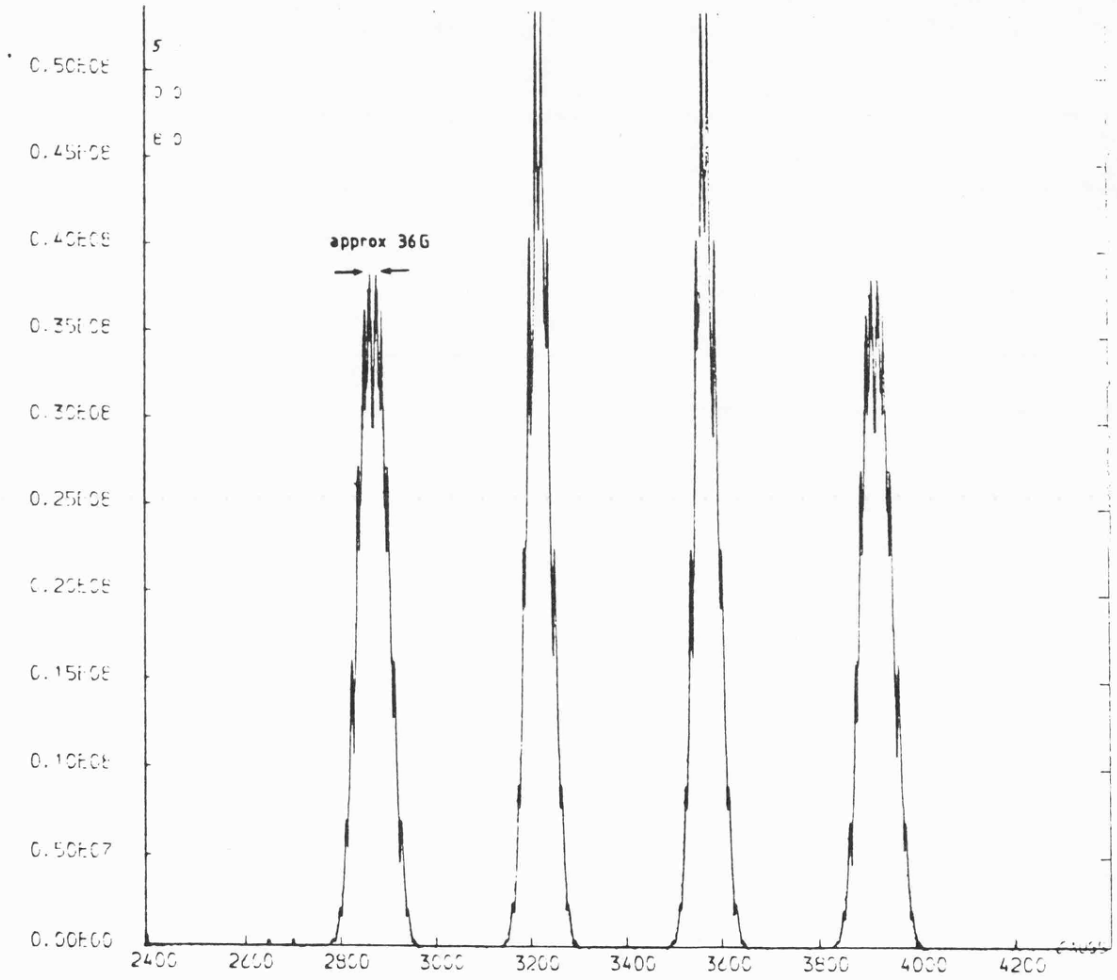

FIGURE 7.1

Simulated first derivative spectrum of $Me_2\dot{C}(Br)CMe_2$, i.e. twelve equivalent protons with a 6 G splitting.

$A_{max}(^{81}Br)$ = 362 G
$A_{max}(^{79}Br)$ = 338 G
Number of data points = 2048
Linewidth = 5.0
Percentage Lorentzian = 80
Truncation width = 8.0

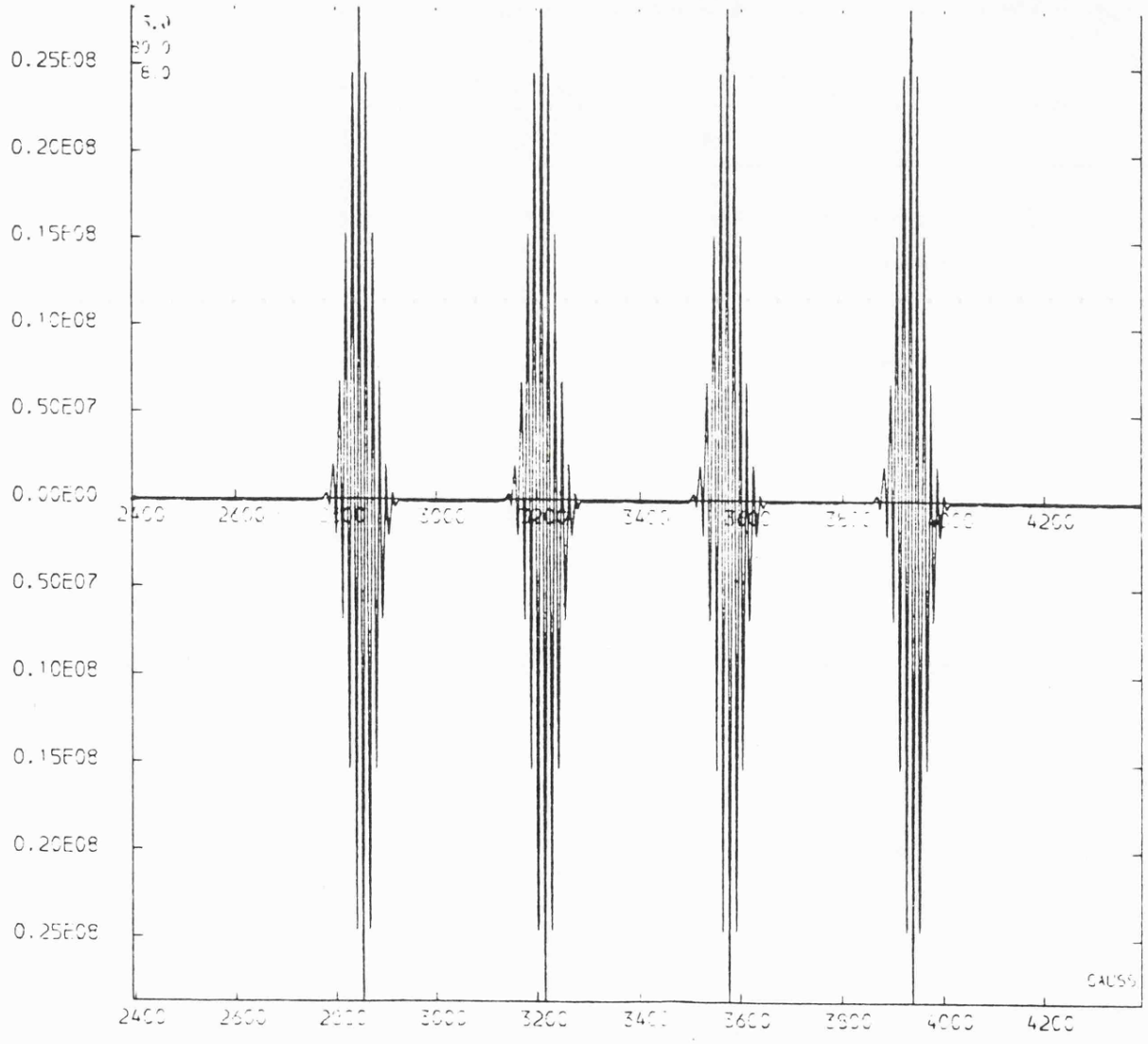

FIGURE 7.2

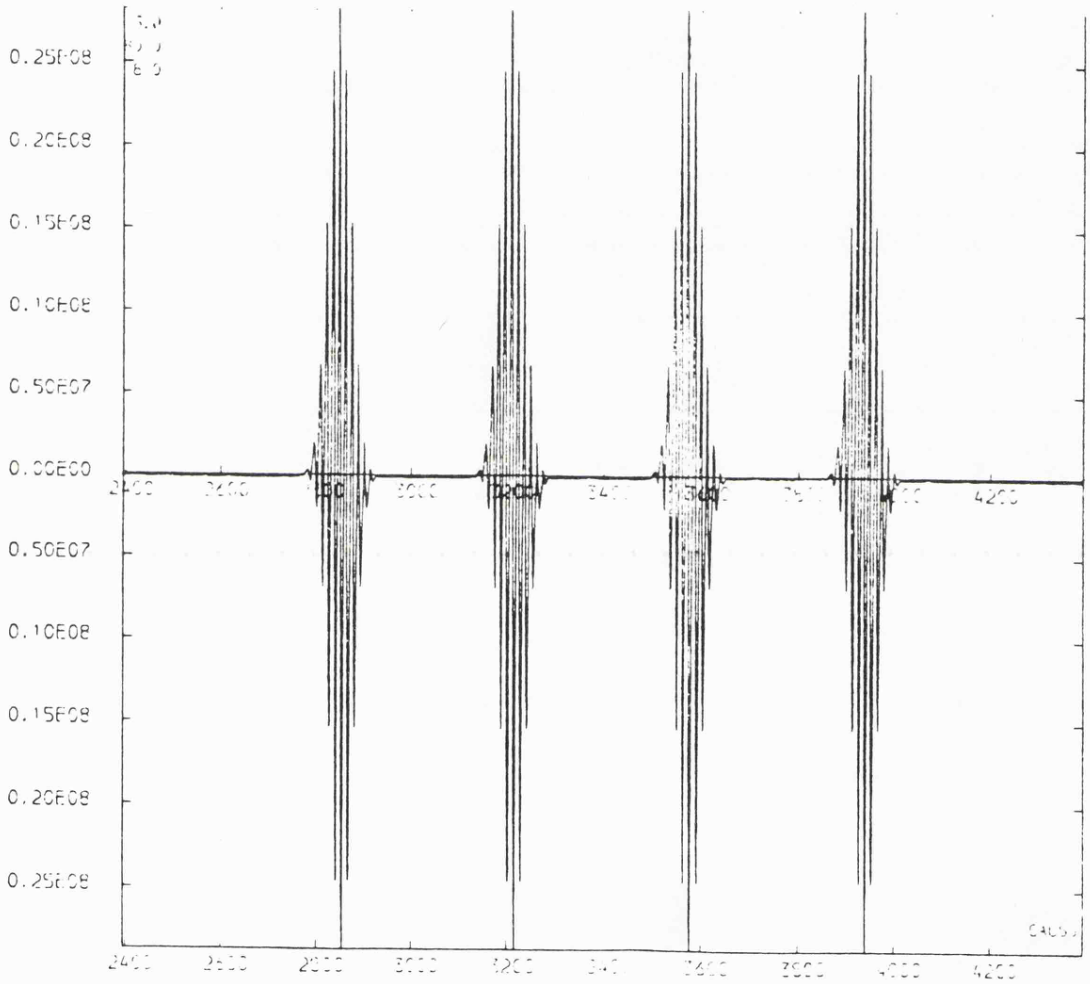
0.25E08
0.20E08
0.15E08
0.10E08
0.50E07
0.00E00
0.50E07
0.10E08
0.15E08
0.20E08
0.25E08
2400
2600
2800
3000
3200
3400
3600
3800
4000
4200

FIGURE 7.3

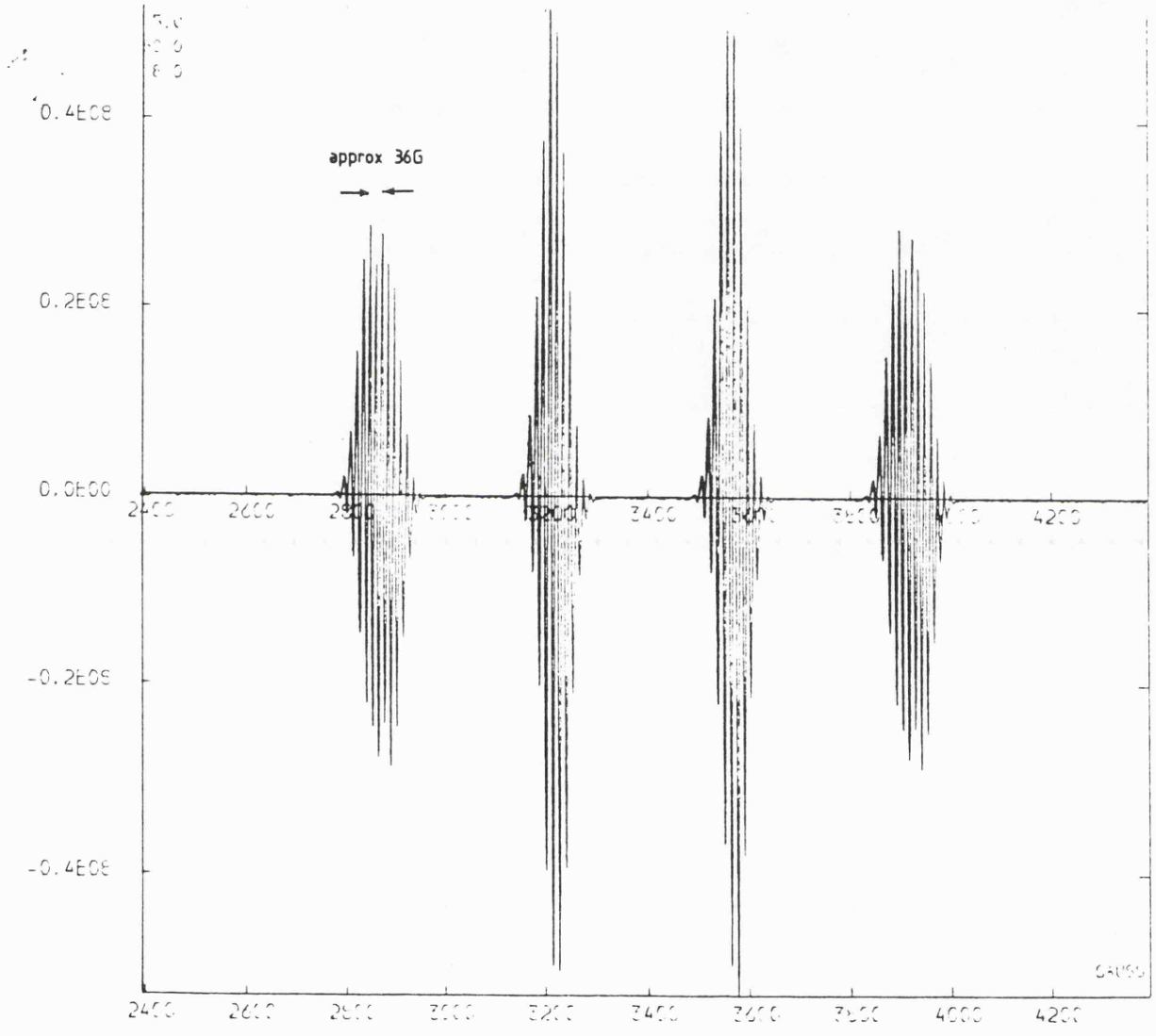
approx 36G
0.4E08
0.2E08
0.0E00
-0.2E08
-0.4E08
2400
2600
2800
3000
3200
3400
3600
3800
4000
4200

on the mainframe 'CYBER'. Initially, data from the ESR spectrometer was digitised and transferred via paper tape. However, at a later date it was possible to transfer data directly.

In the first instance, simple derivative techniques were tried, including the addition of 1st., 3rd. and 5th. derivatives. Some enhancement was observed but was not satisfactory. The signal/noise ratio was poor.

A more powerful technique involved Fourier Transform.[8] The digitised line was converted to the frequency domain, the 1st., 3rd. and 5th. derivatives could be added and/or a change in linewidth could be made. It was also possible to cancel some high frequency noise thereby improving the signal/noise ratio of the final spectrum.

Using this technique several experiments were conducted.

(i) A weak pitch signal was resolved as a control experiment. No hyperfine structure exists on a weak pitch signal and none was found, i.e. no spurious signals generated or artefacts were produced.

(ii) The $Me_2\dot{C}-CBrH_2$ species in which it was possible to resolve hyperfine coupling was overmodulated. Using the enhancement technique, it was possible to extract lines with ca. 13 G coupling.

(iii) The technique was employed on the $+^3/_2$ line of the new (symmetric?) β-species. It was possible to resolve lines with ca. 10 G splitting at 77 K and ca. 6 G splitting at 100 K (Figures 8, 9 and 10).

In the last two experiments not all lines could be detected due to the relative intensities given by the ratio of the degeneracies of the levels between which transitions occur, i.e. coefficients in the expansion of $(1+x)^n$. As a precaution the $+^3/_2$ lines were used, no additional features exist under this line. The $-^3/_2$ lines were too weak to be of use.

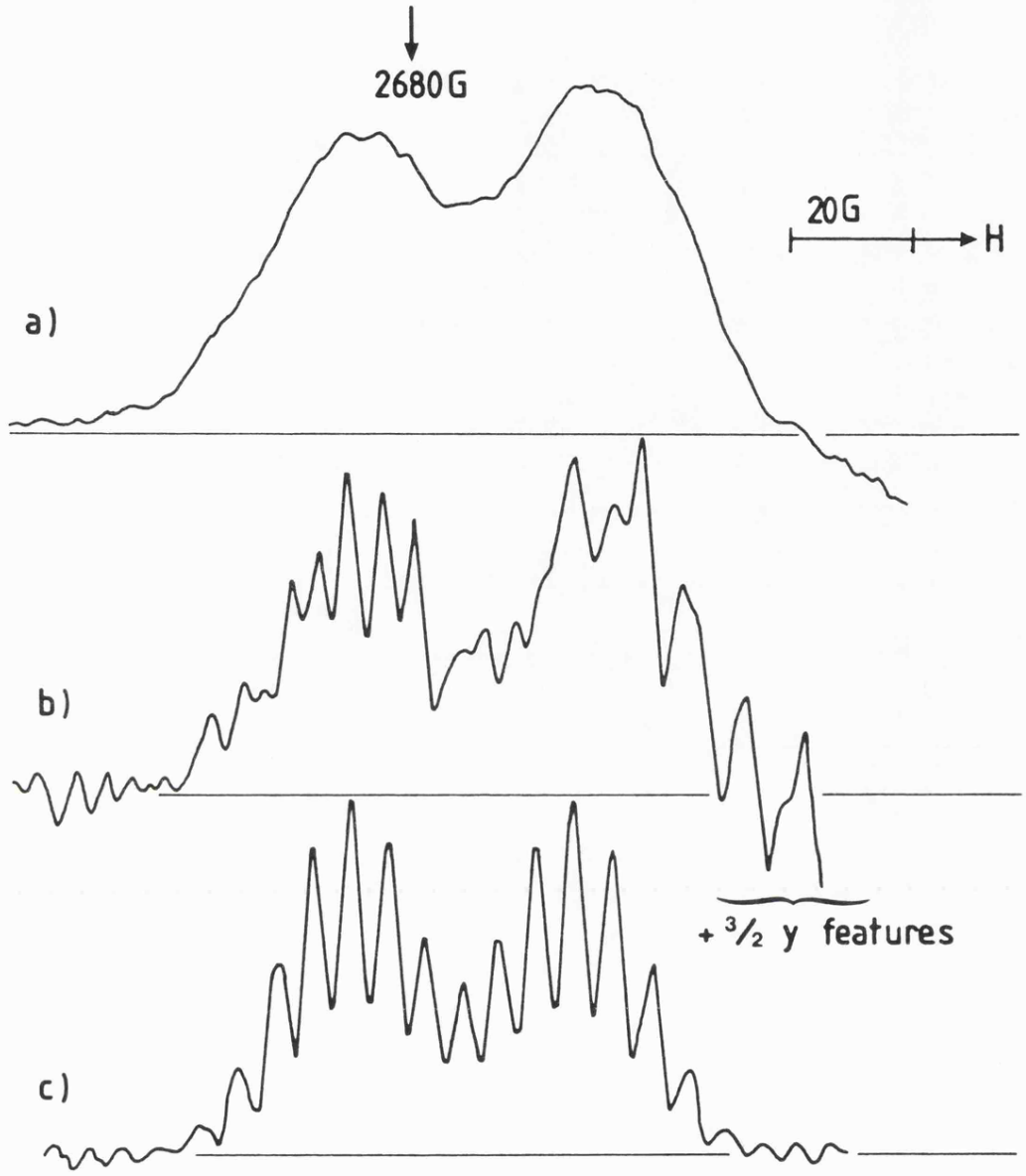

FIGURE 8

a) The $M_I = +3/2$ Z line of the $Me_2\dot{C}CMe_2(Br)$ radical at 100 K. The resolved doublet due to the ^{81}Br and ^{79}Br parallel features is clearly seen.
b) Resolution enhanced spectrum of (a) showing lines split by ca. 5.75 +/-.25 G. Some features from the Y-components interfere in the high-field region.
c) Resolution enhanced spectrum of a synthesised spectrum of 2 sets (split by 34.5 G) of 13 lines split by 5.75 G.

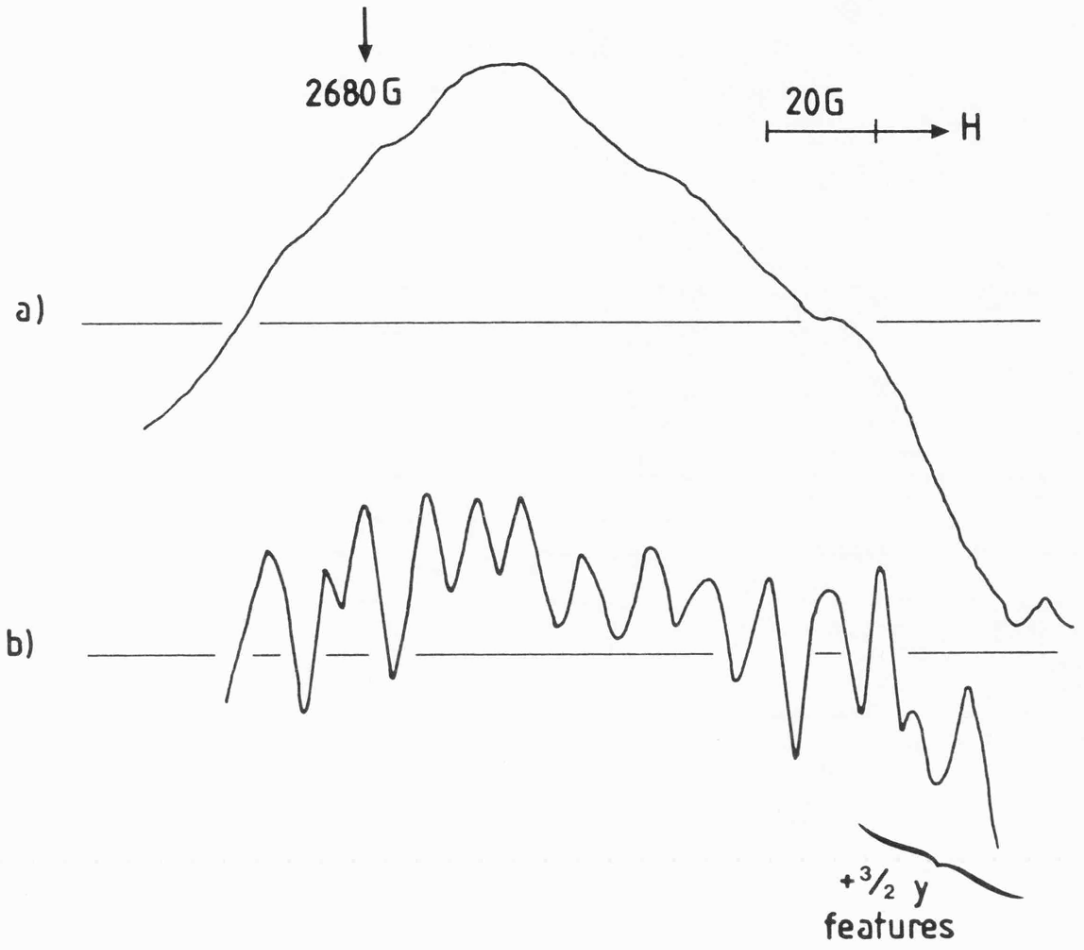

FIGURE 9

a) The $M_I = +3/2$ Z line of the $Me_2\dot{C}CMe_2(Br)$ radical at 77 K. The resolved doublet due to the ^{81}Br and ^{79}Br parallel features is lost at this temperature.
b) Resolution enhanced spectrum of (a) showing lines split by ca. 9.0 ± 1.0 G. Some features from the $+3/2$ Y line interfere in the high-field region.

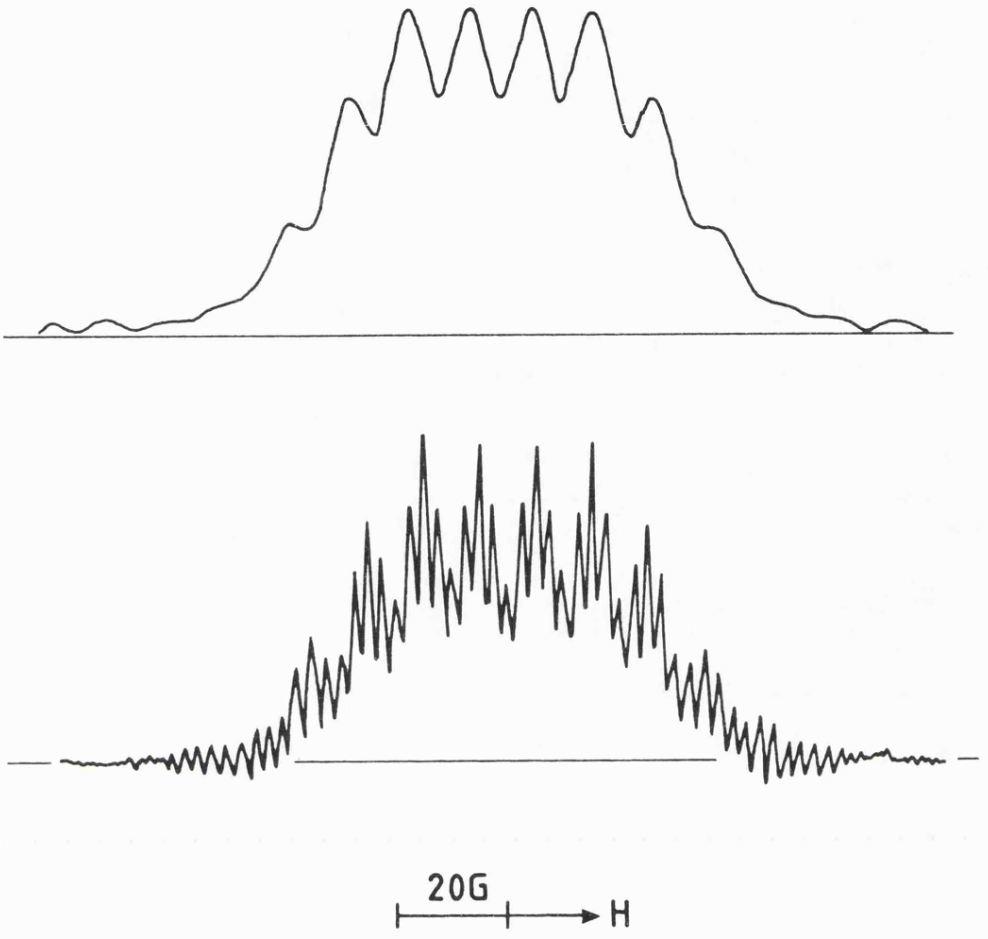

FIGURE 10

a) Resolution enhanced spectrum of a synthetic spectrum of 2 sets (^{81,79}Br split by 30 G) of 7 lines (first group of 6 equivalent H) split by 10 G, each of these being split in a septet (second set of 6 equivalent H) spaced by 1.0 G.
b) Resolution enhanced spectrum of a synthetic spectrum of 2 sets (^{81,79}Br split by 30 G) of 7 lines (first group of 6 equivalent H) split by 10 G, each of these being split in a septet (second set of 6 equivalent H) spaced by 2.5 G.

6.5 ENDOR

If in a system, there are two or more nuclei of the same spin, there is ambiguity in the assignment of hyperfine multiplets. Additionally, if the spacing of a set of hyperfine lines does not exceed their width, the splitting cannot be detected. The brief outlines of this technique were discussed in Chapter 2. A prerequisite of this method is that the ESR signal has to be saturated. With the β-bromo radical this was not possible at 77 K and the temperature had to be reduced to ca. 10 K. Despite intensive investigations, no meaningful signals could be obtained.

6.6 CONCLUSIONS

The outer ($M_I = \pm 3/2$) lines show a 36 G doublet splitting from ^{81}Br and ^{79}Br components at ca. 100 K but no resolution on cooling to 77 K or below. A symmetric structure (I) would give 13 binomial components whereas the asymmetric structure (II) would give strong coupling to 6 protons (7 lines) and very weak coupling to the other six protons. If rapid bromine atom migration occurred, the twelve protons should become equivalent, the hyperfine splitting being ca. half that of the slow exchange situation.

Using the resolution enhancement technique, after signal averaging to reduce noise level two sets of results were obtained. At 77 K, two sets of features were apparent with a splitting of ca. 10 G, whereas at 100 K the doublet revealed a sub-splitting of ca. 6 G in each component.

Simulation of the spectra using these parameters and linewidths just great enough to remove the sub-structure, gave good agreement with the experimental spectra.

The results for the 77 K spectra strongly support the asymmetric

structure (II). Thus the overall spectrum . . . . . of the $Me_2\dot{C}CMe_2(Br)$ radical with a methyl proton coupling (10 G) is comparable with, though significantly less than, that for the $Me_2\dot{C}CH_2(Br)$ radical (13 G). Resolution enhancement techniques were unable to give a measure of the coupling to the other two methyl groups, but the technique known as CEPSTROM gave a figure of < 1 G. The simplest explanation of the spectral changes observed in the 80-100 K region is the onset of a rapid equilibrium between the two potential minima for structure II (1).

$$Me_2\dot{C}-\overset{Br}{\overset{|}{C}}Me_2 \rightleftharpoons Me_2C-\overset{Br}{\overset{|}{\dot{C}}}Me_2 \qquad \ldots\ (1)$$

Only a small relative movement of the two units is needed due to the large size of the bromine atom. In order to obtain an average coupling of ca. 5.5 G one needs a coupling of 10 G and 1 G for the static radical.

Due to the complexities of these spectra and associated spectral analysis techniques, no further parameters could be obtained.

6.7 OTHER DIBROMO PRECURSORS

A variety of other dibromo precursors were tried:

(i) 1,2 Dibromoethane. - A variety of spectral lines were produced in a CD_3OD matrix. Several features could be preferentially lost on annealing. The addition of bromine to the mixture prior to irradiation produce slight changes in the final spectrum (Figures 11 and 12). The same experiments were performed using MeTHF and TMS as a matrix. No β-species could be clearly defined.

(ii) 2,3 Dibromobutane. - A variety of solvents were used and the addition of bromine were used. No β-species was found (Figures 13 and 14).

(iii) ± Trans-1,2-dibromocyclohexane. - A variety of solvents were tried.

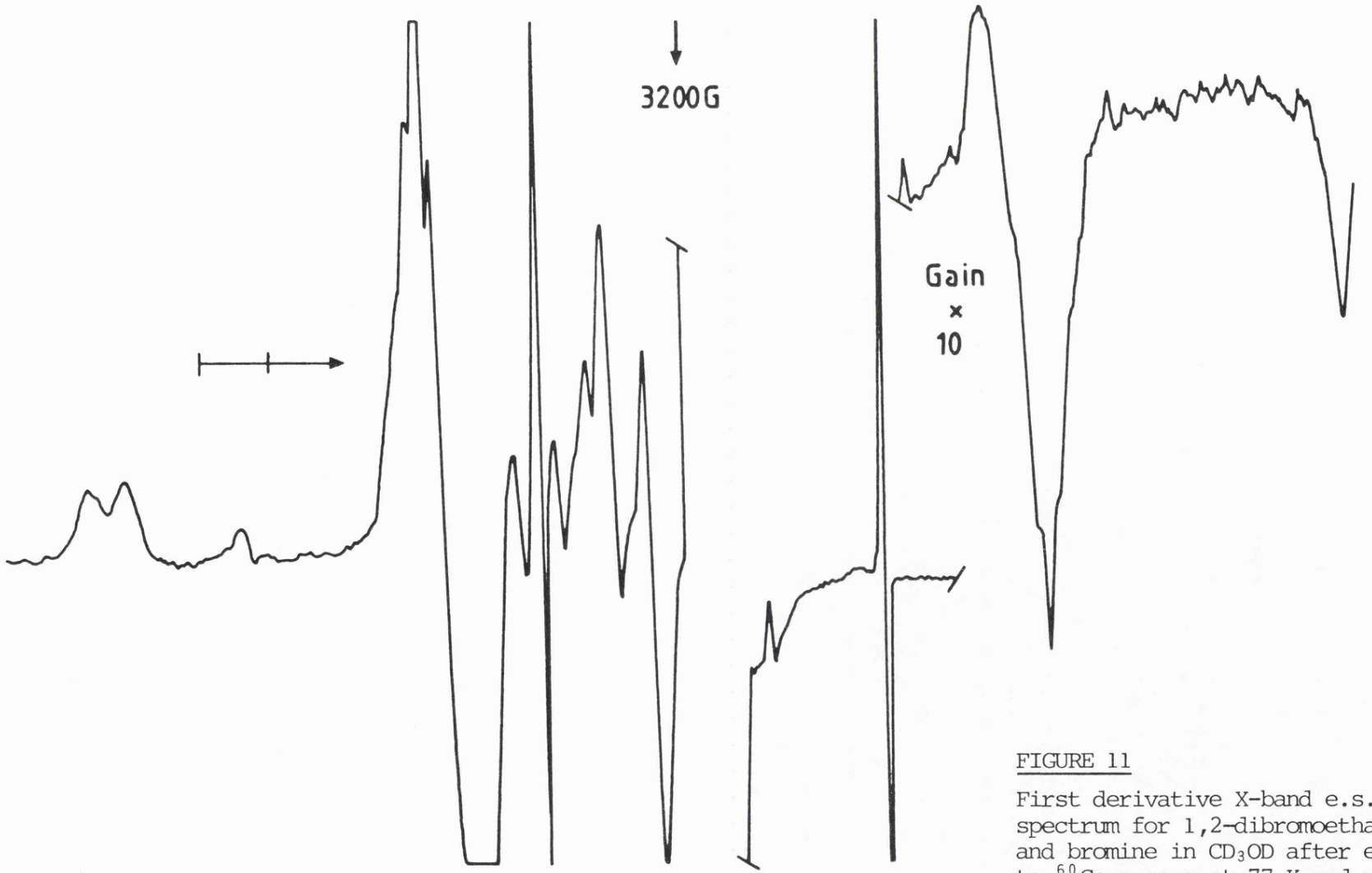

FIGURE 11

First derivative X-band e.s.r. spectrum for 1,2-dibromoethane and bromine in CD_3OD after exposure to ^{60}Co γ-rays at 77 K and warming to ca. 100 K.

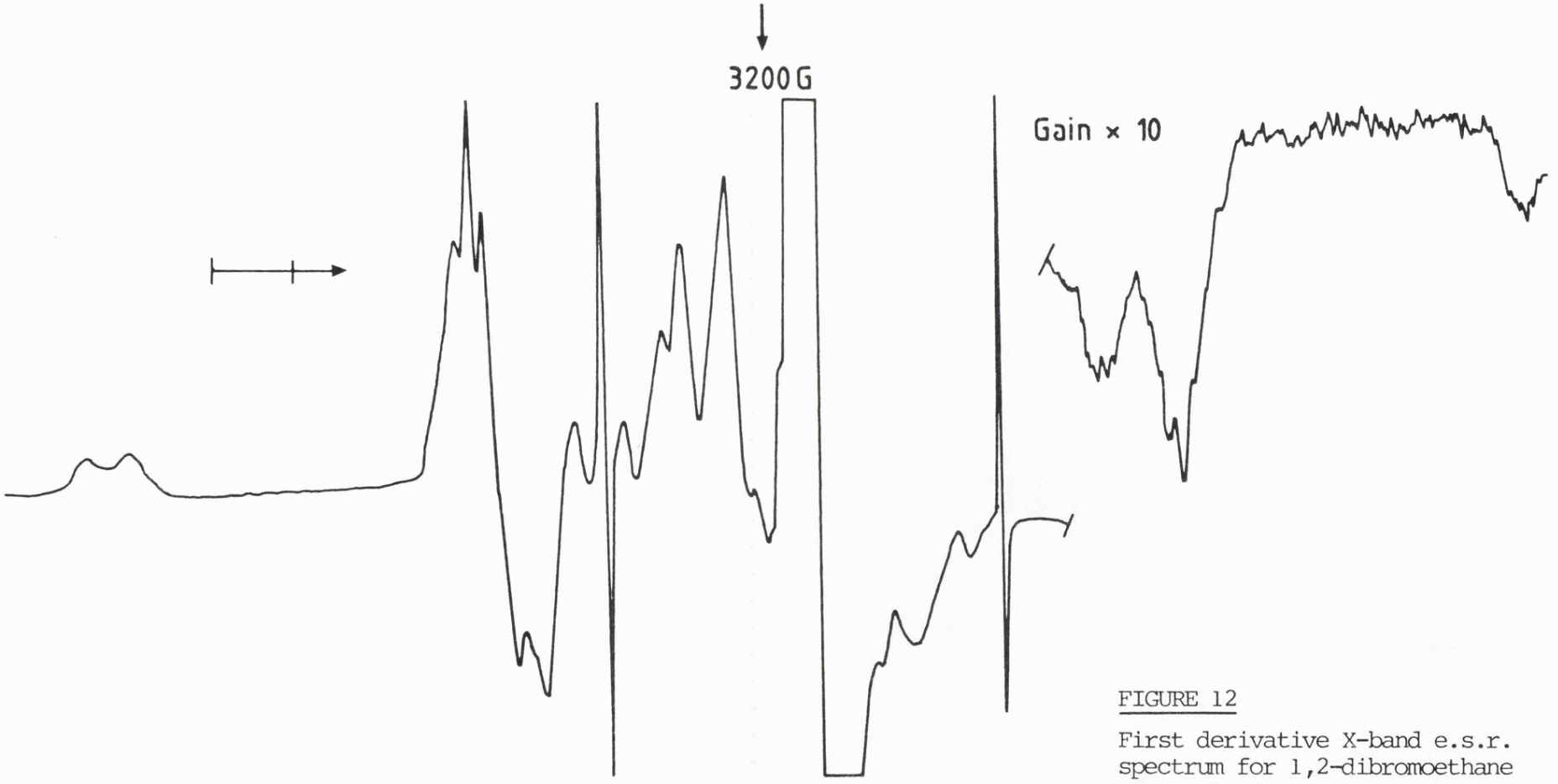

FIGURE 12

First derivative X-band e.s.r. spectrum for 1,2-dibromoethane in CD_3OD after exposure to ^{60}Co γ-rays at 77 K and warming to ca. 100 K.

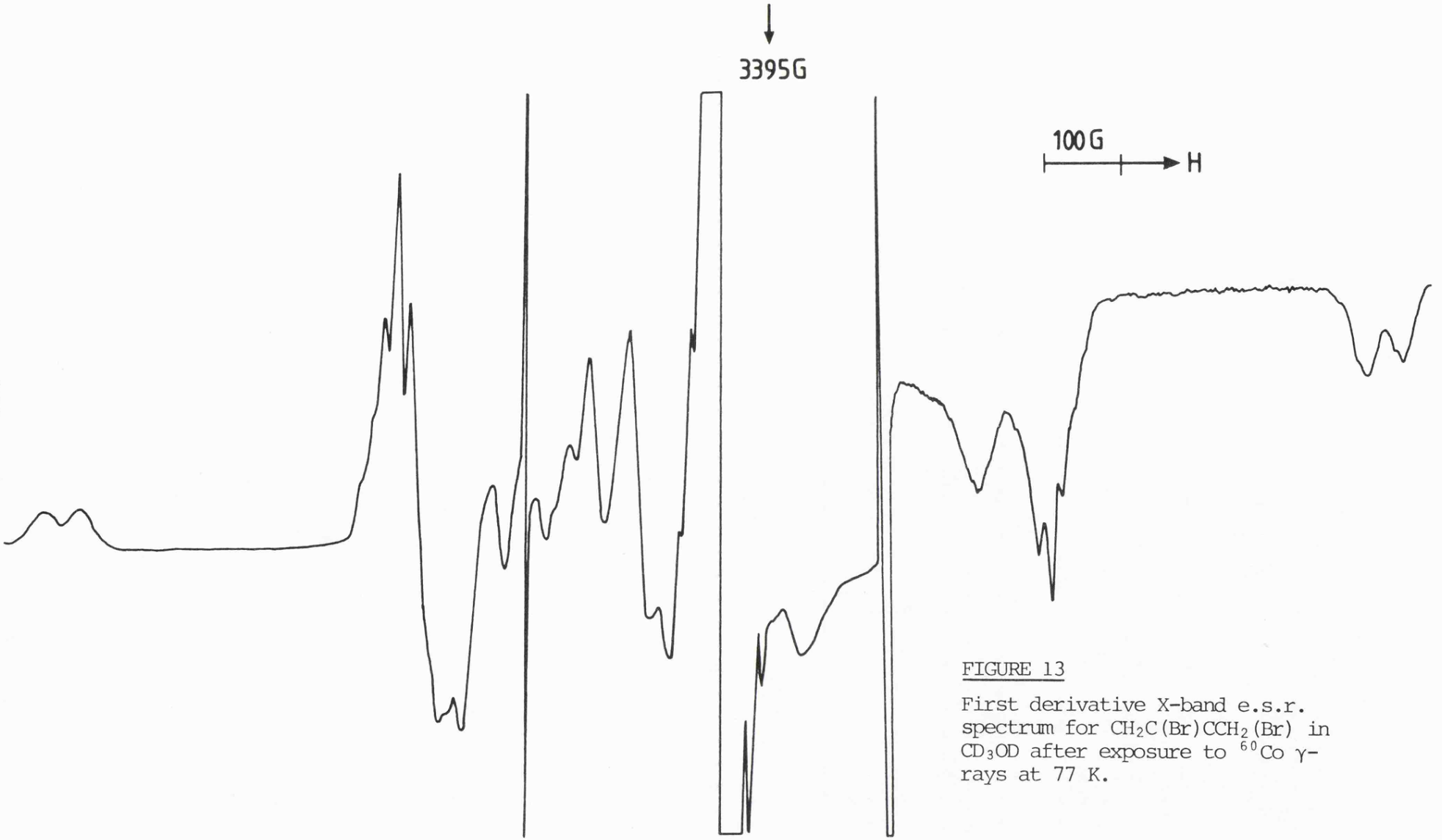

FIGURE 13

First derivative X-band e.s.r. spectrum for $CH_2C(Br)CCH_2(Br)$ in CD_3OD after exposure to ^{60}Co γ-rays at 77 K.

FIGURE 14

First derivative X-band e.s.r. spectrum for $CH_2C(Br)CCH_2(Br)$ in CD_3OD with a trace of bromine after exposure to ^{60}Co γ-rays at 77 K.

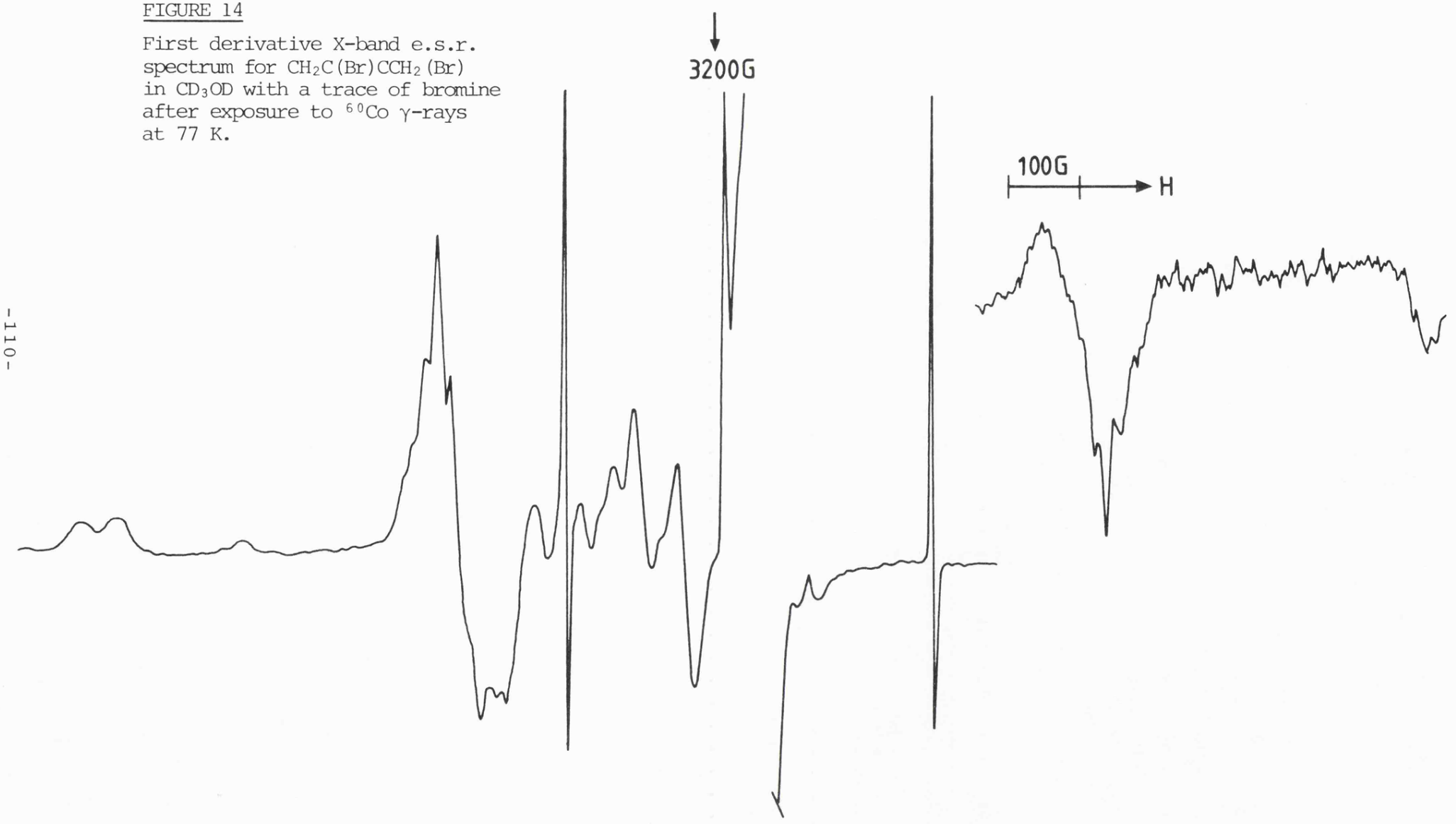

In MeTHF the addition of bromine caused the suppression of one strong line. Q-band was tried but the results were inconclusive.

6.8 CONCLUSIONS

The formation of β-bromo species is sensitive to the nature of the groups attached to the molecule. Electron-donating groups seem to stabilize the radical, thereby increasing the chance of the radical being produced. This stabilizing effect is evident in the 1,2-hal shift in the t-butyl bromide system. Electron-gain species must be produced, the mechanism is probably:

$$R_2CX - R_2CX + e^- \longrightarrow R_2C=CR_2 + X_2^-$$

Due to time limitations, it was not possible to analyse the reaction mixture for any olefins produced.

REFERENCES FOR CHAPTER 6

1. W. A. Pryor, Free Radicals, McGraw-Hill, New York, 1966.

2. P. S. Skell, P. R. Pavlis, D. C. Lewis and K. J. Shea, J. Am. Chem. Soc., 1973, 95, 6735;
K. J. Shea and P. S. Skell, J. Am. Chem. Soc., 1973, 95, 283;
K. J. Shea, D. C. Lewis and P. S. Skell, J. Am. Chem. Soc., 1973, 95, 7768.

3. A. J. Bowles, A. Hudson and R. A. Jackson, Chem. Phys. Letters, 1970, 5, 552.

4. A. R. Lyons and M. C. R. Symons, J. Am. Chem. Soc., 1971, 93, 7330;
A. R. Lyons, G. W. Neilson, S. P. Mishra and M. C. R. Symons, J. Chem. Soc., Faraday Trans. 2, 1975, 363.

5. M. C. R. Symons, J. Chem. Soc., Faraday Trans. 2, 1972, 68, 1897.

6. S. P. Mishra, G. W. Neilson and M. C. R. Symons, J. Chem. Soc., Faraday Trans. 2, 1974, 70, 1165.

7. M. C. R. Symons and I. G. Smith, J. Chem. Soc., Perkin Trans. 2, 1979, 1362.

8. M. C. R. Symons and P. M. R. Trousson, Radiat. Phys. Chem., 1984, 23, 127.

CHAPTER 7

Ethyl Iodide

7.1 INTRODUCTION

Most adducts produced in matrices such as adamantane, tetramethylsilane and acetonitrile d_3 (CD_3CN) have given well-resolved spectra from which parameters could be extracted. One notable exception is the radiolysis of pure polycrystalline alkyl iodides.

7.2 EXPERIMENTAL

Ethyl iodide (Fisons) was used as supplied. Samples were degassed *via* the freeze-thaw method prior to experimentation. A monolithic crystal of ethyl iodide was grown by Dr. T. Chen (ETH) and to whom the author is indebted. The sample tube, containing the ethyl iodide, was moved hydraulically firstly through a heating coil and then through a thermostatted cylinder and then into cold nitrogen gas. The thermostatted cylinder was a few degrees below the melting point of ethyl iodide and the stream of nitrogen gas was tens of degrees colder. The sample tube was moved at the rate of 2 cm in 24 hours. All temperatures were controlled by a Proportional, Integral and Differential control system to within ±0.5°C (Diagram 1).

7.3 RESULTS AND DISCUSSION

Earlier work on ethyl iodide was repeated. Figures 1 and 2 show the spectra at 77 K generated from radiolysis at 77 K of polycrystalline CH_3CH_2I and CD_3CD_2I respectively.

Controversy exists over the species responsible for the spectra and, indeed a range of polycrystalline and glassy n-alkyl iodides from C_2 to C_8. All give 'wide scan spectra' on γ-irradiation. No single strong contender exists that would explain the results. Previous work in this laboratory suggested the spectra were the result of the $R\cdot/I^-$ adduct.

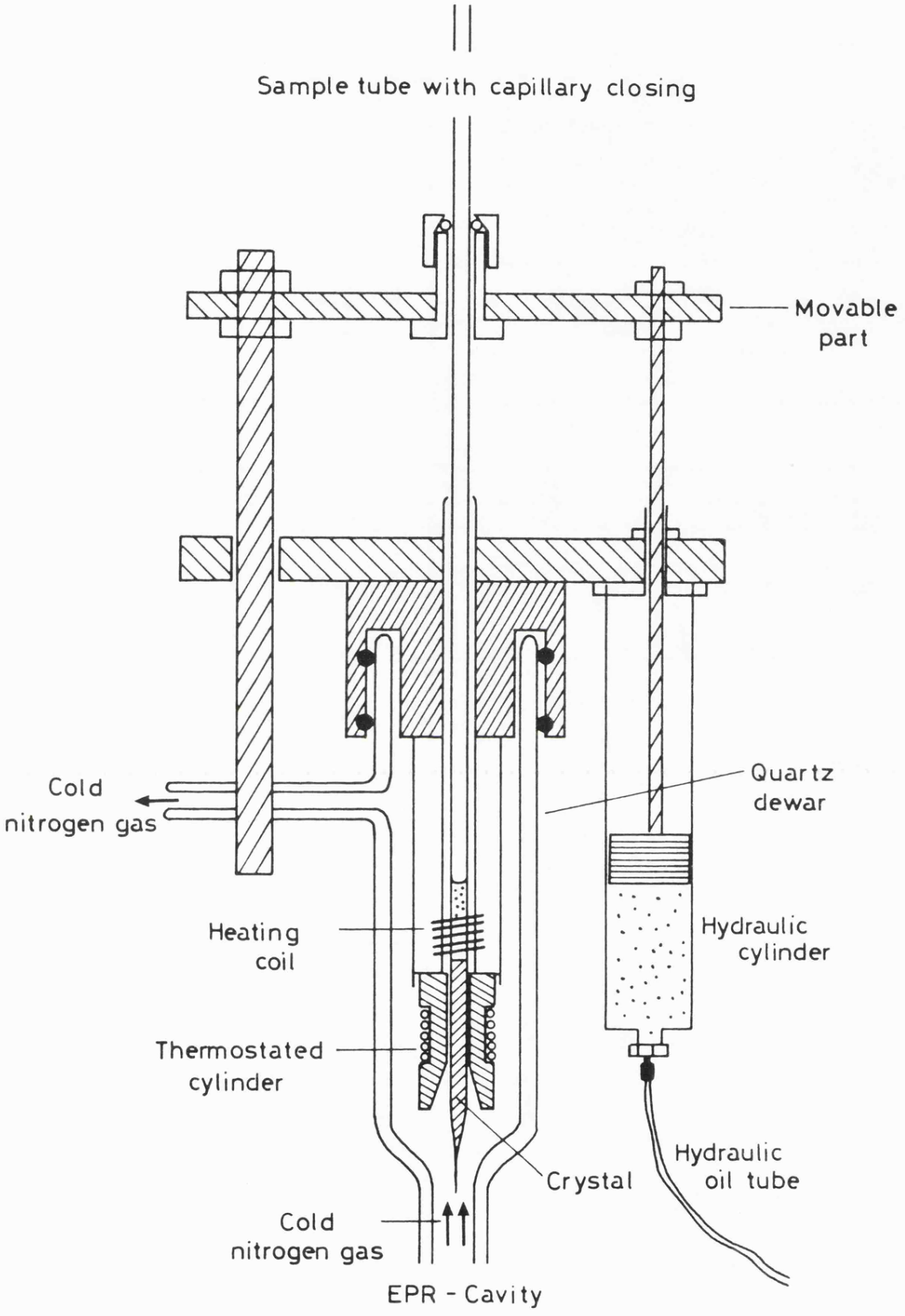

DIAGRAM 1

Crystal growth at low temperature.

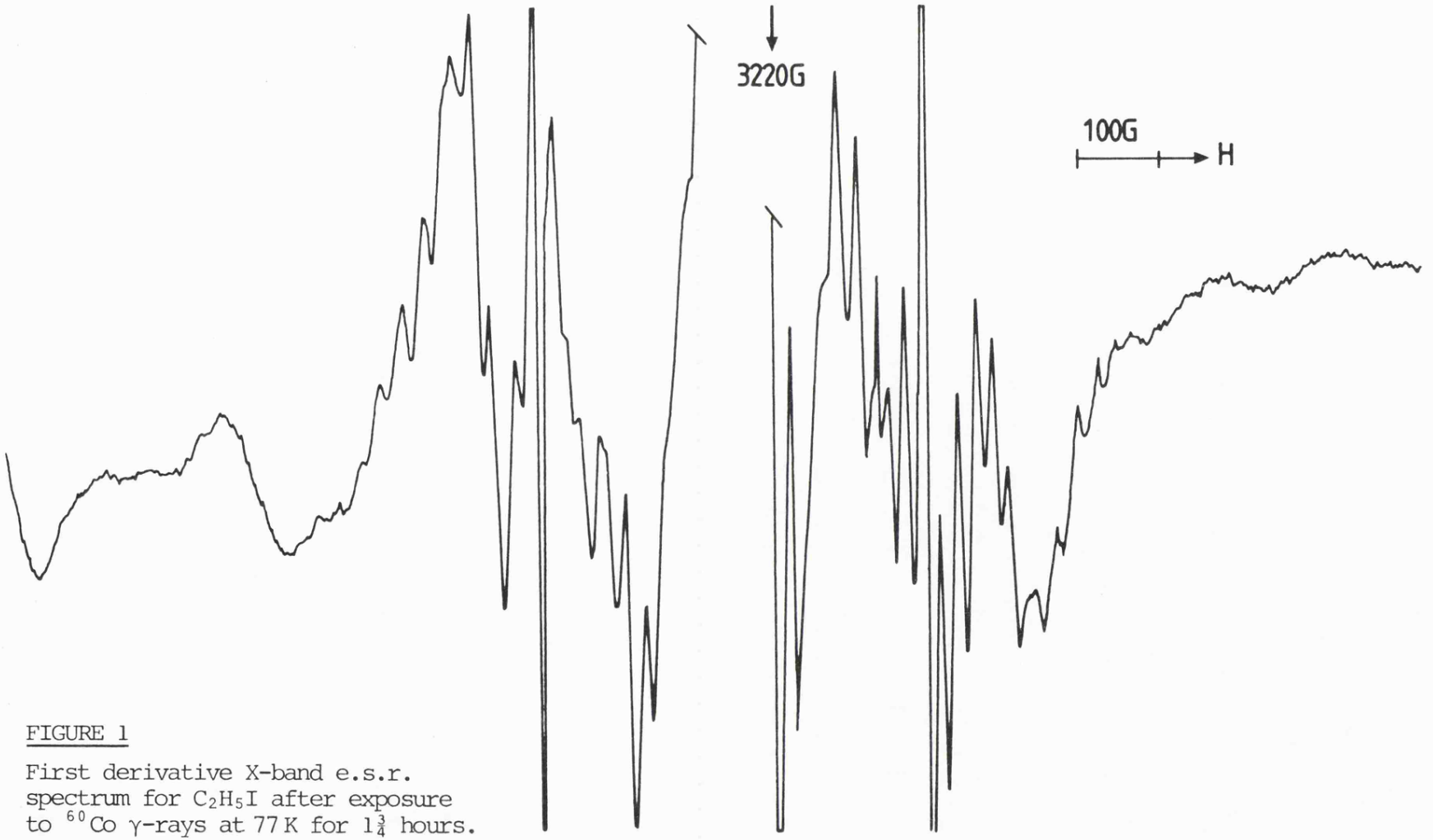

FIGURE 1

First derivative X-band e.s.r. spectrum for C_2H_5I after exposure to ^{60}Co γ-rays at 77 K for $1\frac{3}{4}$ hours.

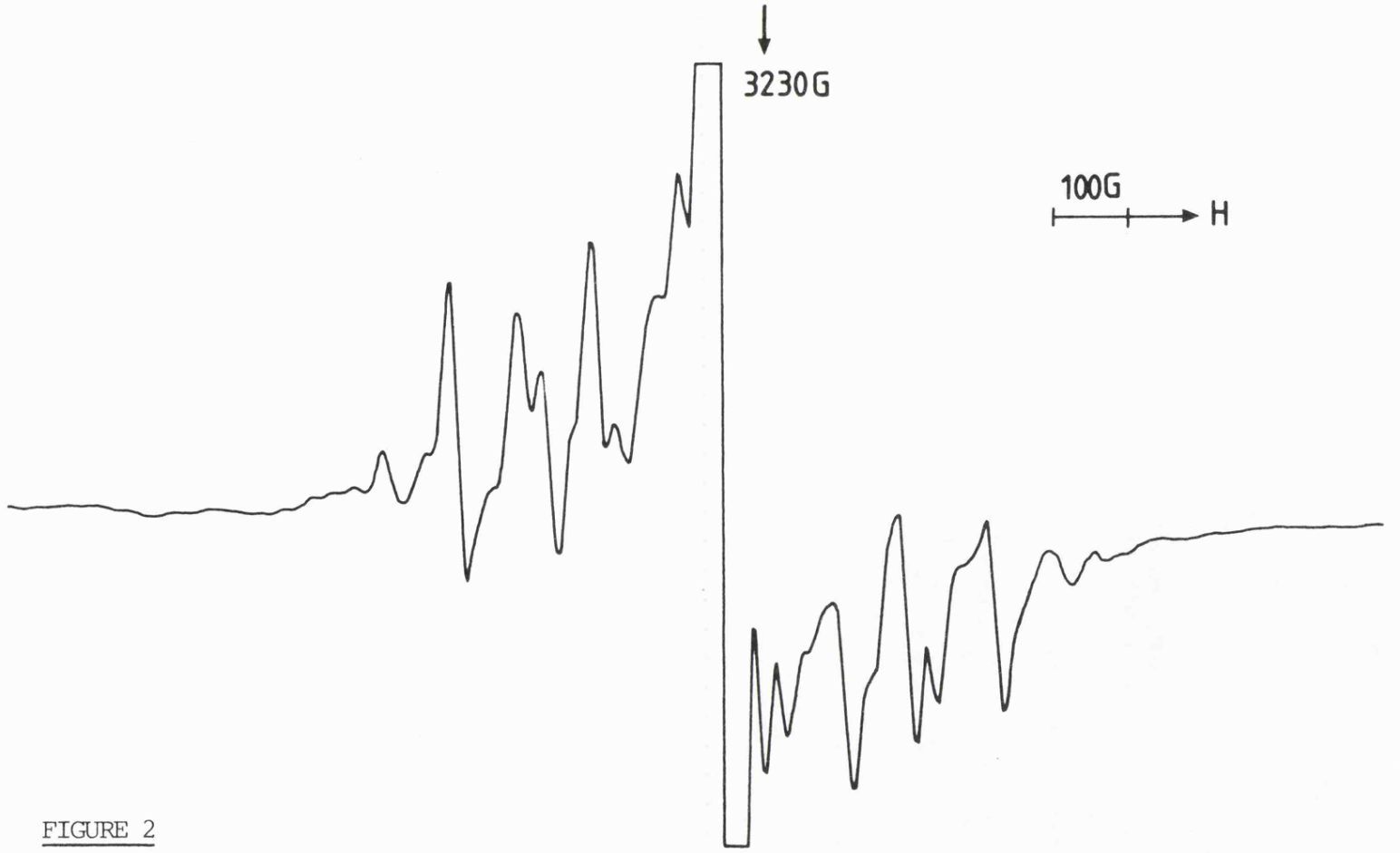

FIGURE 2

First derivative X-band e.s.r. spectrum for C_2D_5I after exposure to ^{60}Co γ-rays at 77 K for 3 hours.

Rehearsing the observations to date made by Willard et al.[1-3] and Smith (Table 1).

(i) "All γ-irradiated polycrystalline n-alkyl iodides with even carbon numbers from C_2H_5I to $C_8H_{15}I$ show broader, more complex ESR spectra than would be produced by the alkyl radical formed by rupture of the C-I bond."

The even n-alkyl iodides produce the adduct in the polycrystalline state with the large iodine coupling being a function of the small $R\bullet\cdots I^-$ distance. In the glassy state no adducts are formed.

(ii) "Spectral features persist longer at 77 K and are stable on annealing almost up to the melting point."

This suggests a rigid matrix.

(iii) "On raising the temperature of the glassy samples at a rate of about 30° per hour, the spectra all disappeared at about 0.6 of the absolute melting point. Polycrystalline signals all persisted to 0.8 of the melting point."

This would suggest that the glassy state is less rigid, allowing migrations to take place.

(iv) "The greater yield of C-I bond rupture in glassy than polycrystalline alkyl iodides, indicated both by the e.s.r. spectra and by earlier studies on the radiolysis yields of I_2, may be due to a greater possibility of cage escape in the glass."

(v) "If polycrystalline, γ-irradiated C_2H_5I, at 77 K, is warmed to 145-150 K for 1 minute then examined at 77 K, the complex polycrystalline pattern decays accompanied by a strong central six-line, 165 G $C_2H_5\bullet$ radical pattern. The radical pattern is the same as that observed in glassy samples."

TABLE 1

ESR Spectra of γ-Irradiated glassy and polycrystalline alkyl iodides [a]

Compound	State	Number of lines	Total spread (G)	Approximate Intensity Ratio	Approximate Anneal Temperature	M.pt. (°C)	Radical
C_2H_5I	glass	6	160	1	100	165	C_2H_5•
	cryst.	30	1000	0.005	150	[c]	?
i-C_3H_7I [b]	cryst.	19	500	0.02	145	182	?
n-C_3H_7I	glass	6	160	0.2	108	172	n-C_3H_7•
	cryst.	7	160	0.2	172	172	n-C_3H_7•
n-C_4H_9I	glass	6	160	0.5	106	170	n-C_4H_9•
	cryst.	4	700	0.03	170	170	?
n-$C_5H_{11}I$	glass	6	160	0.5	118	187	n-C_5H_{11}•
	cryst.	6	160	0.1	187	187	n-C_5H_{11}•
n-$C_6H_{13}I$	glass	6	160	0.2	123	205	n-C_6H_{13}•
	cryst.	15	350	0.05	205	205	?
n-$C_7H_{15}I$ [b]	cryst.	6	160	0.2	213	225	n-C_7H_{15}•
n-$C_8H_{17}I$ [b]	cryst.	15	350	0.05	227	227	?

[a] *Ref. 1;*
[b] *Glassy state not obtained;*
[c] *Figure omitted in original table.*

This sequence of events can be related to normal adduct behaviour, i.e. separation of the alkyl radical and the ion.

(vi) "g-Anisotropy does not make a major contribution to the width of the '1000 G spectrum' of polycrystalline ethyl iodide."
Q-band spectrum of the species are identical to X-band spectra. All adducts examined to date have negligible g-anisotropy.

(vii) "The width and complexity of the spectrum is probably due to hyperfine splitting by iodine."
This has to be the case. However, a satisfactory extraction of parameters is not possible.

(viii) "The unpaired electrons responsible for the spectrum undergo hyperfine coupling with the β-hydrogen atoms of ethyl iodide but little or no interaction with the α-hydrogen atoms."
Resolution due to β-hydrogen atom coupling is distinct, whereas coupling to the α-hydrogen atoms is broad, due to greater anisotropy. This accounts for the greater spectral change when deuterating at the β-position.

(ix) "It is known that some alkyl halides and alkanes show systematic odd-even differences in thermodynamic properties and types of molecular packing within the crystals."
This corresponds to the different lattice structures of the glass/polycrystalline matrix structures.

Considering the possible species responsible for the EtI polycrystalline spectrum, Willard et al. proposed either an electron-loss species $(C_2H_5I)^+$ or an electron-gain species $(C_2H_5I)^-$. The following reactions giving rise to the Et• radical.

$$(C_2H_5I)^+ \longrightarrow C_2H_5\bullet + I^+ \quad \ldots\ [1]$$

$$(C_2H_5I)^- \longrightarrow C_2H_5\bullet + I^- \quad \ldots\ [2]$$

Equation [1] would be contrary to what would be expected for an alkyl halide; also this type of species breaks down to produce the α-halo[4] radical or forms a dimer cation.[5]

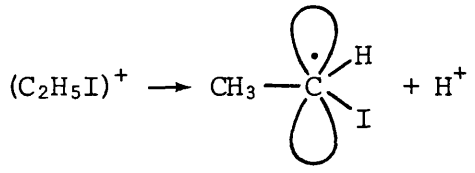

$$(C_2H_5I)^+ \longrightarrow CH_3-\dot{C}(H)(I) + H^+$$

$$(C_2H_5I)^+ + C_2H_5I \longrightarrow [(C_2H_5I)_2]^+$$

Alternative species are α-halo radicals, β-halo radicals and adducts. The α-halo radical would have g-value variation which would lead to spectral asymmetry which is not observed. A β-halo radical would be expected to have a larger hyperfine coupling to the halogen than is observed. Also, the α-protons would give a triplet (<20 G) which is not observed. The spectrum cannot be interpreted as an adduct. A wider scan spectrum reveals a di-iodo species with a maximum iodine hyperfine coupling of ca. 400 G, $(EtI)_2^+$. Hence the complex spectrum must be an electron-gain species. The addition of electron scavengers, e.g. CBr_4, show a decrease in the intensity of the complex spectrum without affecting the strength of signal from the $(EtI)_2^+$ cation.

It is within this context that a single crystal was grown in order to resolve the debate. It was hoped that a comprehensive single crystal study would allow determination of the g-tensor and hyperfine tensor.

7.4 THE THEORY OF THE DETERMINATION OF PRINCIPAL g-VALUES AND THE ELEMENTS OF THE HYPERFINE TENSOR

If a given paramagnetic species in a single crystal has no obvious axis, the principal g-values are measured with respect to an arbitrary set, x, y and z. Now g is a tensor and the spin Hamiltonian may be written:-

$$\hat{\mathcal{H}} = \beta \hat{S} \cdot g \cdot H$$

$$\hat{\mathcal{H}} = \beta[\hat{S}_x\ \hat{S}_y\ \hat{S}_z]\begin{bmatrix} g_{xx} & g_{xy} & g_{xz} \\ g_{yx} & g_{yy} & g_{yz} \\ g_{zx} & g_{zy} & g_{zz} \end{bmatrix}\begin{bmatrix} H_x \\ H_y \\ H_z \end{bmatrix}$$

The product $g \cdot H$ can be considered as a transformation of the actual field H to an effective field $H_{eff} = g \cdot H = g_{eff} H$.

Now $(\Delta W)^2 = \beta^2\, g_{eff}^2\, H^2 = \beta^2 (H \cdot g) \cdot (g \cdot H)$

$$= \beta^2\, H_1 \cdot g^2 \cdot H_2$$

where g^2 is the matrix product of g with its transpose.

H_1 is $H[\ell_x\ \ell_y\ \ell_z]$ $\quad$ ℓ - direction cosines

H_2 is $H\begin{bmatrix} \ell_x \\ \ell_y \\ \ell_z \end{bmatrix}$

i.e. $$g_{eff}^2 = [\ell_x\ \ell_y\ \ell_z]\begin{bmatrix} (g^2)_{xx} & (g^2)_{xy} & (g^2)_{xz} \\ (g^2)_{yx} & (g^2)_{yy} & (g^2)_{yz} \\ (g^2)_{zx} & (g^2)_{zy} & (g^2)_{zz} \end{bmatrix}\begin{bmatrix} \ell_x \\ \ell_y \\ \ell_z \end{bmatrix}$$

The $(g^2)_{ij}$ elements are determined experimentally by rotating the crystal in the planes xz, xy and yz.[6-8] Consider the xz plane; let θ be the angle between H and the z-axis, i.e. $\ell_z = \cos\theta$, $\ell_y = 0$ and $\ell_x = \sin\theta$.

$$g_{eff}^2 = [\sin\theta\ 0\ \cos\theta]\begin{bmatrix} (g^2)_{xx} & (g^2)_{xy} & (g^2)_{xz} \\ (g^2)_{yx} & (g^2)_{yy} & (g^2)_{yz} \\ (g^2)_{zx} & (g^2)_{zy} & (g^2)_{zz} \end{bmatrix}\begin{bmatrix} \sin\theta \\ 0 \\ \cos\theta \end{bmatrix}$$

i.e. $g_{eff}^2 = (g^2)_{xx} \sin^2\theta + 2(g^2)_{xz} \sin\theta \cos\theta + (g^2)_{zz} \cos^2\theta$

Similarly for rotation in the yz plane;

$$g_{eff}^2 = (g^2)_{yy} \sin^2\theta + 2(g^2)_{yz} \sin\theta \cos\theta + (g^2)_{zz} \cos^2\theta$$

and in the xy plane;

$$g_{eff}^2 = (g^2)_{xx} \cos^2\theta + 2(g^2)_{xy} \sin\theta \cos\theta + (g^2)_{yy} \sin^2\theta$$

From the above it can be seen the following measurements should be made; in the xz plane, $\theta = 0$ and $90°$ to give $(g^2)_{zz}$ and $(g^2)_{xx}$ respectively. When $\theta = 45°$ and $135°$ $(g^2)_{xz}$ can be determined.

The tensor must then be diagonalized, i.e.

$$\det (A - \lambda I) = 0$$

giving
$$\begin{bmatrix} (g^2)_{xx} & 0 & 0 \\ 0 & (g^2)_{yy} & 0 \\ 0 & 0 & (g^2)_{zz} \end{bmatrix}$$

The square root of each diagonal element gives the principal component.

The elements of the hyperfine tensor can also be determined. Rotating the crystal in the x-axis with the magnetic field in the yz plane, and the angle between the direction of the applied field and the z-axis of the crystal being θ, then in the yz plane

$$I = [0, \sin\theta, \cos\theta]$$

and
$$\left(\frac{\Delta W}{h}\right)^2 = [0, \sin\theta, \cos\theta] \begin{bmatrix} (A^2)_{xx} & (A^2)_{xy} & (A^2)_{xz} \\ (A^2)_{yx} & (A^2)_{yy} & (A^2)_{yz} \\ (A^2)_{zx} & (A^2)_{zy} & (A^2)_{zz} \end{bmatrix} \begin{bmatrix} 0 \\ \sin\theta \\ \cos\theta \end{bmatrix}$$

$$= [0, \sin\theta, \cos\theta] \begin{bmatrix} (A^2)_{xy}\sin\theta + (A^2)_{xz}\cos\theta \\ (A^2)_{yy}\sin\theta + (A^2)_{yz}\cos\theta \\ (A^2)_{zy}\sin\theta + (A^2)_{zz}\cos\theta \end{bmatrix}$$

$$= A^2_{eff} = (A^2)_{yy}\sin^2\theta + 2(A^2)_{yz}\sin\theta\cos\theta + (A^2)_{zz}\cos^2\theta$$

Similarly for rotation about the z and y axis respectively

$$I = [\cos\theta, \sin\theta, 0]$$

i.e. $$A^2_{eff} = (A^2)_{xx}\cos^2\theta + 2(A^2)_{xy}\sin\theta\cos\theta + (A^2)_{yy}\sin^2\theta$$

and
$$I = [\sin\theta, 0, \cos\theta]$$

i.e. $$A^2_{eff} = (A^2)_{xx}\sin^2\theta + 2(A^2)_{xz}\sin\theta\cos\theta + (A^2)_{zz}\cos^2\theta$$

If the system has axial symmetry, then

$$A^2_{eff} = A^2_{//}\cos^2\theta + A^2_{\perp}\sin^2\theta$$

The A^2 tensor is then diagonalized by subtracting λ from each diagonal element and equating the determinant to zero. The resulting cubic equation is solved. The roots of the equation are then:-

$$^{d}A^{2} = \begin{bmatrix} a & 0 & 0 \\ 0 & b & 0 \\ 0 & 0 & c \end{bmatrix} \qquad [a,\ b \text{ and } c \text{ are rods}]$$

Elements of the direction-cosine are obtained by substituting the three different values of λ into the three equations. The coefficients obtained are the eigen vectors corresponding to the eigenvalues.

7.5 CONCLUSIONS

Spectra obtained clearly demonstrated the existence of a single crystal, rotation by a few degrees producing markedly different spectra. However, complex spectra were still in evidence and the simplification of the spectra was not materialized. Many attempts were made to find some suitable axes but none were found. Variation in microwave power suggested the presence of more than one species, but no positive identification could be made. Finally, in attempts at higher temperatures to preferentially anneal some of the species, all signals were lost.

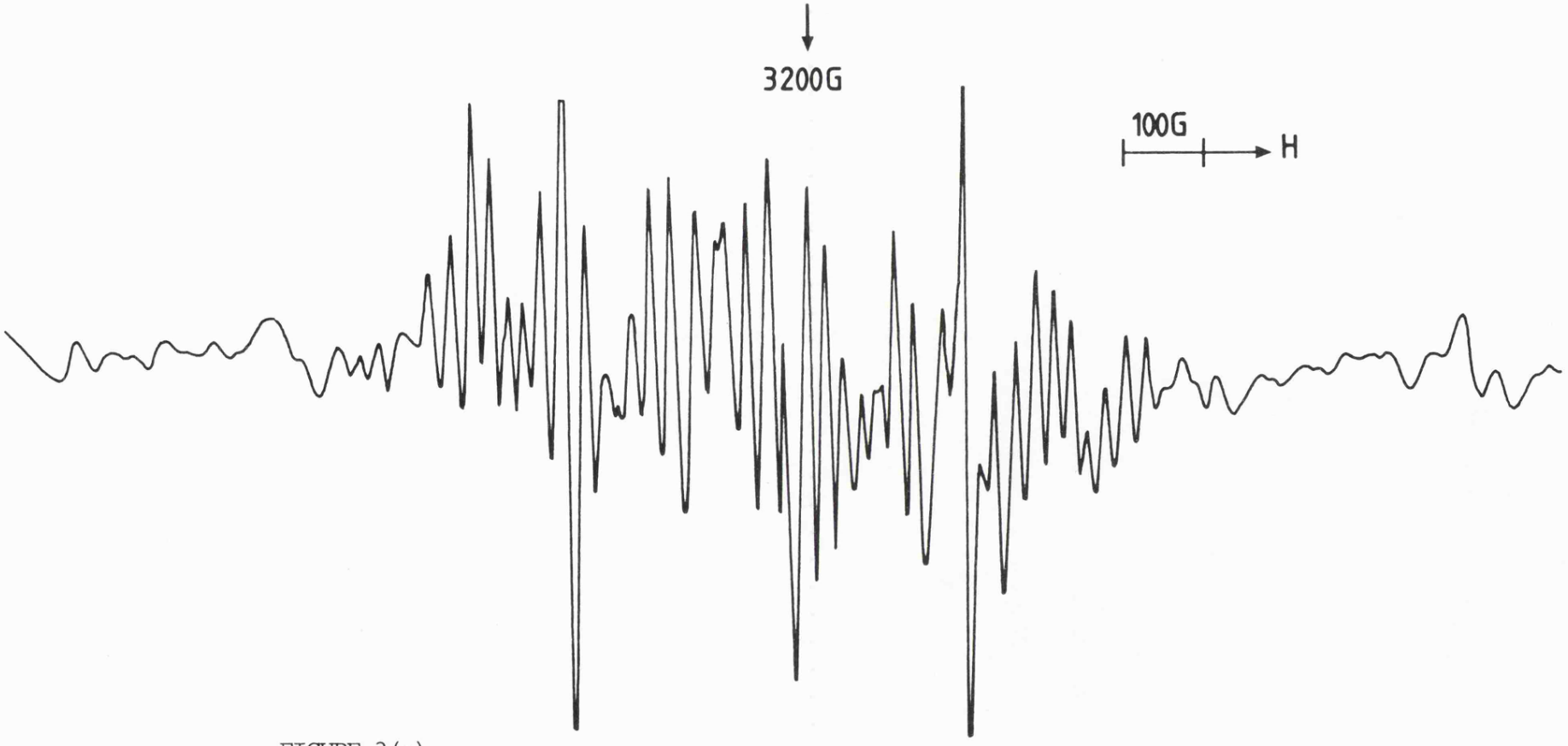

FIGURE 3(a)

First derivative X-band e.s.r. spectrum of a monolithic crystal of C_2H_5I after exposure to ^{60}Co γ-rays at 77 K.

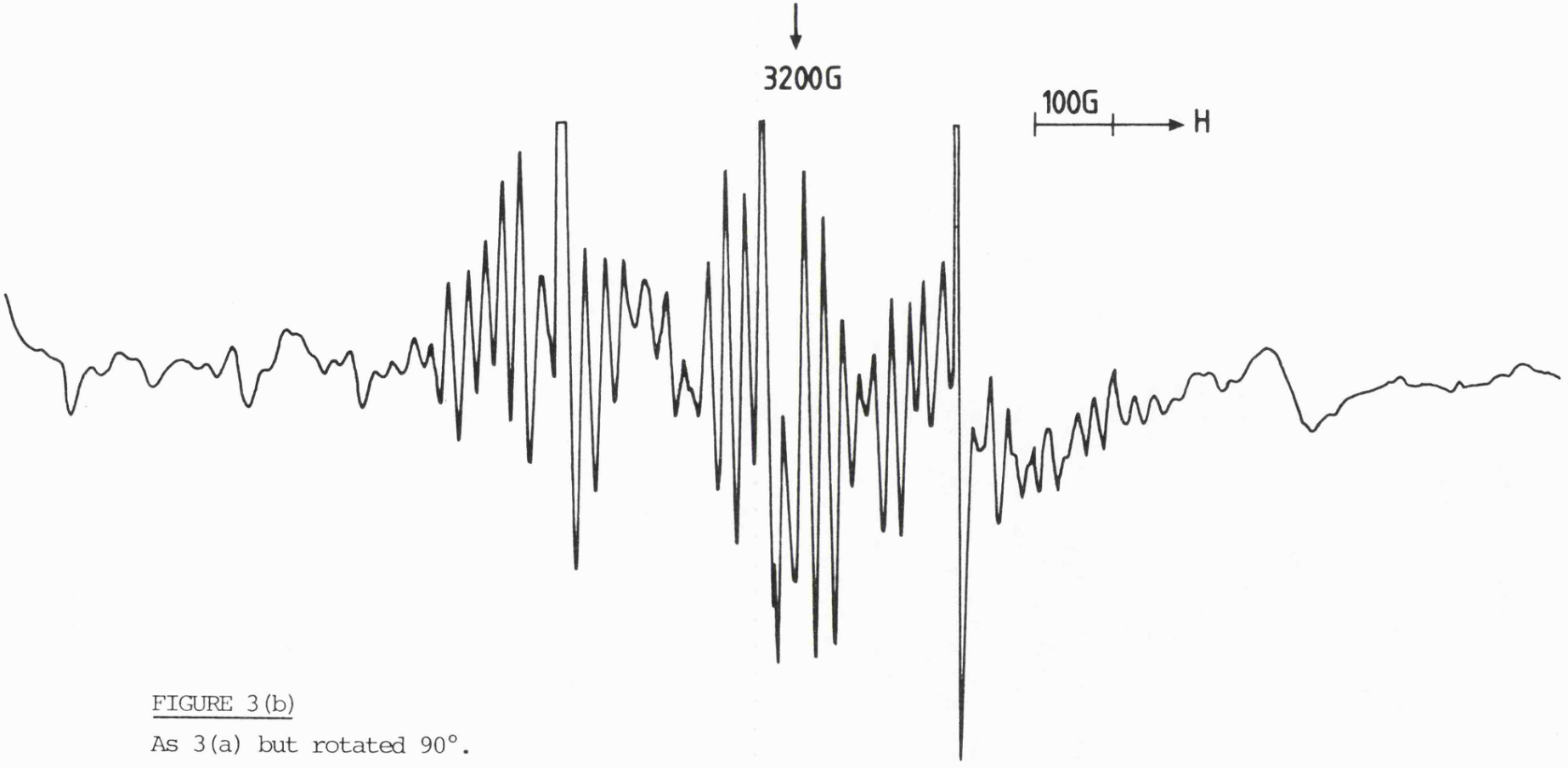

FIGURE 3(b)

As 3(a) but rotated 90°.

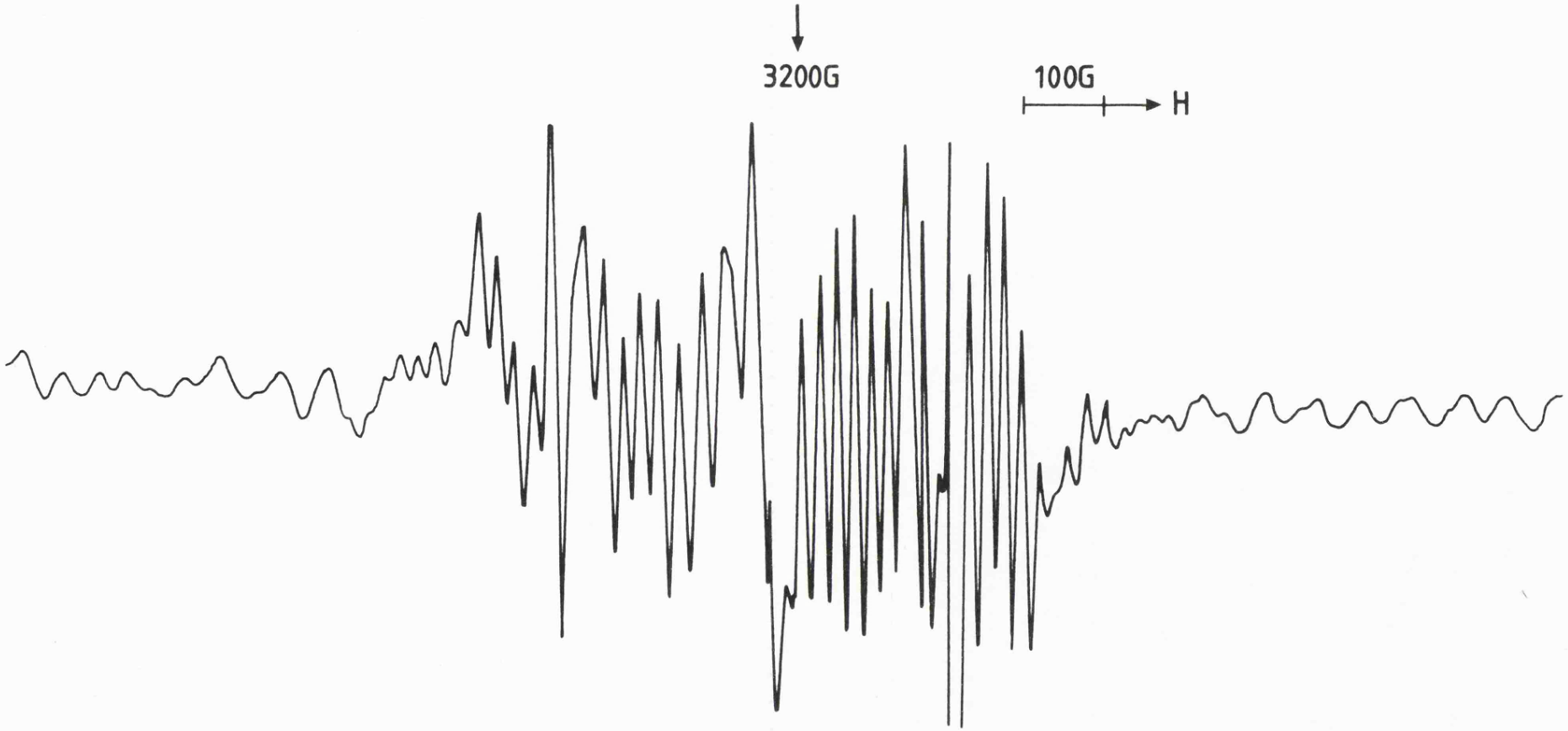

FIGURE 3(c)

As 3(b) but rotated 90°.

REFERENCES FOR CHAPTER 7

1. H. W. Fenrick, S. V. Filseth, A. L. Hanson and J. E. Willard, J. Amer. Chem. Soc., 1963, 85, 3731.
2. H. W. Fenrick and J. E. Willard, J. Amer. Chem. Soc., 1966, 88, 412.
3. R. J. Egland, P. J. Ogren and J. E. Willard, J. Phys. Chem., 1971, 75, 467.
4. S. P. Mishra, G. W. Neilson and M. C. R. Symons, J. Chem. Soc., Faraday Trans. II, 1974, 70, 1165.
5. S. P. Mishra and M. C. R. Symons, J. Chem. Soc., Perkin Trans. 2, 1975, 1492.
6. J. E. Gensic and L. C. Brown, Phys. Rev., 1958, 112, 64.
7. M. H. L. Pryce, Proc. Phys. Soc. A, 1950, 63, 25.
8. J. A. Weil and J. H. Anderson, J. Chem. Phys., 1958, 28, 864.

CHAPTER 8

1 - Bromoadamantane

8.1 INTRODUCTION

After electron capture by the carbon-halogen bond (e.g. MeBr), a relaxation occurs to lower the antibonding character of the extra electron. This results in a flattening of the $H_3\dot{C}$ unit, which in turn increases the 'p' contribution to the orbital. This increases the energy of the carbon contribution and forces the unpaired electron further onto the carbon (Figures 1 and 2). This is a continually adjusting process, with no energy minimum.

FIGURE 1

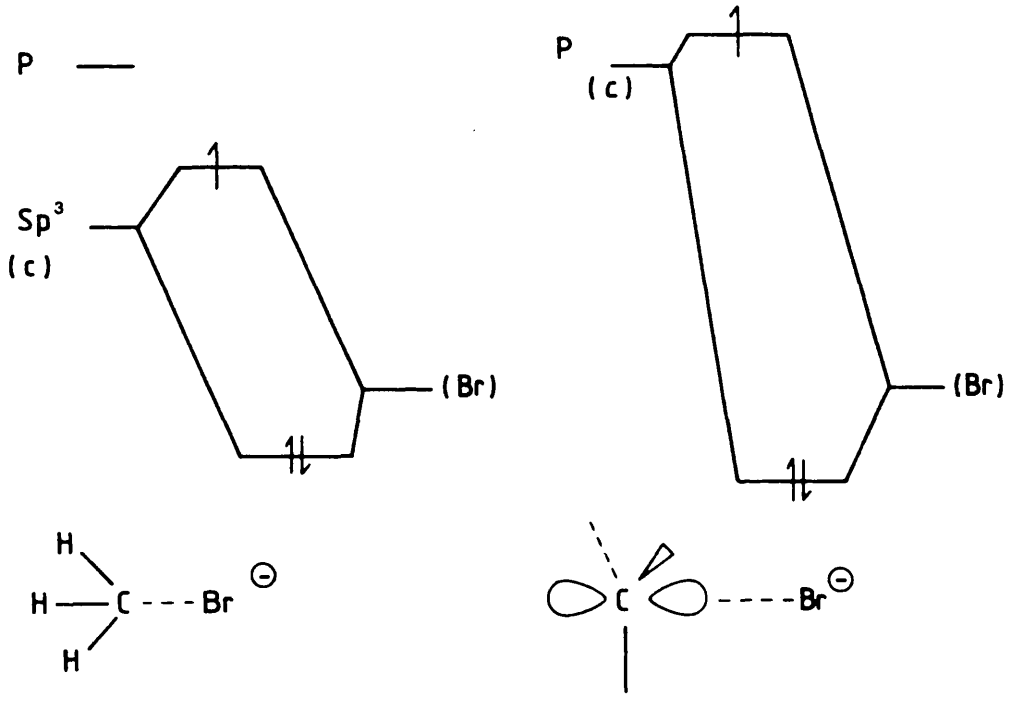

Electron addition to 1-bromoadamantane (Figure 3) stretches the C-Br bond. However, there is little if any tendency for the adamantane unit to become linear, which would be required if the orbital on C contributing to the C-Br σ bond were to become pure 2p. Hence the species remains a σ* anion and a new bond length exists for which there is a potential minimum preventing further departure of the halogen.

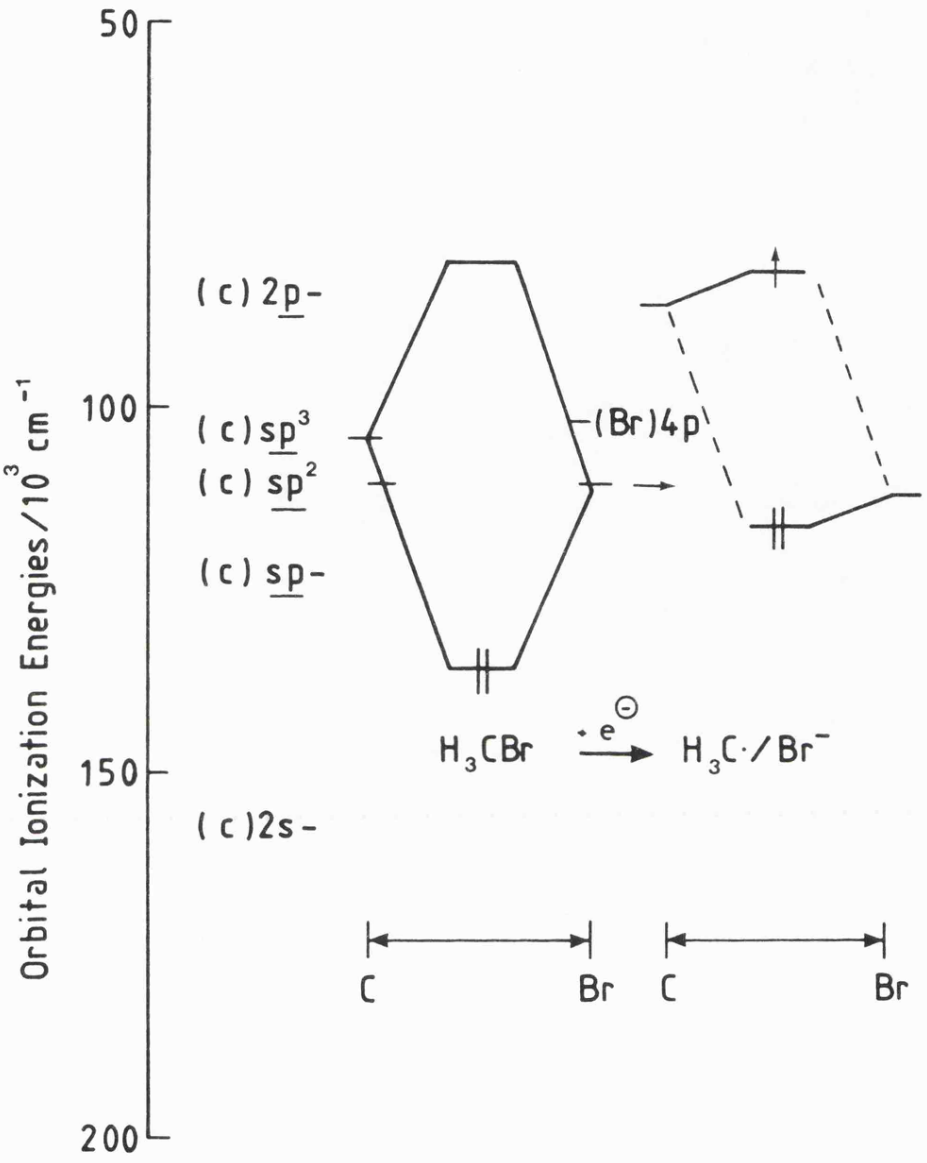

FIGURE 2

Qualitative energy level diagrams for the formation of the $CH_3\cdot/Br^-$ adduct.

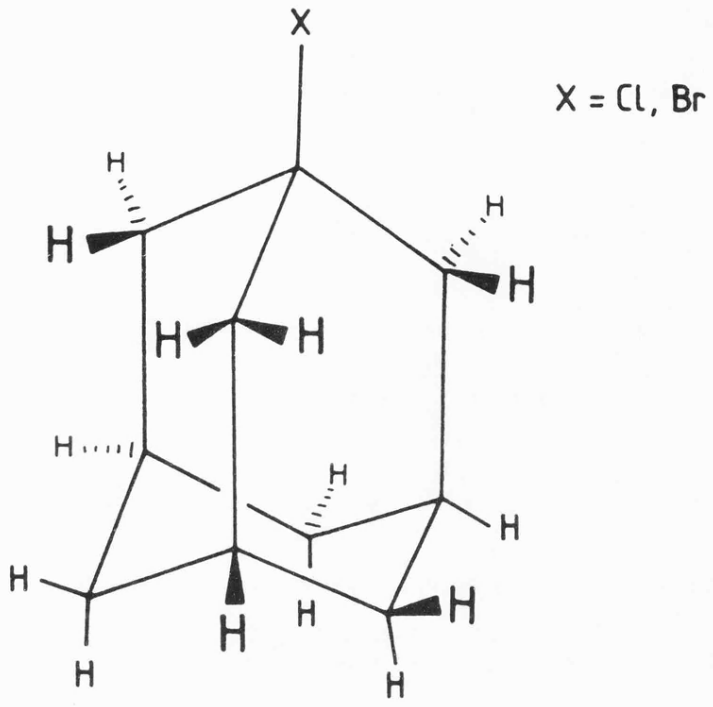

FIGURE 3 1-haloadamantane

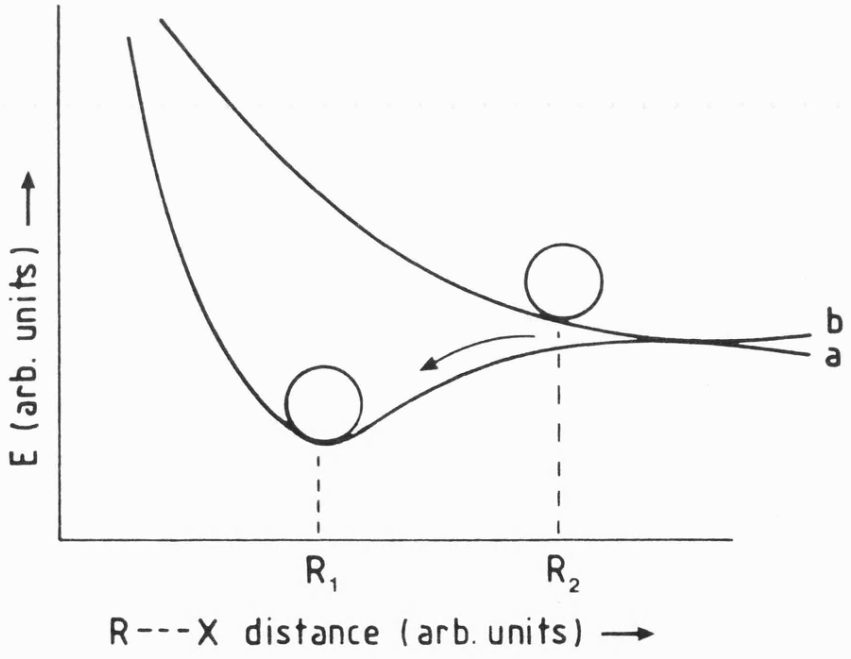

FIGURE 4

Potential energy graph for (a) the σ* anion with a potential energy minimum at R_1 and (b) the adduct with the solvent cage determining the distance R_2.

Thus electron addition into a C-Br bond of an organic radical can result in the formation of an $R\cdot/X^-$ adduct (Figure 4) or the formation of a $(R\overset{\cdot}{-}X)^-$ σ^* anion.[1-5] The electron residing in the σ^* orbital of the C-X bond. Symons proposed that the configurational change will favour the adduct after electron addition to the C-Br σ^* orbital. Inability to allow a configurational change maintains the species as a σ^* anion. Clearly, in both cases, the percentage 'p' and percentage 's' character would be very different[6,7] (Figure 5).

Using the A° values of Morton and Preston and 2B° values of Atkins and Symons[6-9] a plot of percentage 'p' character against percentage 's' character for σ^* anions results in a straight line (Graph 1). From the graph it can be seen that for a 100% 'p' orbital population on the halide a 6% 's' orbital population exists indicative of a weak bond. Adducts with a 100% 'p' orbital population demonstrate only ca. <1% and this is entirely due to spin polarization. The diagnostic characteristic for unknown species is self-evident.

8.2 EXPERIMENTAL

1-Bromoadamantane-h_{16} (Koch-Light) was recrystallised twice from methanol prior to use. All other reagents, adamantane-d_{16} (Merck, Sharp & Dohme), tetramethylsilane (BDH), acetonitrile-d_3 (NMR) and methanol-d_4 (BDH) were all used as supplied.

The co-sublimation experiments employed one of the characteristic properties of adamantane. The ease with which it sublimes was used both as a method of purification and mixing. For purification work, a small sample of adamantane was placed in the bottom of a silica tube which is then sealed under vacuum. Application of a temperature gradient allowed the sample to be sublimed further up the tube. In the case of

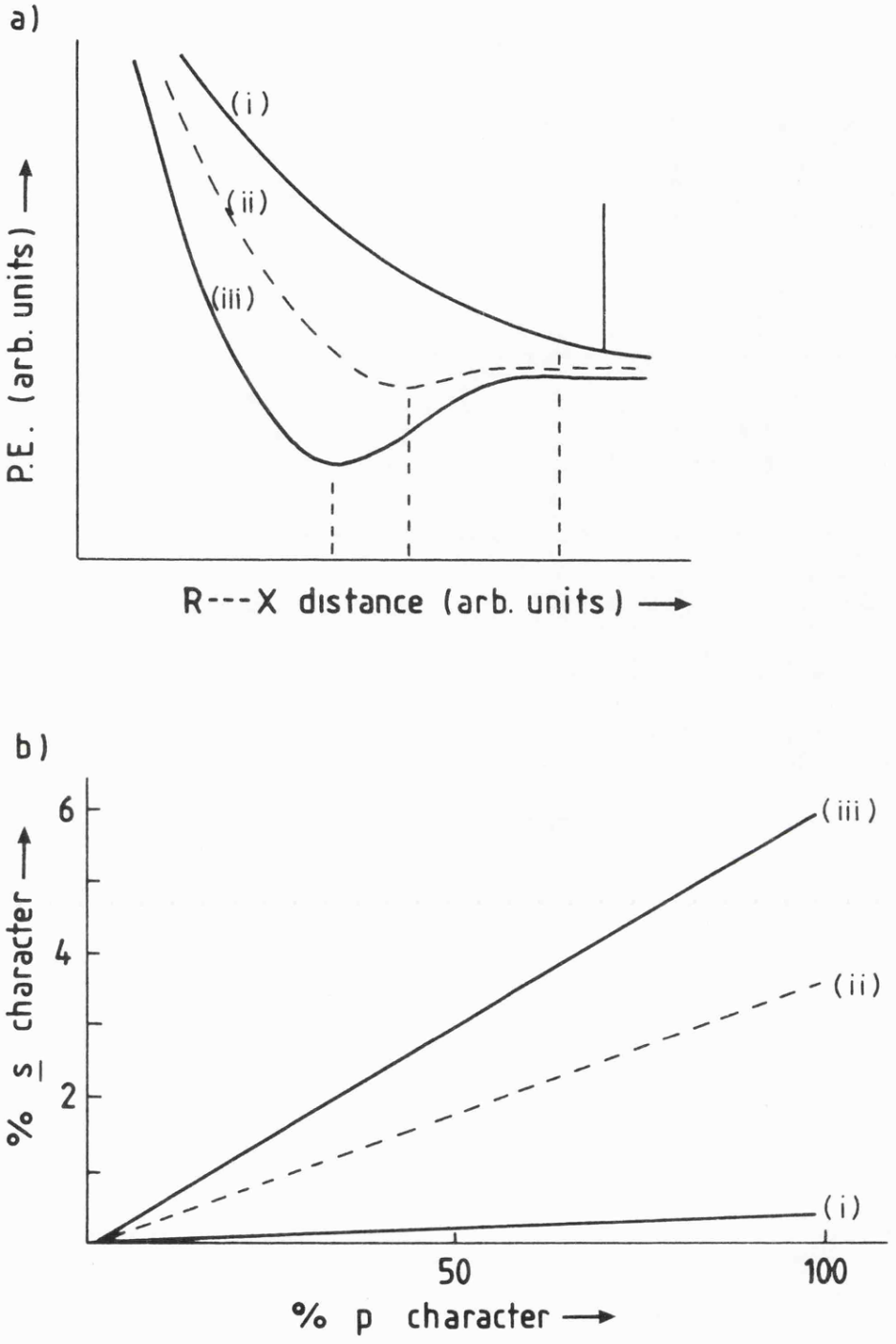

FIGURE 5

(a) The Potential Energy curves;
(b) the %p-character vs. %s-character for:-
(i) adduct, (ii) possible intermediate case and
(iii) the σ* anion.

GRAPH 1

Relative %s and %p character in a range of iodo-, bromo- and chloro- σ* anions.

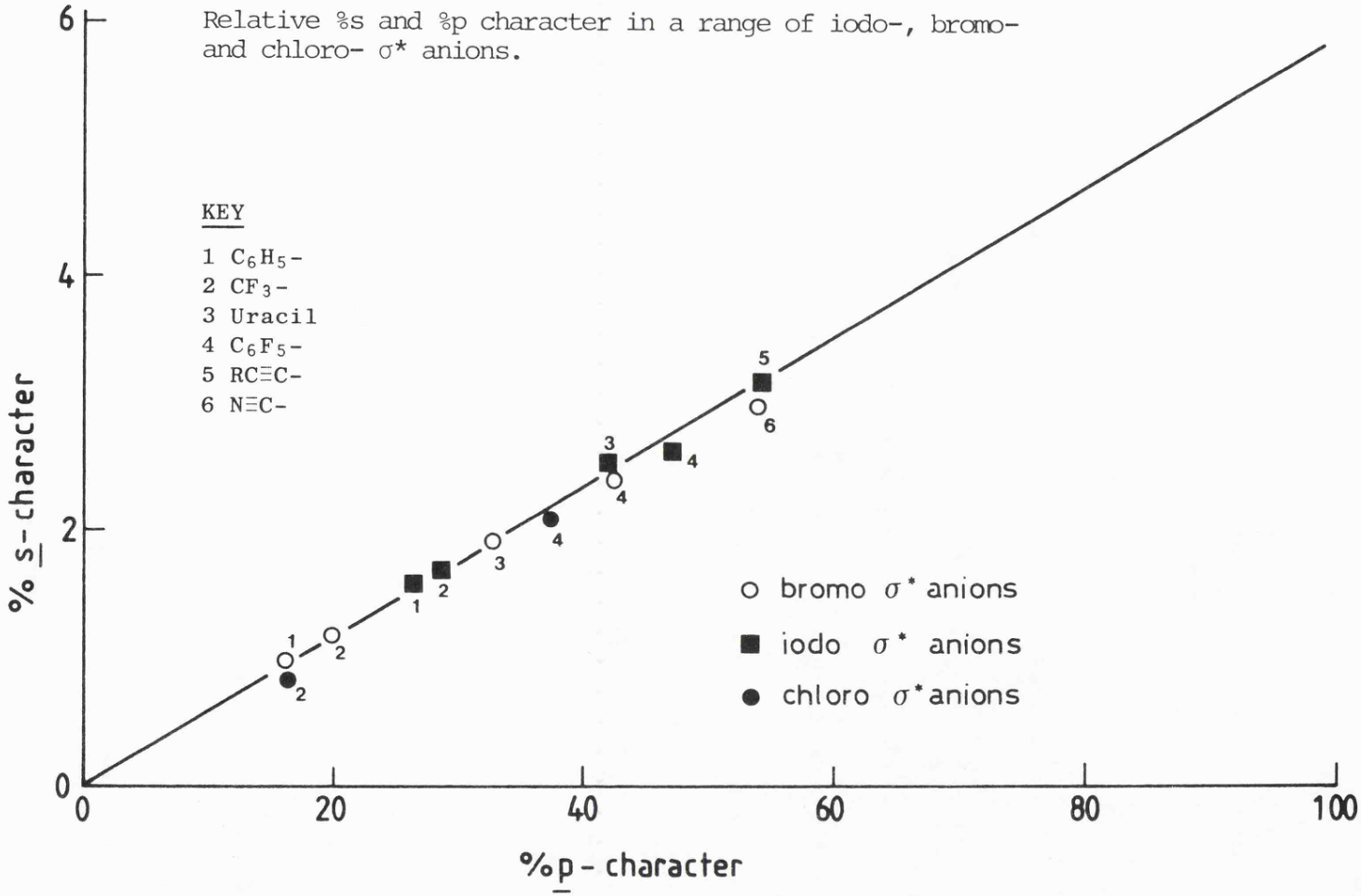

co-sublimation, for example, 1-bromoadamantane and adamantane-d_{16}, an intimate mixture was sealed in the tube which was then heated sufficiently to vapourize the contents. Cooling one end of the tube re-solidified the sample. Extreme care was taken, due to the high vapour pressure of the samples. The sample could then be cooled to 77 K and γ-irradiated.

8.3 RESULTS AND DISCUSSION

Earlier work was repeated and spectra reproduced. Pure 1-monobromo-adamantane on γ-radiolysis gave clear features of a monobromo radical. The approximately equal abundance of ^{79}Br and ^{81}Br and $I = 3/2$ (magnetic moment of ^{79}Br slightly smaller than ^{81}Br) gave rise to seven features in the spectrum, each being sub-divided into multiplets by the different isotopic contributions. The monobromo species had an $A_x(^{81}Br)$ hyperfine coupling of 371 G and $A_x(^{79}Br)$ hyperfine coupling of 344 G split into a doublet of ca. 65 G (Spectrum 1). Radiolysis of the perdeuterated analogue converted the doublet to a single line, i.e. splitting due to a single hydrogen atom (Spectrum 2).

Clearly the bromine hyperfine coupling of ca. 370 G defines the species as a σ* anion. However, there is no explanation of the single proton coupling of ca. 65 G. From the diagram one could expect a small coupling to six equivalent hydrogen atoms.

Broadly speaking, the interaction with the single proton must be due to either an intra- or an inter- molecular interaction. The following experiments were performed.

1. 1-Bromoadamantane was γ-irradiated for 8 hours and the sample examined at various temperatures, -150, -160 and -173°C. The signal annealed away with no significant change. A reversible broadening was apparent on recooling.

SPECTRUM 1(a)

First derivative X-band e.s.r. spectra of 1-bromoadamantane after exposure to ^{60}Co γ-rays at 77 K and warming to 88 K.

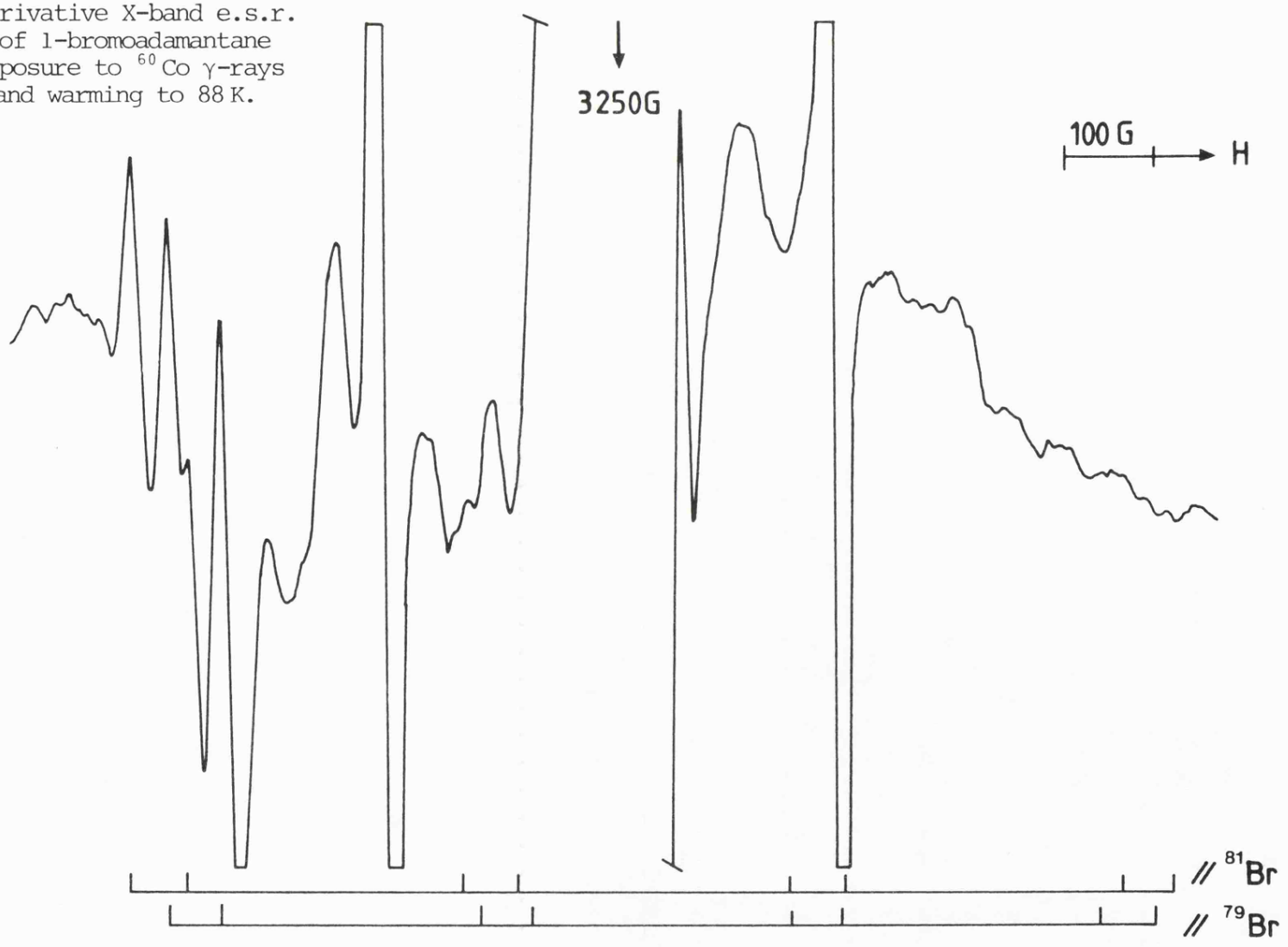

SPECTRUM 1(b)

First derivative X-band e.s.r. spectrum of 1-bromoadamantane after exposure to ^{60}Co γ-rays at 77 K and warming to 108 K.

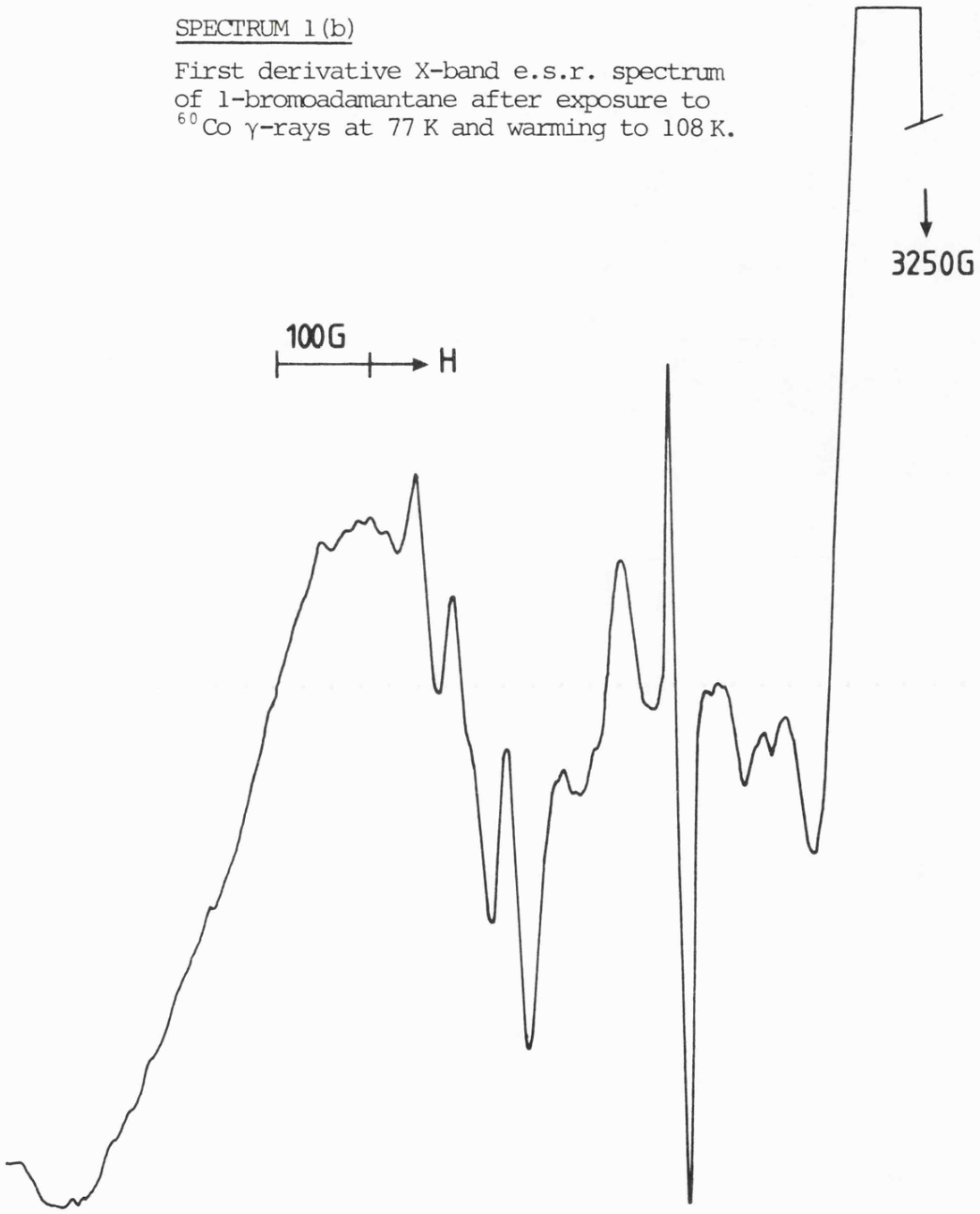

SPECTRUM 1(c)

First derivative X-band e.s.r. spectrum of 1-bromoadamantane after exposure to ^{60}Co γ-rays at 77 K and warming to 88 K.

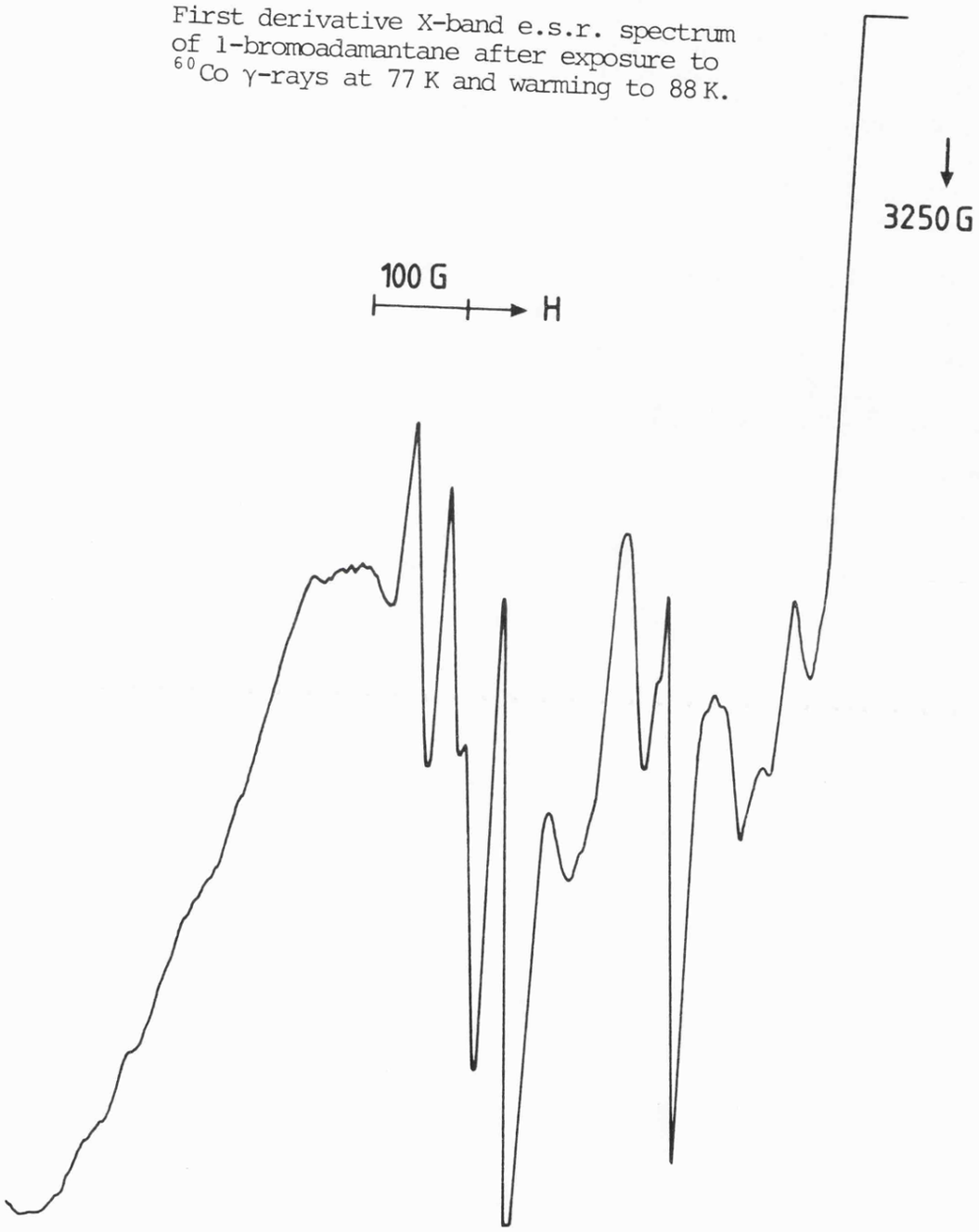

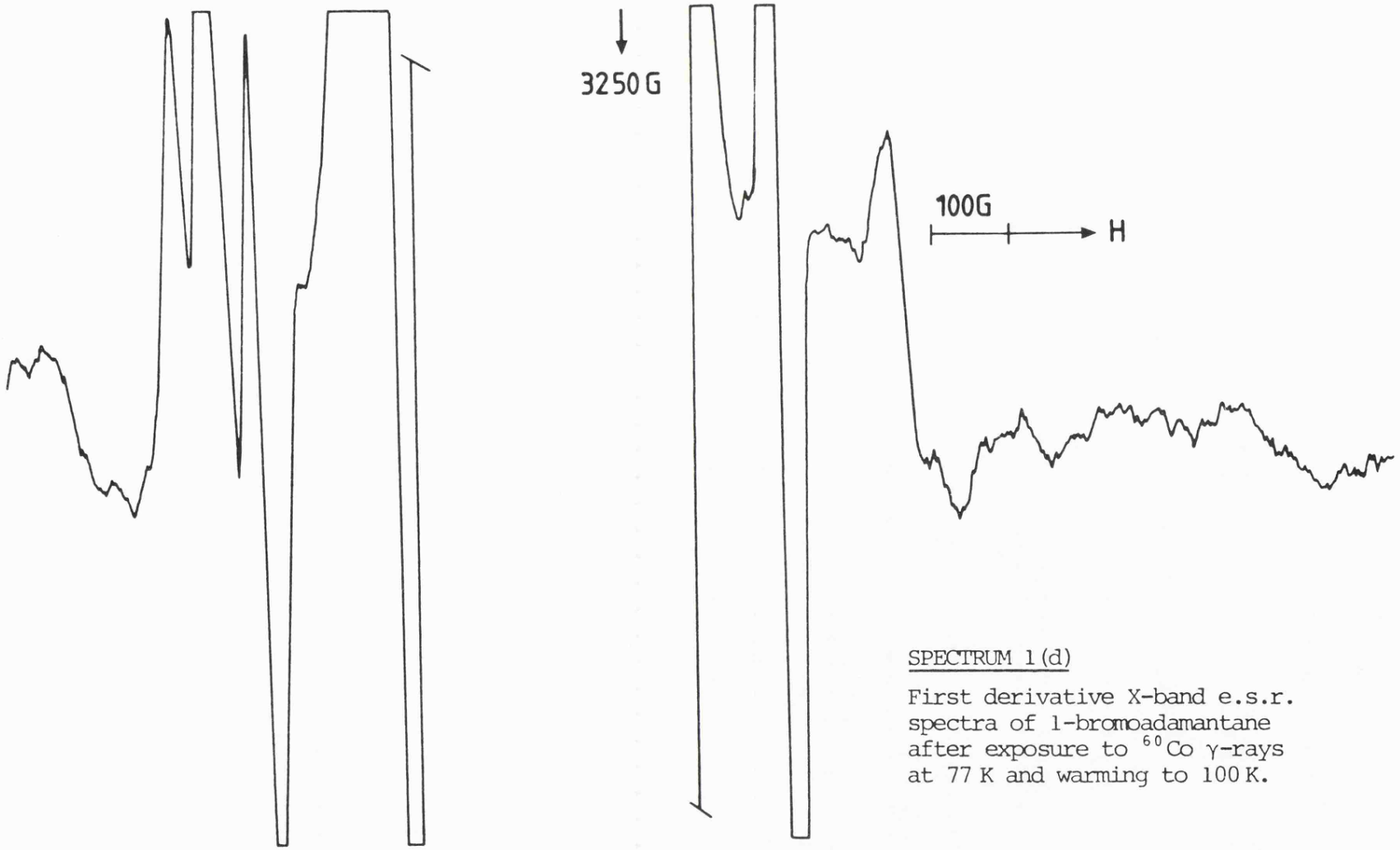

SPECTRUM 1(d)

First derivative X-band e.s.r. spectra of 1-bromoadamantane after exposure to ^{60}Co γ-rays at 77 K and warming to 100 K.

SPECTRUM 2

First derivative X-band e.s.r. spectrum of 1-bromoadamantane-d_{15} ($C_{10}D_{15}Br$) after exposure to ^{60}Co γ-rays at 77 K.

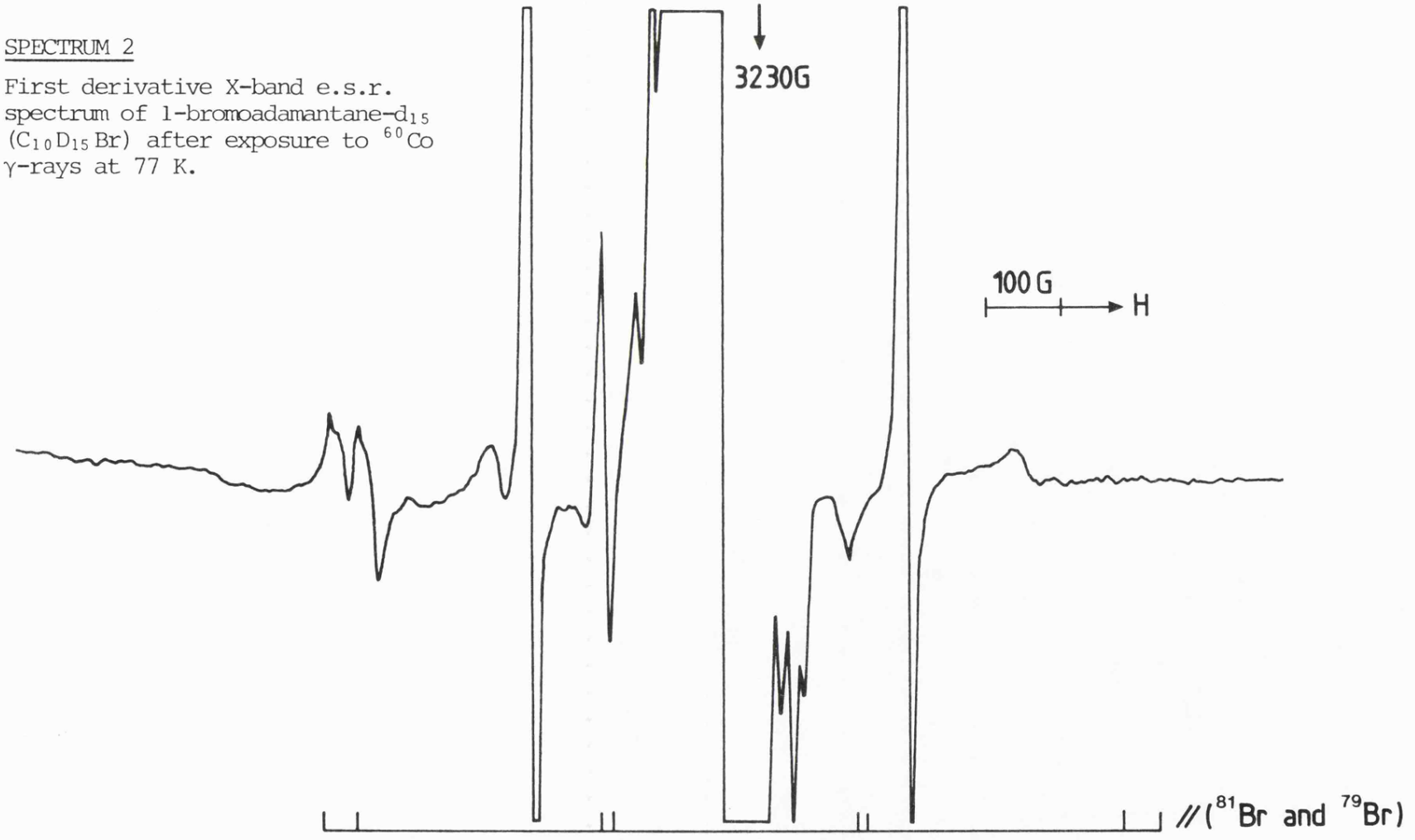

2. A more careful variable temperature experiment was conducted using the PID control equipment. This allowed accurate temperature control over a longer period of time. At -175°C the four lines of interest, 81, 79, 81, 79 + $^3/_2$, collapsed into 3 lines, presumably due to greater molecular librations. At -160°C signal strength was reduced. Returning the sample to -185°C restored the spectra to the four-line splitting with no reduction in signal strength. It was possible to thermally cycle from up to -120°C and back to -185°C with no significant reduction in signal strength. At these higher temperatures, the signal could not be defined [Spectra 1(a) - 1(d)].
3. 1-Bromoadamantane and adamantane-d_{16} were co-sublimed and examined at various temperatures. Similar results were obtained (i.e. 4 lines were seen) with the added complication of other lines possibly due to Br_2^-. No significant spectral changes were observed.
4. 1-Bromoadamantane was dissolved in methanol-d_3 to various concentrations. Solutions of 50% and 25% still produced characteristic spectra. More dilute solutions failed to give any signal.
5. Approximately 50% solutions of 1-bromoadamantane in methanol-d_3 were subjected to various temperatures in the e.s.r. cavity. The species behaved exactly as it had done in the other variable temperature experiments, i.e. reduction in signal strength coupled with a collapse to three lines.
6. Various concentrations of 1-bromoadamantane in TMS were γ-irradiated. The results parallelled the methanol-d_3 work.
7. Pure 1-bromoadamantane samples, after γ-irradiation to produce the σ^* anion, were subjected to high and low pressure mercury vapour lamps. The signals reduced slowly in magnitude over a 15-minute

period but demonstrated no significant change.

Possible radical contenders and explanations for the spectra are:-

(a) σ* anion

(b) β-bromo radical

(c) H-atom addition.

Considering these in turn:-

(a) σ* anion

The $A_x(^{81}Br)$ hyperfine coupling of 371 G would seem to agree with normal σ* bromine anion parameters (Table 1). However, there is no explanation for the 60 G coupling due to a single hydrogen atom. One could expect a small coupling to six equivalent hydrogens but this was not observed.

(b) β-bromo radical

This is a possible contender in that this species would contain a unique hydrogen and the $A_x(^{81}Br)$ hyperfine coupling of 362 G (Chapter 6) from other β-species is of the right order of magnitude. However, the p_z and σ orbitals would be orthogonal, hence no overlap would occur (Figure 6).

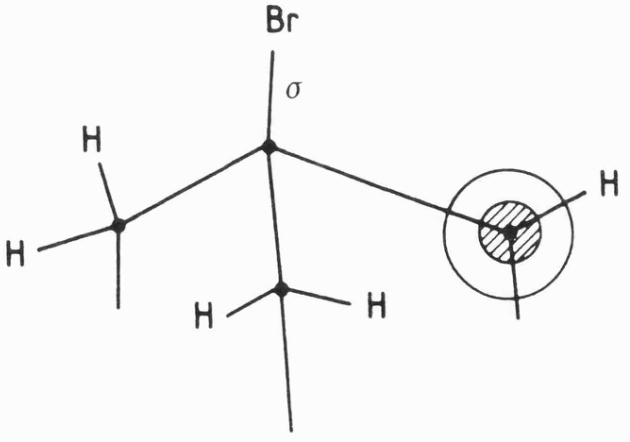

The result of this configuration would produce a maximum bromine coupling of much less than 300 G.[10,11]

TABLE 1

ESR Parameters and Spin-Densities of various bromo- and iodo-σ*-radicals

Radical	Hyperfine tensor components in G			g-tensor		Orbital population on hal		
		$A_{//}$	$A_{\perp}$	$g_{//}$	$g_{\perp}$	a_p^2 (%)	a_s^2 (%)	
$F_3C\dot{-}Br^-$ [a]	^{81}Br	263.6	114.2	2.0036	2.0212	20	1.9 [f]	1.5 [g]
BrU^- [b]	^{81}Br	373	143	1.997	2.030	32	2.7 [f]	1.8 [g]
$N\equiv C\dot{-}Br^-$ [c]	^{81}Br	587	180	2.00	2.07	54	3.7 [f]	2.5 [g]
$F_3C\dot{-}I^-$ [a]	^{127}I	373.1	178.8	2.0002	2.0483	28.5	3.3 [f]	1.6 [g]
IU^- [d]	^{127}I	505	220	1.991	2.044	42	4.3 [f]	2.1 [g]
$PhC\equiv C\dot{-}I$ [e]	^{127}I	639	263	1.98	2.09	55	5.3 [f]	2.6 [g]

[a] *Ref. 5;*
[b] *BrU = 5-bromouracil;*
[c] *Ref. 3;*
[d] *IU = 5-iodouracil;*
[e] *Ref. 4;*
[f] *Using A° values of Refs. 9 and 15;*
[g] *Using A° values of Ref. 10.*

(c) H-atom addition

Another possible species is the result of hydrogen atom addition to 1-bromoadamantane, i.e.

$$Ada\text{-}Br + H\cdot \longrightarrow Ada - \dot{B}r - H$$

This type of reaction is not unknown.[13] This is obviously an intermolecular reaction. Dilution of 1-bromoadamantane by co-sublimation with adamantane-d_{16} failed to alter the spectra. Deuterium atom addition would have resulted in the collapsing of the 60 G coupling.

Consideration was then given to the possibility of a radical cation or anion species. Radical cations are unlikely to be produced in CD_3OD. That aside, if one were to be formed similar to the following species[13] a coupling of the order of 500 G would be expected.

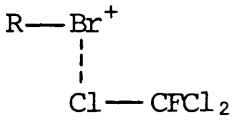

Similarly electron addition, not normally expected, would in CD_3OD produce the adamantane radical and the solvated halide ion.

In summary, no firm conclusions may be drawn with regard to the identity of the species responsible for these spectra.

REFERENCES FOR CHAPTER 8

1. G. W. Neilson and M. C. R. Symons, J. Chem. Soc., Faraday Trans. II, 1972, 68, 1582.
2. G. W. Neilson and M. C. R. Symons, Mol. Phys., 1974, 27, 1613.
3. S. P. Mishra, G. W. Neilson and M. C. R. Symons, J. Chem. Soc., Faraday Trans. II, 1974, 70, 1280.
4. D. J. Nelson and M. C. R. Symons, Chem. Phys. Letters, 1977, 47, 436.
5. A. Hasegawa, M. Shiotani and F. Williams, Faraday Discussions, Chem. Soc., 1977, 63, 157.
6. M. C. R. Symons, Radicaux Libres Organique, 1977, p.105.
7. M. C. R. Symons, J. Chem. Research, 1978, 360.
8. P. W. Atkins and M. C. R. Symons, 'Structure of Inorganic Radicals', Elsevier, 1967.
9. J. R. Morton and K. F. Preston, J. Mag. Res., 1978, 30, 577.
10. M. C. R. Symons, 'Chemical and Biochemical Aspects of Electron Spin Resonance Spectroscopy', Van Nostrand Reinhold Co. Ltd., Wokingham/Berkshire, 1978.
11. A. R. Lyons and M. C. R. Symons, J. Am. Chem. Soc., 1971, 93, 7330.
12. W. C. Danen and D. G. Saunders, J. Am. Chem. Soc., 1969, 91, 5924.
13. G. W. Eastland, S. P. Maj, M. C. R. Symons, A. Hasegawa, C. Glidewell, M. Hayashi and T. Wakabayashi, J. Chem. Soc., Perkin Trans. 2, 1984, 1439.

CHAPTER 9

Benzyl Cations

9.1 INTRODUCTION

This Chapter is a study of the radical cations of benzyl chloride, benzyl bromide and derivatives thereof produced by dilution in trichlorofluoromethane and exposed to ^{60}Co γ-rays at 77 K. The e.s.r. spectrum of benzyl chloride ($C_6H_5CH_2Cl$) was dominated by a hyperfine coupling to three inequivalent protons. These have been assigned to the para ring proton (12 G) and the two methylene protons (26 and 21.5 G). No coupling was given by the chlorine nucleus. This would suggest the preferred conformation allows the chlorine atom to be close to, but not in, the plane of the benzene ring, with a significant barrier for the in-plane site.

Benzyl bromide produced cations with strong hyperfine coupling to bromine nuclei. The two major species were $A_{//}$ (^{81}Br) 193 and 133 G.

The degree of delocalisation onto halogen can be compared with β-halogeno alkyl radicals, $R_2\dot{C}\text{-}CH_2hal$.[12,13] Andrews et al. have used electronic absorption spectroscopy to study such cations in inert gas matrices.[14,15]

These studies indicate the preferred conformation of β-halogeno radicals. There is considerable evidence that β-substituents, X, in alkyl radicals, $R_2\dot{C}CH_2X$, tend to prefer the extreme out-of-plane site with $\theta = 0$[16,17] (Diagram I). The σ-π delocalisation involves overlap

I

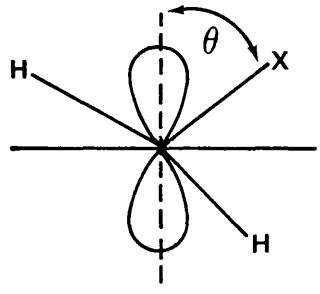

between the C-X σ-bond and the half-filled carbon 2p-orbital.[17]

Evidence for chlorine preferring the $\theta = 0$ site in $R_2\dot{C}CH_2Cl$ radicals is strong in both solid[18] and liquid states.[12] Work by Wood and Lloyd

indicates that bromine in $Me_2\dot{C}CH_2Br$ radicals prefer a site which is close to the in-plane position ($\theta \rightarrow 0$).[19] This laboratory considers that the radical giving a very small bromine hyperfine coupling has been incorrectly identified. The spectrum is not from a β-bromo radical but was an $Me_3C\cdot$ radical interacting weakly with a bromide ion in the adduct $(Me_3C\cdot\text{----}Br)^-$. A full treatment of this has been given elsewhere.[20,21] We strongly suggest that both chlorine and bromine strongly prefer the out-of-plane site with $\theta \rightarrow 0$.

9.2 EXPERIMENTAL

Freon ($CFCl_3$) was purified as previously noted. Benzyl halides were the best grades available commercially and were all purified by vacuum distillation. Purity was checked by proton magnetic resonance. Perdeuterated benzyl chloride (d_7) was 99% enriched.

Samples (ca. 1:1000 $^{v}/_{v}$) were frozen as small beads by floating drops of the solution in liquid nitrogen. The beads were then irradiated at 77 K with ^{60}Co γ-rays.

For annealing the samples were either allowed to warm up in the insert Dewar after decanting the liquid nitrogen and recooling to 77 K to capture significant spectral changes, or using a variable temperature system.

9.3 RESULTS AND DISCUSSION

Benzyl Chloride Cations

From the spectrum (Figure 1a) no hyperfine coupling to chlorine could be assigned. That the coupling is a function of coupling to three inequivalent protons (Table 1) was confirmed by using $C_6D_5CD_2Cl$ which gave only a single isotropic feature. It is suggested that the chlorine must lie close to the plane of the benzene ring (as in I,

TABLE 1

ESR Parameters for Radical Cations of Various Benzyl Halides and Related Species

Cation	Proton Hyperfine Coupling/G[a]	Halogen Hyperfine Coupling/G[a] (^{35}Cl or ^{81}Br) //	⊥[b]
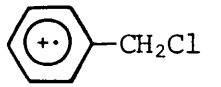	12(1H) 21.5(1H) 26(1H)[c]	0	0
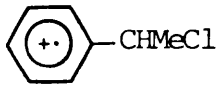	[d] ——		
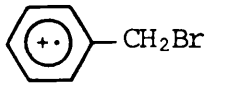	[e] ——	(α) 193 (β) 133	[b]
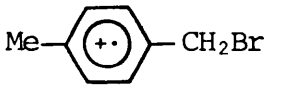	15(3H) ——	162	±45
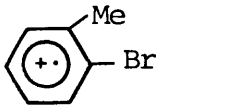	[e] ——	160	[b]

[a] G = 10^{-4} T; [b] ⊥ features not identifiable with any certainty;

[c] Broad singlet for $(C_6D_5CD_2Cl)^+$; [d] Broad singlet covering ca. 60 G;

[e] Proton hyperfine features not resolved.

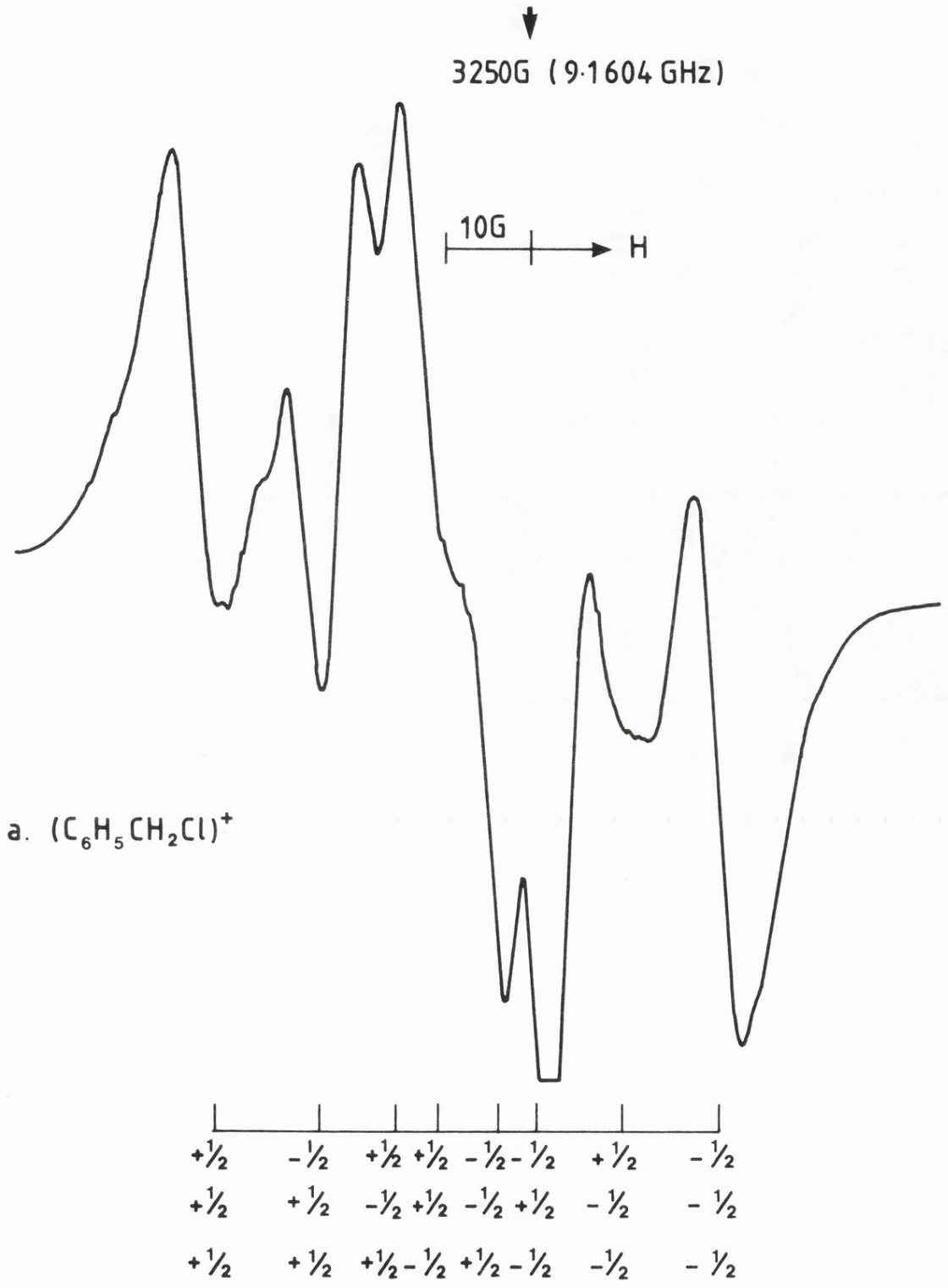

FIGURE 1a

First derivative X-band ESR spectra for benzyl chloride in $CFCl_3$ after exposure to ^{60}Co γ-rays at 77 K, showing features assigned to benzyl chloride cations.

$\theta \rightarrow 90°$). The inequivalence of the methylene protons indicates that the symmetry is not complete and it does not lie directly in the plane.

1-Methylbenzyl Chloride Cations

These cations gave a very broad e.s.r. spectrum with no clear resolution into hyperfine components. It was not possible to improve resolution even using variable temperature annealing. The total width was comparable with that for the species obtained from benzyl chloride. It is suggested that the steric effect of the methyl group is to reduce the magnitude of the energy barrier, thereby allowing a range of different conformers to be present.

Para-methylbenzyl Bromide Cations

Only one conformation was formed (Figure 2). The parallel features are well-defined and show quartet splitting from the para-methyl protons in addition to the splitting between ^{81}Br and ^{79}Br on the $M_I = \pm 3/2$ lines. No splitting could be resolved from the methylene protons. The species is characteristic of species exhibiting large hyperfine coupling to bromine in that the parallel ($\underline{z}$) features are clear, but $\underline{x}$ and $\underline{y}$ are unspecified. All attempts to obtain satisfactory computer simulations have failed.[22]

Benzylbromide Cations

The e.s.r. spectrum produced is more complex than the other cases. Two major conformations (Figure 2$\underline{b}$) can be identified each with parallel quartets. Annealing failed to significantly alter the spectrum. No full explanation can be given for the spectrum. It is suggested that there are two or three slightly different conformations in different abundancies. The broad lines could not be further resolved.

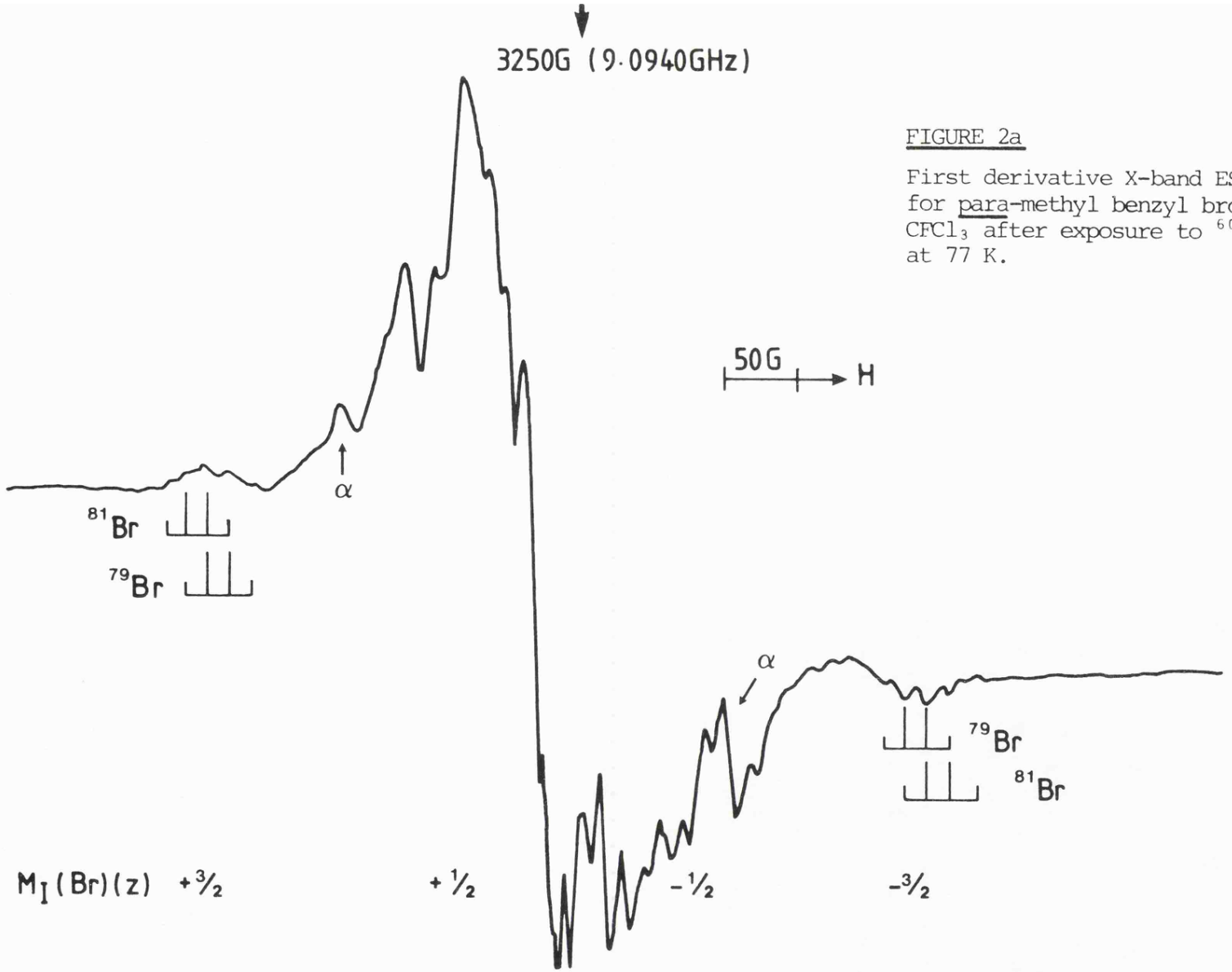

FIGURE 2a

First derivative X-band ESR spectrum for para-methyl benzyl bromide in $CFCl_3$ after exposure to ^{60}Co γ-rays at 77 K.

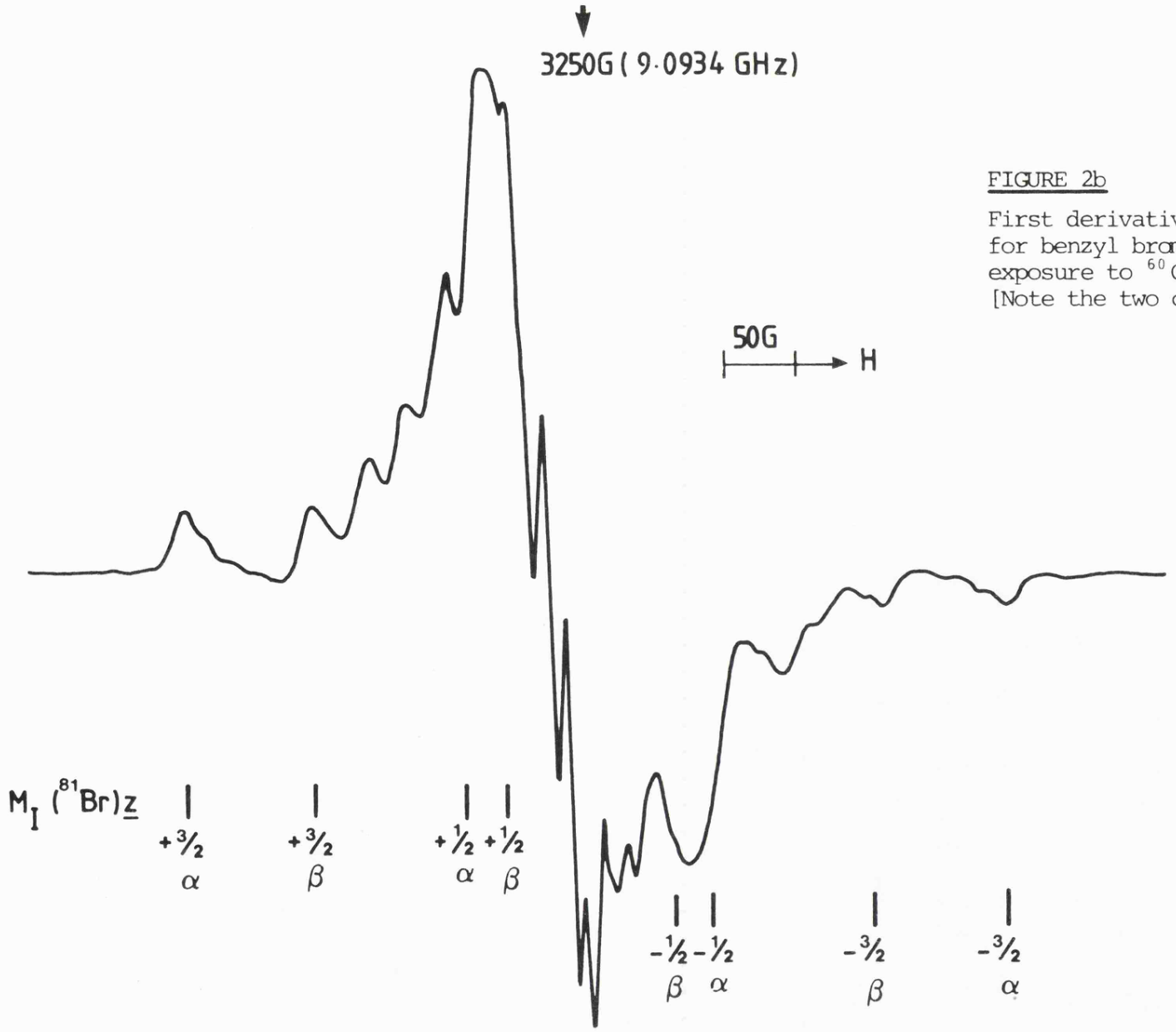

FIGURE 2b

First derivative X-band ESR spectrum for benzyl bromide in $CFCl_3$ after exposure to ^{60}Co γ-rays at 77 K. [Note the two conformations α and β.]

Identification

Considerable success has been achieved with this method of producing electron loss species.[1-10] The possibility of other mechanisms can be considered, e.g. unimolecular isomerisation or breakdown which would give rise to structures other than those proposed.

In the case of the chloro-derivative it was difficult to suggest any other breakdown products that would give rise to the parameters observed. The migration of chlorine is a well-documented occurrence[13,18] and the most probable change would be the migration of chlorine from the CH_2 group into the ring system. In the 1,2-halogen shift systems, the radical first formed was $H_2\dot{C}$-$C(Me)_2$hal (hal being Cl or Br) that rearranged producing the only detectable species of $Me_2\dot{C}$-CH_2hal. Migration of the halogen into the ring is perhaps possible but unlikely. Such an event would produce substituted benzyl radicals such as II or III. For II the spin-density on the carbon atoms that flank the

II

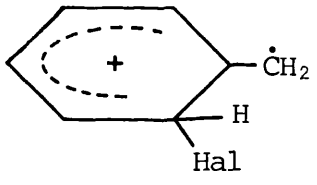

III

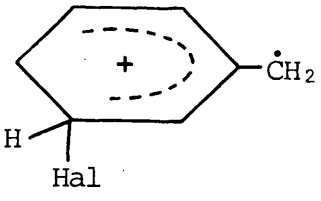

CH(hal) group should be low producing a small halogen coupling but one could expect coupling to several protons with splittings considerably less than the observed 21.5 and 26 G. The largest proton coupling for the structurally similar hexamethyl benzyl radical cation is 5.4 G.[23]

For structure III one could expect a large coupling to halogen and the hydrogen but the expected large unique proton coupling that could

be expected is not seen.

The cations (II and III) could rearrange by intramolecular proton transfer giving perhaps species IV. In order to check this possibility, cation IV was produced from the precursor ortho-bromotoluene (Figure 3). The spectrum is typical of an α-bromo species.[11] Species IV gave $A_{//}$ (^{81}Br) = 160 G and $C_6H_5Br^+$ gave 185 G.

IV 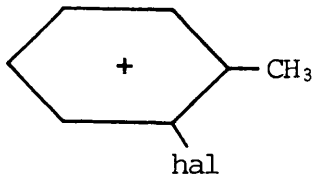

Comparisons can be made between the bromine hyperfine characteristics for this α-bromo species and that of the β-bromo species (Figure 2). In the case of the α-bromo radicals, the $M_I = +3/2$ line is of greater intensity than the $-3/2$ line. In the β-bromo case the intensities are comparable - this being due to the g-values being all relatively close to the free-spin value. For the same reason, the $M_I = +1/2$ features for α-chloro and bromo radicals are usually nearly isotropic and hence of far greater intensity than the remainder. This effect is much less marked for β-bromo radicals. Also typical of α-bromo radicals, the difference in quadrupole shifts causes a negligible ^{81}Br and ^{79}Br isotopic splitting to occur on the $M_I = \pm 3/2$ lines.[24] This does not occur for the β-bromo species.

In conclusion the possibility of rearranged species can be ignored.

9.4 ASPECTS OF STRUCTURE

The results indicate the preference of chlorine for the sterically unfavourable in-plane site rather than the $\theta = 0°$ conformation that is favoured by β-chloroalkyl radicals. This would suggest that C-H hyperconjugation is favoured over C-Cl hyperconjugation due to the positive

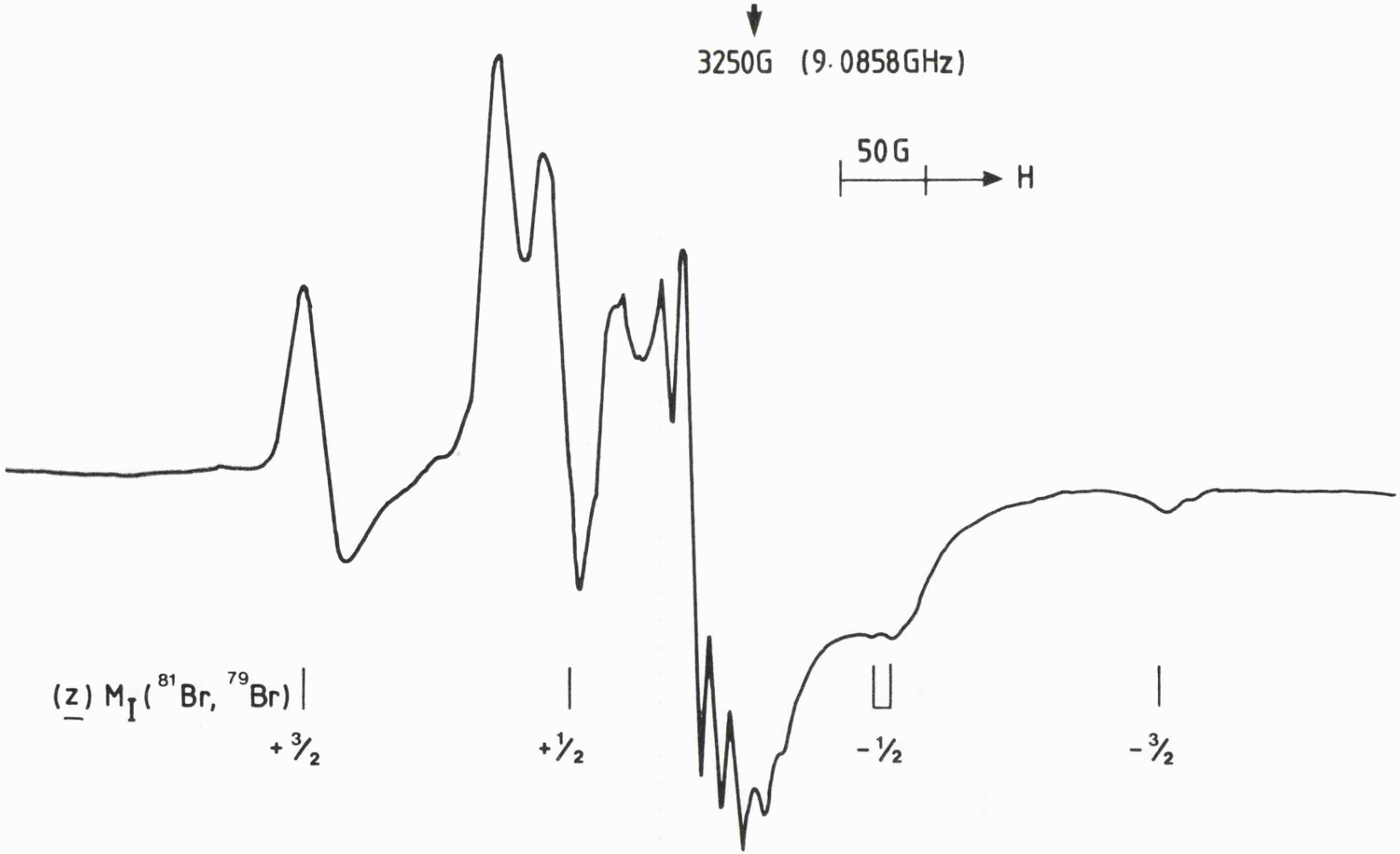

FIGURE 3

First derivative X-band ESR spectra for ortho-bromotoluene in $CFCl_3$ after exposure to ^{60}Co γ-rays at 77 K, showing features assigned to the corresponding radical cations.

charge effect.[8,25] Actual electron transfer from the C-H σ-orbitals may be favoured over the C-Cl σ-orbital contribution. An additional factor could be weak hydrogen-bonding between chlorine and an ortho-proton, as in V. The positive charge will make this bond slightly acidic.

V

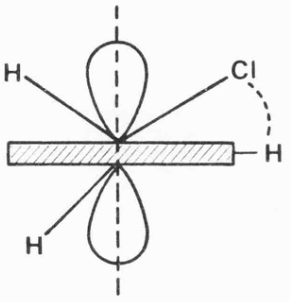

In the case of $(C_6H_5CH_2CH_3)^+$ cations[26] there are two main points. For the ethyl derivative, the two CH_2 protons are equivalent (A = 29 G). This implies no major barrier to placing the methyl group in the benzene plane. The larger proton coupling for the chloro-derivative (26 G) is less than the 29 G of the ethyl derivative despite the fact that overlap must be more favourable. It is therefore possible to assign the electron-withdrawing effect to the chlorine atom which inhibits electron-donation from the C-H σ-orbitals into the ring.

In the case of β-bromo cations, electron donation from the C-Br bond is more favourable than that from C-Cl bonds - additionally, steric resistance must be larger. In spite of this, the expected structure with $\theta = 0$ is not preferred as different conformations are formed. For the para-methyl derivative, the methyl-proton coupling (15 G) is significantly less than that for para-xylene cations (18.2 G).[8] The implication is that a significant delocalisation of the unpaired electron into the C-Br bond exists. Results from $Me_2\dot{C}-CH_2Br$ radicals give no resolution for $-CH_2$ protons where the coupling is less than 5 G. Absence of similar detectable coupling in the β-bromo cations is in accord with this.

The ^{81}Br parallel hyperfine coupling is ca. half that of $Me_2\dot{C}-CH_2Br$ radicals.[13] To a first approximation one could expect a spin-density of 0.33 on the carbon atom bonded to the CH_2Br group and hence only a maximum coupling of ca. one-third that of the alkyl radical derivative. The difference is only partly accounted for in terms of delocalisation onto the two methyl groups of the $Me_2\dot{C}-CH_2Br$ radical. Hence, a positive charge effect occurs for the C-Br electrons as well as the C-H electrons.[8]

Assuming $A_\perp$ (^{81}Br) of 45 G then an approximation for the spin-density on bromine can be made.[27] This gives $A_{iso}(^{81}Br)$ = 84 G and 2B = 78 G. The 4s-character is trivial and can be understood in terms of spin polarisation or minor 4s-admixing, but the 4p-population is ca. 15%; a measure of the spin-density on the bromine. Data is not available for bromine spin-densities in β-bromoalkyl radicals, hence no comparison can be made. Assigning all the proton hyperfine coupling for the CH_3 protons in the toluene cation to delocalisation, the total is only ca. 11%. To a first approximation, this explains why bromine is preferred to hydrogen in the optimum overlap site for the bromo species.

REFERENCES FOR CHAPTER 9

1. K. Toriyama, K. Nunome and M. Iwasaki, J. Chem. Phys., 1982, 77, 5891.
2. M. C. R. Symons and I. G. Smith, J. Chem. Res. (S), 1979, 382.
3. H. Kubodera, T. Shida and K. Shimokoshi, J. Phys. Chem., 1981, 85, 2563.
4. J. T. Wang and F. Williams, J. Am. Chem. Soc., 1981, 103, 6994.
5. M. C. R. Symons and B. W. Wren, J. Chem. Soc., Chem. Commun., 1982, 817.
6. Y. Takemura and T. Shida, J. Chem. Phys., 1980, 73, 4133.
7. M. C. R. Symons and L. Harris, J. Chem. Res., 1982, (S) 268, (M) 2746.
8. M. Iwasaki, K. Toriyama and K. Nunome, J. Chem. Soc., Chem. Commun., 1983, 320.
9. M. C. R. Symons, A. Hasegawa and S. P. Maj, Chem. Phys. Lett., 1982, 89, 254.
10. S. P. Maj, A. Hasegawa and M. C. R. Symons, J. Chem. Soc., Faraday Trans. 1, 1983, 79, 1931.
11. S. P. Mishra, G. W. Neilson and M. C. R. Symons, J. Chem. Soc., Faraday Trans. 2, 1973, 69, 1425;
S. P. Mishra, G. W. Neilson and M. C. R. Symons, J. Chem. Soc., Faraday Trans. 2, 1974, 70, 1165.
12. A. J. Bowles, A. Hudson and R. A. Jackson, Chem. Phys. Lett., 1970, 5, 552.
13. A. R. Lyons, G. W. Neilson, S. P. Mishra and M. C. R. Symons, J. Chem. Soc., Faraday Trans. 2, 1975, 71, 363.
14. B. W. Keelan and L. Andrews, J. Am. Chem. Soc., 1981, 103, 822.
15. L. Andrews, B. J. Kelsall, C. K. Payne, O. R. Rodig and H. Schwarz, J. Phys. Chem., 1982, 86, 3714.
16. A. R. Lyons and M. C. R. Symons, J. Chem. Soc., Faraday Trans. 2, 1972, 68, 622.
17. M. C. R. Symons, Tetrahedron Lett., 1975, 10, 793.
18. M. C. R. Symons, J. Chem. Soc., Faraday Trans. 2, 1972, 68, 1897.
19. R. V. Lloyd and D. E. Wood, J. Am. Chem. Soc., 1975, 97, 5986; Tetrahedron Lett., 1976, 5, 345.
20. M. C. R. Symons and I. G. Smith, J. Chem. Soc., Perkin Trans. 2, 1979, 1362.
21. M. C. R. Symons and I. G. Smith, J. Chem. Soc., Perkin Trans. 2, 1981, 1180.
22. H. Riederer, J. Hüttermann and M. C. R. Symons, J. Phys. Chem., 1981, 85, 2789.
23. R. Hulme and M. C. R. Symons, J. Chem. Soc. (A), 1966, 446.

24. H. Oloff, J. Hüttermann and M. C. R. Symons, J. Phys. Chem., 1978, 82, 621.

25. R. Hulme and M. C. R. Symons, J. Chem. Soc., 1965, 1120.

26. H. Chandra, D. N. R. Rao and M. C. R. Symons, J. Chem. Soc., Perkin Trans. 2,

27. M. C. R. Symons, Chemical and Biochemical Aspects of Electron Spin Resonance Spectroscopy, Van Nostrand Reinhold Co. Ltd., Wokingham/Berkshire, 1978.

APPENDIX

Electron Spin Resonance Data for Mono- and Di- Anions of m-dinitrobenzene: Radiation Induced Addition of Two Electrons at 77 K

MARTYN C. R. SYMONS,* S. PAUL MAJ, DAVID E. PRATT
and
MISS LYNN PORTWOOD

[Department of Chemistry, The University, Leicester, LE1 7RH]

Exposure of dilute solutions of m-dinitrobenzene or s-trinitrobenzene in methyltetrahydrofuran to ^{60}Co γ-rays at 77 K gave two species detectable by ESR spectroscopy. One, favoured at low doses, had features characteristic of mono-anions with the unpaired electrons primarily localised on one nitro-group. Similar anions were formed from the nitro-derivatives in methanol (CD_3OD).

At high γ-ray doses a second species grew in at the expense of the mono-anions. These had half-field ($\Delta M_S = \pm 2$) transitions characteristic of triplet-states, and well defined features in the parallel regions of the anisotropic $\Delta M_S = \pm 1$ transitions. These parallel features, which exhibited no resolved hyperfine coupling to ^{14}N were used to estimate average effective separations between the two unpaired electrons, giving values in the region of 5-6 Å. The $\Delta M_S = \pm 1$ perpendicular features were poorly defined but gave clear evidence of ^{14}N hyperfine coupling. The (^{14}N) parallel features were better resolved in the $\Delta M_S = \pm 2$ transitions, which showed five shoulders indicating two equivalent nitrogen nuclei with ca. half the coupling of the mono-anions.

These results are all in accord with the postulate that the species involved are di-anions in triplet-states. Each unpaired electron must be strongly localised on one nitro-group which cannot be twisted far from

the limit of co-planarity. Absence of ^{14}N coupling on the $\Delta M_S = \pm 1$ parallel features can then be understood since the ^{14}N parallel axes are perpendicular to the principal axis for the zero-field coupling.

The alternative explanation for these results, that solvent radicals are trapped close to the radical anions is considered but ruled out on the grounds that the $\Delta M_S = \pm 2$ features should then be triplets rather than quintets and because there would be no barrier to chemical reactions between such radicals and the nitrobenzene anions.

IT is well established that radiolysis of dilute solutions of substrates in solvents such as methanol or methyltetrahydrofuran (MeTHF) is an excellent method for adding electrons to give radical-anions of the substrates.[1] We established some time ago that nitrobenzenes can be converted into their anions using this procedure.[2] We showed that the spectra were usually similar to those obtained by freezing solutions of the anions prepared chemically, and that the data could be used to give approximate spin-densities on nitrogen.

Recently, Konishi *et al.*[3] have shown that for *m*-dinitrobenzene (*m*-DNB) and *s*-trinitrobenzene (*s*-TNB) in MeTHF solution, a triplet-state species can be formed by radiolysis at 77 K. No such species could be obtained from mono-nitrobenzene, or from the *o*- and *p*- dinitro derivatives. Only the outermost (parallel) features of the $\Delta M_S = \pm 1$ transition were resolved, but for both the *m*-dinitro and tri-nitro derivatives, two pairs of parallel features were detected. This was taken to mean that two different sets of radical-pairs were formed.[3] These workers failed to detect ESR features for the mono-anions, but established their presence by visible spectroscopy. The anion ESR features would have been completely

concealed beneath the intense features for MeTHF radicals. One significant aspect of their results was that the initial rate of formation of the triplet species was much less than that of the radical-anions as gauged by optical spectroscopy.

These results were interpreted in terms of pair-trapping. The possibility that di-anions were being formed was briefly considered but dismissed. The phenomenon of pair-trapping of radicals in solids, first observed by ESR spectroscopy in potassium persulphate crystals,[4] is now well established.[5] However, it has never previously been postulated for MeTHF systems. In order to explain the specificity of m-DNB and s-TNB, structure I was proposed. This, it was suggested, is such a

I

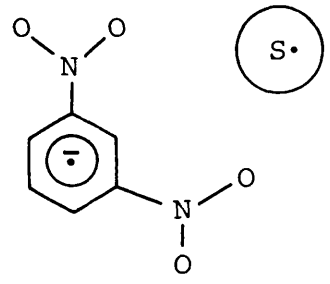

stable configuration that radical-radical reactions do not occur: for the other nitro-derivatives it was supposed to be efficient. The slow initial growth of the pair-species was explained in terms of the following mechanism:

$$\text{MeTHF} \xrightarrow{\gamma} (\text{MeTHF})^+ + e^- \quad \ldots\ [1]$$

$$e^- \longrightarrow e_t^- \quad \ldots\ [2]$$

$$e^- + \text{ArNO}_2 \longrightarrow (\text{ArNO}_2)^- \quad \ldots\ [3]$$

$$(\text{MeTHF})^+ + \text{MeTHF} \longrightarrow \text{MeTHF} + (\text{MeTHF})^+ \quad \ldots\ [4]$$

$$(\text{MeTHF})^+ + \text{MeTHF} \longrightarrow \text{MeTHF}\cdot + \text{MeTHFH}^+. \quad \ldots\ [5]$$

It was supposed that hole migration occurred [4] until the cations and anions were close together, the cation then being stabilised by

reaction [5].

It occurred to us that these results were better explained in terms of the formation of di-anions in their triplet-states. We have therefore repeated and extended this work in the hope of differentiating between the two alternative interpretations.

EXPERIMENTAL

The nitrobenzenes were of the best grades available and were used as supplied. Solutions (between 10^{-4} and 10^{-3} M) were degassed *in vacuo* by freeze-thaw procedures and were frozen as small glassy beads in liquid nitrogen prior to exposure to ^{60}Co γ-rays at 77 K in a Vickrad source. Doses varied from 0.1 - 6 MRad.

ESR spectra were measured with a Varian E-109 X-band spectrometer calibrated with a Hewlett-Packard 5246L frequency counter and a Bruker B-H12E field probe, which were standardised with a sample of DPPH. Samples were annealed until the central ESR features due to MeTHF radicals were lost or reduced and then re-cooled to 77 K for measurement.

RESULTS AND DISCUSSION

Mono-Anions. - The ESR spectra for the mono-anions (Figure 1 and Table 1) establish that for both *m*-DNB and *s*-TNB the excess electrons are confined to only one nitro-group. Thus broad triplets were obtained, characteristic of mono-nitro derivatives, each of the outer (parallel) components being split into quartets from three nearly equivalent protons. The perpendicular coupling is small and is lost in the width of the intense central component. This is typical of solid-state ESR spectra for aromatic nitro-anions. This is, perhaps, surprising since the LUMO for both these molecules is normally symmetric so that two or three equivalent

TABLE 1

ESR Parameters for Mono- and Di- Anions of m-Dinitrobenzene and s-Trinitrobenzene at 77 K

Anion	Solvent	Hyperfine Coupling Constants/G[a]			Zero-field Splitting/G[a]	
		$^{14}N_{//}$	$^{14}N_{\perp}$	^{1}H	$D_{//}$	$D_{\perp}$
(m-DNB)$^{-}$ [b]	MeTHF	27 (1N)	0±3	ca. 3.5 (3H)		
	CD_3OD	30 (1N)	0±3	ca. 3.5 (3H)		
(m-DNB)$^{2-}$	MeTHF	13 (2N) [d]	0±3	e	363	ca. 182
	MeTHF [c]	e	e	e	350 + 295 [g]	e
(m-DNB)$^{2-}$	CD_3OD	15 (2N) [d]	0±3	e	240	ca. 120
(s-TNB)$^{-}$	MeTHF	27 (1N)	0±3	ca. 3.5		
	CD_3OD	29 (1N) [f]	0±3	ca. 3.5		
(s-TNB)$^{2-}$	MeTHF	13 (2N) [d]	0±3	e	463	ca. 232
	MeTHF [c]	e	e	e	458 + 273 [g]	e
	CD_3OD	15 (2N) [d]	0±3	e	284	ca. 142

[a] $G = 10^{-4}$ T; [b] DNB = dinitrobenzene, TNB = trinitrobenzene; [c] Ref. 3;
[d] Based mainly on $\Delta M_S = 2$ transition. $A(^{14}N) = 0$ on $D_{//}$ features; [e] Not resolved;
[f] Possible 2N species - see text; [g] Assigned to separate species in Ref. 3.

nitrogen nuclei would have been expected. However, we have previously shown that relatively minor perturbations from cations or even protic solvent molecules are sufficient to move the anions of m-DNB from the symmetric to the antisymmetric state.[6-8] The situation envisaged is shown schematically in Figure 2. These are two equivalent asymmetric orbitals, each centred on one of the two nitro-groups. We suggest that, in the present examples, the perturbations introduced by the added electron sets in preferably around one nitro-group. This is expected for methanolic solutions since hydrogen-bonding develops readily at 77 K when anions are formed from neutral molecules,[9] and marked line-width alternation is exhibited by fluid solutions.[7,8] It is less clear that the asymmetric structure should be favoured in MeTHF solution and we have looked carefully for a switch to the thermodynamically favoured symmetric structure on annealing, to no avail. The spectra leave no doubt that, for both compounds, the first formed structure is one having an asymmetric wavefunction for the HOMO (Figure 1).

The Triplet Species. - As stressed by Konishi et al.,[3] the ESR spectra for these species leave no doubt that they are triplets. The issue is purely one of identification: are they radical-pairs[3] or are they di-anions?

Our results are not identical with those already published (Table 1). In particular, we failed to detect the inner shoulders separated by 295 G reported for m-DNB in MeTHF.[3] We do not understand this difference. We have been able to get further details of the $\Delta M_S = \pm 1$ transitions and, as indicated in Figure 3, have obtained some hint that the "perpendicular" features include ^{14}N hyperfine coupling. This idea also accommodates the inner features found for s-TNB by Konishi et al.[3] However, clear evidence for ^{14}N hyperfine coupling is shown by the $\Delta M_S = \pm 2$ transitions

(Figure 4). This was not resolved in the previous study.[3] The zero-field splitting is not present in these half-field transitions, so the spectra are dominated by the ^{14}N features. As with the mono-anions, only the parallel features are resolved, but in these spectra there are five shoulders, indicating two equivalent nitrogen nuclei. The splitting is ca. half those for the mono-anions, indicating fast exchange, as expected for the doubly charged anions.

This constitutes the strongest evidence in favour of the concept that the triplet-state species are doubly charged anions. The radical-pair model (I) would exhibit coupling to only one coupled ^{14}N nucleus, as for the mono-charged anion. In slow exchange the hyperfine coupling should be the same, whilst in fast exchange half the normal value should be obtained. The fact that 5 rather than 3 features are seen strongly supports our spectral interpretation.

Structure. - Here we consider what is to be expected if a second electron is added to the mono-anions. Since the first electron is strongly confined to a single NO_2-group, this should also be true of a second electron. Hence a triplet-state giving a species with two equivalent nitrogen atoms is to be expected for both substrates. The effect of charge-repulsion should be to localise the electrons even more on the two NO_2-groups. This is required by the relatively small values of the zero-field parameters. These have been used to derive mean values for the separation between the two unpaired electrons (Table 2). These values require that the two electrons be strongly confined to the nitro-groups since if they were both delocalised into the benzene rings the coupling would be much larger. The separation between the two nitrogen atoms is ca. 5 Å, but there is considerable delocalisation onto oxygen, so that, for confined electrons, values between 5 and 6 Å are reasonable.

TABLE 2

Mean separation (r) between the Unpaired Electrons for the Di-anions estimated from the zero-field splitting parameters

Di-anion/solvent	(m-DNB)$^{2-}$/MeTHF	(m-DNB)$^{2-}$/CD_3OD	(s-TNB)$^{2-}$/MeTHF	(s-TNB)$^{2-}$/CD_3OD
r/Å	5.3	6.1	4.9	5.8

It is not clear why the zero-field splitting for these species in methanol (CD_3OD) is less than those for MeTHF solutions. Probably solvation at oxygen increases the extent of localisation. Even though localisation must be extensive for the species in MeTHF, a small increase can have a disproportionate effect on the zero-field splitting because of the large contribution from electrons delocalised into the benzene rings. That such a shift of spin-density onto NO_2 is induced by solvation is clearly evidenced by the enhanced value of $A_{//}(^{14}N)$ for the mono-anions on going from MeTHF to methanol solutions (Table 1). A measure of the spin-densities on nitrogen for these forms of the mono-anions can be obtained from the hyperfine tensor components. Taking reasonable values for A_{iso} from liquid-phase data,[6-8] and using the usual procedures,[5] we get values of ca. 58% and 61% for solutions in aprotic MeTHF and alcohol solvents respectively.

The degree of localisation must be at least as great for the di-anions. The measured values for $A_{//}$ will only be principal values (A_{zz}) if the nitro-groups are coplanar. This is unlikely to be exactly true, so that they represent lower limits for A_{zz}. The extent of localisation can also be gauged, in principle, from the proton hyperfine coupling. If it remains the same as for the mono-anions, we expect $A(^1H) \approx 3.5$ G, but if localisation on the NO_2 groups is increased, this value should fall. The narrowest features are the parallel lines for the $\Delta M_S = \pm 1$ transition. No proton splitting can be detected for these lines, so we can place an upper limit of ca. 3 G on the coupling constants. Unfortunately, no firm conclusions can be placed on this result. Nevertheless, we conclude that the di-anion model is in reasonable accord with all the results.

The objection that m-DNB should not give a triplet species on the addition of two extra electrons is not valid. Since addition of one

electron gives the asymmetric structure found, for example, in fluid aqueous solutions,[8] then the second electron must, by symmetry, occupy the alternative orbital and hence a triplet state is to be expected. It is particularly significant that mono-nitrobenzene and o- or p-dinitrobenzene do not give these species since they have no low-lying states that can mix in this way. Thus their di-anions should not be triplet species.

The Radical-Pair Model. - The strongest argument against this model is that it predicts a triplet for the ^{14}N hyperfine structure in the $\Delta M_S = \pm 2$ transition, whereas a quintet is observed. However, we consider this concept to be innately improbable from a mechanistic viewpoint. Firstly, it is unlikely that positive charge migration is efficient (process [4]). There is no evidence that substrates with low ionization potentials give radical-cations in this medium: indeed, its great efficacy as a medium for specifically forming electron-addition products[1] is evidence against hole migration. If it were efficient, then we require the coincidence that reaction to give the neutral MeTHF radicals should occur only when the separation between cations and anions is in the 5-6 Å region. At that separation charge transfer from the anion to the cation would be extremely efficient, so that pair-trapping would be a rare event. Even if such pairs could be formed, there would seem to be no barrier to reaction between the highly reactive MeTHF radicals and the reactive radical-anions. Ring or oxygen addition would, in our view, be expected even at 77 K.

Aspects of Mechanism. - If our conclusions are correct, these results have important implications for radiation chemistry. Our results suggest that the ease of electron capture by the mono-anions is comparable with that for addition to the neutral molecules. At high doses we have been

able to reach a point at which the intensity of the mono-anion features appeared to fall. It is difficult to quantify these changes and only qualitative trends could be relied on. This was attempted by Konishi et al.[3] but it seems to us most probable that their optical data relate to the total concentration of mono- and di- anions rather than to just the concentration of mono-anions. If this is correct, their Figure 5 compares the total increase in the mono- and di- anion concentration together with that of the di-anions alone. These trends are in qualitative agreement with expectation and confirm that second electrons add with remarkable efficacy. These conclusions may have some significance with respect to the problems of radiation damage in electron-microscopy.[9]

Acknowledgement. - We thank the SERC and ICI Limited for a CASE Award to SPM.

REFERENCES

1. M. C. R. Symons, Pure and Appl. Chem., 1981, 53, 223.
2. W. M. Fox, J. M. Gross and M. C. R. Symons, J. Chem. Soc. (A), 1966, 448.
3. S. Konishi, M. Hoshino and M. Imamura, J. Phys. Chem., 1981, 85, 1701.
4. P. W. Atkins, M. C. R. Symons and P. A. Trevalion, Proc. Chem. Soc., 1963, 222;
   S. B. Barnes and M. C. R. Symons, J. Chem. Soc. (A), 1966, 66.
5. M. C. R. Symons, Chemical and Biochemical Aspects of Electron Spin Resonance Spectroscopy, Van Nostrand Reinhold Co. Ltd., Wokingham, Berkshire, 1978.
6. T. A. Claxton, W. M. Fox and M. C. R. Symons, Trans. Faraday Soc., 1967, 63, 1.
7. C. J. W. Gutch, W. A. Waters and M. C. R. Symons, J. Chem. Soc. (B), 1970, 1261.
8. D. Jones and M. C. R. Symons, Trans. Faraday Soc., 1971, 67, 961.
9. M. C. R. Symons, Ultramicroscopy, 1982, 10, 15.

CAPTIONS TO FIGURES

FIGURE 1 First derivative X-band ESR spectra for dilute solutions of m-DNB and s-TNB in CD_3OD or MeTHF after low exposure to ^{60}Co γ-rays at 77 K, followed by annealing to reduce the concentration of solvent radicals: a for m-DNB in MeTHF at 77 K showing features assigned to $(m\text{-DNB})^-$ anions. Feature α is the $M_I = +1$ parallel line measured during the annealing process, showing proton hyperfine lines from 3 nearly equivalent protons. b For s-TNB in MeTHF at 77 K showing features assigned to $(s\text{-TNB})^-$ anions and c for s-TNB in CD_3OD at 77 K showing features assigned to $(s\text{-TNB})^-$: [central features are for $\cdot CD_3$ + $D_2\dot{C}OD$ radicals].

FIGURE 2 Combination of the ground state SOMO ($\psi_{S(1)}$) for $(m\text{-DNB})^-$ and the low-lying excited state ($\psi_{S(2)}$) to give two equivalent asymmetric levels ($\psi_{M(1)}$ and $\psi_{M(2)}$) which are selected in the present study on the addition of either one or two electrons.

FIGURE 3 First derivative X-band ESR spectra for dilute solutions of m-DNB and s-TNB in MeTHF or CD_3OD after prolonged exposure to ^{60}Co γ-rays at 77 K, showing outer features assigned to $(m\text{-DNB})^{2+}$ or $(s\text{-TNB})^{2-}$ anions: only the outer (parallel) features are well defined: a for m-DNB in MeTHF, b for m-DNB in CD_3OD, c for s-TNB in MeTHF and d for s-TNB in CD_3OD.

FIGURE 4 First derivative X-band ESR spectra for dilute solutions of m-DNB and s-TNB in MeTHF or CD_3OD after prolonged exposure to ^{60}Co γ-rays at 77 K, showing half-field transitions ($\Delta M_S = \pm 2$) assigned to $(m\text{-DNB})^{2-}$ or $(s\text{-TNB})^{2-}$, a for m-DNB in MeTHF, b for m-DNB in CD_3OD and c for s-TNB in CD_3OD.

Fig. 1a

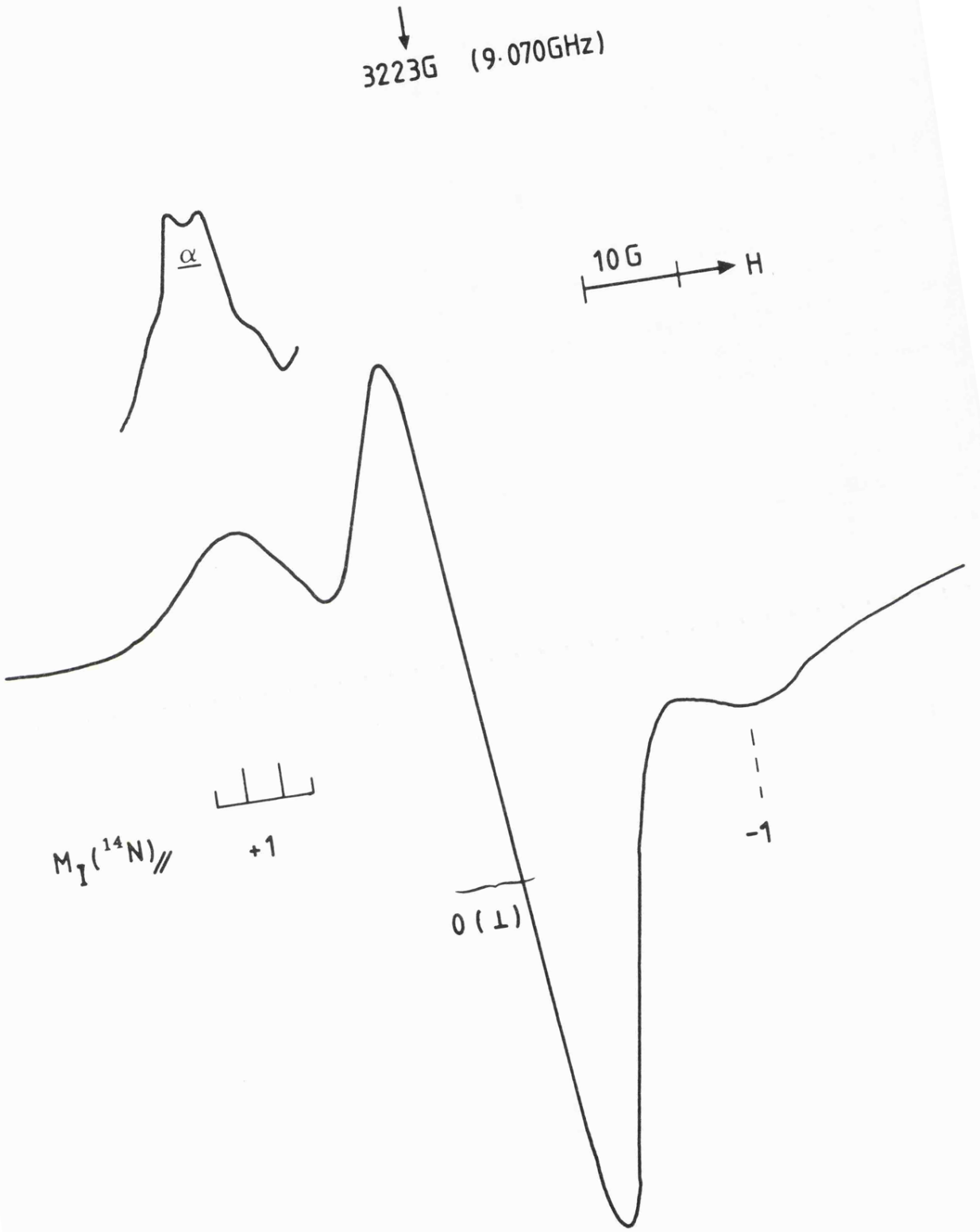

Fig. 1b

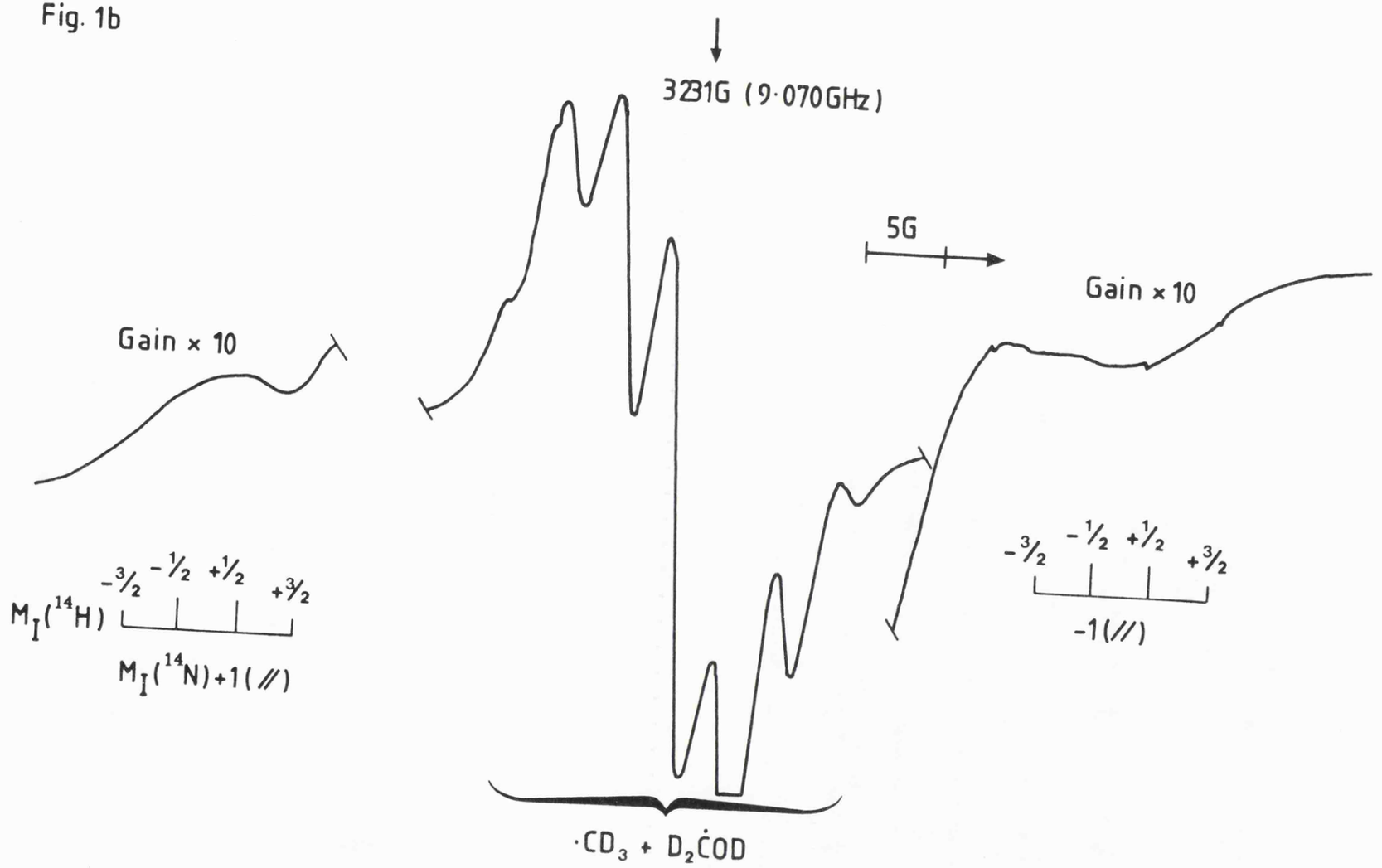
3231G (9·070GHz)
5G
Gain × 10
Gain × 10
$M_I(^{14}H)$ $-3/2$ $-1/2$ $+1/2$ $+3/2$
$M_I(^{14}N)+1(//)$
$-3/2$ $-1/2$ $+1/2$ $+3/2$
$-1(//)$
$\cdot CD_3 + D_2\dot{C}OD$

Fig. 1c

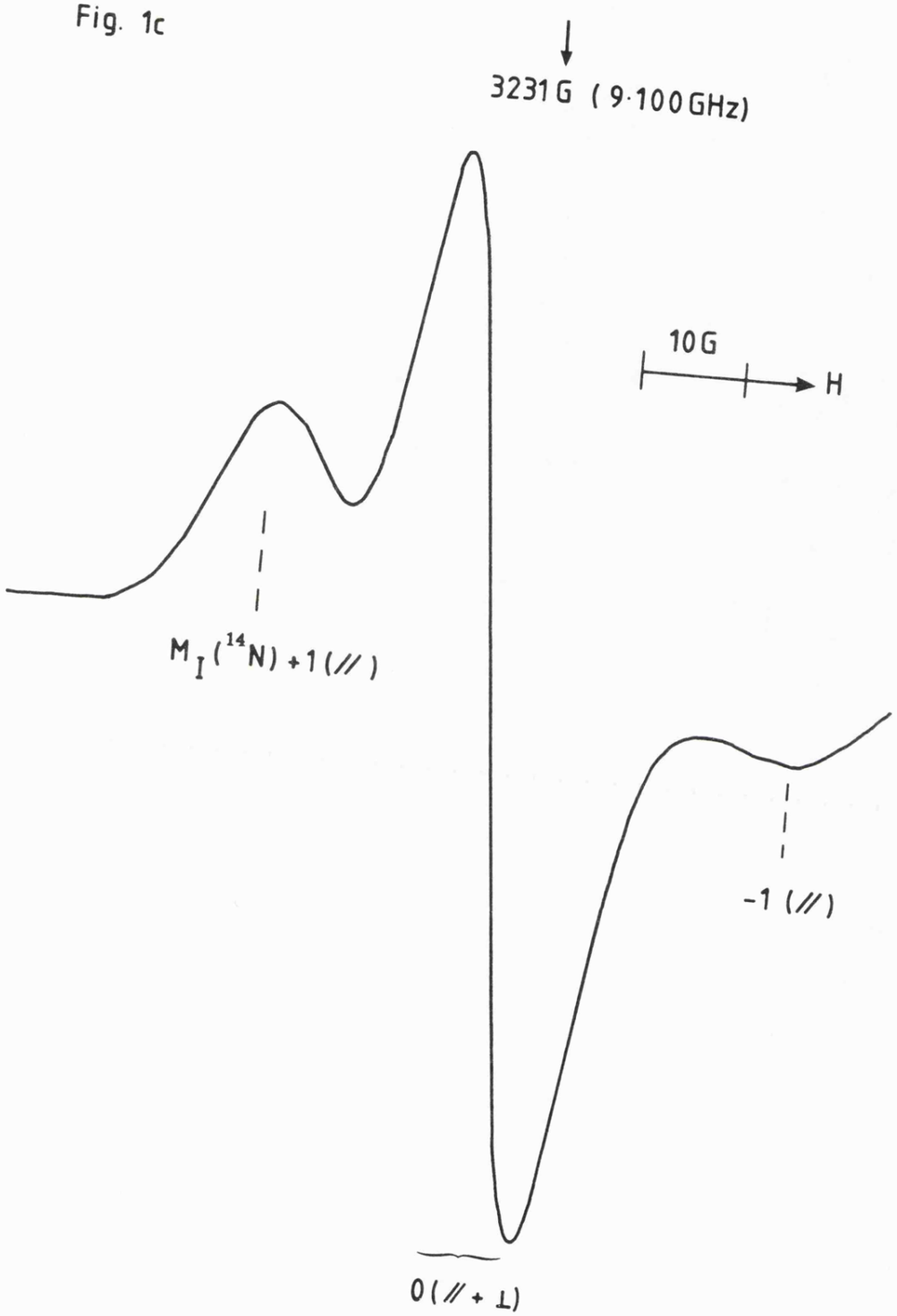

Fig. 2

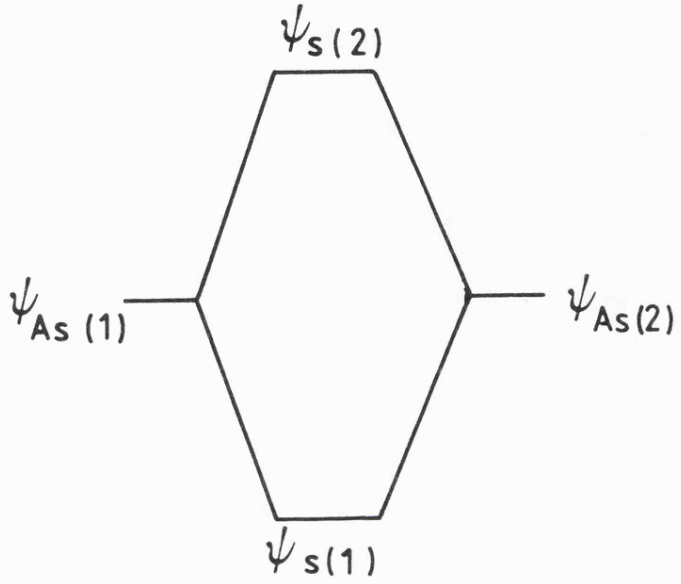

Fig. 3a

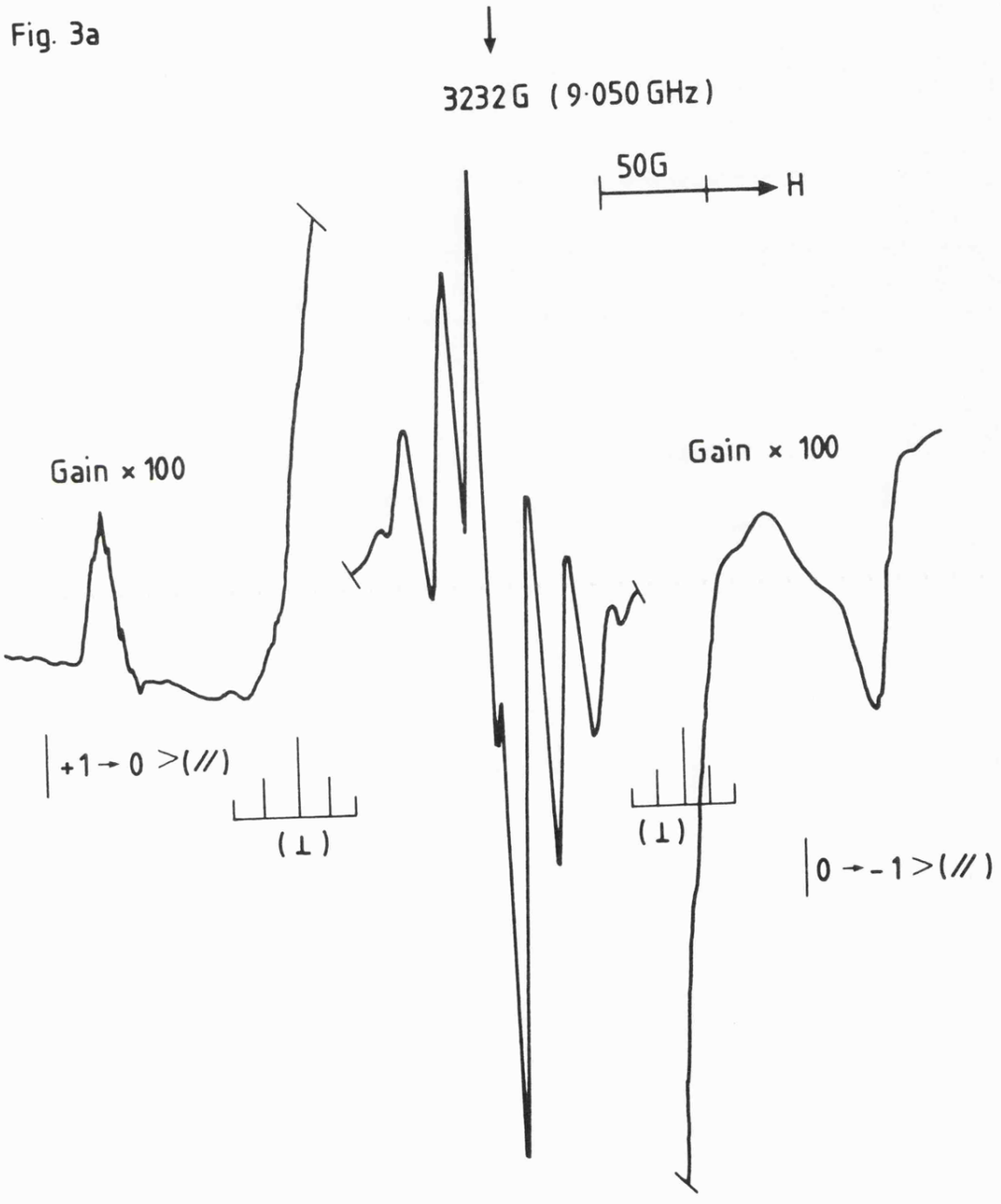

Fig. 3b

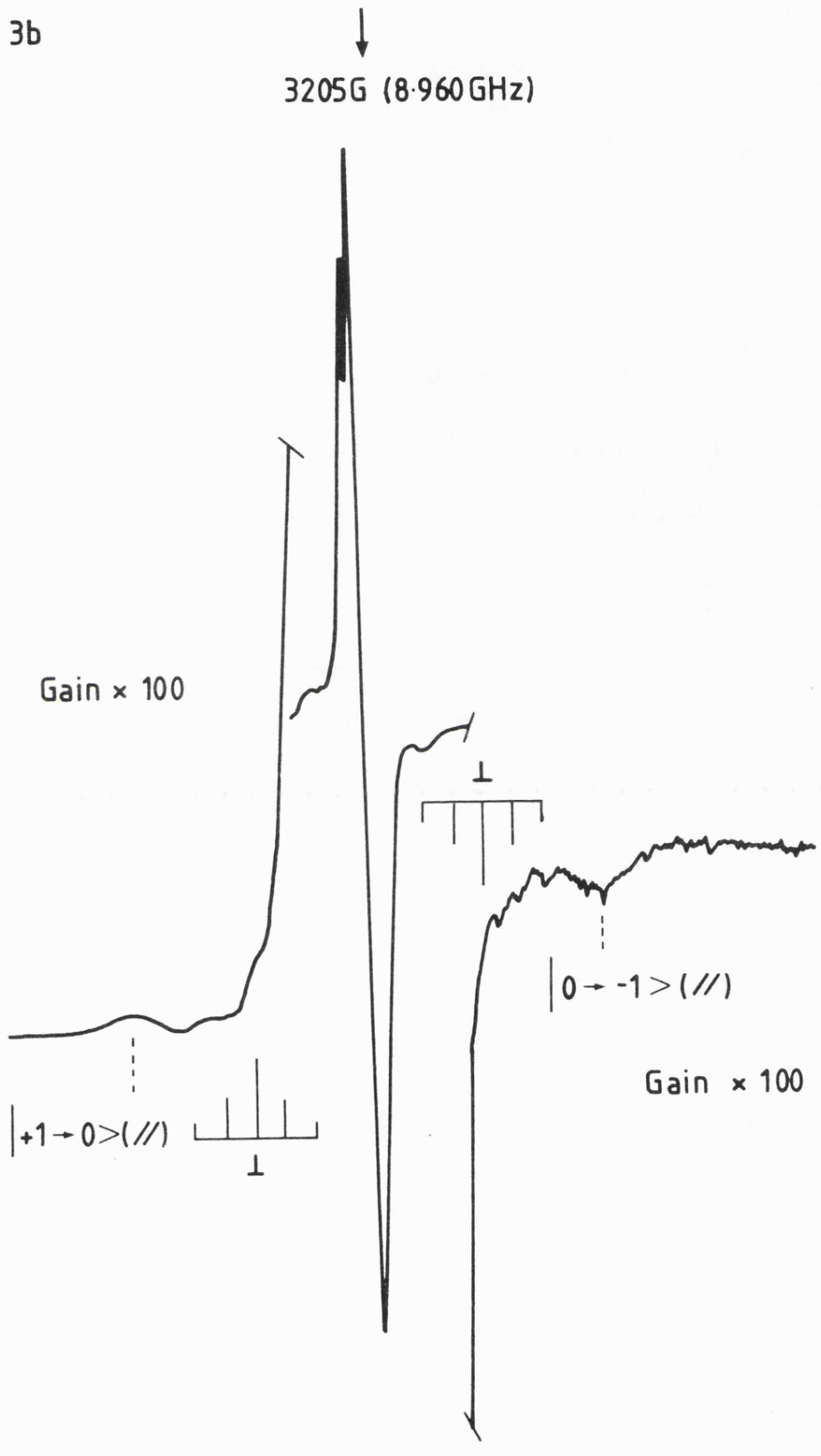

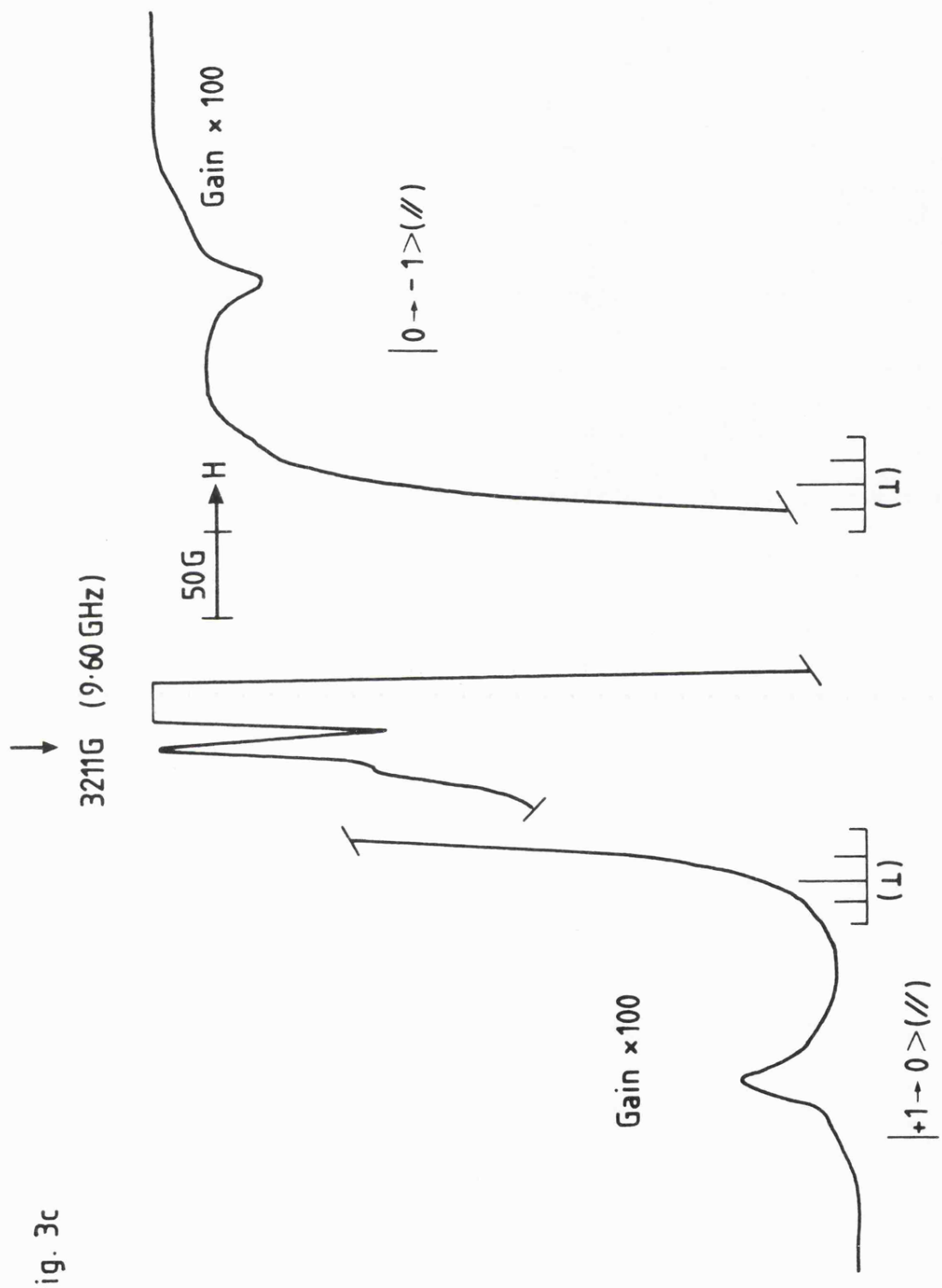

Fig. 3c

Fig. 3d

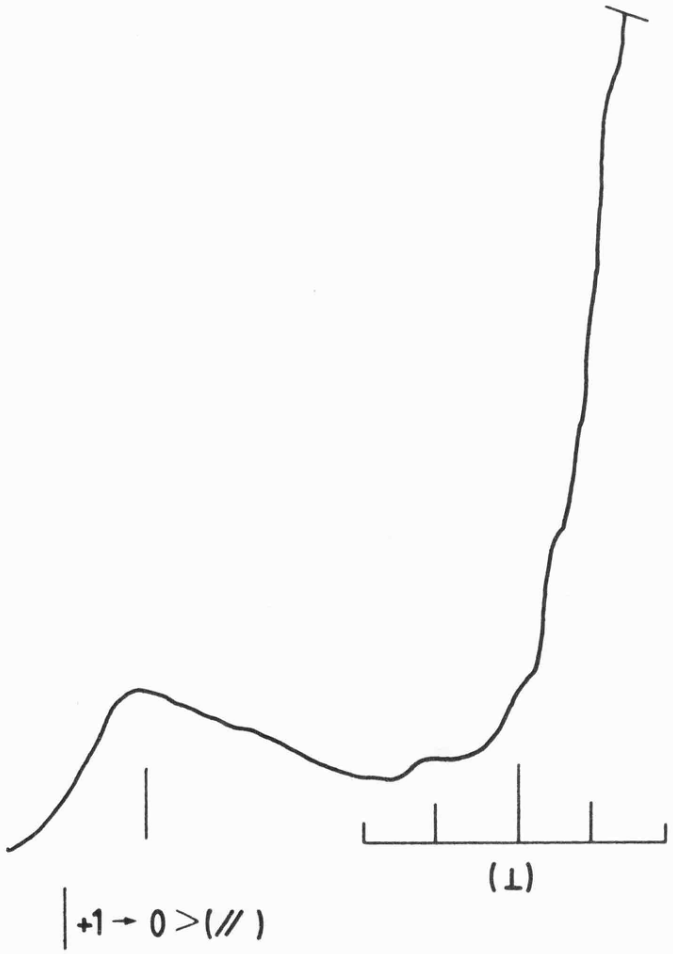

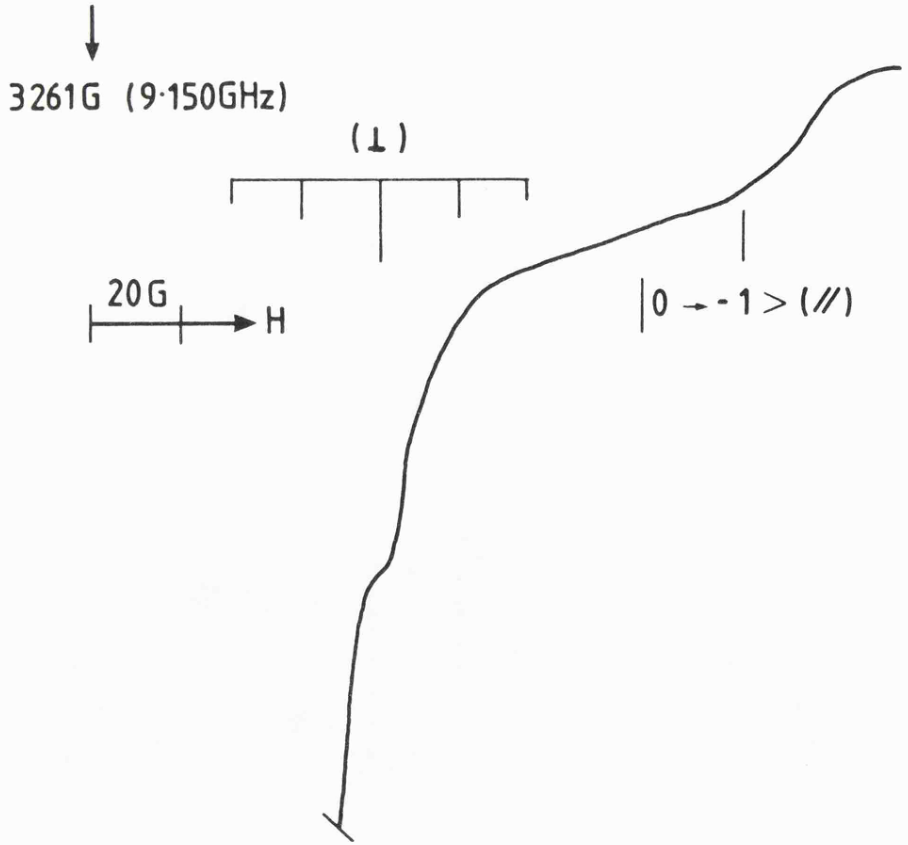

Fig. 4a

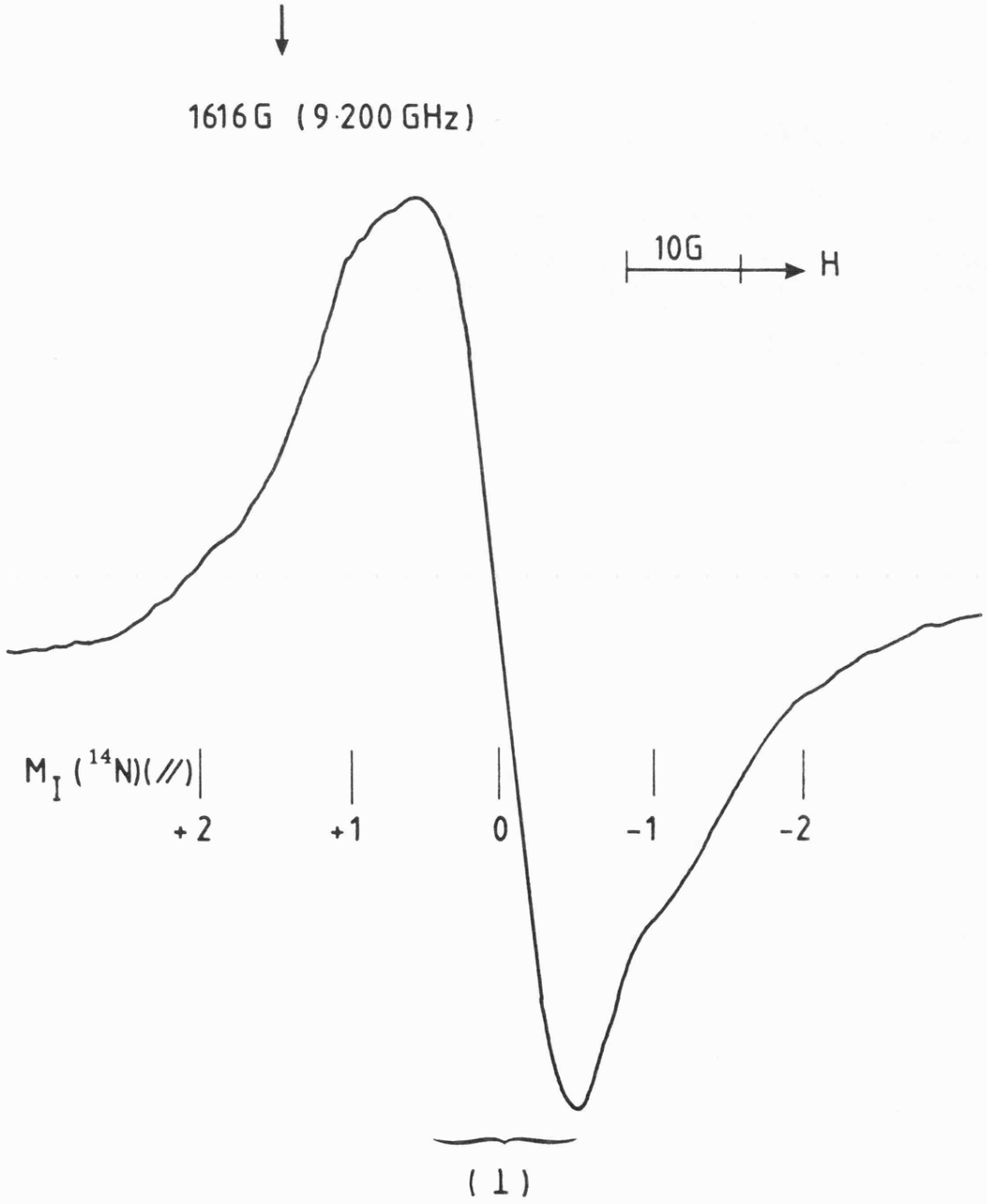

Fig. 4b

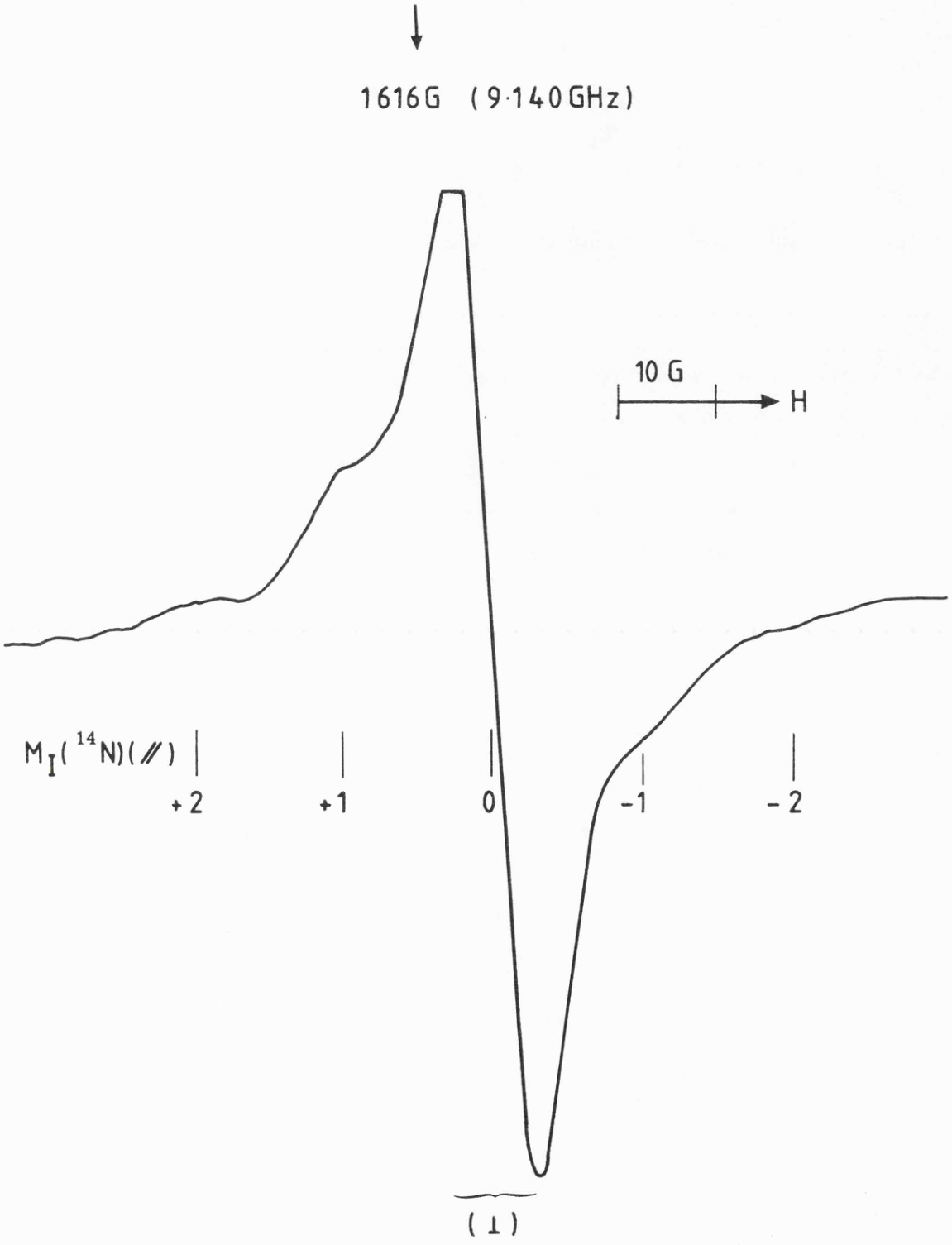

Fig. 4c

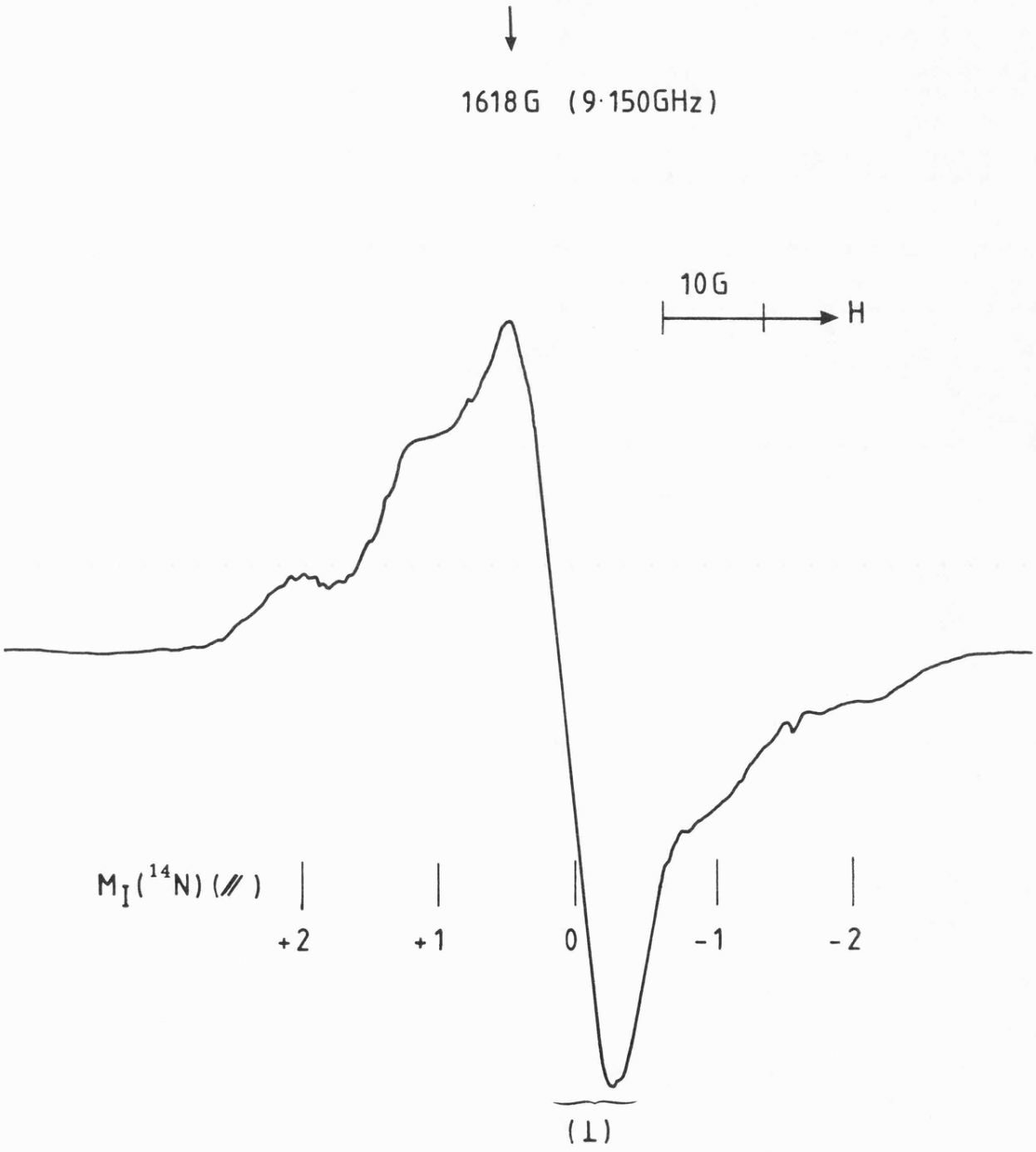

ESR STUDIES OF ORGANO-HALIDE RADICALS

Stanislaw Paul Maj

Abstract

Exposure of a range of dilute solutions of halogenobenzenes in fluorotrichloromethane to ^{60}Co γ-rays at 77 K gave the corresponding cations characterised by their ESR spectra. The approximate spin-densities on the halogens were greater than predicted by comparison with neutral α-bromo radicals and increased from *ca.* 8% for PhF^+ to 23% for $PhCl^+$, 30% for $PhBr^+$ and 46% for PhI^+ in accord with the fall in the ionization potential for this series of halogen. For $PhBr^+$, replacement of *para* hydrogen by Br, OH and SH gave a steady fall in spin-density on Br reflecting increasing π delocalisation onto the *para* substituent. Evidence for dimer cation formation in concentrated solutions is presented. The major species obtained from benzyl chloride suggested a preferred conformation with the chlorine close to, but not in, the plane of the benzene ring, with a significant barrier for the in-plane site, in contrast with benzyl bromide with strong hyperfine coupling to bromine [Chapters 3, 4 and 9].

Exposure of dilute solutions of $Me_2C(Br)\dot{C}(Br)Me_2$ in CD_3OD and MeTHF to ^{60}Co γ-rays at 77 K gave the radical $Me_2\dot{C}C(Br)Me_2$. From changes in the e.s.r. spectrum of this radical, it is deduced that the stable structure is asymmetric, but that the rate of migration of bromine between the two equivalent sites becomes fast on the e.s.r. time-scale at *ca.* 100^{-1} [Chapter 6].

Evidence is given for the 1,2-intramolecular proton shift in the interconversion of isobutyl to tert-butyl radicals. The parent material was dissolved in a variety of matrices and exposed to ^{60}Co γ-rays at 77 K. The reaction was observed using an in-cavity Proportional, Integral and Differential (PID) temperature control system [Chapter 5].

A single crystal of ethyl iodide was grown and irradiated at 77 K with a ^{60}Co γ-ray source. The spectra were orientation dependent but it was not possible to determine the principal *g*-values and the elements of the hyperfine tensor [Chapter 7].

1-Bromo adamantane was dissolved in a variety of deuterated matrices and exposed to ^{60}Co γ-rays at 77 K. No firm conclusions can be drawn regarding the single proton coupling of *ca.* 65 G to the bromine.

Exposure of dilute solutions of m-dinitrobenzene or s-trinitrobenzene in methyltetrahydrofuran to ^{60}Co γ-rays at 77 K gave two species at 77 K. One, favoured at low doses, had features characteristic of mono-anions with the unpaired electron localized on one nitro-group. At high γ-ray doses a second species with triplet state characteristics grew at the expense of the first. The average separation between the two unpaired electrons was estimated to be 5-6 Å.